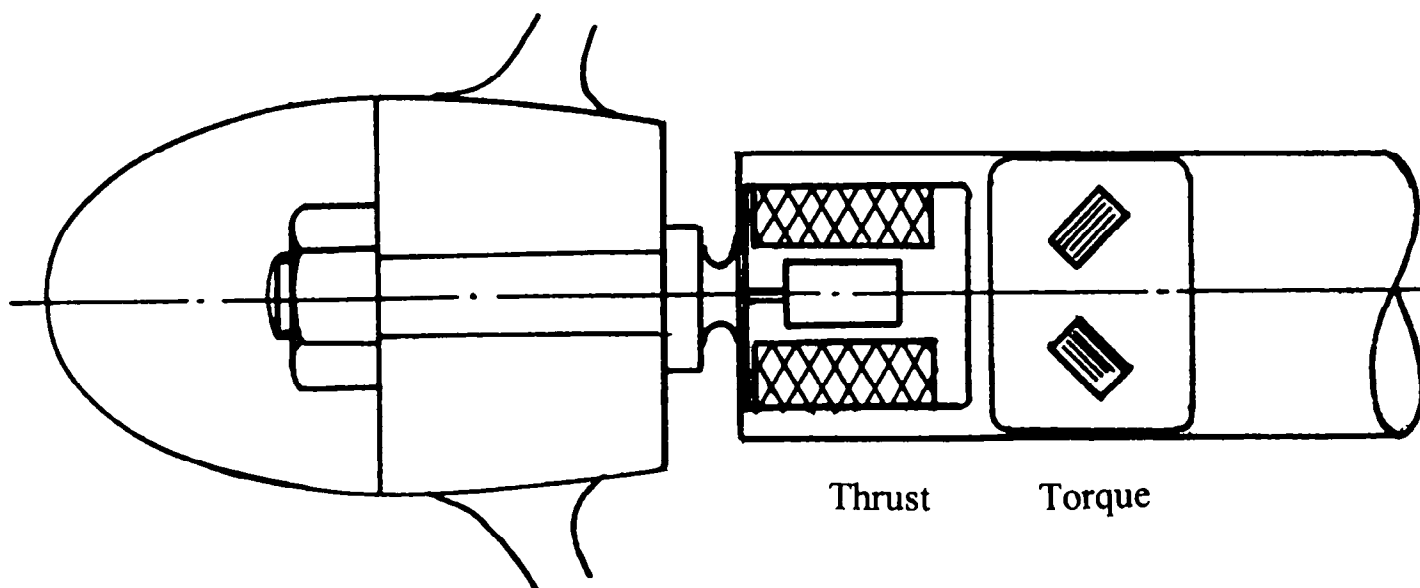




LECTURE NOTES

TMR7

Experimental Methods in Marine Hydrodynamics



Sverre Steen

Revised August 2014

CONTENTS

1	INTRODUCTION	3
1.1	Background	3
1.2	Why model tests	4
2	GENERAL MODELLING LAWS	6
2.1	Geometrical similarity	6
2.2	Kinematic similarity	6
2.3	Dynamic similarity	7
2.4	Scaling Ratios	10
2.5	Hydroelasticity	11
2.6	Cavitation	13
3	EXPERIMENTAL FACILITIES	14
3.1	Introduction	14
3.2	Towing Tanks	14
3.3	Cavitation Tunnel	18
3.4	Ocean Laboratories	20
3.5	Generation of environment	21
4	INSTRUMENTATION	28
4.1	General description of equipment	28
4.2	Strain and displacement measurements	28
4.3	Position measurements	32
4.4	Accelerations	34
4.5	Pressure Transducers	35
4.6	Velocities	38
4.7	Force measurements - Dynamometers	41
4.8	Wave Measurements	42
4.9	Data Acquisition	44
4.10	Sampling Frequency	48
4.11	Length of Records	50
4.12	Calibration	53
4.13	Zeroing	54
5	PHYSICAL MODELLING	55
5.1	General	55
5.2	Rigid Models	55
5.3	Elastic Models	57
6	CONVENTIONAL SHIP TESTING	61
6.1	General	61
6.2	Towing and propulsion tests in towing tank	61
6.3	Cavitation tunnel tests	65
6.4	Maneuvering tests	67
7	SEAKEEPING TESTING	71
7.1	General	71

7.2	Test Requirement	71
7.3	Test set up	72
7.4	Test Procedure.....	73
7.5	Tank wall effects	75
8	OFFSHORE STRUCTURE TESTING	77
8.1	General	77
8.2	Test Requirements.....	77
8.3	Deep water structures requirements	78
8.4	Test Procedure.....	80
9	REAL TIME HYBRID MODEL TESTING	82
9.1	Testing of floating offshore ships and platforms with mooring and flexible riser systems. ..	83
9.2	Testing of hydrofoil ships.....	83
9.3	Testing of floating offshore wind turbines.	83
9.4	Challenges in hybrid model testing	83
10	ANALYSIS OF MEASURED DATA.....	85
10.1	General	85
10.2	Static tests	85
10.3	Decay test	85
10.4	Regular Wave Test.....	88
10.5	Irregular Wave Test	91
11	FULL SCALE MEASUREMENTS.....	103
11.1	Delivery trials	103
11.2	Ship monitoring systems	110
12	ERROR ANALYSIS	113
12.1	Introduction	113
12.2	Uncertainty analysis	113
12.3	Discussion of Error Sources	119
13	MODEL TESTS VS NUMERICAL CALCULATIONS	127
13.1	General	127
13.2	Model tests for Validation of Numerical Calculations.....	128
14	REFERENCES	130
15	INDEX	132
ANNEX A	Example of Reporting from Model Test	
ANNEX B	Example of Model Test Specification	
ANNEX C	Viscous Surge Damping of Floating Production Vessel Moored at Sea	
ANNEX D	Error Analysis of Experiments. Lecture note by S. Ersdal	
ANNEX E	ITTC standard for powering performance prediction	

1 INTRODUCTION

This compendium has been prepared for the course “Experimental Methods in Marine Hydrodynamics”. Parts of the notes are based on earlier lecture notes within this field; see Huse (1999) and Walderhaug (1983). Extensive revisions of the compendium written by Aarsnes in 2001 were made by Steen in 2004, 2005, and 2006, followed by smaller revisions in 2010 and 2012.

Although the name of this course is “Experimental Methods in Marine Hydrodynamics”, we will mainly be talking about model testing, since most experiments in marine hydrodynamics are made in model scale. Also, model testing involves many interesting issues, like scaling and modelling. Full scale testing is handled as a special case, see chapter 11.

Throughout the text, many references are given to supplementary literature, and it is recommended to consult those for a more in-depth treatment of special topics. A good textbook that covers most of the topics in these lecture notes at an introductory but still more thorough level is the book by Dunn (2005).

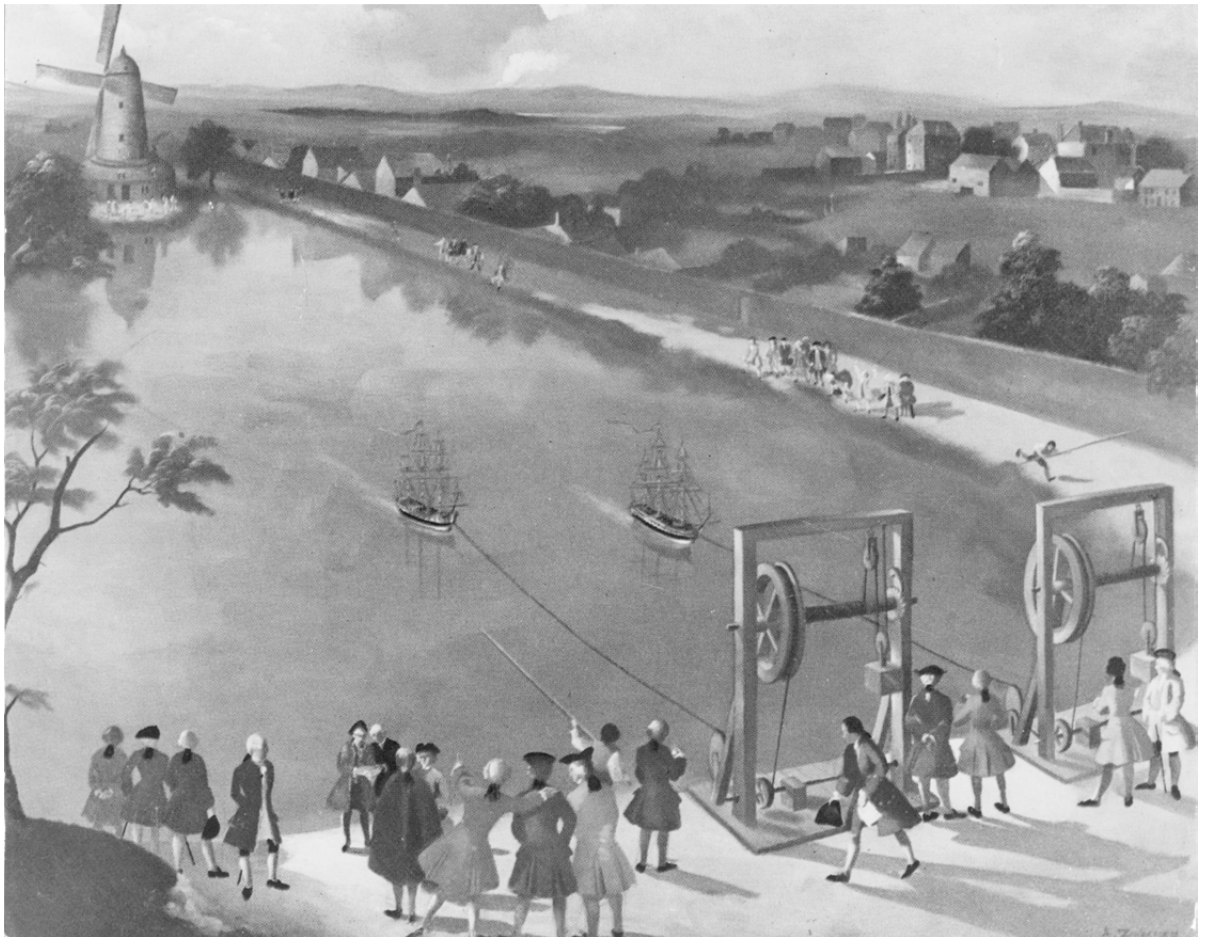


Figure 1.1 Model tests in Peerlesspool in London in 1761

1.1 Background

Experimental facilities for model testing of ships have a long tradition. Improved resistance performance of the ships was early the main driving force behind the development of ship model

testing. It is known that Leonardo da Vinci (about year 1500) carried out tests with 3 models of ships, all with equal length, but with different fore and aft shape. Based on his experiments he was able to give recommendation about which shape gives the highest speed. Later Samuel Fortey (1622-1651) also did tests with ship models and in 1721 Emanuel Swedenborg gave a detailed proposal for ship model testing introducing the principle with falling weight for towing of the models. In this way he was able to achieve a known and constant towing force. In 1761 this principle was used in Peerlesspool in London as shown on the picture given in Figure 1.1. At that time no scaling laws were available to predict full scale behaviour and one had to assume that the winner was the best also in full scale.

William Froude (1810-1879) is often given the honour for the method of really using model testing for ship design by the development of a method for scaling from model resistance to the actual ship resistance. This may be right, but several other works from the same time also contribute significantly to this development. The establishing of the scaling methods should therefore more be regarded as a result of the increasing interest and activities within this field.

Froudes towing tank was built in South England in ca 1870 and is regarded as the beginning of modern model testing. The main dimension of the tank was $L \times B \times d = 85 \text{ m} \times 11 \text{ m} \times 3 \text{ m}$. It was equipped with a rail in the roof, which carried the dynamometers. Maximum speed was 5 m/s. Shortly after this tank was established, several other tanks were built in England, Germany and elsewhere. The towing tank in Trondheim was completed in 1939 with dimension $L \times B \times d = 170 \text{ m} \times 10.5 \text{ m} \times 5 \text{ m}$, which was a normal tank size at that time.

Later, the development within ship technology has initiated development and building of specialised facilities as cavitation tunnels, manoeuvring and sea keeping basins. During the last 20-25 years the needs from the offshore industry have pushed this development even further, and complex laboratories with the possibility of testing structures in realistic conditions including wind, current as well as multidirectional waves, have been built. An example of this type of laboratory is the Ocean Basin at MARINTEK.

Different types of facilities are described in more details in chapter 3.

A further description and review of the history and development of ship model testing can be found in SNAME (1967) and in Stoot (1959)

1.2 Why model tests

Hydrodynamic model testing will basically have three different aims:

1. To achieve relevant design data to verify performance of actual concepts for ships and other marine structures
2. Verification and calibration of theoretical methods and numerical codes
3. To obtain a better understanding of physical problems.

All the aims can be associated to the often very complicated nature of problems connected to the interaction between fixed and floating structures and the marine environment.

Aim 1 is specially the case if the analysis is very complicated for which verified numerical tools are not available. Model test can be used to investigate effects of simplifications used as basis for

analytical or numerical models. In this way model test results can be used to assist development of more reliable numerical tools.

2 GENERAL MODELLING LAWS

Physical models are intended to represent the full-scale system as close as possible at a (much) smaller scale. To be able to determine the proper properties of the model we need modelling or scaling laws that ensure a similar behaviour in model and full scale.

Dimensional analysis can be used to derive a group of meaningful dimensionless quantities for applicable variables. This is particularly useful if the problem is complex. Typically all the various quantities assumed to be of importance for a certain phenomena is listed. A functional relationship between the different parameter groups is then established for all flow governing quantities. The scaling laws are obtained by taking the ratio of the different forces. A detailed description of dimensional analysis can be found in Taylor (1974). A derivation of the most common dimensionless variables used in fluid dynamics, using Buckingham's Pi-theorem is found in chapter 5 of White (2005).

To achieve similarity in forces between the model scale and full scale situation the following conditions must be fulfilled:

- Geometrical similarity
- Kinematic similarity
- Dynamic similarity

In the following these requirements will be discussed. A more comprehensive discussion about model laws is given by Chakrabarti (1998)

2.1 Geometrical similarity

Geometrical similar structures in model and full scale have the same shape. This means that a constant length scale between them exist:

$$\lambda = L_F / L_M$$

where L_M and L_F are any dimensions of the model/full scale structure. The requirement to equal length ratio for all dimensions does not apply only to the structures, but also to the surrounding environment. At the first view this seems to be an easy requirement to satisfy for practical testing. However this need not be the actual situation. For example the actual surface roughness of a ship cannot be accurately modelled. Another example is the almost unrestricted extent of the surrounding water for a sailing ship (except for water depth in some cases). This situation is not possible to reproduce in model scale, which implies that physical boundaries always present in model testing can influence the test results.

2.2 Kinematic similarity

The ratios between velocities in model scale have to be equal to the corresponding ratios in full scale. This implies that flow will undergo the geometrical similar motions in both cases. As an example the ratio between the forward speed of a ship and the rotational speed of the propeller has to be the same:

$$\frac{V_F}{n_F(2\pi R_F)} = \frac{V_M}{n_M(2\pi R_M)}$$

or

$$\frac{V_F}{n_F D_F} = \frac{V_M}{n_M D_M} \Rightarrow J_F = J_M$$

where V is the ship speed, n is the rate of revolution of the propeller, R is the propeller radius, D is the propeller diameter and J is the advance coefficient.

2.3 Dynamic similarity

2.3.1 Forces

Dynamic similarity is achieved if we have the same ratio at model scale and full scale for the different force contributions present in the problem. In principle the following force contributions will be of importance:

1. Inertia Forces, F_i
2. Viscous forces, F_v
3. Gravitational forces, F_g
4. Pressure forces, F_p
5. Elastic forces in the fluid, F_e .
6. Surface forces, F_s .

In addition, for elastic models the elastic relative deformations must be identical in model and full scale.

We will use the following different physical quantities to characterise the different force contributions; physical length; L , velocity; U , fluid density; ρ , gravitational acceleration; g , and the fluid viscosity coefficient; μ . The following dependence of the physical parameters L , U , ρ , g and μ will exist for the different force contributions:

Inertia Forces:
$$F_i \propto \rho \frac{dU}{dt} L^3 = \rho \frac{dU}{dx} \frac{dx}{dt} L^3 = \rho U^2 L^2$$

Viscous Forces:
$$F_v \propto \mu \frac{dU}{dx} L^2 = \mu U L$$

Gravitational Forces:
$$F_g \propto \rho g L^3$$

Pressure Forces:
$$F_p \propto p L^2$$

Elastic fluid Forces:
$$F_e \propto \varepsilon_v E_v L^2$$

Surface Forces:
$$F_s \propto \sigma L$$

where ε_v is the relative elongation (compression), E_v is the volume elasticity and σ is the surface tension.

2.3.2 Froude Number

The dynamic similarity requirement applied on the ratio between inertia and gravity forces gives the following relation:

$$\frac{F_i}{F_g} \propto \frac{\rho U^2 L^2}{\rho g L^3} = \frac{U^2}{gL}$$

Applied on model and full scale this requirement gives:

$$\begin{aligned} \frac{U_M^2}{gL_M} &= \frac{U_F^2}{gL_F} \\ \frac{U_M}{\sqrt{gL_M}} &= \frac{U_F}{\sqrt{gL_F}} = F_N \end{aligned}$$

where F_N is the Froude number. Geometrical and kinematic similarity, and equality in Froude number in model and full scale will therefore ensure similarity between inertia and gravity forces. Since surface waves are gravity waves, this implies that equality in Froude number should give equality in wave resistance coefficient.

2.3.3 Reynolds Number

Equal ratio between inertia and viscous forces will give:

$$\frac{F_i}{F_v} \propto \frac{\rho U^2 L^2}{\mu UL} = \frac{\rho UL}{\mu} = \frac{UL}{\nu} = Re$$

where Re is the Reynolds number and $\nu = \mu/\rho$ is the kinematic viscosity. Equality in Reynolds number between full scale and model scale will therefore ensure that the viscous forces are correctly scaled.

2.3.4 Mach's number

The elasticity of water will influence the pressure transmission in water and will therefore be important for some type of model testing. Equal ratio between inertia and elastic forces gives:

$$\frac{F_i}{F_e} \propto \frac{\rho U^2 L^2}{\varepsilon_v E_v L^2}$$

Using the geometrical similarity requirement that ε_v are equal in model and full scale this requirement gives:

$$\begin{aligned} \left(\frac{\rho U^2 L^2}{\varepsilon_v E_v L^2} \right)_M &= \left(\frac{\rho U^2 L^2}{\varepsilon_v E_v L^2} \right)_F \\ \frac{U_M}{\sqrt{E_{v,M}/\rho}} &= \frac{U_F}{\sqrt{E_{v,F}/\rho}} = M_n \end{aligned}$$

where M_n is the Mach number and $\sqrt{E_v/\rho}$ is the speed of sound in water.

2.3.5 Webers number

The ratio between inertia and surface tension forces is given from:

$$\frac{F_i}{F_s} \propto \frac{\rho U^2 L^2}{\sigma L} = \frac{\rho U^2 L}{\sigma}$$

Similarity requirement for this force ratio in model and full scale will now give the following requirement:

$$\left(\frac{\rho U^2 L}{\sigma} \right)_M = \left(\frac{\rho U^2 L}{\sigma} \right)_F$$

which gives:

$$\frac{U_M}{\sqrt{\sigma_M/(\rho L)_M}} = \frac{U_F}{\sqrt{\sigma_F/(\rho L)_F}} = W_n$$

where W_n is the Weber's number

2.4 Scaling Ratios

The following dimensionless quantities are commonly used for testing of ship and offshore structures:

Symbol	Dimensionless Number	Force Ratio	Definition
Re	Reynolds Number	Inertia/Viscous	$\frac{UL}{\nu}$
F_N	Froude Number	Inertia/Gravity	$\frac{U}{\sqrt{gL}}$
M_n	Mach's Number	Inertia/Elasticity	$\frac{U}{\sqrt{E_v/\rho}}$
W_n	Weber's Number	Inertia/Surface tension	$\frac{U}{\sqrt{\sigma/\rho L}}$
St	Strouhall number	-	$\frac{f_v D}{U}$
KC	Keulegan-Carpenter Number	Drag/Inertia	$\frac{U_A T}{D}$

The Strouhal Number is not derived from a force ratio. f_v is the vortex shedding frequency and St is the non-dimensional vortex shedding frequency, which again determine the oscillation frequency of the transverse lift forces acting on a cylinder with cross dimension D .

The Keulegan-Carpenter Number is determined from force ratio between drag and inertia forces for the case with oscillating flow past a cylinder. T is the period of oscillation and U_A is the velocity amplitude. Equal KC in model and full scale is for example achieved if the same ratio between wave height and cylinder diameter is used.

In practical testing it will not be possible to satisfy simultaneously the different scaling laws. For example ships and offshore structures are for most practical situation influenced by surface wave effects, either from incoming waves or wave generated by the forward speed or motions of the structure. Gravitational forces will govern the surface wave formation. This implies that for these conditions equality in Froude number in model and full scale must be achieved. If viscous forces are important for the actual situation, the requirement of equality in Reynolds number should in principle also be satisfied. This is not possible to achieve. The viscous forces will not be correctly scaled and in the scaling process from model to full scale this effect has to be evaluated.

Other practical limitations for achieving equality in Re are model size and necessary model speed. The requirement of constant UL (assuming ν constant) will for most cases be impossible to achieve.

In conventional model testing of ships and offshore structures, physical scaling and test execution are most commonly carried out based on Froude Scaling. The effect of different Reynolds number is accounted for by different scaling procedures. A typical example is ship resistance tests, where scaling methods for correcting for effect of different Reynolds number is well established. For other applications no established method exists for accounting for the effect of Reynolds number. This will be discussed in more details in chapter 12.2.

Assuming Froude scaling is applied and geometrical similarity with scale ratio $\lambda = L_F / L_M$, from the equality in Froude number we have:

$$\frac{U_M}{\sqrt{gL_M}} = \frac{U_F}{\sqrt{gL_F}}$$

$$\Downarrow$$

$$U_F = U_M \sqrt{\frac{L_F}{L_M}} = U_M \sqrt{\lambda}$$

The other physical parameters can now be derived from the dimensional analysis's follows:

Structural mass: $M_F = \frac{\rho_F}{\rho_M} \lambda^3 M_M$

Force: $F_F = \frac{\rho_F}{\rho_M} \lambda^3 F_M$

Moment: $M_F = \frac{\rho_F}{\rho_M} \lambda^4 M_M$

Acceleration: $a_F = a_M$

Time: $t_F = \sqrt{\lambda} t_M$

Pressure: $p_F = \frac{\rho_F}{\rho_M} \lambda p_M$

The ratio ρ_F / ρ_M is included to account for possible difference in fluid density between full scale and model scale (usually sea water in full scale relative to fresh water in the test tank).

2.5 Hydroelasticity

In hydroelastic problems the hydrodynamic forces are influenced by the elastic deformation of the structure. This deformation is governed by the inertia forces and elastic forces in the structure. The modelling of the elastic properties of structures will therefore give several additional problems compared to the modelling of wave induced dynamic response of rigid structures. Examples where correctly scaled elastic behaviour of the model will be important is springing and whipping of ships, and dynamic behaviour of marine risers and mooring lines.

Additional requirements to the elastic model can be summarised as follows:

- Correctly scaled global structural stiffness
- Structural damping must be similar to full scale values
- The mass distribution must be similar.

Geometrical similarity between model and full scale for an elastic structure will require that the elastic deformations are similar. To illustrate this we will consider the deflection of a cantilever beam as an example. The deflection, δ , is given from:

$$\delta \propto \frac{FL^3}{EI}$$

where EI is the flexural rigidity and F is the hydrodynamic force which can be expressed as:

$$F \propto C\rho U^2 L^2$$

where C is a force coefficient dependent on F_N , Re etc. The requirement of similarity in deformation in model and full scale gives:

$$\frac{\delta_F}{L_F} = \frac{\delta_M}{L_M} \Rightarrow \delta_F = \lambda \delta_M$$

Using the above equations this requirement is satisfied if the ratio:

$$\frac{C\rho U^2 L^4}{EI}$$

is equal in model and full scale. Assuming equal force coefficient and density we obtain the following requirement to the structural rigidity:

$$\left(\frac{U^2 L^4}{EI} \right)_F = \left(\frac{U^2 L^4}{EI} \right)_M \Rightarrow (EI)_F = (EI)_M \lambda^5$$

If all dimensions of the cross sectional shape of the beam are scaled geometrical similar, the moment of inertia, I , will satisfy the relation:

$$I_F = I_M \lambda^4$$

We are then left the following requirement to the Young's modulus, E :

$$E_F = E_M \lambda$$

This implies that the Young's modulus for the model must be $1/\lambda$ times the value of the full scale structure.

It should be noted that the two last equations is not to be regarded as requirements to the model. The bending stiffness requirement is given for EI . In practical model testing the requirement given to scaling of EI is often satisfied by manipulating the different parameters by applying other materials, other wall thickness, or by modifying the structural build-up of the beam. The outer geometry, which is exposed to the hydrodynamic forces, has to be modeled geometrically correct. Also the requirement to correct modeling of mass distribution and structural damping has to be satisfied. This will be further discussed as part of the physical modeling, see chapter 5.3.

Similar results will be found for the axial and torsion stiffnesses. The requirement for the axial stiffness case is:

$$(EA)_F = (EA)_M \lambda^3$$

where EA is the axial stiffness. This relation gives equal strain in model and full scale. The cross sectional area, A , will satisfy the relation $A_F = A_M \lambda^2$, which gives the same requirement to the Young's modulus as shown above.

2.6 Cavitation

If cavitation occurs, dynamic similarity also requires that the law of equal cavitation number is accounted for in the experiments. The requirement is that the cavitation number given as:

$$\sigma = \frac{(\rho gh + p_0) - p_v}{1/2 \rho U^2}$$

has to be the same for the model as in full scale. p_0 is the atmospheric pressure, ρgh is the hydrostatic pressure and p_v is the vapour pressure. To satisfy this requirement a cavitation tunnel, with possibility to lower the atmospheric pressure has to be applied.

3 EXPERIMENTAL FACILITIES

3.1 Introduction

The different type of experimental facilities used for ships and offshore structures can be categorized as follows:

- Towing tanks, conventional and facilities tailor made for specific purposes.
- Cavitation tunnels
- Ocean basins

Usually we will find two or more different type of tests facilities at each research and testing institution. For example at MARINTEK there is three towing tanks, a cavitation tunnel and an ocean basin. In Figure 3.1 an overview of the test facilities at MARINTEK is presented.

The experimental facilities for testing of ship and offshore structures are not only the physical tank/basin where the tests are executed. The testing facilities have also to cover different additional functions as workshops for construction and building of models, instrumentation, simulation of environment and software and tools to record and analyze the measured data. A typical lay out of a towing tank, including utility functions, is shown in Figure 3.2. For testing of realistic behavior of structures in a seaway, equipment for generation of wind, waves and current and efficient wave absorption are of vital importance.

3.2 Towing Tanks

The first towing tanks were built for performing towing and propulsion tests. The length of the towing tank has to be long enough to get a sufficient long time with steady flow conditions for measurements of towing and propulsion forces. The required size will therefore be dependent on type of ships to be tested, scale ratio and forward speed. Today a large number of towing tanks exist, more than 200 are in regular use. The length of the towing tanks is from 20 m to more than 1000 m.

The small tanks are typically connected to teaching and research institutions. The very long tanks are mainly connected to naval activities. An example is the high speed tank at David Taylor Naval Ship Research and Development Centre with dimensions 900m x 6.4m x 3m with a maximum towing carriage speed of up to 50 m/s. This tank was built especially for testing of high-speed ships. The construction of this tank was a direct result of the requirements: "Navy in 50 kn", defined in about 1960 as a target for the US Navy. A similar facility also exists in St. Petersburg.

A typical size for commercial working towing tanks is $L \times B \times d = 250\text{m} \times 10\text{m} \times 5\text{m}$. Typical ship model length is 5-8 m. This size of facilities seems to represent a reasonable compromise between cost for tank construction, cost for model manufacture and operational costs (which together determine the cost of model testing) and the required scale ratio and corresponding accuracy that can be achieved. The size of the large hydrodynamic laboratories at the Marine Technology Centre is shown in Figure 3.1, with more details about the towing tanks given in Figure 3.3.

Almost all towing tanks use a towing carriage to move the model through the water. A typical towing carriage design is shown in Figure 3.3. The typical max carriage speed is 10 m/s. During calm water towing and propulsion the model is kept fixed in surge sway and yaw, but free to heave and pitch.

Ocean basin data:

Length: 80 m
 Width: 50 m
 Depth: 0-10 m

Maximum Current velocity: 0.2 m/s

Wave maker 1

Hydraulic driven, hinged double-flap type

Wave characteristics:

Regular waves:

Max height: 0.9 m
 Wave periods: 0.8 s and above

Wave spectra:

Max Hs=0.5 m

Wave maker 2

Electrically driven, hinged single-flap type
 144 individually controlled flaps

Wave characteristics:

Regular waves:

Max height 0.4 m
 Wave periods: 0.6 s and above

Wave spectra:

Max Hs=0.3 m

HP CODA data acquisition system
 6 DoF optical position measurement

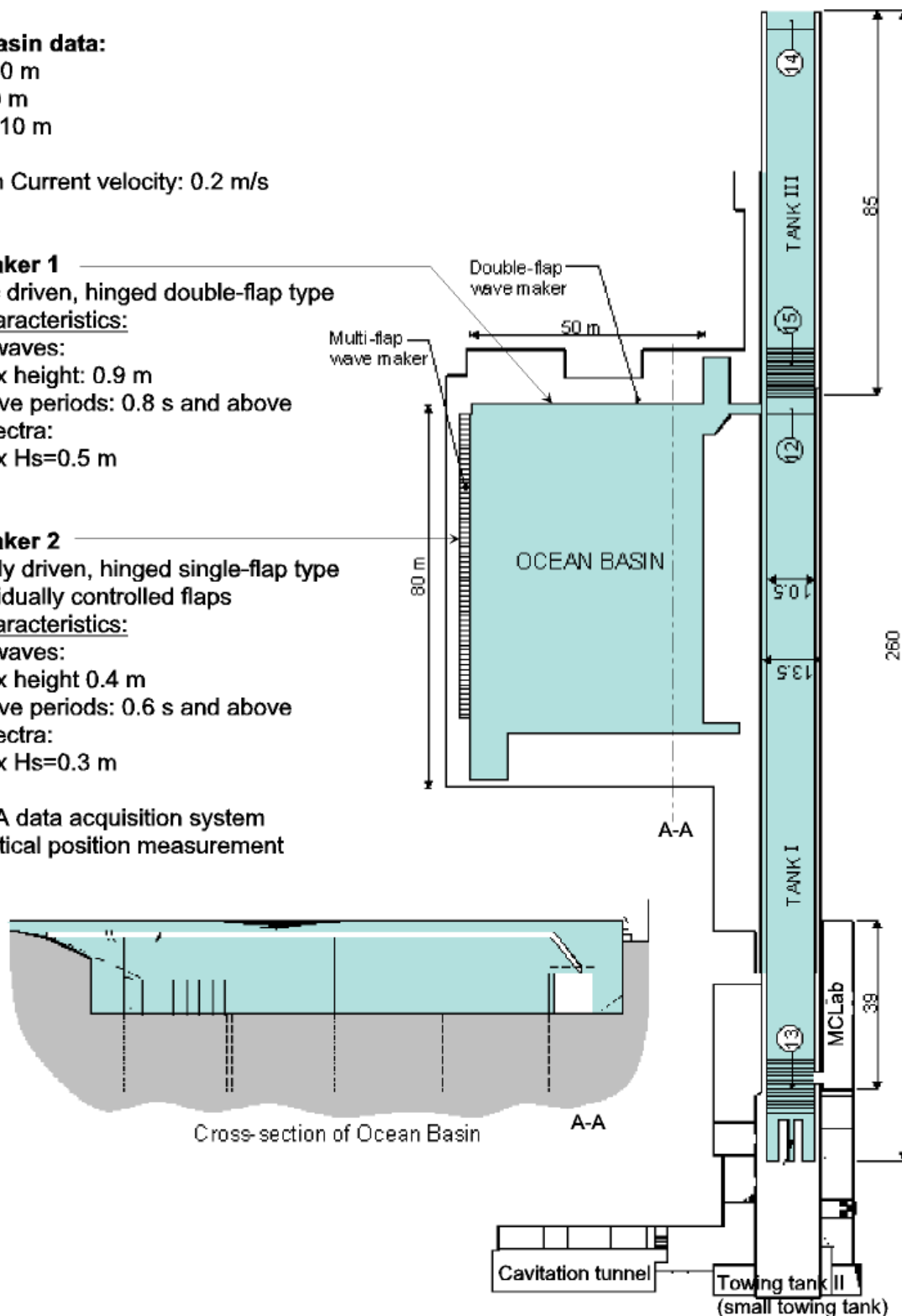


Figure 3.1 Overview of test facilities at MARINTEK

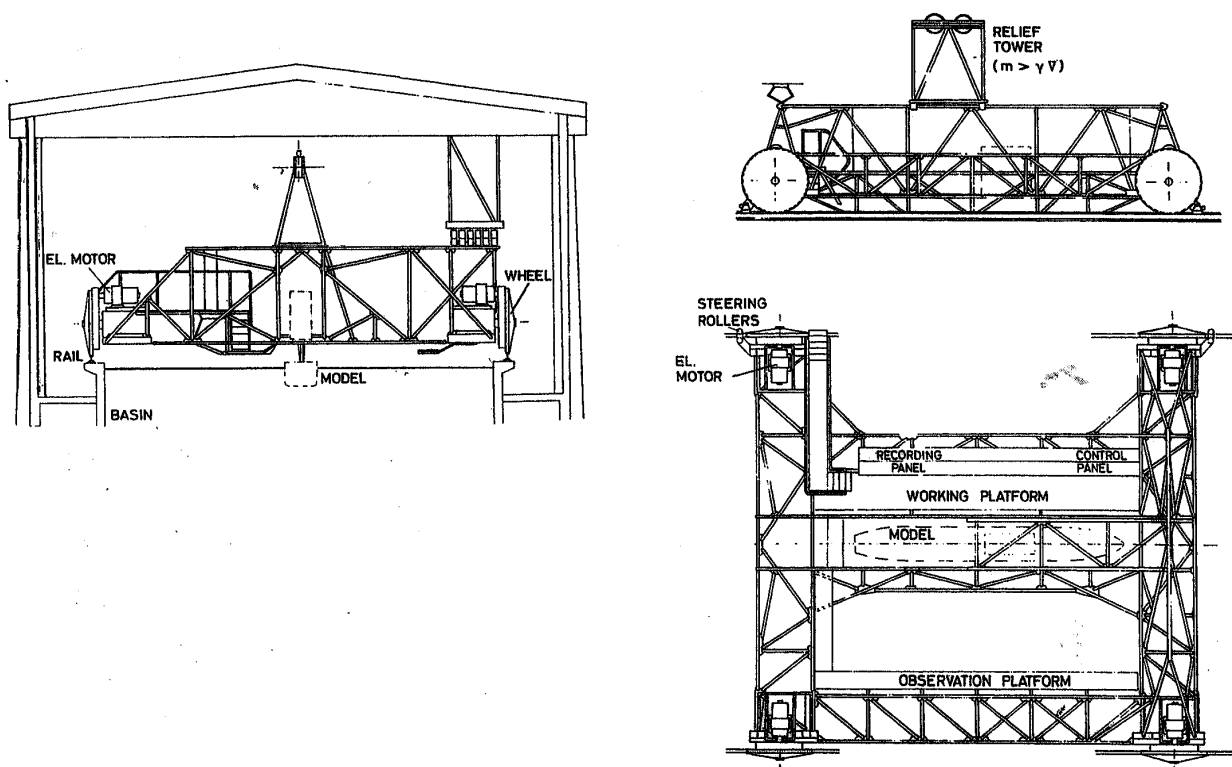


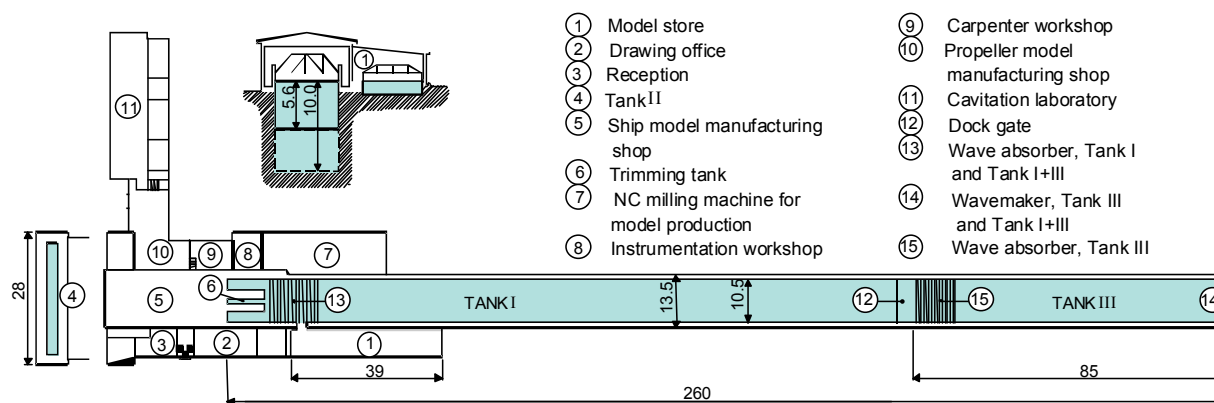
Figure 3.2 A typical towing carriage design.

To be able to perform seakeeping tests or other type of testing in surface waves, many towing tanks are equipped with a wave maker at one end of the tank. Generation of waves and type of wave generators are discussed in more details in chapter 3.5.1. In order to prevent reflections of waves from the opposite side, a wave beach, which is absorbing the wave energy, has to be installed at this side of the towing tank.

It has also been constructed towing tanks that are highly specialised for a given purpose. An example is the Dutch and Chinese vacuum tanks, where the entire space above the tank is evacuated and air pressure down to 0.04 bar can be achieved. The purpose of this type of facility is to do propulsion tests with surface effects and complete ship model present, at the low pressure required for equality in cavitation number.

Another example of a specialised tank is the ice tanks in Hamburg and Helsinki. Ice is modelled by freezing, using high salinity water and chemicals to control the mechanical properties of the ice. These tanks are used for testing of icebreakers and offshore structures exposed to the action of drifting ice.

The towing tank at MARINTEK was completed in 1939 with dimensions 170 x 10.5 x 5 m. Later, in 1978, extended to 260 m where the depth of the extension is 10.0m. The layout of the towing tank is shown in Figure 3.4. The towing carriage is of conventional type. For testing of high-speed vessels the carriage is equipped with a "Free to Surge" rig. The 8 m long rig is mounted in front of the towing carriage as shown in Figure 3.4. Using this rig the wind disturbance at the position of the model is eliminated and the model is allowed to freely surge, heave and pitch during wave testing.



Towing tank data

	Tank I	Tank II	Tank III	Tank I+III*
Length:	175 m	25 m	85 m	260 m
Width:	10.5 m	2.8 m	10.5 m	10.5 m
Depth:	5.6 m	1.0 m	10 m	5.6/10.0 m
Tot. weight carriage:	20 tons	0.2 ton	15 tons	20/15 tons
Wheelbase:	11.04 m	3 m	11.04 m	11.04 m
Speed range:	0.02-10 m/s	0.05-1.75 m/s	0-0.9 m/s	0.02-10 m/s
Max. acceleration:	1 m/s ²	1 m/s ²	1 m/s ²	1 m/s ²
Model size range:	8 m	1 m	-	8 m
Wave maker:		Single flap Regular and irregular waves	Double flap Regular and irregular waves	Double flap Regular and irregular waves
Max. wave height:		0.3 m	0.9 m	0.9 m
Wave period range:		0.25-3 sec.	0.8-5 sec.	0.8-5 sec.
Max. wave steepness:		1:8	1:10	1:10
Wave spectra:		Computer generated		

* Tank I and III can be used separately and also as one long tank (Tank I + III) by removing the gate (12) and wave absorber (15). In Tank I + III either of the two carriages can be used.

Figure 3.3 Towing Tanks at MARINTEK.

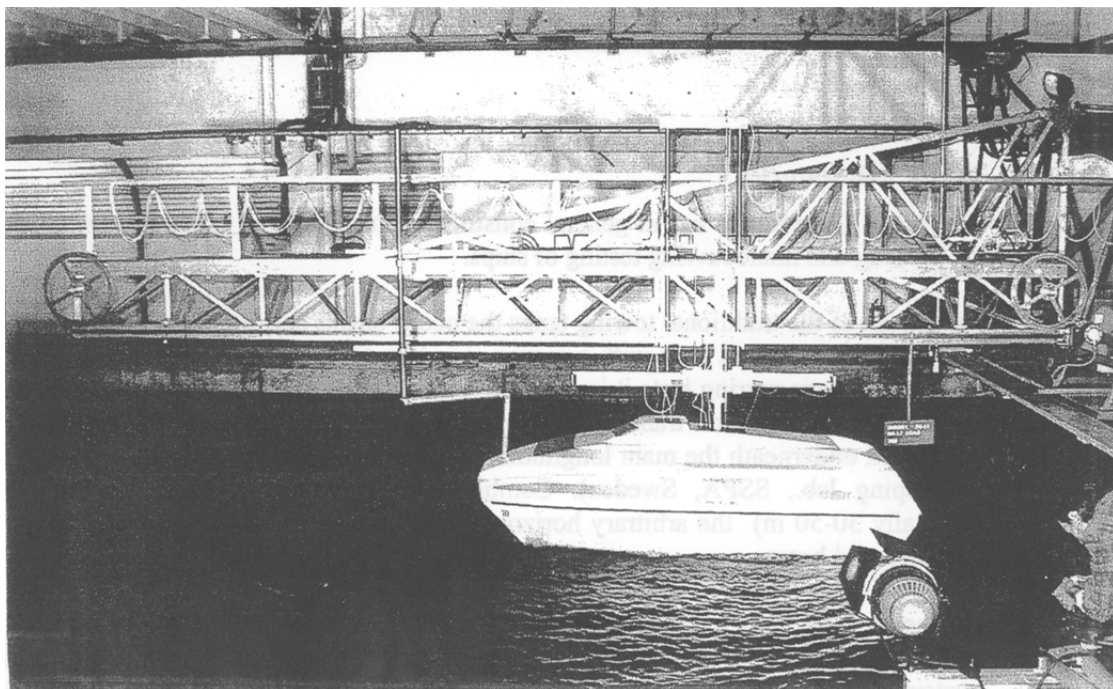


Figure 3.4 “Free to surge” rig in front of towing carriage.

3.3 Cavitation Tunnel

Cavitation tunnels are designed to be able to test propellers and other lifting surfaces at a sufficiently low pressure to achieve correct cavitation number. Most commercial model test institutions have one or more cavitation tunnels, and about 100 tunnels is today in regular use.

A wide range of different size cavitation tunnels exist, from small size tunnels for research and education, with test section area of typically 0.25 x 0.25 m, to very big circulating water tanks, with test section dimension up to 3 x 6 m and length of 11 m (the Berlin tunnel). A typical size conventional tunnel is with circular test section with diameter of about 1 m. Maximum flow speed at measuring section is usually 10-20 m/s. Large tunnels often have test sections allowing for mounting of a complete ship hull model.

For tunnels that cannot allow testing of entire ship hull models, an afterbody model of the ship is often applied to produce correct inflow to the propeller, and mesh screens are used to produce the specified wake distribution. The benefit of using afterbody models and mesh screens, instead of a complete model, is the possibility of having the mesh screen simulate full scale wake, not only model scale wake. When testing the entire ship model, only model scale wake might be tested.

Some cavitation tunnels are of the free surface type. Such tunnels can be used for testing of high-speed propellers operating in full or submerged condition. This type of tunnels is especially well suited for studying ventilation problems for propeller, water jets and foil sections. Large tunnels with free surface enable test with normal ship models.

The cavitation tunnel at MARINTEK is shown in Figure 3.6. The diameter of the working section is 1.2 m and the length of working section is 2.08 m. Maximum water velocity is 18 m/s. The minimum working pressure is 0.1 atm. Afterbody models and mesh screens are applied.

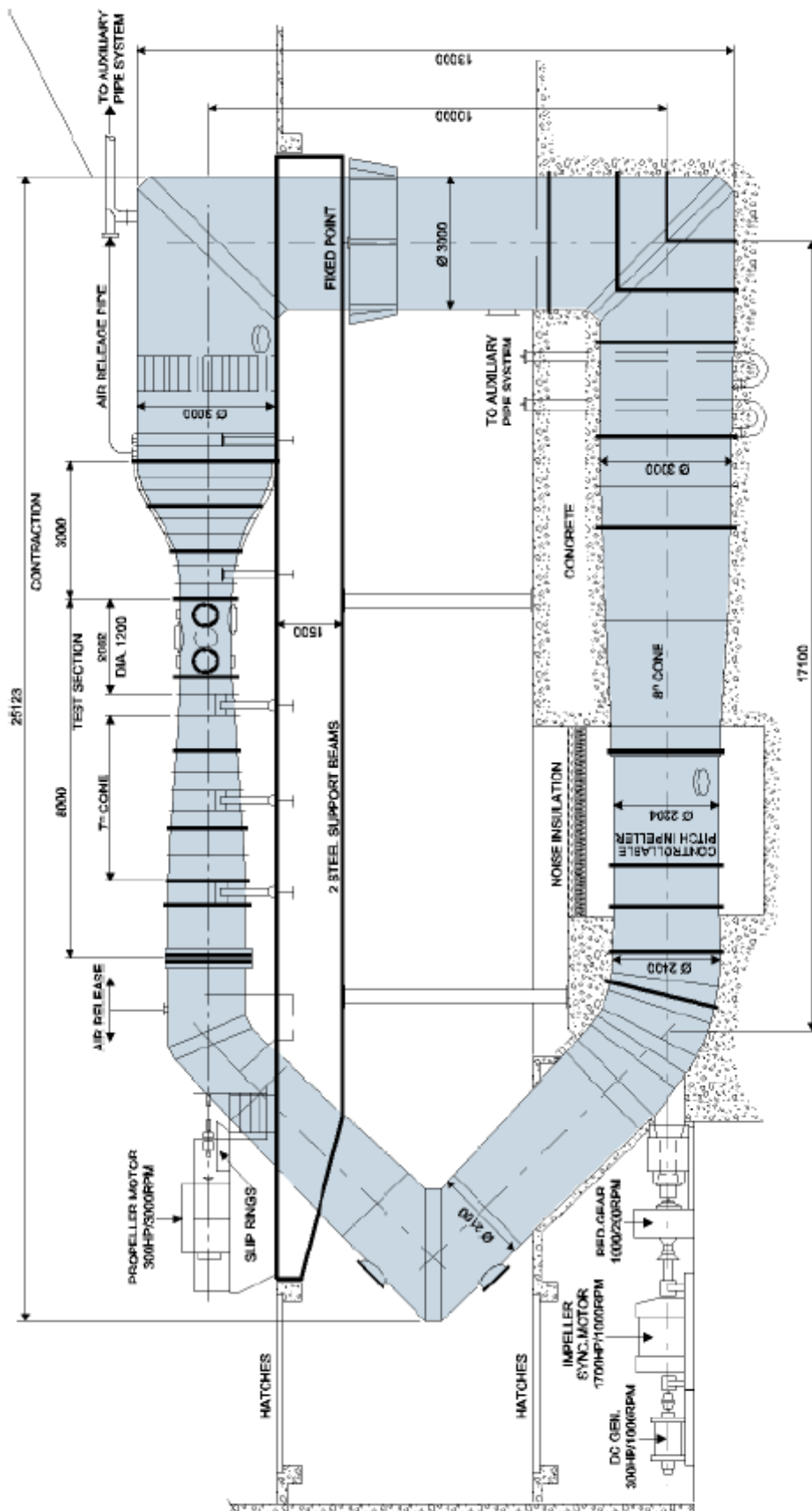


Figure 3.5 Cavitation Tunnel at MARINTEK.

3.4 Ocean Laboratories

The ocean laboratories are in general constructed for testing of offshore structures and for seakeeping and manoeuvring testing of ships.

In contrast to the traditional towing tanks the ocean basins and seakeeping laboratories make it possible to carry out tests with any wave heading (oblique waves) for ships with forward speed. For manoeuvring tests it is required with a towing carriage with controlled motions in both longitudinal and transverse direction. This is achieved by a sub-carriage, which is connected underneath the main longitudinal motion carriage (see Figure 3.7, taken from the seakeeping laboratory at SSPA, Sweden). Combined with the large width of these facilities (typically 30-50 m) the arbitrary horizontal motion requirement tends to make the carriage system complex and heavy.

Basins purpose built for offshore testing is for most cases built after 1980. For offshore testing a large carriage system is not required. Ocean laboratories are usually equipped with advanced systems for generation of waves, often capable of generation of both long-crested and multidirectional (or short-crested) waves as well as wind and current. In this way it is possible to give a realistic representation of the marine environmental conditions.



Figure 3.6 Carriage system in Ocean Basin (from SSPA, Sweden).

Examples of commercial ocean laboratories for testing of coastal and offshore structures are:

MARINTEK, Trondheim;	LxB= 80mx50m, d=0-10 m
MARIN, Netherlands;	LxB= 45mx36m, d=0-10.5m, pit in centre with d=30 m
Hydraulic Lab, Ottawa, Canada:	LxB= 50 m x 30 m, d=3 m
OTRC, Texas A&M:	LxB= 45.7 m x 30.5 m, d=5.8 m, pit with d=16.8 m

Some basins are equipped with a false bottom that can be set to different depths. In this way the actual water depth can be correctly modeled in the test set up. This property also enable mounting of models, mooring system and other subsea equipment on a dry bottom, which after installation of the system to be tested, is lowered down to the wanted water depth. This largely simplifies the preparation work for the test.

The ocean laboratory at MARINTEK is fitted with two sets of wave makers. Along the 50 m side of the basin there is a double-flap wave maker capable of generating long-crested waves. Along the 80 m side there is a multi-flap wave maker consisting of 144 individually controlled flaps for generation of short-crested and long-crested waves. Wave absorption beaches are installed on the two opposite sides to reduce the problems with wave reflections. Current can be modeled in direction along the basin (in wave direction of the double flap wave maker). The water depth is adjustable from 0 m (surface position) to 10 m by moving the false bottom. A more detailed description of the Ocean Laboratory at MARINTEK is given by Huse and Tørum (1981) and Naeser. (1981).

3.5 Generation of environment

Reliable model testing requires controlled generation of wind, waves and current in both time and space to achieve a realistic and well-defined environment. Commonly used equipment for environment generation is described in the following.

3.5.1 *Wave generation and absorption*

There are two main classes of wave generators, the horizontal driven flap type wave maker and the vertical driven wedge (plunger) type wave maker. In modern test facilities almost only the flap type is used. Two examples of flap type wave makers are shown in Fig 3.8. The first one is a double flap wave maker as installed in the towing tank and in the ocean basin at MARINTEK. Hydraulic actuators are used. The other is the single flap wave maker as installed in Marine Cybernetic Laboratory (MCLab) at MARINTEK. This wave maker is electrically driven. The rear side of the flap may be either dry or wet. The double flap type is usually used for deeper water. By the possibility of using the upper, the lower or both flaps in combinations for the double flap type, it is possible to generate waves with a minimum of distortion for larger wave length range than what is possible for a single flap solution.

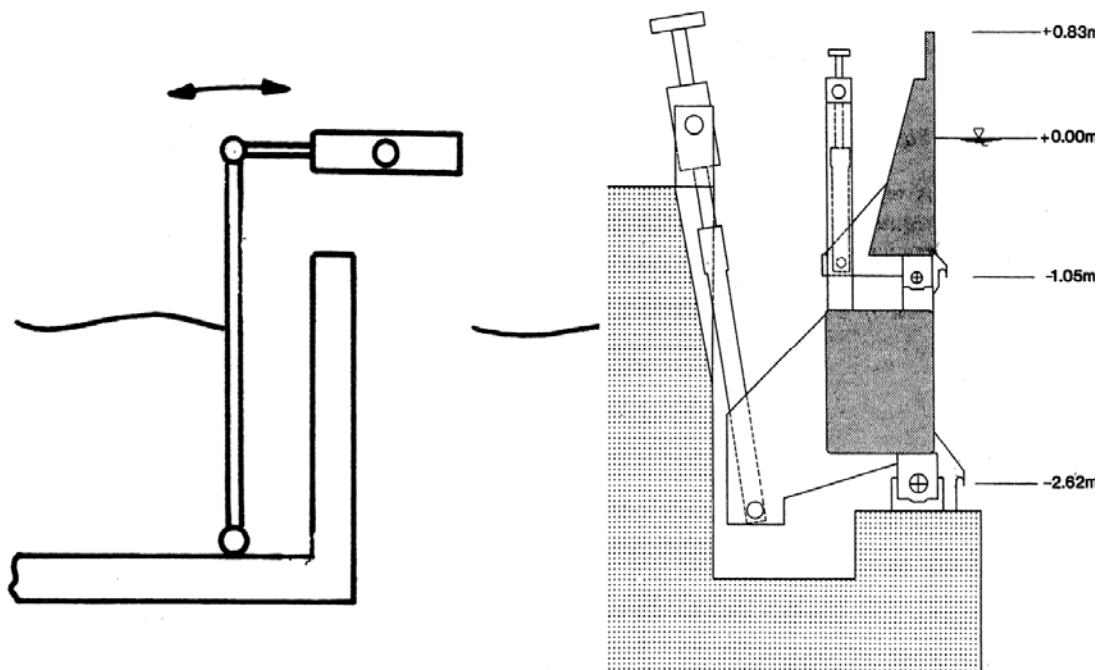


Figure 3.7 Examples of flap type wave maker; single flap and double flap.

Other types of wave makers are piston type (a small sketch is shown in Figure 3.9), and pneumatic wave makers. Pneumatic wave makers use variable air pressure in a chamber above the water at the edge of the basin to create waves. David Taylor Model Basin in Washington DC has a pneumatic wave maker in their ocean basin, except for that the principle is little used, and is considered inferior relative to flap type wave makers.

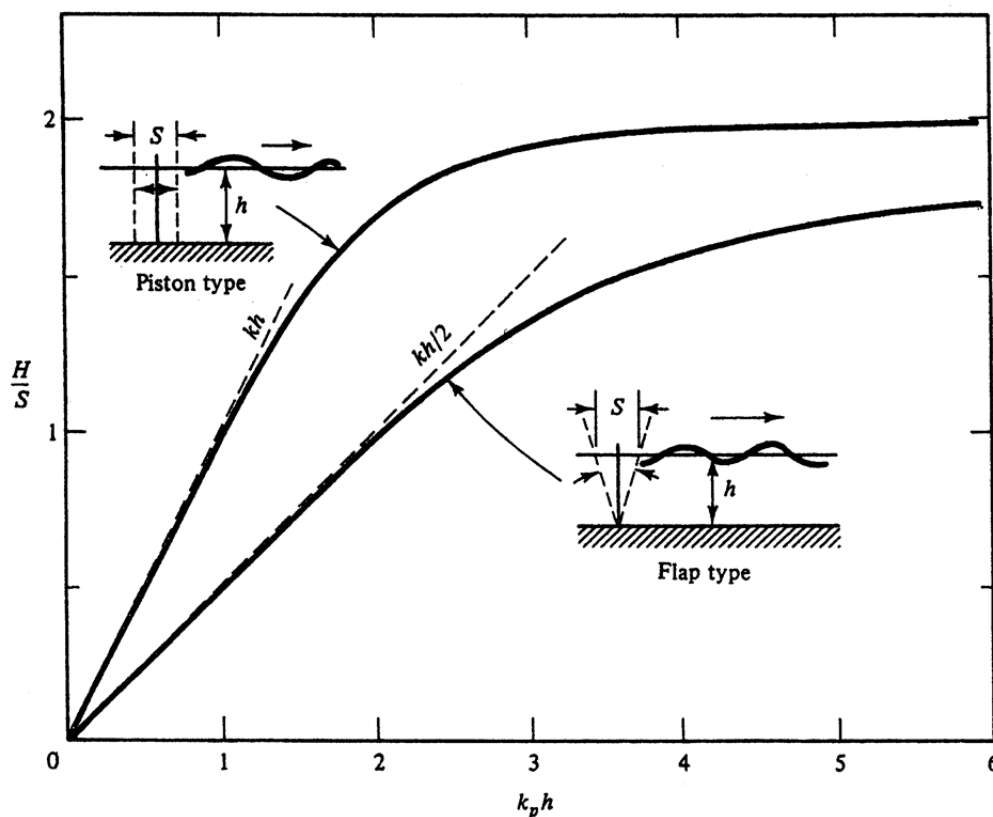


Figure 3.8 Wave-maker theory, Wave height to stroke ratio as function of relative depth.

The generation of waves are controlled by the frequency and amplitude of the flap. In Figure 3.9 the relation between flap stroke, S , and wave height H , is shown for flap type wave maker. The resulting wave height is shown as a function of the parameter kh where $k = 2\pi/\lambda$ is the wave number, λ is the wave length and h is the water depth. The results are based on wave-maker theory see e.g. Dean and Dalrymple (1984). This ratio between the mechanical displacement of the flap to the wave amplitude is the transfer function of the wave maker.

A regular wave elevation can be generated using the transfer function to determine the required control signal to the wave maker. In Figure 3.10 the maximum wave height for regular waves as function of wave period is shown for the double flap wave makers in the towing tank at MARINTEK. It is observed that increasing wave period (and hence wave length), gives decreasing maximum wave height.

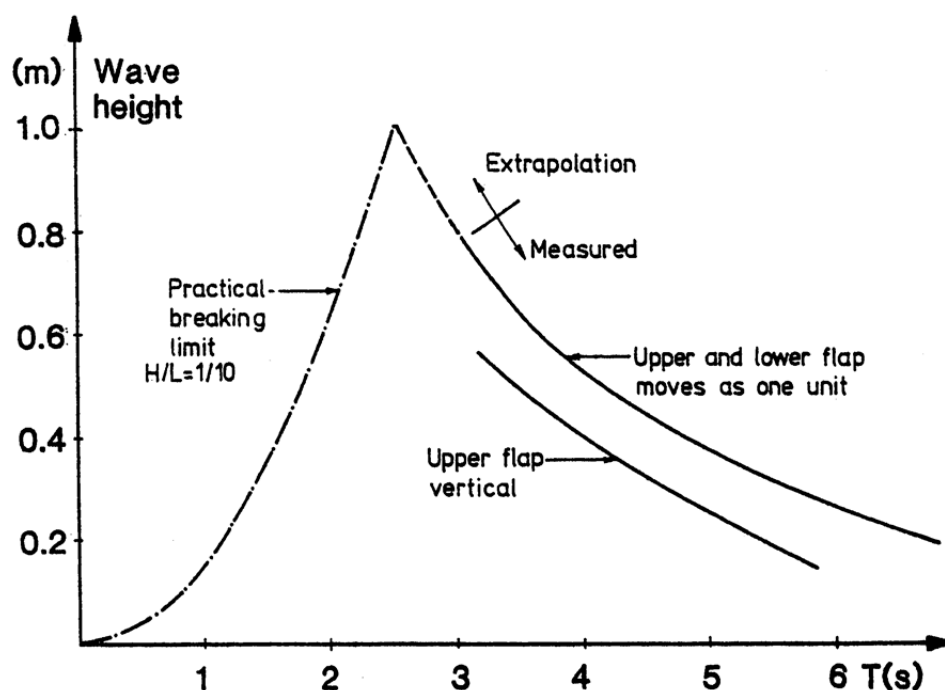


Figure 3.9 Maximum wave height as function of wave period, Double Flap wave maker at MARINTEK

The generation of irregular waves is controlled by an input signal based on the selected wave spectrum combined with the transfer function of the wave maker. The commonly used assumption that the sea surface elevation is a stationary Gaussian process with zero mean is applied. The surface elevation as function of time, $\eta(t)$, can then be represented by a finite number of Fourier components:

$$\eta(t) = \sum_{n=1}^N a_n \cos(\omega_n t + \varepsilon_n)$$

where ε_n is the phase angle of component n created from a random phase generator. Random phase is necessary to eliminate any coherent features developing in the wave signal. a_n is the Fourier amplitude of component n determined from the input wave spectrum density $S(\omega)$ as:

$$a_n = \sqrt{2S(\omega_n)\Delta\omega}$$

$\Delta\omega$ is the frequency interval for each component. It is important with a sufficient number of components in the wave generation to avoid repetition of the wave signal and aliasing, see Newland (1975) for further details. Typically, 2000 components are used.

For most cases the wave spectra are generated according to the JONSWAP formulation:

$$S(\omega) = \alpha g^2 \omega^5 \exp\left[-1.25(\omega/\omega_0)^{-4}\right] \gamma^{\exp\left[(\omega-\omega_0)^2/(2\sigma\omega_0^2)\right]}$$

where:

$$\sigma = 0.07 \text{ for } \omega < \omega_0$$

$$\sigma = 0.09 \text{ for } \omega > \omega_0$$

ω_0 is the spectral peak frequency

γ is the peakedness parameter.

In Figure 3.11 a typical example of theoretical JONSWAP spectrum and measured wave spectrum in the wave tank are shown. The agreement in energy distribution is seen to be very good.

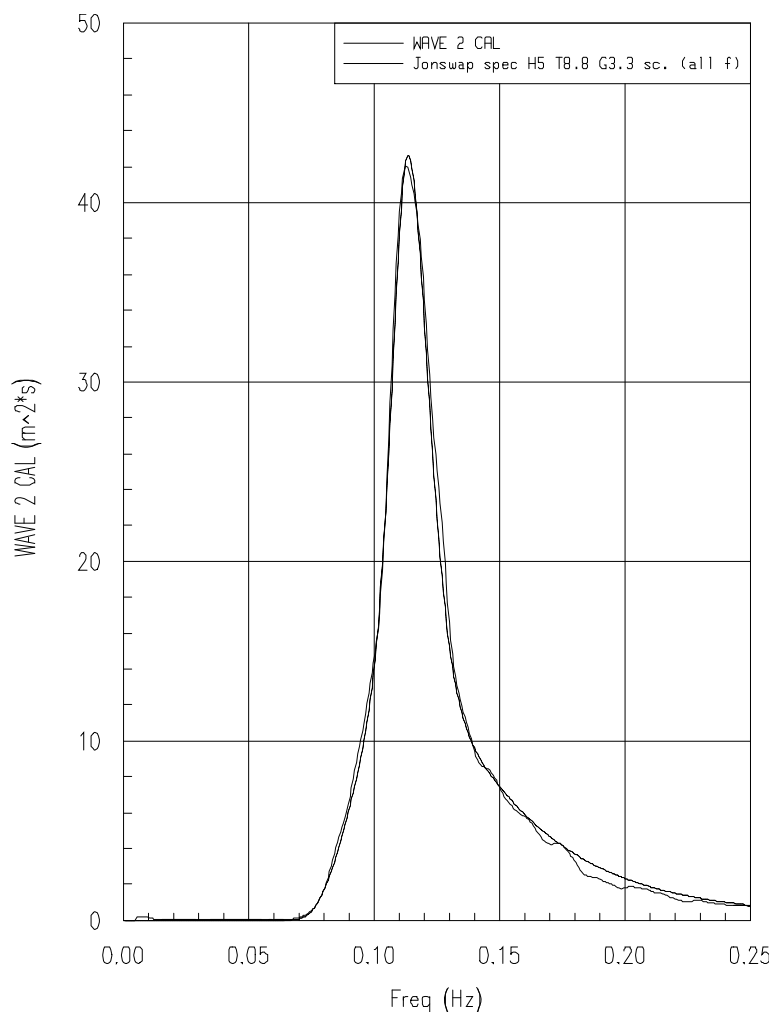


Figure 3.10 Typical example of theoretical JONSWAP spectrum and measured wave spectrum in the wave tank

Multidirectional (or short crested) waves can be generated using an array of flaps along one side of the basin. There are typically about a hundred individual flaps. The multi-flap wave generators can

also be used to generate long crested waves with an arbitrary wave heading. To generate short crested wave the directional spreading function must be specified in addition to the energy density spectrum. This gives the following generalisation for the surface elevation as function of space and time, $\eta(x,y,t)$:

$$\eta(x, y, t) = \sum_{n=1}^N a_n \cos[k_n (x \cos \theta_n + y \sin \theta_n) - \omega_n t + \varepsilon_n]$$

where a_n now is the Fourier amplitude of component n including the spreading function:

$$a_n = \sqrt{2S(\omega_n)D(\omega_n, \theta_n)\Delta\omega\Delta\theta}$$

To avoid reflection and wave building up in the basin, an efficient wave absorption system is also essential. The most used system for wave absorption is wave beaches. An example is shown in Figure 3.12. The shape is parabolic which has been found to be more efficient for a large wave period range compared to a straight beach. Reflected wave height of less than 5 % of the incoming wave height will typically be achieved with this beach design. In ocean basins wave absorbers are usually mounted on the sides without wave makers, typically with two sides with wave makers and two sides with wave absorbers (as in MARINTEK ocean basin).

In towing tanks the main problem will be reflection of the ship generated wave system from the tank walls. It is not practical to mount a beach alongside the tank wall and transverse waves will be generated. For tests with forward speed this is usually not a problem, since the reflected waves will hit the test area after the model has left. For tests with zero or very low forward speed, the problem of wave reflections must be taken very seriously. For long test runs, like is typical for a test in irregular waves, some kind of wave absorption along the tank wall is required.

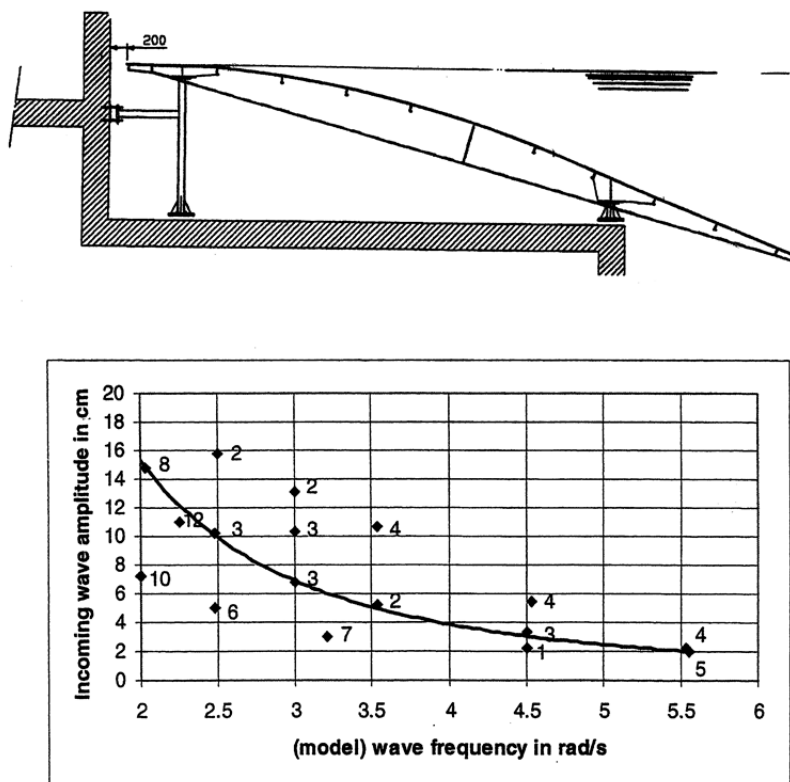


Figure 3.11 Upper; Wave absorber, beach type. Lower; measured wave reflection from beach, in % of incoming wave amplitude.

3.5.2 Wind generation

Wind generation is most connected to stationary model tests in ocean basins. For freely moving models wind is not easily applied in practical testing. The wind in the basin is usually generated by means of a battery of portable electrical fans. The fans are placed some distance from the testing area to achieve a homogeneous wind speed distribution at the position of the test model. The wind direction can be changed by moving the position of the fans.

Two different methods for calibrating the wind speed are commonly used:

1. Froude scaling of wind speed, i.e: $U_{M,Wind} = U_{F,Wind} / \sqrt{\lambda}$
2. Using pre-calculated wind force acting on the model and tuning the model wind speed to this force is achieved.

For the first case the wind speed is calibrated at the position of the model, but without the model present. Using this procedure require a very accurate modelling of the model superstructure to obtain reliable wind forces. The last procedure requires that reliable wind force estimates are available on beforehand. If this is the case the scale effects on wind forces can be avoided. Usually this procedure will give about 20 % higher wind speed than the speed established from Froude scaling law.

The effect of wind will be important for almost all types of moored structures. The wind speed is in general non-steady and the dynamic effects of the winds can be an important excitation source for resonance motions of moored structure and in special cases for roll motions of ships. The dynamic

effect of wind can be simulated in the test by controlling the power to the fans. A frequently used wind energy spectrum for offshore applications is the NPD spectrum.

The frequency range of a wind spectrum is quite broad-banded, often covering a range from 0.005 to 1 Hz.

3.5.3 Current

To simulate current two different approaches are commonly used:

1. Direct generation of current in the basin using pumping of water
2. Towing of the model set up with speed equal to the current speed.

The first approach requires large pumps with re-circulation ducts. For basins with a false bottom (as at MARINTEK) the pumps can re-circulate the water under the false bottom. Also external piping (outside the basin, as used in MCLab at MARINTEK and at Marin in the Netherlands) can be used for recirculation of water.

Local current can be generated by placing portable current generators in front of the model (in principle as for the wind generation). However for this method it is difficult to achieve a reasonable stationary current field at the position of the model due to large eddies of back-flowing water. The effect of current on wave forces will not be realistically accounted for by this procedure due to large space variation in current field between the wave maker and model.

The effect of current is especially important for moored structures, both due to the direct forces due to the current and due to the interaction between current and waves. The interaction between current and waves effect can largely influence the wave drift forces and hence influence mean offset and forces as well as the slow drift motions. For the case with moored structures the simulation of the current effect by towing the model with a speed equal to the current speed is not a practical solution. For this case a basin with direct current generation will be required.

The generation of current speed is based on the Froude scaling law. This is necessary to properly represent the wave-current interaction effects, but it may introduce some scale effects for the current forces due to difference in Re number, resulting in possibly different flow regimes in model and full scale.

Current calibration of speed and profile should be performed without the model in the basin. Velocity fluctuations will always be present in basin-generated current (in real full scale current, fluctuations will also be observed). Large fluctuations in current may represent an excitation source for slowly varying resonance oscillations and the magnitude should therefore be as low as possible. A standard deviation for the current fluctuation of about 5% of mean current is typically achieved in basins with closed re-circulation solutions. Correct modelling of the current fluctuations might be important for the dynamics of deepwater systems, but we still not know enough about this, and no model testing facilities currently have possibilities to create controlled current fluctuations.

4 INSTRUMENTATION

4.1 General description of equipment

A large range of different type of measuring equipment is used for testing of ships and offshore structures. Usually, instruments are designed to generate an analog voltage or current signal which is linearly proportional to the measured parameter. Non-linear characteristics occur in rare cases. Instruments with digital output are increasingly used, but analog output is still preferred, in order to avoid the complexities of dealing with different digital signal protocols.

The system required for performing measurements includes the following components:

- The transducers
- Amplifiers
- Filters (analog and/or digital)
- AD converter
- Data storage unit
- Cabling between the different components

A typical set up is shown in Figure 4.1. It is common practice to use two or more independent computer systems for operating the tank facility. One machine is used for real time generation of control signal for the wave maker and an additional machine is used for the data acquisition and analysis. Additional machines might be used for control of rudders or other control devices, or for control of the carriage.

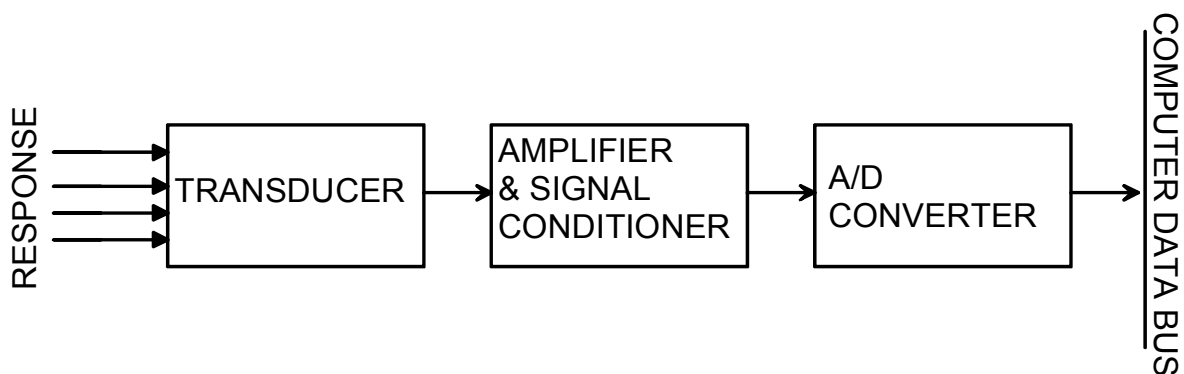


Figure 4.1 Schematic of typical set up of a data acquisition system for model testing

A further description of instrumentation and transducers relevant for model testing can be found in Olsen (1992). A detailed description of measurement techniques for fluid measurements is given by Goldstein (1983)

4.2 Strain and displacement measurements

The most used methods for strain and displacement measurements in model testing are based on the following principles:

- Resistive transducers, based on change of resistance due to strain; strain gauges
- Inductive transducers
- Capacitance transducers.

In addition to a direct measure of strain and displacements, these type of transducer are also commonly used as the basis for pressure cells, force transducers, velocity measurements and accelerometers. These applications will be discussed separately.

4.2.1 Strain gauges

The strain gauge measured the elongation in the material to which it is glued. Strain gauges are commonly used in a number of different types of transducers. Examples of strain gauge constructions are shown in Figure 4.2. The threads are usually CU-Ni alloys.

The use of strain gauges is based on that the elongation of the strain gauge will change the resistance. The gauge factor k , is defined as:

$$k = \frac{\Delta R/R}{\Delta L/L}$$

where R is the resistance and L is the length and Δ represent the change of length or resistance. The factor k is typically about 2 for metallic materials. Increasing the factor k will increase the sensitivity of the strain gauge. k values up to about 100-200 can be achieved using piezoresistive materials.

The elongation of the strain gauges us usually measured in *micro-strain*, $\mu S=10^{-6} S$, where $S = \Delta L/L$.

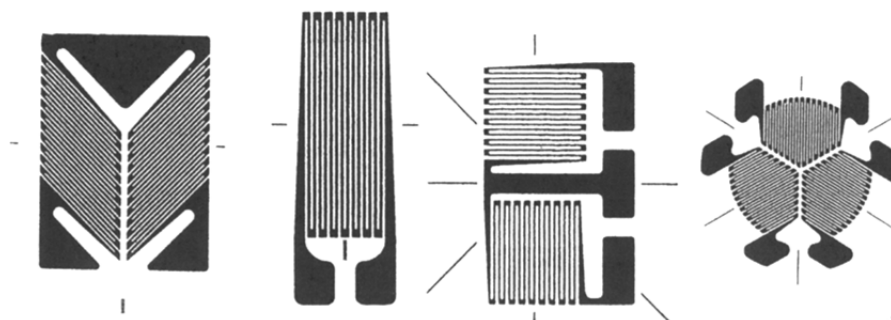


Figure 4.2 Examples of strain gauges designs

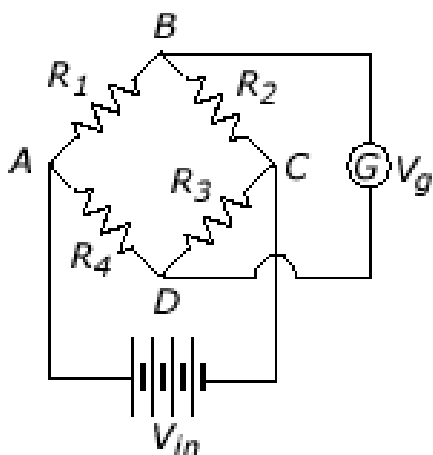


Figure 4.3 Wheatstone bridge circuit

To measure the change of resistance over a strain gauge, a Wheatstone bridge circuit is used. A basic Wheatstone bridge circuit contains four resistances, a constant voltage input, and a voltage gage. For a given voltage input V_{in} , the currents flowing through ABC and ADC depend on the resistances, i.e.,

$$V_{in} = V_{ABC} = V_{ADC}$$

$$\Rightarrow I_{ABC}(R_1 + R_2) = I_{ADC}(R_3 + R_4)$$

The voltage drops from A to B and from A to D are given by:

$$V_{AB} = I_{ABC} R_1 = \frac{V_{in}}{R_1 + R_2} R_1$$

$$V_{AD} = I_{ADC} R_4 = \frac{V_{in}}{R_4 + R_3} R_4$$

The voltage gage reading V_g can then be obtained from:

$$V_g = V_{AB} - V_{AD} = \frac{V_{in}}{R_1 + R_2} R_1 - \frac{V_{in}}{R_4 + R_3} R_4$$

$$= \frac{R_1 R_3 - R_2 R_4}{(R_1 + R_2)(R_4 + R_3)} V_{in}$$

Now suppose that all resistances can change during the measurement. The corresponding change in voltage reading will be:

$$V_g + \Delta V_g = \frac{(R_1 + \Delta R_1)(R_3 + \Delta R_3) - (R_2 + \Delta R_2)(R_4 + \Delta R_4)}{(R_1 + \Delta R_1 + R_2 + \Delta R_2)(R_4 + \Delta R_4 + R_3 + \Delta R_3)} V_{in}$$

If the bridge is initially balanced, the initial voltage reading V_g should be zero. This yields the following relationship between the four resistances:

$$V_g = \frac{R_1 R_3 - R_2 R_4}{(R_1 + R_2)(R_4 + R_3)} V_{in} = 0$$

$$\Rightarrow R_1 R_3 = R_2 R_4 \quad \text{or} \quad \frac{R_1}{R_2} = \frac{R_4}{R_3} = \frac{1}{r}$$

We can use this result to simplify the previous equation that includes the changes in the resistances. Doing so results in the solution for the change in V_g :

$$\Delta V_g = \frac{r}{(1+r)^2} \left(\frac{\Delta R_1}{R_1} - \frac{\Delta R_2}{R_2} + \frac{\Delta R_3}{R_3} - \frac{\Delta R_4}{R_4} \right) (1+\eta) V_{in}$$

where η is defined by:

$$\eta = \frac{1}{1 + \frac{1+r}{\frac{\Delta R_1}{R_1} + \frac{\Delta R_4}{R_4} + r \left(\frac{\Delta R_2}{R_2} + \frac{\Delta R_3}{R_3} \right)}}$$

Moreover, when the resistance changes are small (<5%), the second order term η is approximately zero and can be ignored. We then have:

$$\Delta V_g = \frac{r}{(1+r)^2} \left(\frac{\Delta R_1}{R_1} - \frac{\Delta R_2}{R_2} + \frac{\Delta R_3}{R_3} - \frac{\Delta R_4}{R_4} \right) V_{in}$$

which is the basic equation governing the Wheatstone bridge voltage in strain measurement. The coefficient $\frac{r}{(1+r)^2}$ is called circuit efficiency.

In practice, one often uses the same resistance value for all four resistors, $R_1=R_2=R_3=R_4=R$. Noting that $r=1$ in this case, the change in voltage can be further simplified to

$$\Delta V_g = \frac{\Delta R_1 - \Delta R_2 + \Delta R_3 - \Delta R_4}{4R} V_{in}$$

Different types of Wheatstone bridge circuits are used to measure the change of resistance over a strain gauge. A very simple example for measurement of force is shown in figure 4.4. One strain gauge is mounted to each side of a beam. Two dummy resistances (usually integrated in the amplifier) are used for balancing the bridge. This set up is called a half-bridge. A constant voltage is used as excitation, V_{in} . The force gives rise to an elongation of strain gauge 1 and compression of strain gauge 2. This introduces an unbalance in the bridge and a voltage can be measured at the exit at V_g . In a full bridge circuit, all four branches of the bridge are strain gauges. Mounting two strain gauges on each side of the beam in Figure 4.4 in a full bridge arrangement would give twice the sensitivity of the half bridge arrangement.

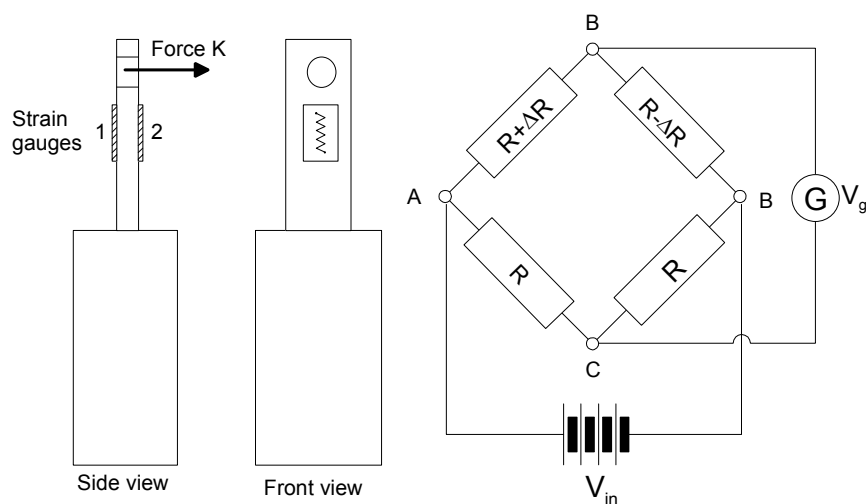


Figure 4.4 Examples of half-bridge circuit for measurements of change of resistance of strain gauges.

4.2.2 Inductive transducers

The inductive transducers are based on the voltage induced by a movable core. An example of an application is shown in Figure 4.5. The shown system is called LVDT (linear variable differential transformer). One set of the coil is excited by AC voltage and the induced voltage is measured in the second set.

This type of transducer is available in a wide range of sizes, frequency ranges and accuracy's. It is used for direct position measurements, but also as basis for pressure cells force transducers, velocity measurements and accelerometers.

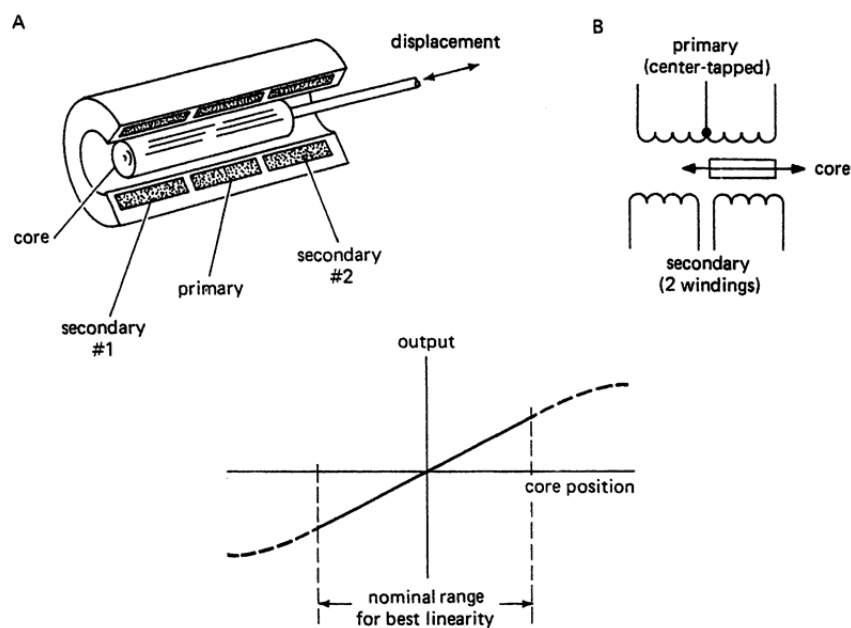


Figure 4.5 LVDT transducer for displacement measurements.

4.2.3 Capacitance transducers

The capacitance transducers consist of two closely spaced plates or a plate suspended between a pair of outer plates as shown in Figure 4.6. The plates are conductive and relative movement between the plates introduce a variation of the capacitance

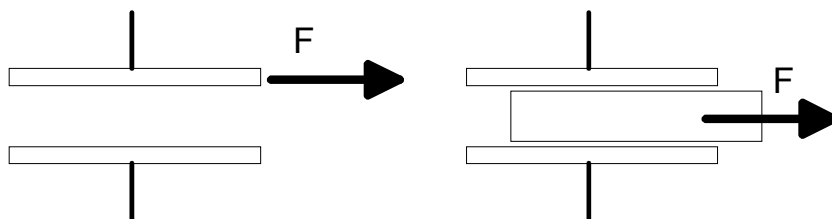


Figure 4.6 Capacitance transducers for displacement measurements.

This type of transducers require a much smaller driving force compared to inductive transducers, but have a higher noise level and are therefore less frequently used in practical model testing.

4.3 Position measurements

Typical position measurements of interest for floating structures will be the 6 degrees of freedoms rigid body motions of ship/platforms and motions of mooring lines and risers. Other examples are measurements of deflections of elastic models as for springing and whipping response of ships.

4.3.1 Optical and Video systems

For free running models and moored structures the global motions are measured by optical or video based systems. For optical system minimum 3 light emitting diodes are located on the model.

For video systems ball shaped reflectors mounted on the model is used. Onshore cameras, minimum 2, are used for reading the position of each diode. Based on the instantaneous position (x, y and z) of each of the 3 diodes, the motions in 6 DoF are determined.

The accuracy of the measured motions will for both optical and video systems be of the order of ± 1 mm for position (in model scale) and ± 0.05 degrees for roll, pitch and yaw. For most cases this is an acceptable accuracy for the rigid body vessel motions.

4.3.2 Gyros

The roll and pitch motions can also be measured using gyros. The principle behind the gyro is shown in Figure 4.7. A rotating mass keeps the inner part of the gyro in a continuous horizontal position. The next link can be tilted about one axis and the angle is measured using a potentiometer. The outer link can be tilted about an axis perpendicular to the first axis and the angle can be measured in the same way. From the measured angles and the known sequence of the angles the roll and pitch motions are uniquely determined.

The gyro is a robust tool and is commonly used both in model testing and in instruments applied in full scale. However, since it involves complex mechanical components, it is fairly large and fairly expensive. The size limits the use in models, and the cost limits the use both in model and in full scale experiments.

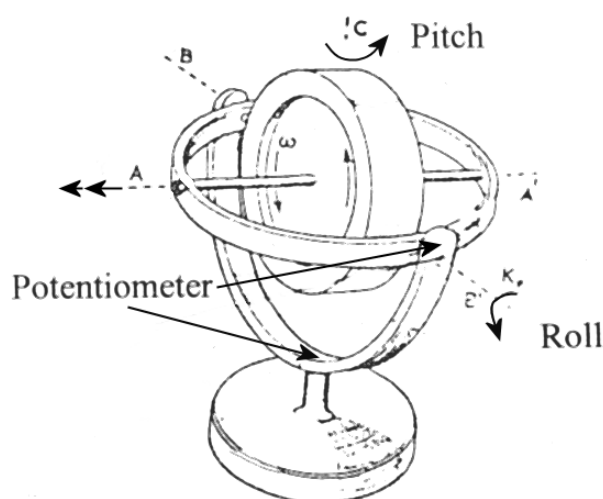


Figure 4.7 Principle of a gyro for measurement of roll and pitch.

4.3.3 Potentiometer

Low friction potentiometers can be used for measurement of motion in one direction. A Nylon line is connected to the model, then passed around the pulley on the potentiometer spindle and tensioned by springs. The motion of the model will therefore be directly transduced into a voltage signal by the potentiometer.

A commonly used set up for measurements of heave and pitch (trim) for towing tests is shown in Figure 4.8. The potentiometers are used for measurements of the motions between the ship model and the towing carriage. The set up is used both for measurements of running heave and trim in calm water testing and for measurements of wave induced motions in head sea waves.

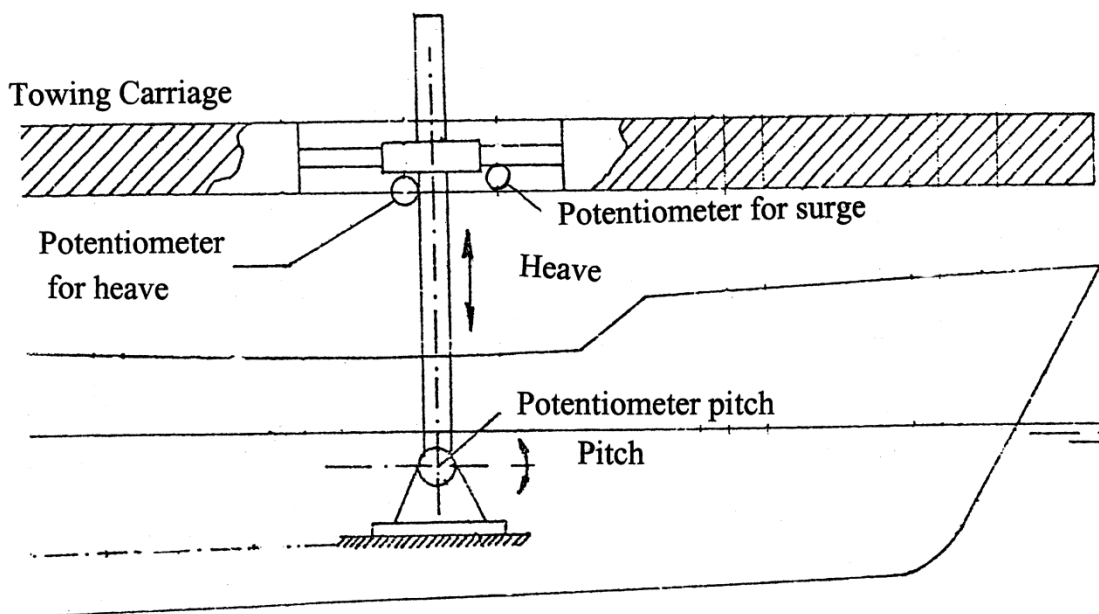


Figure 4.8 Example of using potentiometers for measurements of heave and pitch motions in towing tests.

4.3.4 Position based on measured force and acceleration.

Measurement of position can in principle be obtained from measured acceleration (see below) by a double integration of the measured acceleration signal:

$$x(t) = \iint a(t) dt dt + At + B$$

As can be seen, position based on integrated acceleration cannot give information about mean level or possible constant drift of the position. Increasing period of oscillation will give reduced accuracy of the derived position. For practical applications this method are therefore usually limited to measurements of the wave frequency part of the motions.

Another indirect way to establish the position is using measured force in combination with a linear spring:

$$x(t) = \frac{F(t)}{k}$$

The method requires a spring connection between the model and a fixed point (e.g towing carriage, sea bed etc.). It is necessary that the spring stiffness is sufficient low to avoid any influence on the dynamic behavior of the model.

4.4 Accelerations

Measurements made by accelerometers are based on the ratio between force, mass and acceleration:

$$a(t) = \frac{F(t)}{m}$$

A mass can be connected to a beam. When exposed to acceleration the beam will be deflected by the inertia forces. The deflection of the beam is proportional to the acceleration. Strain gauges can be used for measuring the deflection of the beam and hence the acceleration is obtained.

Another type of accelerometers is based on the piezo-electrical effect. A piezo-electrical material is a material which when deformed produces an electrical field. The voltage generated is proportional to the surface pressure applied. Combined with a mass this gives a signal proportional to the acceleration. The principle is shown in Figure 4.9. The charge is transferred to voltage in a charge amplifier, but some of the charge leaks out. This gives the accelerometer a lower limit for which frequencies that can be covered. This type of accelerometers can therefore only be used for dynamic measurements.

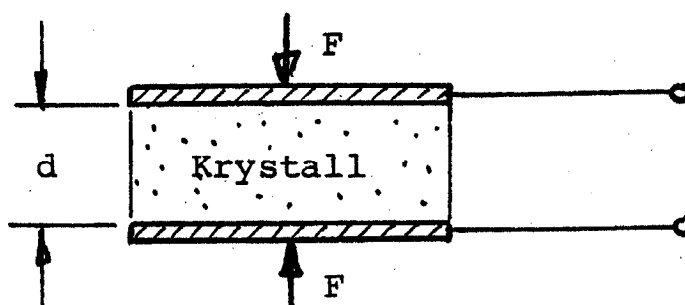


Figure 4.9 Piezo –electric material exposed to surface pressure.

The resonance of the mass – spring system may influence the measurement of accelerations. For frequencies well below the resonance frequency the mass will follow the motions of the housing and we have a linear relation between the acceleration and the signal out. For frequencies in the resonance region the mass will be excited and the signal out will be frequency dependent. The dynamic amplifications will be dependent of the damping of the system, but in general accelerometers should only be used for measurements of responses with oscillation frequencies well below the natural frequency of the accelerometer. Accelerometers based on Piezo-electricity can be made very stiff with resonance frequency higher than 500 KHz. This makes them useful for applications of measurements of response due to impact loads. To increase the sensitivity of the accelerometer the mass must be increased or the stiffness reduced. Accelerometers with low natural frequency will therefore be more sensitive than the accelerometers with high resonance frequency.

The accelerometers add weight to the structure and it is therefore important to ensure that that weight is sufficiently low to avoid any influence on the dynamic behaviour. The weight of the accelerometer can be made very small, typically down to a few grams.

4.5 Pressure Transducers

Pressure measurements are mostly performed using pressure cells. Three types of pressure cells are commonly used:

1. based on piezo-electricity
2. based on inductive transducers
3. based on strain gauges.

Pressure cells are basically force measurements over a small area. Typical dimensions of pressure cells used for model testing is $D=2-10$ mm. The different types of pressure measuring devices are illustrated in Figure 4.10.

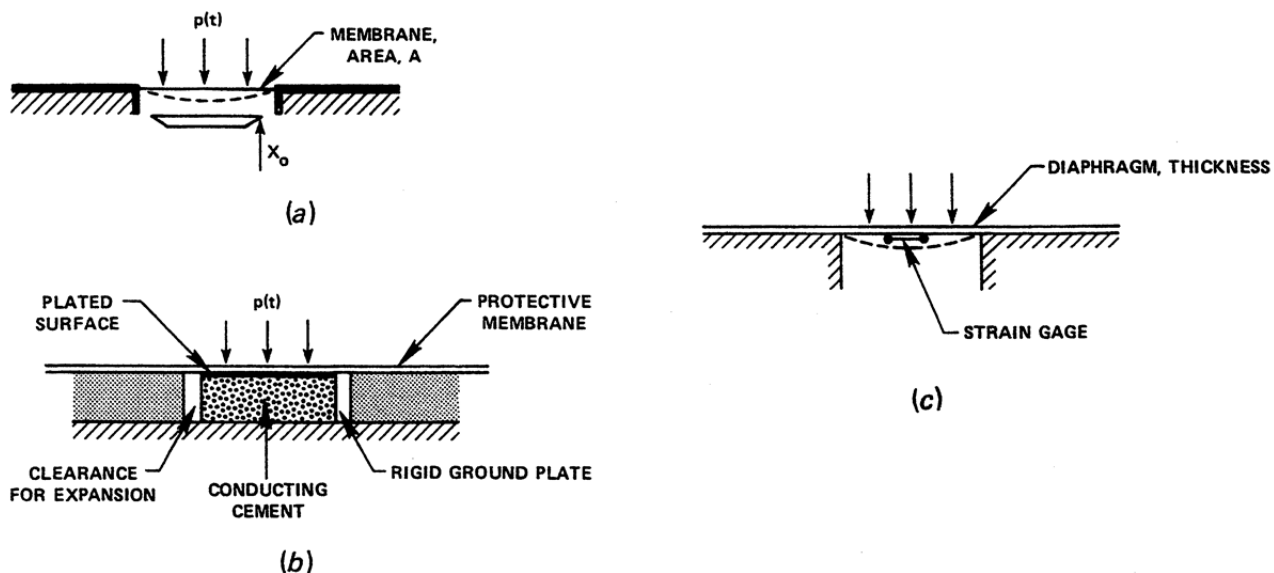


Figure 4.10 Schematic representation of the most common type of pressure transducers.

(a): Capacitance transducer, (b): Piezoelectric and (c): Strain gauge

Pressure cells behave in many ways similar as an accelerometer and the resonance of the mass – spring system may influence the measurements. The dynamic amplifications will be dependent of the damping of the system, but in general pressure cells should only be used for measurements of responses with frequencies well below the natural frequency of the cell. Strain gauge type cells responds to displacements from dc to 5 kHz. It is therefore well suited for most practical model testing. Pressure cells based on piezo-electricity can be made very stiff with resonance frequency up to more than 500 kHz. An example of this type of pressure cell is shown in Figure 4.11. This transducer is therefore well suited to measurements of pressure behavior with very low rise time as will be the case for slamming pressure measurements. An example of measured slamming pressure for the impact of a flat, elastic plate towards a wave crest is shown in Figure 4.12. It is observed that close to the center of the plate bottom where the wave crest hit, the rise time is less than 0.0001 s and the duration of the peak extremely short. Consequently a pressure cell with very high resonance period will be required to accurately reproduce this pressure behavior.

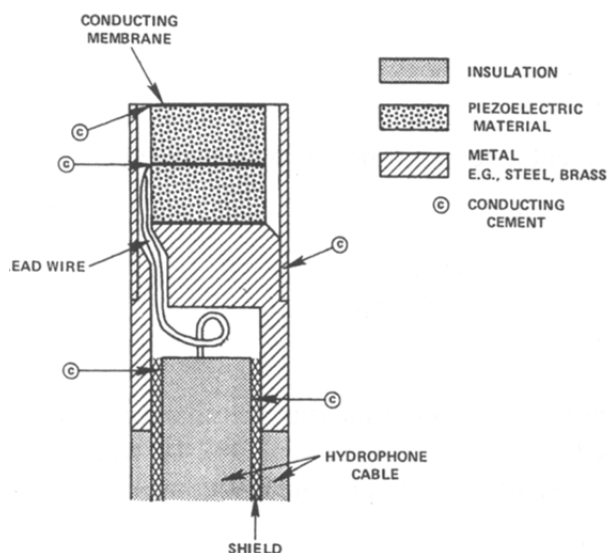


Figure 4.10 Piezo-electric pressure transducer for pressure measurements.

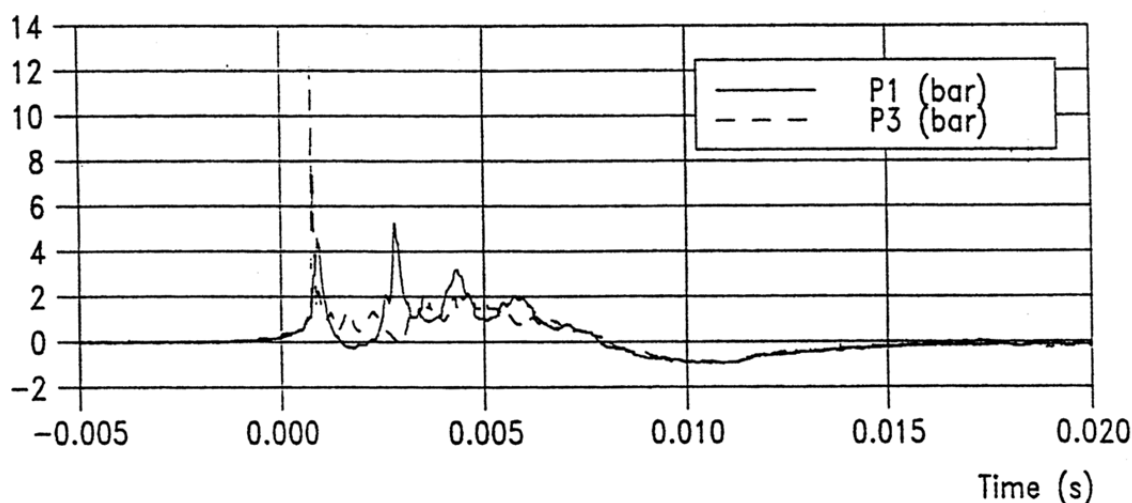


Figure 4.11 Example of measured slamming pressure. Impact of a horizontal circular cylinder towards calm water surface.

4.5.1 Measurement of pressure distribution

In the later years, pressure sensing film has been developed by several different companies. The film is basically a matrix of small pressure cells integrated into a flexible plastic film that can be applied to curved surfaces, and will effectively return the pressure distribution over the surface. The pressure cells are made of a layer of semi-conducting material where the degree of conductivity depends on the pressure applied to the material. Two companies that develop pressure sensing film are Tekscan <http://www.tekscan.com/> and Pressure Profile Systems <http://www.pressureprofile.com/>. This technology has mainly been developed for “dry” applications, like testing and development of car seats, sports equipment, and similar. Thus, it is not straight forward to apply it to marine hydrodynamics problems, but the possibility of easily measuring the pressure distribution, not only point pressures, means that this technology is probably going to be applied also to marine hydrodynamics in the future.

A slightly similar technology is pressure sensitive paint (PSP) . The color of the paint is changing with the pressure, when a special light source is used. This is also a recent measurement technique, developed in the former Soviet Union and known in the West since an advertisement in Aviation Weekly in 1990. It is primarily used in wind tunnel testing of aircraft. The pressure sensitive paint is sensitive not only to pressure, but to temperature and oxygen content in the flow, something that complicates the application.

4.6 Velocities

The velocity in a point can be obtained by a straight forward integration of measured acceleration or by a derivation of measured position. Both methods are commonly used for velocity measurements of structural components.

For measurement of fluid velocity different principles are possible:

- Based on measurements of pressure, e.g. pitot tubes
- LDV
- Ultrasonic transducers
- By measuring rate of revolution of a small impeller.

The two first methods are discussed in the following.

4.6.1 Pitot tubes

The pitot tube sensor is commonly used for measurement of the wake surveys, flow through water jets etc. The Prandtl pitot tube is shown in Figure 4.13. The pressure difference between the total pressure head at the front (in pos. A in the figure) and the static pressure at the side (at position B) is measured by a differential pressure cell. Basically the pitot tube is a pressure difference measure, but the velocity is obtained from the well-known relation:

$$\Delta p = 1/2 \rho U^2$$

To improve accuracy this theoretical relation is not used, instead the calibrated relation between pressure and velocity will be applied.

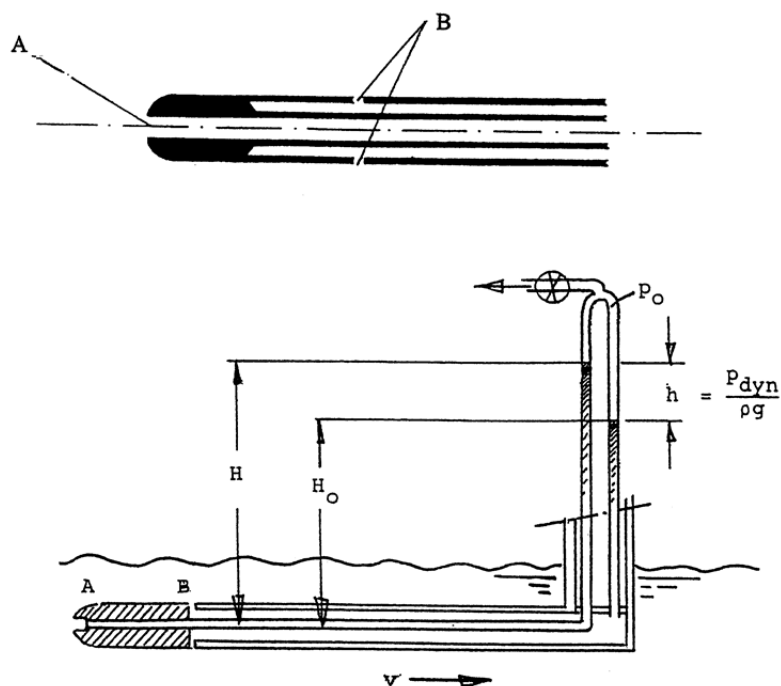


Figure 4.12 Prandtl pitot tube.

To cover more positions in the same run, several pitot tubes can be mounted together as shown in Figure 4.14.

Using pitot tubes with five holes located in different angular position on a spherical head, the velocity in all three directions can be measured, in case of wake surveys; axial, tangential and radial velocity.

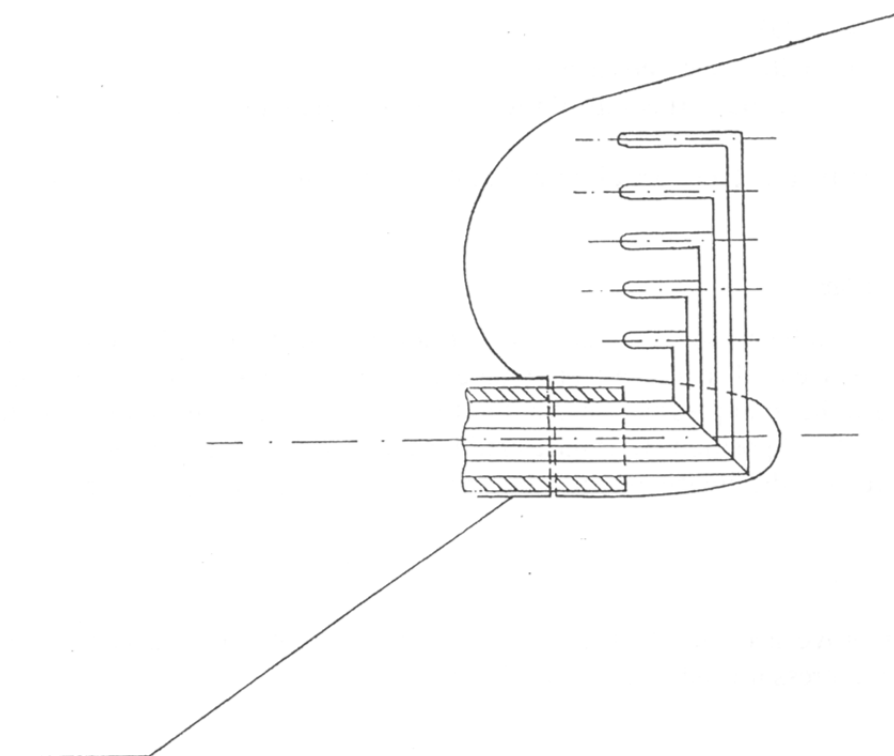


Figure 4.13 Pitot tube arrangement for measurement of velocity in several positions.

4.6.2 Laser Doppler Velocimetry - LDV

Laser Doppler Velocimetry (LDV) has been used for more than 20 years for measurements of flow around ships and propellers. The use has been mainly for validation of prediction tools for velocity distribution around lifting surfaces, within boundary layers and for wake flow. Generally LDV measurements are time consuming and expensive to perform and the use for commercial model testing have been very limited. See ITTC, (1996) for a further discussion for application of LDV in model testing.

LDV uses the Doppler shift in the reflected light frequency (color) to determine the velocity and direction of the flow. By using two beams from different direction, the 3-D velocity vector in a single point can be measured. To measure velocity in different positions, the transmitting and receiving optics must be moved (see Figure 4.14). This is commonly done using an automatic traversing system.

One of the main benefits of LDV is that it is a non-intrusive measurement technique, which means that one does not have to put any sensors into the area where one wants to measure, thus one is not interfering with the flow field of interest. LDV do also give very quick response, which means that it is suitable for measurement of turbulence and similarly rapidly changing flow phenomena. For measurement of average velocity in one direction, it is generally recommended to use pitot tubes or similar techniques.

For LDV to work there needs to be light-reflecting particles dissolved in the water in order to provide light scattering. If there is no particles in the water the light from the laser will not be reflected. In fact, one is not measuring the water velocity, but rather the particle velocity. There might be sufficient "dirt" in the water from the start, but it is common to have to apply particles for the purpose of LDV measurement. This process is called *seeding*. Proper seeding is one of the keys to successful application of LDV. When testing in large facilities, like a large towing tank, seeding might be one of the main challenges. Seeding the entire tank is difficult and expensive. Seeding locally in the area of measurement might disturb the flow, and it might be difficult to obtain a reasonably homogeneous distribution of particles.

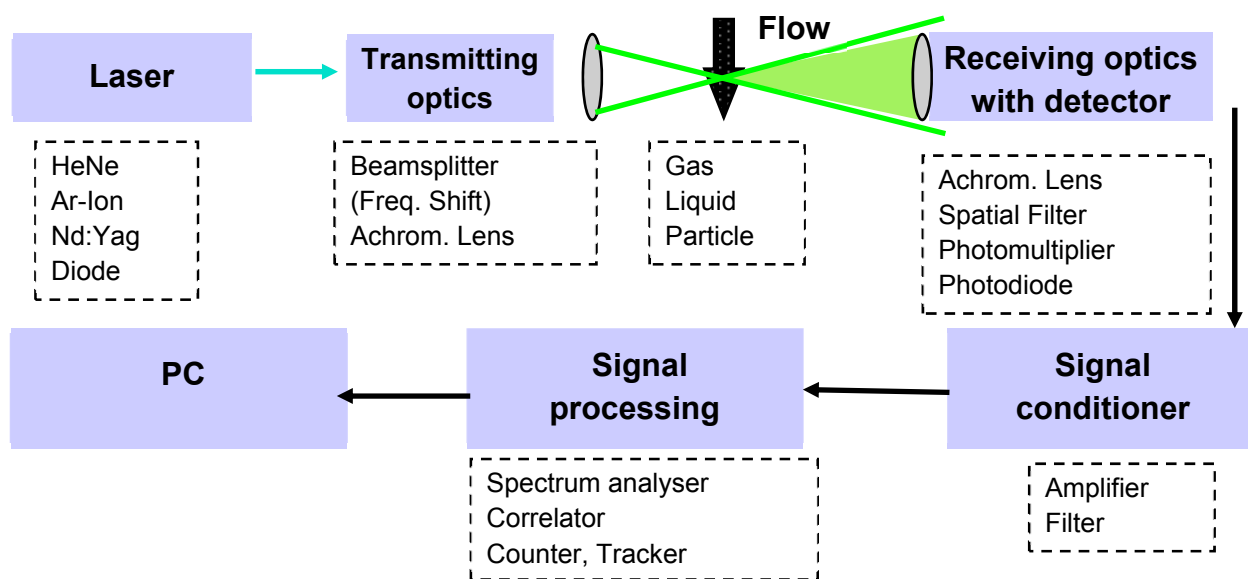


Figure 4.14 Principles of a LDV measurement system

4.6.3 Particle Image Velocimetry - PIV

Particle Image Velocimetry, or PIV, is a non-intrusive, optical technique for measurement of velocity vectors. As for LDV laser light is used, and similar to LDV the water needs particles – seeding – to provide light scattering. While LDV measures velocity in a single point at a time, PIV measures the velocity in an area, so it is considered a field measurement technique. PIV uses a laser light sheet, created by putting a spreading lens in front of the laser beam. By taking two stereo photographs (or one double-exposure stereo photograph) with very short time interval the velocity of the particles can be determined from how far they have moved. By using stereo photographs, the movement in space, not only in a single plane, can be determined. PIV has been in use for a long time, but it is the advance in digital high speed video and image analysis that quite recently has made PIV interesting to apply in regular hydrodynamics research. In the time one used film based pictures and more or less manual analysis, PIV was extremely tedious and time consuming. Now, semi-automating analysis of the digital video images means that large amounts of measurement data can be generated fairly quickly. Also, the accuracy has been greatly increased. PIV is increasingly used instead of LDV, since it is much faster to map a velocity distribution – actually the distribution in an area is captured at one instant, and not over some time, as with LDV.

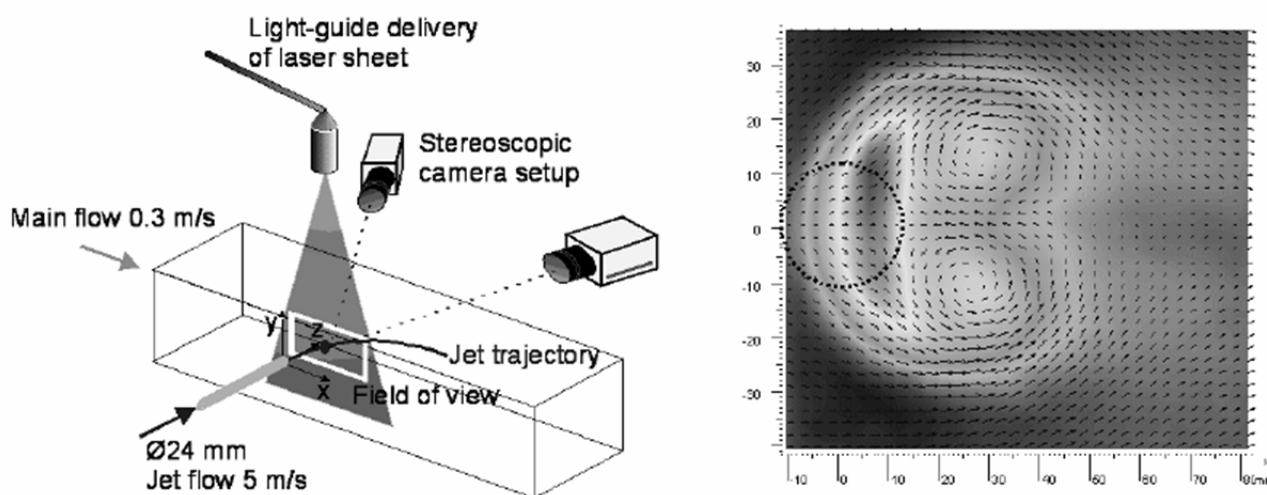


Figure 4.15 Principles of a PIV measurement system

4.7 Force measurements - Dynamometers

The load cells used in model testing are often designed to fit a specific purpose and to cover the expected range of loads during the tests. For example for towing tests, very high accuracy in measured force will be required and the transducer will be tailor made to measure force in one direction with a high as possible resolution. This is called a resistance dynamometer and is standard equipment in a towing tank. In Figure 4.15 a dynamometer for measurements of propeller thrust and torque directly on the propeller hub is shown. The thrust is measured by an inductive position transducer and the torque by strain gauges which measure shear deformation on a hollow part of the propeller shaft.

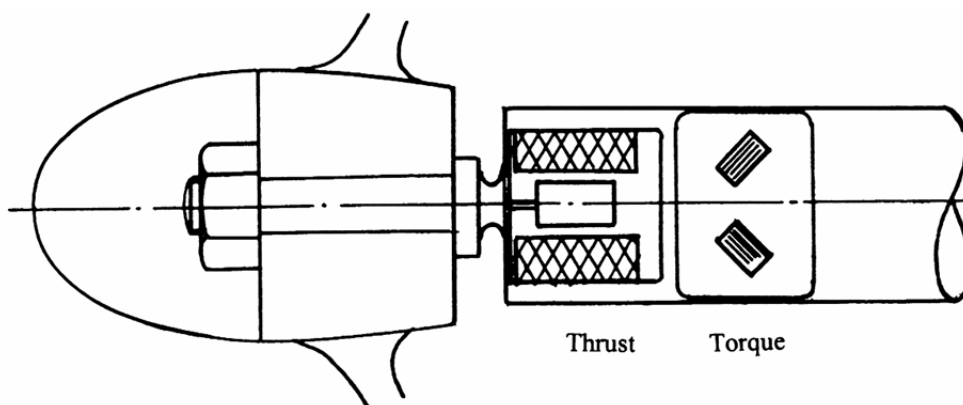


Figure 4.16 *Dynamometer for measurements of propeller thrust and torque.*

Transducers for measurements of forces in one or more degrees of freedom are often produced as a purpose machined piece with strain gauges glued to the base material. A typical design for measurement of forces in 3 d.o.f's (axial force and shear forces) is shown in Figure 4.17.

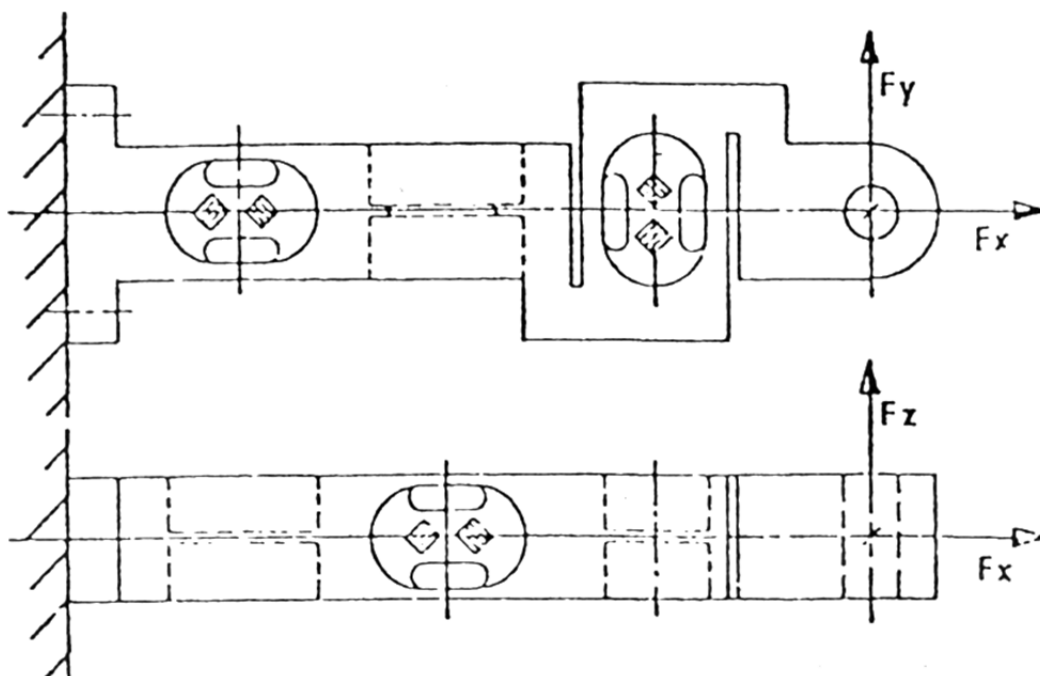


Figure 4.17 *Example of force transducer based on strain gauges. Axial forces and shear forces are measured.*

The machining of the material gives areas with high shear stresses where the strain gauges are mounted. By careful design of the transducer the "cross talk" can be kept at a minimum. "Cross talk" means coupling effects between the different degrees of freedom. For example for the transducer in Figure 4.17, if a pure tension in x-direction is applied, the measured response from the transducer in y and z direction is a result of "cross-talk". For transducer design it is important with minimum "cross-talk".

Using 3 transducer of this type mounted between two plates a 6 d.o.f transducer is obtained.

4.8 Wave Measurements

Wave elevation is most commonly measured by means of wave probes of the conductive (or resistance) type. A voltage is applied on to parallel rods. The resistance is determined by the length

Lecture notes in Experimental Methods in Marine Hydrodynamics, issued August 2014

of the rods which is wetted (or submerged). By measuring the current due to the applied voltage across the rods the wetted part and hence surface elevation, is directly achieved. Arrays of three or more of this type of sensors can be used to measure the directional distribution in short-crested waves.

Wave probes are also used for measurement of relative motions between the structure and the water surface. The wave gauge may then be mounted on the structure and the relative motion in the point is directly obtained. Examples of transducer solutions for this purpose are shown in Figure 4.18. Both rods and conductive tape glued to the model are used for this purpose. Rods are preferable at zero speed due to easier mounting and calibration, while conductive tape is often required for models with forward speed, to avoid resistance and water spray from the rods.

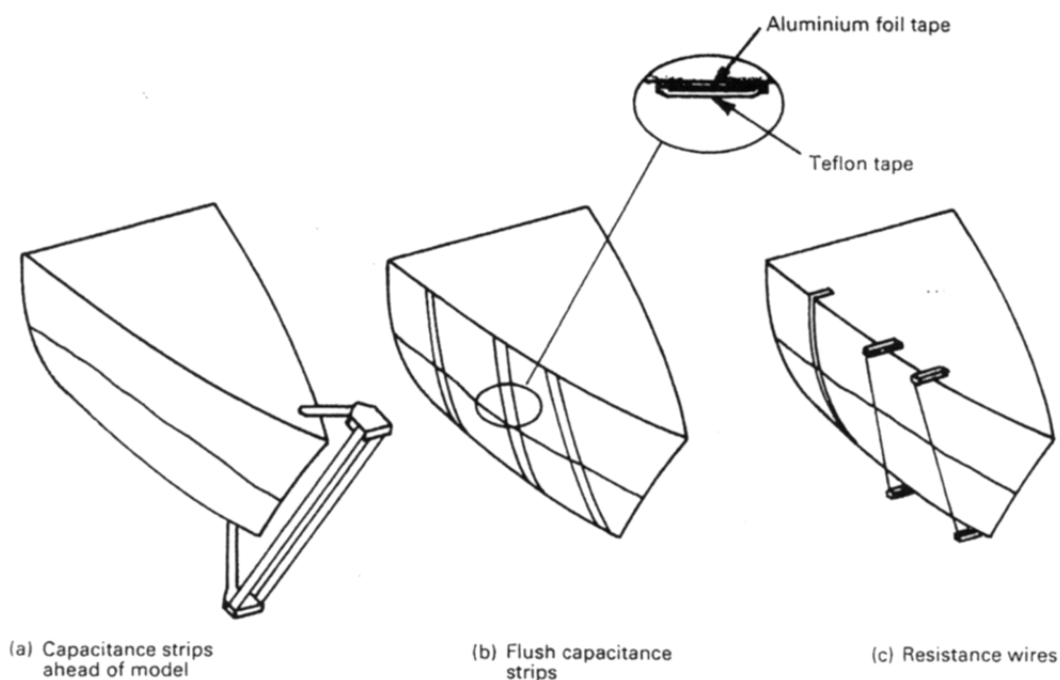


Figure 4.18 Example of wave transducers for measurements of relative motions.

For measurement of waves at high forward speeds, the wire-based probes don't work well, due to the spray and wave-making of the surface-piercing wires. Run-up in front of the wires and ventilation behind the wires leads to large errors in the measurements. For forward speeds of more than 2 m/s, the wire based probes should not be used. Alternatives are mainly:

- Ultrasound wave probes
- Servo needle wave probes

Ultrasound wave probes works by sending out a high frequency sound pulse, and measuring the time it takes before the reflected sound wave reaches the probe. The technique has been used for a long time for level measurement in tanks and dams, but it is not until fairly recently that instruments with sufficient accuracy for towing tank wave measurement has been available. The UltraLab systems from General Acoustics is in practical use in the hydrodynamic laboratories at the Marine Technology Centre. Some of these systems have limitations with respect to forward speed

and wave steepness, while the most advanced systems cover all conditions of practical interest for towing tank work.

Servo needle wave probes consist of a sensing needle mounted on a servo mechanism. The sensing needle measures the degree of contact with the water, and the servo mechanism makes sure the needle has a fairly constant submergence. Then, the actual wave height is found by measuring the position of the needle. This is a fairly complex and fragile instrument, and the only reason to use such an instrument is the capability of wave measurement at high forward speed.

4.9 Data Acquisition

The different instruments applied in the test set up are connected by cables to a data acquisition system to record the measured data. A schematic of a data acquisition system is shown in Fig 4.1.

4.9.1 Amplifiers

A typical analog transducer signal is with output in microvolts. It is therefore amplified by an amplifier, usually to +/-10 Volt range.

Depending on type of transducer different type of amplifiers is used. Amplifiers for analog signals from strain gauge and similar type of transducers can have bridge excitation and bridge balancing built in. This means that the amplifier will provide the current and voltage required for the measurement bridge (see section 4.2.1 *Strain gauges*), in addition to amplification of the output signal. Piezo-electrical transducers require a charge amplifier. Induction type transducers require AC excitation, which means that the driving current of the transducer is AC rather than DC. Strain gauge transducers can use either AC or DC excitation.

4.9.2 Filters

Filters can be either analog or digital filters. Analog filters are applied before the signals are converted to digital units by the AD converter and may be built in as an integrated part of the amplifier. The digital filters are applied after the AD conversion and can be implemented either as a digital circuit or as software in the computer used for analysis.

The filters remove signals at certain frequency bands. Depending on which frequency band is removed they can be split into three classes:

- Low pass, i.e. for removing of high frequency components
- High pass, i.e. for removing of low frequency components
- Band pass

the different types are illustrated in Figure 4.19.

Analog low pass filter is commonly used for removing of noise as the noise is usually appearing at a significantly higher frequency than the physical measuring signal. To avoid Nyquist phenomena (see discussion below) the cut off frequency of the analog low pass filtered should be set to be lower than half the sampling frequency f_s . The general recommendation is to set the cut-off frequency much lower than half the sampling frequency – 1/10 of the sampling frequency is the preferred value, but it might mean that high sampling frequencies are required, and therefore compromises are often made.

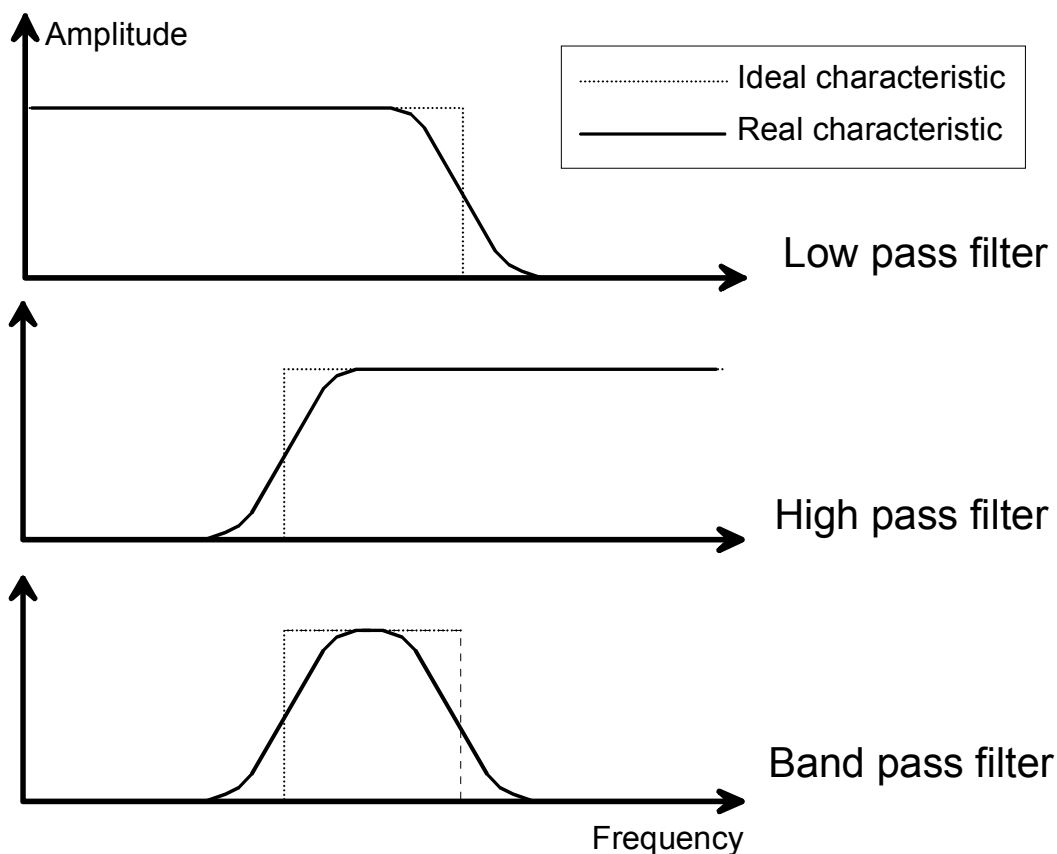


Figure 4.19 Illustration of different type of filters.

Low-pass filters applied in real time causes a time delay. This might be illustrated with an example of a very simple low-pass filter, which is created by creating the low-pass filtered signal from an average of the unfiltered signal over a certain period of time. In the example, shown in Figure 4.20, a sinusoidal signal with period of 30 seconds has had another sinusoidal signal with period 1.2 seconds superimposed. The filter is implemented as a running average over 2.4 seconds, seen in Figure 4.20 as the time it takes before the filtered signal appears. It is clearly seen from the figure that the filtered signal lags behind, with half the averaging time. The longer the average period, the lower the filter frequency, and the longer the time delay. If the averaging window could have been symmetrically placed relative to the time of the filtered value the delay would be avoided. This can be achieved when filtering an existing data set, but not when filtering in real time, since it would require the ability to look into the future.

It should be noted that filtering is in practice not performed by simple averaging. There is a large variety of methods, which is not covered here. See for instance Dunn (2005) for a discussion of filter algorithms.

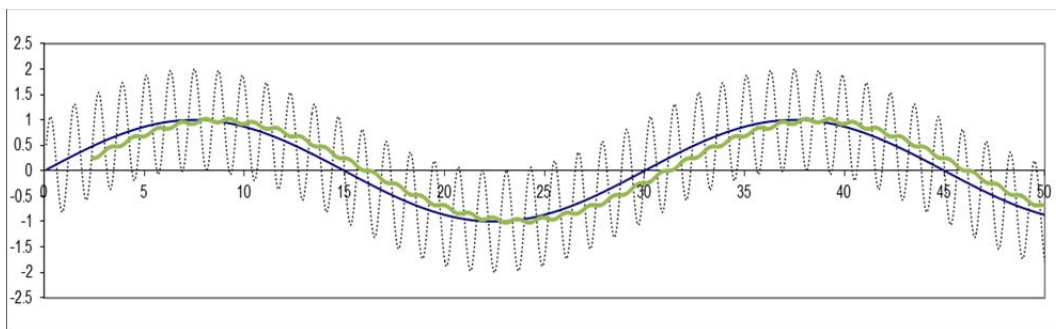


Figure 4.20 Illustration of time-delay due to filtering

4.9.3 Analog to Digital (AD) Conversion

Most transducer types, including the large group of strain gauge based transducers, are analog transducers, meaning that they produce an analog output signal. To represent this signal in a computer it has to be digitized. The process of digitalization is performed in the AD-converter.

The AD-converter is usually a physically separate unit; a box or an extra card for the computer. The line-in part of a computer sound card is an AD-converter custom-made for sound, but really quite similar to the AD-converters used for other measurements. The AD-converter unit will often also have a possibility for digital to analog conversion – DA – similar to the line-out of a computer sound card. The DA-converter might for instance be used to produce a signal for a control system. The AD-converter might be integrated with the measurement amplifier. This is the case for the Hottinger MGC+ digital measurement amplifiers in use in the hydrodynamic laboratories at the Marine Technology Centre.

The AD-converter unit will, depending on the actual model, have a certain number of channels, which means how many signals can be converted simultaneously. Limitations in the AD-converter will determine how fast the data can be sampled – the sampling frequency. It means that for experiments requiring very fast sampling, special AD-converter equipment might have to be acquired.

One should also be aware that some AD-converters sample all channels at exactly the same instant, while others will sample the channels sequentially during the sampling interval. If for instance 10 channels are sampled at 10 Hz, the sequential AD-converter will sample a single channel every 1/100 second, so that each channel is sampled every 1/10 second, but not at the same time. This is usually not a problem, since the sampling frequency should be much higher than the frequency of the phenomena to be studied.

The *range* of the AD-converter means what input voltage values are accepted. Most AD-converters accept values in the range $\pm 10V$. If the input signal exceeds the range, an overflow occurs, resulting in an invalid value, and possibly in an error situation that disturbs the other channels and/or disrupts the measurement.

Another important feature of the AD-converter is the *resolution* – how many bits are used to represent one sample. An 8-bit AD-converter will represent the analog value by choosing the nearest of only $2^8=256$ different values. 12 bit AD-converters are common for the less expensive models, producing a range of 4096 different values. Expensive models, like the MGC+, use 20 bit,

giving 1048576 different values. Especially for low resolution AD-converters it is very important to use as much as possible of the range of the AD converter. If you have a 8 bit AD-converter and use only 10% of the range you get an effective resolution of only 25 different values, and that will seriously impact your measurement accuracy – you get as much as $100/25=4\%$ error only on the AD-conversion! To use as much of the range as possible, you should select a transducer with a capacity that is close to what you will measure, but where you are pretty sure that the capacity is not going to be exceeded. This means you need to know approximately the magnitude of your measured values prior to the experiment. In addition to selecting the correct transducer, you can also adjust the *amplification* of the amplifier. The reason why you should not just use a large-capacity transducer and turn up the amplification is that this will also amplify the noise in the measurement chain, resulting in a poor *signal-to-noise ratio* in the resulting measurement.

4.9.4 **Wireless data transmission**

Examples of cases where wireless data transmission is required in a test set-up are measurements on a rotating shaft, for instance a propeller shaft, and measurements onboard a small ship model. There are various alternatives and currently a rapid development of technology and available products. A fundamental question is at what “stage” shall the data transmission take place – before or after the A/D-conversion? For strain gauge and similar sensors, the transmission should take place after the amplification. This means that the amplifier should be placed onboard the model or the rotating shaft. This again means that for the smallest models, and indeed for the rotating shaft, the amplifier must be of a special, very small kind. Previously, it was most common to transmit the amplified analog signal, for instance using an analog radio link. Now it is more common to include the A/D-converter in the instrumentation package onboard the model and transmit the digital signal. We will provide two examples of this.

For a free-running ship model to be used in seakeeping tests, MARINTEK is using a MGC+ digital measurement amplifier onboard the model. The amplifier is running on 24V DC power, supplied by two motorcycle batteries mounted in series. The MGC+ is communicating with the computer by an ordinary IP connection. Usually this connection is by cable, but in case of the free running model the cable is replaced by a wireless link of standard 802.11 b/g type. The only drawback of this set-up is the size and weight of the MGC+, which means it cannot be used for really small models. Also, the amplifier is by no means waterproof, which means you can easily destroy this very costly piece of equipment if the model gets flooded.

For measurement of forces on a propeller on a thruster or pod, NTNU, MARINTEK and the electronics company Norbit have developed a measurement system using on wireless transmission. In this system, a small amplifier and A/D-unit is mounted to the rear end of the propeller shaft. In the centre of this unit is an infrared (IR) sender/receiver unit of the same type used in mobile phones for the phone to communicate with a PC or another phone. Directly in front of the rotating amplifier and A/D unit is a similar electronics unit that contains the same type IR sender/receiver. Power is supplied to the unit on the rotating shaft by means of a coil with one rotating and one stationary part, as seen in Figure 4.20. Figure 4.21 shows the physical dimensions of the unit.

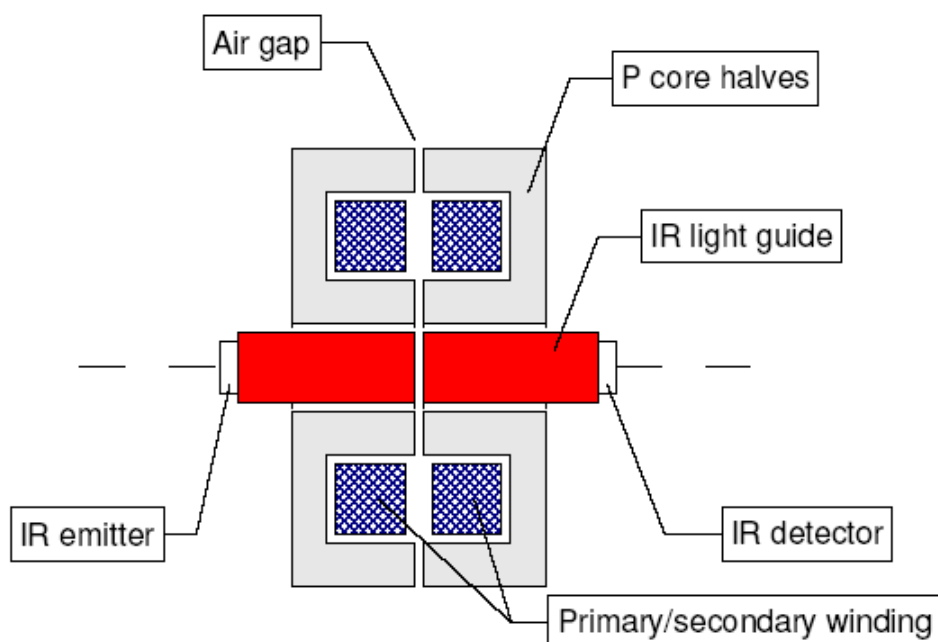


Figure 4.21 Principle of wireless data transmission from rotating shaft.

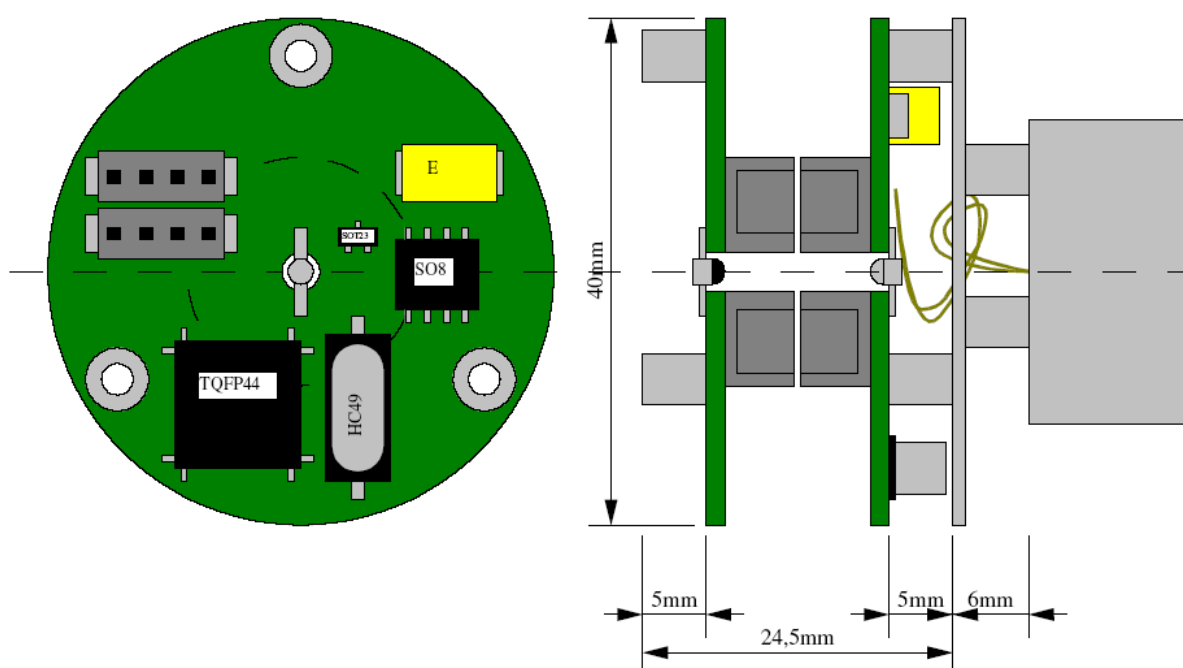


Figure 4.22 Sketch of electronics units for wireless data transmission from rotating shaft. The end of the rotating shaft is seen to the right. To the left is drawn the electronics unit seen from the rear

4.10 Sampling Frequency

The recording of the data during the test is done by sampling of the signal, i.e. the signal is recorded and stored digitally in the computer with a certain time interval, h , between each sampling. $1/h$ is called the sampling frequency f_s . The required data storage capacity for each measuring channel is

Lecture notes in Experimental Methods in Marine Hydrodynamics, issued August 2014

determined by the product $T \cdot f_s \cdot n_{bit}$, where T is the total measuring time and n_{bit} is the number of bits required to store each number. The sampling frequency will therefore determine the data storage capacity required, and the size of the result files is a major reason not to select a higher than necessary sampling frequency.

The sampling frequency has to reflect the time dependency of the process to be recorded. It has to be quick enough to cover all variations. On the other hand using high sampling frequency increases the amount of data collected through the tests and data processing and storage will be demanding.

In Figure 4.22 is shown that sampling can lead to generation of erroneous components in the record. A relatively high-frequency sinusoidal is sampled at a sampling frequency $1/h$. The apparent signal stored in the computer is a much more low-frequency sine wave, which did not exist in the original signal. The information in the original signal is lost and can not be restored in the subsequent analysis.

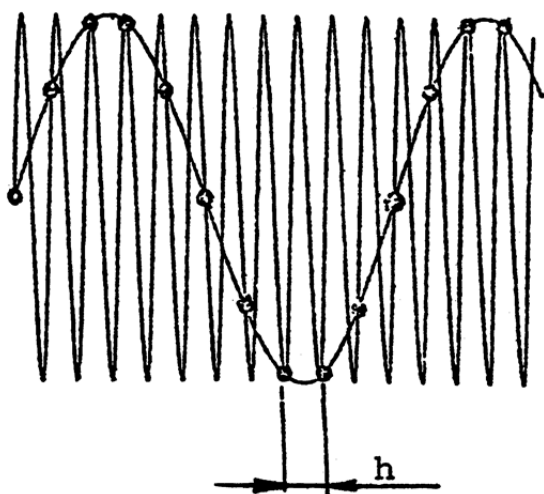


Figure 4.23 *Illustration of consequence of too low sampling frequency*

In order to define the amplitude and phase of a pure sine wave we theoretically need a minimum of 2 samples per cycle. In other words the highest frequency that can be determined from the signal is:

$$f_c = \frac{1}{2h}$$

This frequency is called the Nyquist frequency of the sampling process.

If the original signal contains components above f_c they will be “folded back” into the low frequency part of the spectrum and appear there as erroneous, non-physical components. This is shown in Figure 4.23. Two methods can be used to avoid this error:

1. Choose a sufficiently high f_s that all possible frequencies in the signal are correctly recorded in the sampling
2. Apply analog low-pass filtering of the signal, removing all signal components at frequency above f_c before the signal is sampled.

The latter method is most commonly applied in practice. For practical measurements, it is recommended to set the cut-off frequency of the low-pass filter significantly lower than the Nyquist

frequency. The recommendation is to set the low-pass filter cut-off frequency to 1/10 of the sampling frequency. Since the low-pass cut-off frequency must be sufficiently high to retain all frequencies of interest, following the recommendation leads to high sampling frequencies. Thus, compromises might be made, but it is strongly recommended to keep the filter cut-off frequency well below the Nyquist frequency.

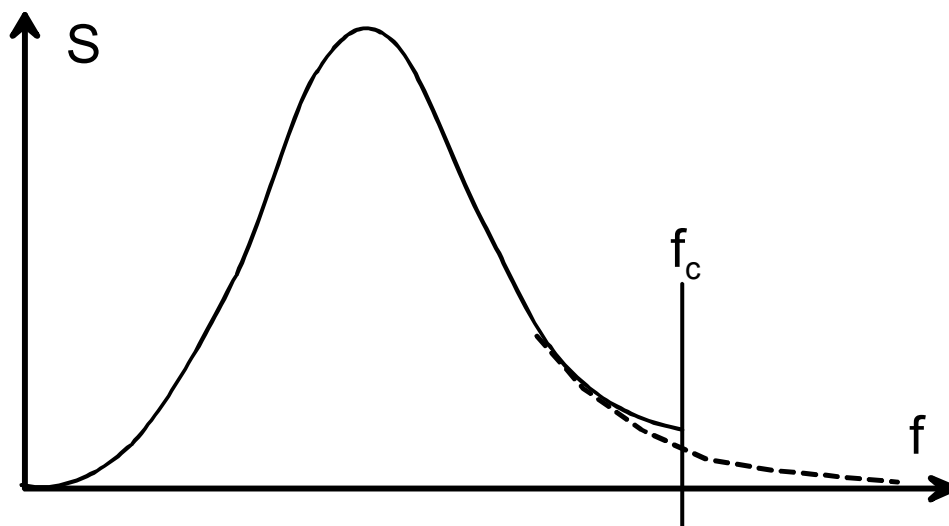


Figure 4.24 *Effect of Folding*

Wave frequency motions will follow the wave frequency, and a moderate sampling frequency is required. Typically, a low-pass filter frequency equal to minimum 10 times the wave frequency (or peak frequency in case of irregular waves) should be applied for this purpose.

Impact loads is an example where very high sampling frequency is required. This is especially the case if the local rise angle at the position of impact between model and wave surface is close to zero. An example of measured pressure on a horizontal plate dropped vertically towards a wave crest is shown in Figure 4.11. The tests were carried out to simulate impact loads against a catamaran wet-deck. The rise time is seen to be about 0.0001s and a sampling frequency of 100 kHz was required to cover the pressure peak. The time duration of the impact is very short and it is associated with very high local pressure peaks. This will also require that the amplifiers have a sufficiently large frequency range with linear relation between measured and amplified results. For the transducers very low rise time and high resonance frequency are required.

This example illustrate that the properties of equipment to be used, including sensors, amplifiers, filters and data acquisition unit has to be carefully selected based on the actual behaviour at each application. A good understanding of the physics of the tests situation is therefore of vital importance to decide type of equipment that shall be used and hence to achieve reliable and high quality test results.

4.11 Length of Records

Required duration of the tests will depend on type of testing. For regular waves a short duration of test is usually used. Typically only 10 cycles is used for the analysis, but make sure that the actual test is sufficiently long to establish a steady-state response. For decay tests the requirements to duration is similar.

For irregular waves the statistical accuracy of measured data is improved by increasing the length of the record. The required duration depends on the following parameters:

- The period of the most low frequent phenomena which occur in the tests
- The system damping
- The required standard deviation of the quantities determined by the statistical analysis

In commercial testing there is a very simple rule of thumb that the test duration should preferably be at least 100 times the period of the most low frequent phenomena to be investigated. For testing where only the wave frequency phenomena are of interest this gives a required time of typically 1000 s full scale time. For cases where slow drift motions are important, natural periods in the order of 1-5 min can be expected. This will require test duration up to 10 hours. In practice, often 3-hour duration of test is used for this case.

Referring to the spectral analysis requirement shows that there exist certain relationships between the following quantities (see Bendat and Piersol (1966) for further details):

$$m = \frac{1}{Bh}$$

$$N = \frac{m}{\varepsilon^2}$$

$$T = Nh$$

where:

- B ; the desired frequency resolution in the resulting spectrum (in Hz)
- h ; sampling interval (in s)
- m ; number of time shifts in the calculation of the autocorrelation function (from which the spectrum is calculated, see chap 9.5.2)
- N ; number of samples
- T ; length of recording (in s)
- ε ; normalised standard deviation of the spectrum calculation

Let us consider model tests with measurements of the heave motions of a ship in irregular waves as an example. Assuming the following data:

- Spectral peak period $T_p=10$ s.
- Resonance heave period $T_3= 8$ s.
- Scale ratio $\lambda=40$.

For this case we can assume that there will be almost zero energy of the response spectrum for frequencies above 0.25 Hz. The Nyquist frequency can then be set to $f_c=0.5$ Hz. Wanted frequency resolution in the resulting spectrum is set to $B=0.02$ Hz. This gives:

Sampling interval $h = \frac{1}{2f_c} = 1.0s$

Number of time shifts $m = \frac{1}{Bh} = 50$

Number of samples $N = \frac{m}{\varepsilon^2} = 2222$

Length of record $T = Nh = 2222s \approx 22$ min

4.12 Calibration

The data acquisition process described so far gives a signal in Volts (or millivolts). However, what is needed is a signal in the relevant physical unit. To obtain a link between the measured voltage signal and the correct physical value, we usually apply *calibration*. The process of calibration is to apply a known load to the transducer and measure the output voltage. This is done for a number of different loads, covering the expected range of measured values. Then, a *calibration curve* can be drawn. For ease of application, most transducers are made such that they will give a linear relation between load and output signal. The *calibration factor* will then be the slope of the straight line fit to the measured calibration data (see Figure 4.24).

To be able to apply a known load in an easy and well controlled manner; the calibration of each transducer is usually done before the test is set-up – before the transducer is mounted in the set-up. When doing the calibration this way, one must make sure that the mounting of the transducer in the test set-up doesn't alter the calibration factor. Also, because one is measuring the amplified signal in Volts, the amplifier settings will influence the calibration. Thus, one should make sure to use the same amplifier settings, and preferably also the same amplifier as in the real test set-up.

It is furthermore recommended to perform a check of the calibrations when the test set-up is completed. This ensures that the calibration factors haven't been significantly changed by the mounting, and also that all connections are correct. An example of such a check is when the ship model is connected to the carriage and the resistance dynamometer in preparation for a towing test, a known force is applied to the model in the direction of towing and the resulting output of the resistance dynamometer is compared with the known force.

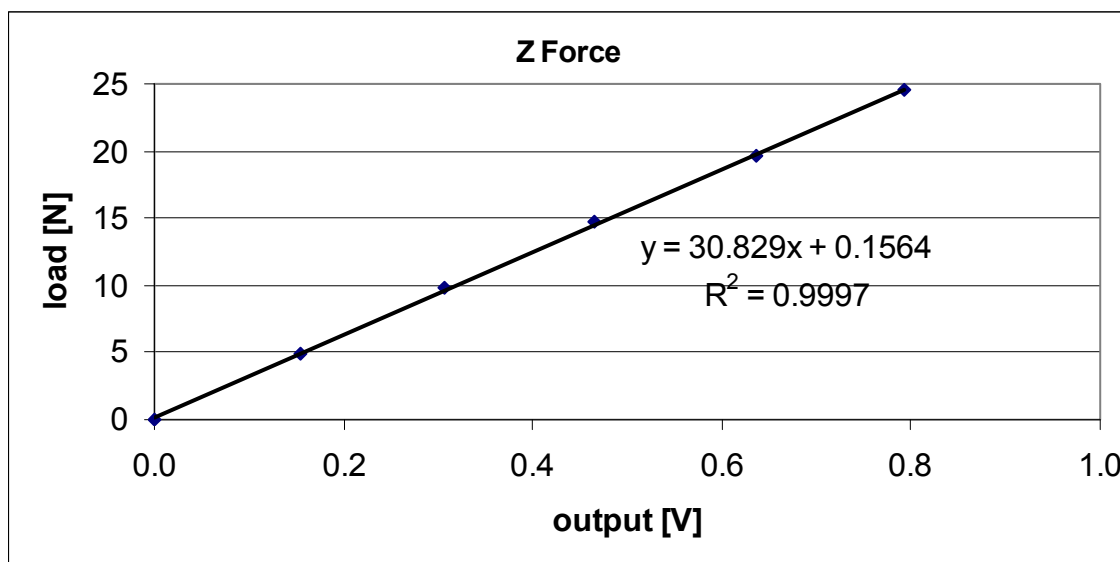


Figure 4.25 Example calibration curve for a force transducer. The calibration factor obtained from this curve is 30.829 N/V.

4.13 Zeroing

The calibration described above will ensure that the proportionality between the output signal and the correct physical property is correct (remember that the calibration factor is the slope of the curve relating output in Volts to the physical unit). However, we also need to make sure that the absolute value is known. This is done by defining a reference level and referring all measurements to this level. Typically, the reference level is zero, and in the following, we assume that this is the case.

Before the test, we measure the zero level of all relevant transducers. For instance for a resistance test, we measure the zero level for resistance, carriage speed, and sinkage fore and aft with the model at rest. The output measured in this condition is stored, and later subtracted from the real measurements at the wanted forward speeds. The data acquisition programs in use at the Marine Technology Centre have zero measurement functionality built in.

4.13.1 Bridge balancing

The zero measurement outlined above is like an ordinary measurement, involving an average over a time selected by the experimenter. In addition to this kind of zeroing, the measurement amplifier usually has additional means of zeroing the output. The most basic one is bridge balancing, which is to adjust the built-in resistances in order to make sure that the Wheatstone measurement bridge for the transducer gives zero output in the selected condition. It is important to balance the bridge before starting the measurements, as this makes subsequent measurements more accurate.

In addition, the amplifier might have a tare or zeroing function, which in principle is similar to the zero measurement described above, except that it bases the zero reading on a single, or a very limited number of samples. Thus, this kind of zero is less accurate, due to the risk of environmental disturbances.

4.13.2 Temperature drift

Zero readings are done many times during a measurement campaign because many transducers have a tendency to drift. Drift in a transducer means that for a constant load, the output changes slowly with time. Zeroing must be performed sufficiently often to reduce the error caused by transducer drift to an acceptable level. If the drift is quick compared to the length of a measurement, it means the transducer is not suitable for the test. Transducer drift for strain gauge based transducers is usually related to temperature changes in the transducer. When the temperature increases, the material to which the strain gauge is attached will be elongated, so the strain gauge will get a reading that is "false". A strain gauge emits significant amounts of heat compared to its small area, so shortly after the transducer is connected to the amplifier (or the amplifier turned on), the transducer will typically drift quite significantly due to heating-up of the transducer material. The drift due to heat from the strain gauge will reach a stable equilibrium within a few minutes (might be up to about 30 minutes), but when the environment around the transducer changes, for instance due to a change of the air velocity around the transducer, the equilibrium is changed and drift will again occur. Especially for transducers immersed in water, the change of cooling of the transducer due to changes in water velocity can cause serious problems for the accuracy.

5 PHYSICAL MODELLING

5.1 General

Design and construction of effective test models is an important part of the model testing process. Typical materials used for construction of ship hull models are wax, wood, aluminum, glass reinforced plastic (GRP) and foam material. Use of GRP will require that a plug is made with the exact finished shape of the hull. The type of construction material to be used will depend on shape, model size, weight and strength requirement, and cost. For ship like models computer controlled milling machines are commonly used for model production.

For almost all type of model testing, very accurate modeling of the part of the model geometry that is exposed to water will be required. For testing where viscous forces are important also the roughness of the surface has to be carefully controlled.

The selection of scale will be limited by several factors:

- The experimental facility available
- Requirements from instrumentation and physical modeling of the actual structure
- Required scale to avoid severe scaling effects, very often connected to viscous forces (Reynolds number).
- Cost of models and test execution

In general a too small scale will give problems with scale effects and measuring accuracy, while large models will be costly and can be difficult to handle. If the models get large compared to the size of the test tank, blockage effects are likely to occur, which means that the tank walls influence the results. Requirements to correctly scaled mass distribution and (when relevant) structural elasticity will be more difficult to satisfy for small models.

5.2 Rigid Models

For dynamic testing where the model is freely moving and the inertia forces will be of importance, the mass distribution needs to be correct. In practical terms the following requirements should be satisfied:

- Total mass
- Moment of inertia expressed through the gyration radius, r_{xx} , r_{yy} and r_{zz}
- Longitudinal and vertical position of centre of gravity
- If internal loads shall be measured, the mass distribution must also be correctly modelled

The mass is determined simply by weighing of the model, or by ensuring that the model is floating at the correct water line.

A practical tool for determining the position of CoG and moment of inertia of a model is to use the pendulum test. The model is arranged in a pendulum, free to rotate about a point A, as shown in the sketch in Figure 5.1. The period of a physical pendulum is given from:

$$T_0 = 2\pi \sqrt{\frac{I}{Mgh}}$$

where M is the mass of the model, I is the moment of inertia referring to the point A, G is the position of center of gravity, h is the distance from A to G and g is gravity. The above equation can be rewritten as:

$$4\pi^2 I - MgT_0^2 h = 0$$

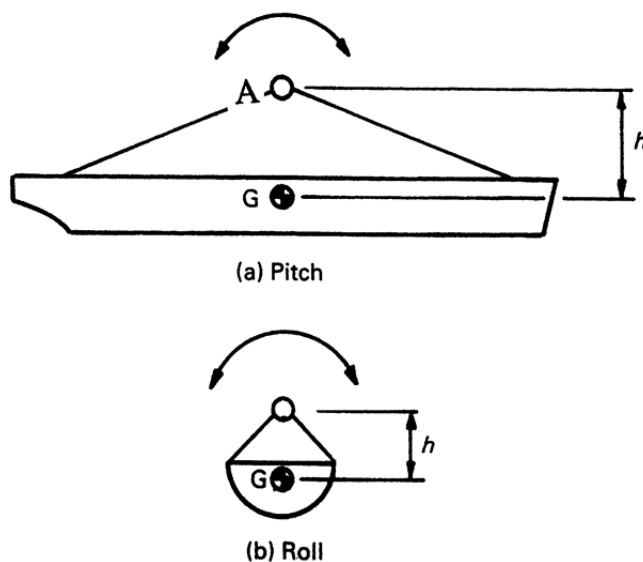


Figure 5.1 Sketch of a Pendulum for determination of centre of gravity and moment of inertia

In the pendulum test one first measure the period T_0 . Then two additional masses, m , are fitted at each end of the pendulum at a distance a from the rotation centre A. Then the pendulum period T_1 is measured with the additional weights fitted. We now have:

$$4\pi^2 (I + \Delta I) - (M + 2m)gT_1^2 (h + \Delta h) = 0$$

where $\Delta I = 2ma^2$ and $\Delta h = \frac{2mh}{(M + 2m)}$. Inserting into the above equation gives:

$$4\pi^2 (I + 2ma^2) - MmgT_1^2 h = -8\pi^2 ma^2$$

We now have two equations with two unknowns, I and h . The solution is:

$$h = \frac{8\pi^2 ma^2}{Mg(T_1^2 - T_0^2)}$$

$$I = \frac{2ma^2T_0^2}{T_1^2 - T_0^2}$$

To obtain the moment of inertia of the model referring to the centre of gravity we have:

$$I_m = I - Mh^2$$

The radius of gyration can be adjusted to the required values by moving the internal ballast weights. It is therefore important to have sufficient amount of ballast weights to be able to achieve the correct weight distribution.

When the position of centre of gravity is available, the metacentric height is also easily obtained. It is common practice to measure the metacentric height also by a static inclination test after the model is in the water. If any deviation from the results from the pendulum test is observed, the inclination test is usually considered to be most accurate.

When the model is divided in several sections for measurement of global loads (shear forces and bending moments) in given transverse cuts, it is not sufficient that the total model has the correct mass and moment of inertia. For this case each section of the ship must have correct mass and moment of inertia to get correct forces. The pendulum tests have then to be carried out for each section.

5.3 Elastic Models

5.3.1 General

For test conditions where the elastic deformation of the model is important the elastic properties of the model need to be correctly scaled. Examples where this will be the case are:

- Marine risers (bending stiffness) and loading hoses (bending stiffness and axial elasticity)
- Tethers for Tension Leg Platforms (both axial and bending stiffness)
- Mooring lines (axial stiffness)
- Springing and whipping of ships, both monohulls and catamarans (bending stiffness and torsional stiffness)
- Floating bridges
- Fish farming plants
- Seismic cables

This implies that for offshore and coastal structure testing one or more elements will usually require modelling of elastic properties. For a test case where the elasticity is not important, the

model is made “sufficient” stiff or “as stiff as possible” to avoid any artificially hydroelastic effects in the model.

The general scaling laws to be applied for elastic modelling is discussed in chap. 2.5. As outlined, a direct geometrical scaling using material with the same modulus of elasticity, gives a model that is λ times too stiff. This implies that in practical modelling the problem is to get the model sufficiently elastic.

For the dynamic response of an elastic structure the mass distribution and structural damping should also be correctly modelled. It is therefore a requirement that the modelling do not introduce additional damping. Materials that show hysteretic behaviour should therefore not be used for modelling. Other source for unwanted damping can be frictional forces between different components in the buildup of the model.

5.3.2 Slender Structure Modelling

A frequently used method for modelling of long and slender structures (eg. riser or tethers) is to apply a steel or aluminium core with dimensions determined to give correct bending stiffness. Around the core is fitted buoyancy material to obtain the correct outer geometry and weight. Using this method it is important to avoid motions and resulting friction between the core and the buoyancy material to avoid introducing artificial structural damping. In Figure 5.2 an example of modelling of a long and slender tube bridge using this method, is shown. Friction forces between core and outer buoyancy are in this case avoided by connecting the buoyancy foam to an outer pipe, which is welded to the core. The gap between the buoyancy elements ensures that the bending stiffness is not influenced by the buoyancy elements.

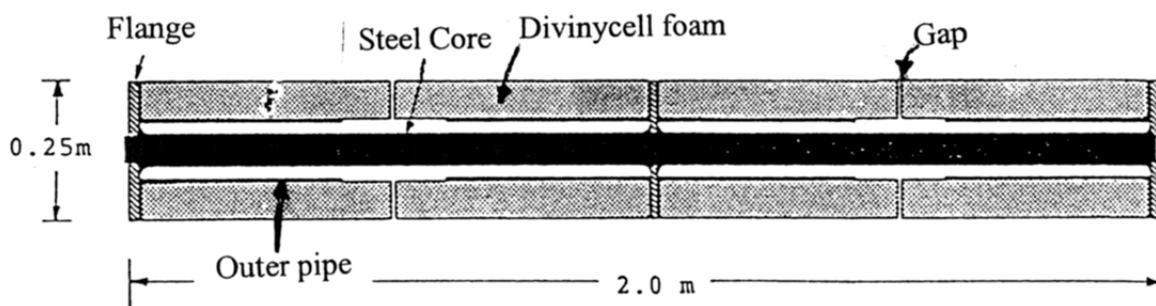


Figure 5.2 Example of elastic modelling of marine riser.

5.3.3 Mooring Lines modelling

The axial elasticity of mooring lines can be modelled by introducing axial springs in one or more positions along the lines. This will be important especially for mooring system including fibre ropes, but also for conventional mooring system designs consisting of chain and/or wire segments, the axial elasticity can be important for the total restoring stiffness and should therefore be accurately modelled.

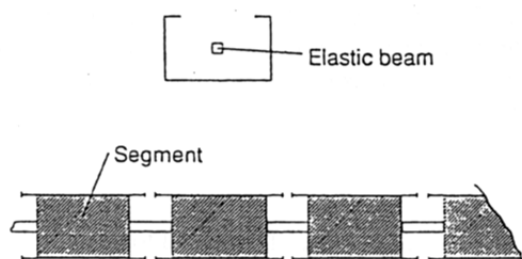
5.3.4 Ship modelling

For elastic modelling of ships, three different solutions have so far been used. (See Maeda (1991)):
Lecture notes in Experimental Methods in Marine Hydrodynamics, issued August 2014

- Backbone model
- Fully elastic model
- Hinged model

In Figure 5.3 the two first alternatives are shown schematically for a monohull. For the backbone modelling, the elasticity of the model is represented by an elastic beam to which rigid segments are connected (similar to the solution discussed above). Using this modelling technique it is relatively easy to model the stiffness and materials as steel or aluminium with stable and well-documented properties can be used. Further it is easy to modify the structural properties, and the structural damping is low. One problem with this modelling is the gap between the different sections. They may be closed using an elastic membrane, but it is difficult to avoid transfer of tension through the membrane. If the gaps are open, each section has to be built watertight. Further the dynamic pressure in the gaps may to some extent influence the results. For ship models with forward speed the gaps will give additional resistance due to the influence on the flow field around the ship.

Backbone model



Fully elastic model

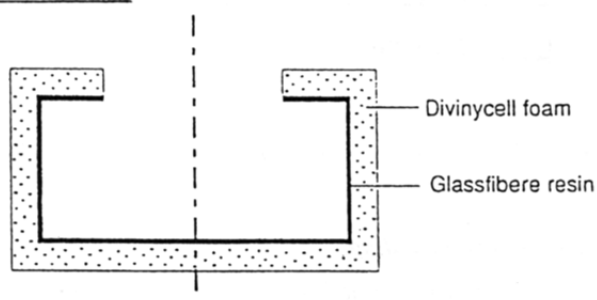


Figure 5.3 *Methods for modelling of an elastic monohull*

The fully elastic model is built up using cross sections with one or two layers with different elasticity as shown in Figure 5.3. Glass-fibre resin in combination with a foam material can be used. The thickness of the inner resin layer can be varied to achieve the correct elasticity. This method of modelling avoids the gap problems, but it is difficult to achieve the correct bending stiffness distribution. Further, the use of foam material introduces some hysteretic effects and the structural damping may be too high for the model. For testing of springing response this is critical for the results. For whipping response the structural damping level is less critical.

While the backbone and fully elastic model is best suited for monohulls the hinged model solution has also been used for catamarans, see Hermunstad et.al. (1995). An example of elastic modelling of a catamaran using the hinged model is shown in Figure 5.4. Each hull is divided into three rigid segments that are connected by springs. The springs are slender steel beams with dimensions determined to give correct bending and torsional stiffness. The two hulls are connected through three transverse springs as shown in the figure. The hull segments are made of Foam/GRP similar to what is used for standard rigid model production. To make the segments stiff, an aluminium frame is mounted within each section. Rubber membranes are attached between each segment to make the model watertight.

In general, a requirement for correctly scaled elasticity of a ship model will significantly increase the complexity (and hence the cost) for model production and also for test execution. In addition detailed information about the elastic properties of the full-scale ship will be required.

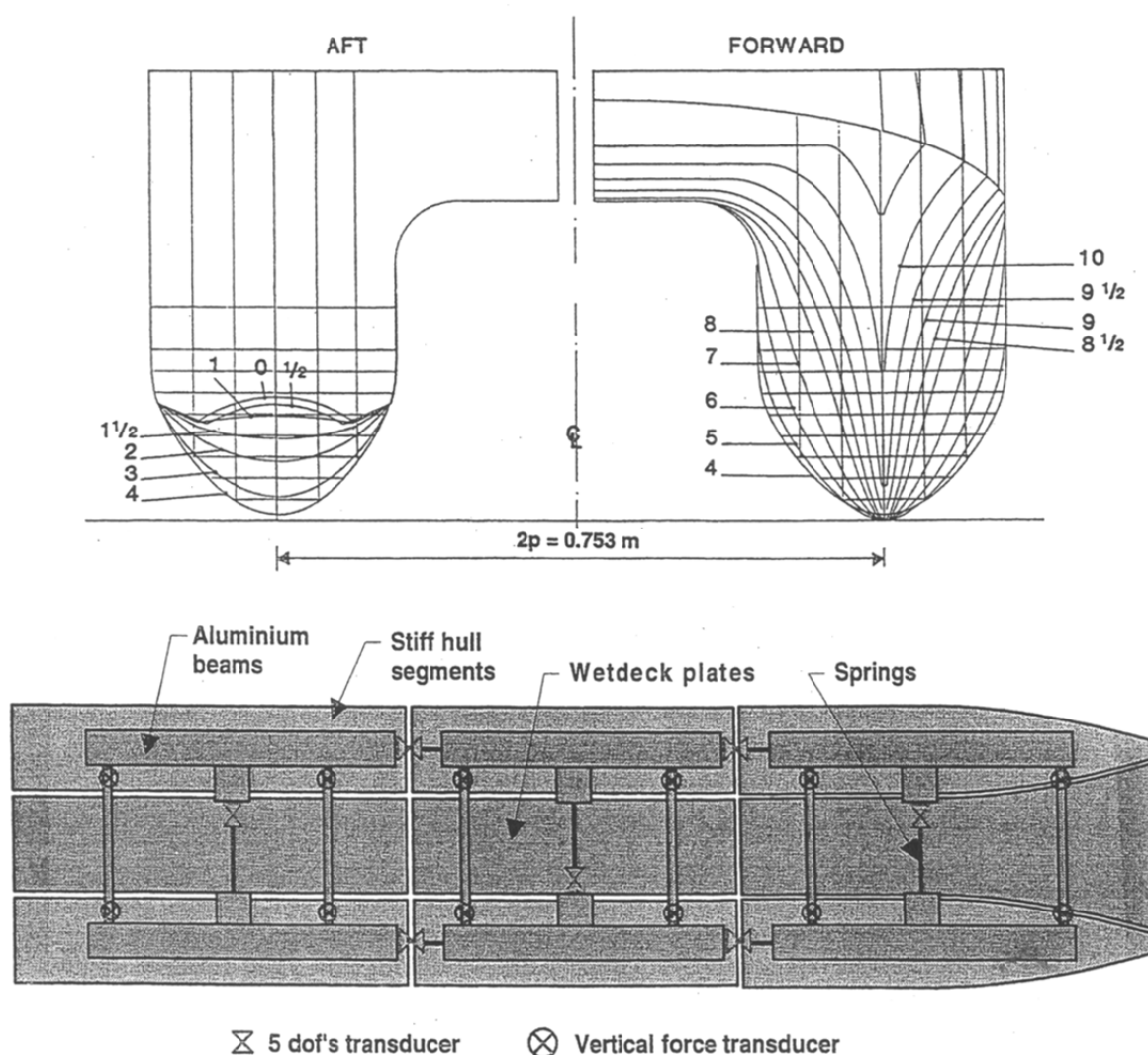


Figure 5.4 Hinged model of an elastic catamaran

6 CONVENTIONAL SHIP TESTING

6.1 General

Conventional ship testing includes the following type of model testing:

- Towing test for resistance measurements
- Propeller Open Water Test – to determine the propeller characteristics in open water (without a ship model present)
- Propulsion test in towing tank, either to determine the propulsion power directly, or to find the propulsion factors (thrust deduction, effective wake, and relative rotative efficiency) when done in combination with resistance test and propeller open water test
- Wake survey – towing test where the velocity distribution in the position of the propeller is measured. The wake distribution resulting from this test is important input to a cavitation tests and for the propeller design.
- Streamline paint test – usually performed with working propeller(s) – to determine the flow pattern around the hull, in order to detect flow separation and optimise inclination of propeller shaft brackets, position of bilge keels, and direction of tunnel thruster opening grids.
- Cavitation tests - for identification of propeller cavitation problems.
- Manoeuvring tests - for check of manoeuvrability

6.2 Towing and propulsion tests in towing tank

The traditional purpose of ship model tests, and still the main activity of “commercial” towing tank testing, is to predict the speed-power relation for a ship before it is built.

All shipbuilding contracts contain strict requirements to the speed the new ship shall do for a given engine power. Failure to meet the contractual speed requirement leads to heavy fines for the yard, and ultimately that the ship owner may refuse to take ownership of the vessel. Thus, it is important for the ship yard to determine before the building has started how fast the ship will go on the trials. Even when main dimensions are fixed, the speed performance of the design can be improved significantly (up to 20% on power) by careful design of bow (including bulb!), stern and propulsion arrangement. Thus, it is common to make modifications to the details of the ship design based on the observations during the model tests.

Conventional towing tests, propulsion testing and scaling of results to full scale are discussed in details in the basic course in Hydrodynamics. Reference is made to Steen (2011). A short summary will be given here.

6.2.1 *Towing tests for resistance measurements*

In a towing test, the model is connected to the towing carriage through a force transducer, commonly called resistance dynamometer, so that all forces in the direction of towing is taken by

the transducer. In addition, the model is kept on a straight course by so-called trim posts, which are devices that only provides lateral forces, but leaves the model free to heave, trim, and surge. Usually, the trim posts have an arrangement for measurement of the sinkage fore and aft. The speed is usually measured as the speed of the carriage. A sketch of the set-up for towing tests is shown in Figure 6.1

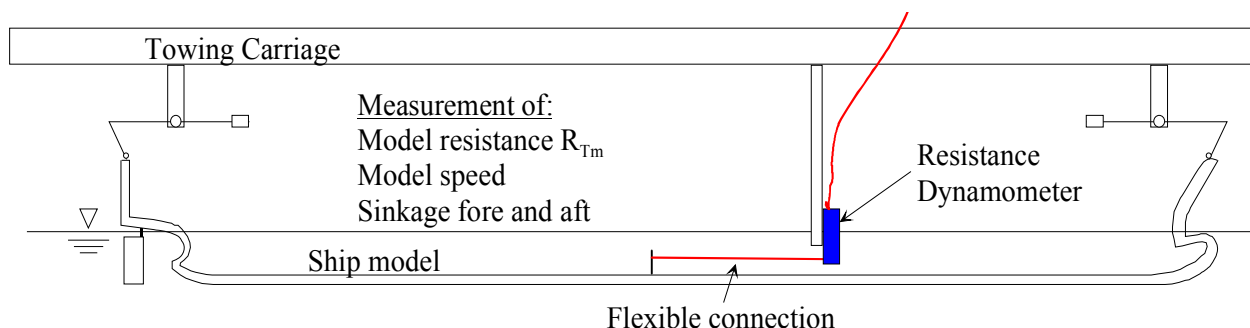


Figure 6.1 Test set-up for towing tests

The procedure for the test is to accelerate the model to wanted speed, then measure the resistance at constant speed for at least ten seconds, and then gradually stop the carriage. For heavy models, it is common practice to have a locking mechanism (“clamp”) to unload the resistance dynamometer during acceleration and deceleration.

In the resistance test, the model is usually equipped with rudder and propeller shaft(s), but with the propeller(s) replaced with dummy bosses made of lead, so that the weight of the dummy boss equals the weight of the propeller model. Furthermore, the model is equipped with a turbulence stimulator, to make sure that the flow over the hull is turbulent also at low speeds. The turbulence stimulator is usually placed 5% of L_{pp} aft of FP. The turbulence stimulator is commonly a 1 mm diameter tread glued to the hull normal to the flow direction. For high speed models, studs are commonly used for turbulence stimulation. Studs are 2-3.5 mm diameter cylinders mounted normal to the hull surface, protruding 2-2.5 mm from the surface, with about 20-25 mm distance between the studs. Sand strips are also used. That is a 5-10 mm wide strip of sharp edged sand with grain size of about 0.5 mm which is glued to the hull. Turbulence stimulation might in addition be required on appendices and separate parts of the hull protruding out of the boundary layer of the hull, like a sonar dome, or the keel of a sailing yacht. On appendices, sand strips are the most common form of turbulence stimulation.

6.2.2 Propulsion tests

In the propulsion test, the model is the same as for the resistance test, except that the dummy bosses are replaced with geometrically scaled model propellers. The propellers are driven by electric motors. Between the electric motors and the propellers are mounted propeller dynamometers, which measure propeller thrust and torque. In addition, the propeller revs are measured. See Figure 6.2 for a sketch of the set-up.

For conventionally shafted propellers, the propeller dynamometers are located inside the hull. Thus, the friction in the propeller shaft seals and bearings will influence the measurement of torque (since one measure the torque inside the hull, but want to know the torque delivered to the propeller). Thus, it is common to do measurements of the so-called idle torque, which is the torque

measured with only the propeller boss present. This is done for several propeller speeds, so that corrections of the measured propeller torque can later be done by interpolation.

Since the frictional resistance coefficient is larger in model than in full scale, it is required to partly tow the model, in order to obtain the correct loading of the model propeller. This can be done in two different ways:

1. Application of a constant force F_D , by using a weight and pulley system as indicated in Figure 6.2. The propeller revs has to be adjusted so that the model reaches the specified speed. This is called *continental method* of propulsion test.
2. The model is connected to the resistance dynamometer in the same way as in the resistance test. The speed is then decided by the carriage speed. The propeller revs are varied to obtain a towing force equal to F_D . It is usually required to do about three runs in the tank at each speed to find the propeller revs that give a towing force equal to F_D . This is called the British method of propulsion test. Since it requires more runs, it is less used. However, the fact that it gives results for different values of F_D means that the results can easily be re-scaled to different scale ratios and different powering prediction methods.

The towing force F_D is found from the difference in resistance coefficients in model and full scale. This difference is primarily due to the difference in frictional resistance coefficients, but differences in air resistance, transom stern resistance, and appendage resistance might also be included.

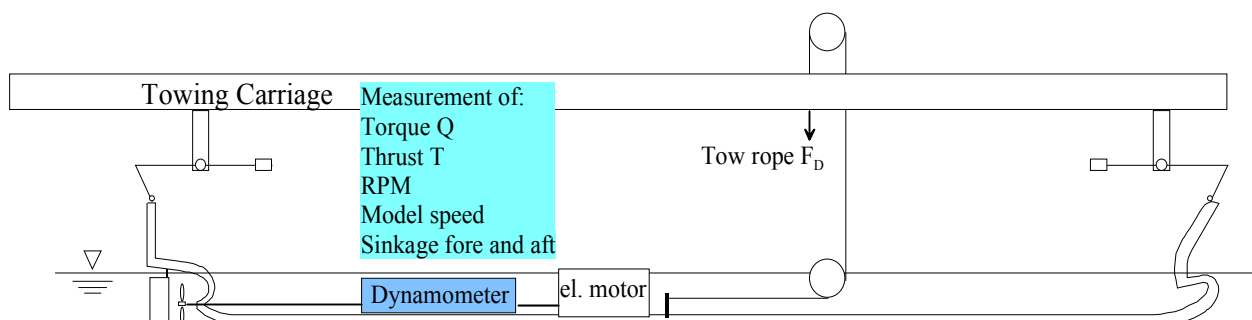


Figure 6.2 Test set-up for propulsion tests. Continental method

6.2.3 Propeller open water test

The purpose of the propeller open water test is to measure the performance of the propeller alone, without the hull present. When combined with the results of the resistance and propulsion tests one can identify the interaction effects between the propeller and hull, like effective wake, relative rotative efficiency and thrust deduction.

In the propeller open water test, the propeller is mounted on a propeller open water dynamometer, which is like an extremely slender thruster with pulling propeller (see sketch in Figure 6.3). The propeller is equipped with a dummy propeller cap. The resistance (thrust) and torque of the dummy propeller cap and propeller hub is measured in separate runs and subtracted from the results, so that one effectively gets the performance characteristics of the propeller blades. One measures the propeller torque, thrust, and revs, as well as the speed. Tests are usually

done at constant propeller revs, varying the speed from zero to a speed that gives zero propeller thrust.

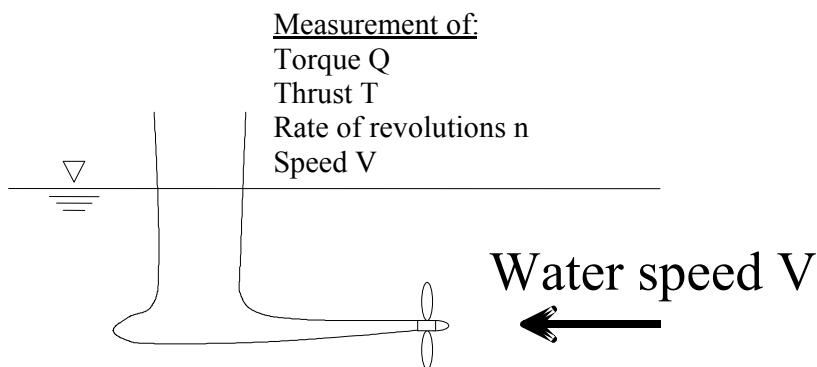


Figure 6.3 Test set-up for propeller open water tests.

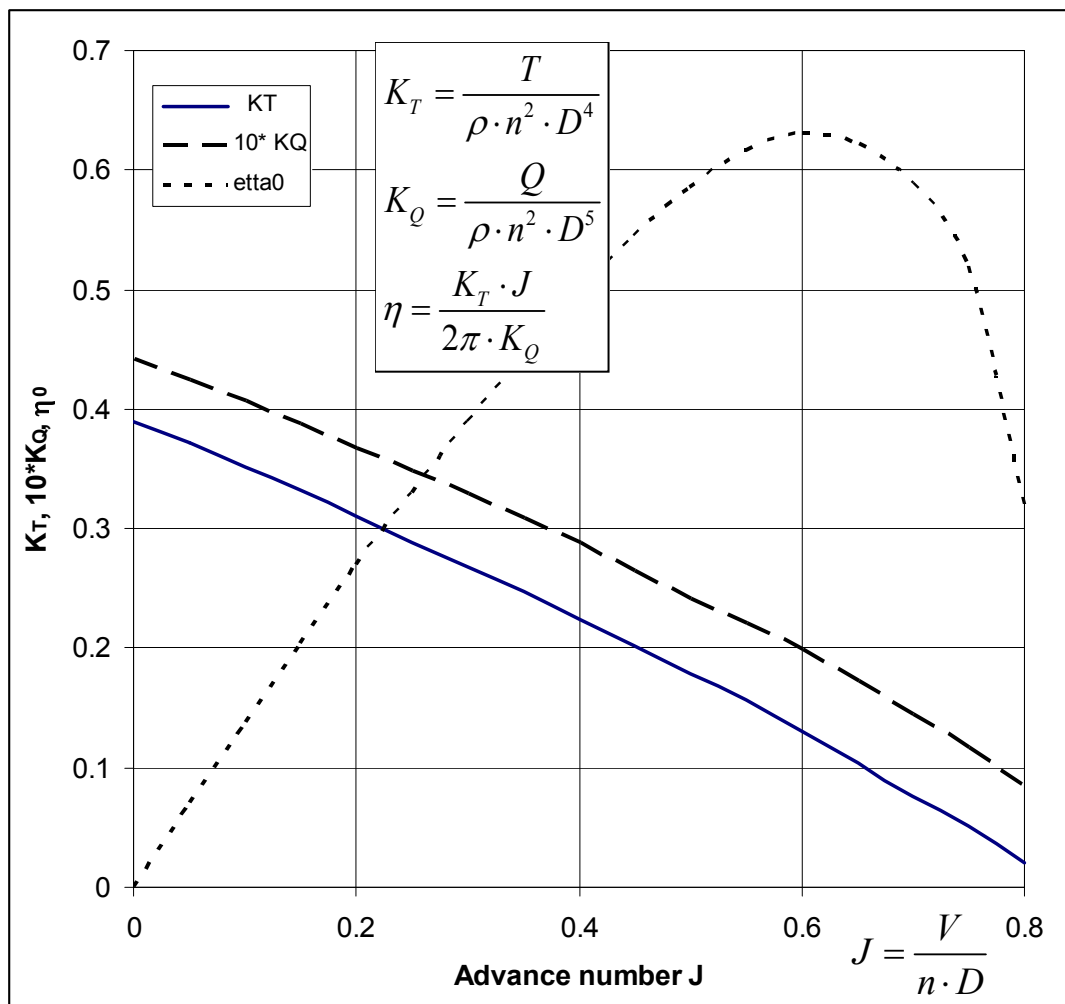


Figure 6.4 Propeller open water diagram, as resulting from a propeller open water test.

The results of the open water test are compiled into an open water diagram, as shown in Figure 6.4.

For ships with ducted propellers, the ducts are not present in the resistance test, but included in the propeller open water tests. In the propeller open water test, the duct thrust is measured separately.

For ships with thruster propulsion, the entire thruster unit is used for the propeller open water test. Thus, the thruster unit itself is considered as “the propulsor”, and the resistance of the thruster body should not be included in the resistance measured in the resistance test.

6.2.4 Powering performance prediction

The purpose of the resistance, propulsion and propeller open water tests is mainly to determine the required shaft power of the full scale ship at different speeds. The ITTC standard for powering prediction is given in Annex E. A detailed description of powering performance prediction is also found in Steen (2011). The details of the powering prediction method differs between towing tanks, so that for instance the method in use at MARINTEK is not exactly the same as the method described in Annex E. A brief outline of the performance prediction method is given here.

With the results from the mentioned tests available, the powering performance prediction is done as follows:

1. The model scale values of the propulsive coefficients thrust deduction t , relative rotative efficiency η_R , and effective wake w are found from analysis of the propulsion test result, using also the resistance and open water test results.
2. Full scale propulsive coefficients are determined by assuming that thrust deduction and relative rotative efficiency are free of scale effects, while the wake is scaled (at least for single screw vessels).
3. The resistance is scaled to full scale, by separating viscous and residual (or “wave”) resistance, and scaling the two parts differently.
4. The propeller open water diagram is scaled to full scale. (This is not done by all model basins – MARINTEK is using the model scale open water diagram also in full scale)
5. The full scale propulsion point is determined by interpolation in the full scale propeller open water diagram. The propulsion point means the value of J , which by use of the full scale open water diagram gives the value of K_Q .
6. The full scale propeller revs and torque are calculated from the full scale propulsion point values of J and K_Q . Then power is calculated.

6.3 Cavitation tunnel tests

6.3.1 General

Testing of cavitation problems will require a facility that gives the possibility to test with correct cavitation number. Cavitation testing facilities is described in chapter 3.3. The purpose of cavitation testing can be one or more of the following reasons:

- Cavitation induced erosion of propeller blades.

- Effect of cavitation on propulsion efficiency
- Vibrations and noise.

The pressure fluctuations caused by the cavitation will introduce pressure variations on the hull, which again can lead to hull vibrations and generation of noise. Another problem is that the cavitation induced pressure pulses can introduce noise, which is disturbing to passengers, or affecting acoustic positioning system or other type of instrumentation. This type of noise can also be a problem for fishing vessels by the direct effect on the fish.

6.3.2 Modelling requirements

The cavitation test has to be carried out in such a way that the main forces as thrust and torque are similar in model and full scale. In principle this will require geometrical similarity of both propeller shape and ship hull. Due to the limited dimensions of most cavitation tunnels, there will be a problem with the tunnel wall effects and with the free surface.

Kinematic similarity requires that the inflow velocity distribution to the propeller is correct and that the tests are run at same advance ratio as in full scale:

$$J_M = \frac{V_M}{n_M D_M} = J_F = \frac{V_F}{n_F D_F}$$

where V is the speed of advance of the propeller, n is the rate of revolution and D is the propeller diameter.

For the dynamic similarity requirement, it is often assumed that the propeller is sufficiently well submerged to avoid surface waves. The requirement to equal Froude number can then be abandoned. The Reynolds number has to be high enough to ensure turbulent boundary layer at the propeller blades, as the actual flow regime will influence the cavitation. As a practical lower limit,

$Re = \frac{UL}{\nu} = 5 \cdot 10^5$ is often used. L is here taken as the chord length of the propeller blade at 0.7 radius.

To ensure the same risk of cavitation in model and full scale, equality in cavitation number is required as discussed in chapter 2.6.

The Weber number (see chap 2.3.5) may also have an effect, especially for the start up of cavitation. Closely related is the requirement of a certain amount of cavitation nuclei in the water, see Huse (1999). The physics of incipient cavitation is such that if the water is completely pure, the cavity (cavitation bubble) must necessarily start as an infinitely small bubble, with infinitely small radius of curvature and thus infinitely large inside pressure due to the surface tension. But with an inside pressure larger than the saturated vapour pressure the cavity will collapse. Thus, infinitely small cavities cannot exist, and since larger cavities have to start as infinitely small ones, they should also be physically impossible. In natural sea water there will always be a certain amount of cavitation nuclei's and the cavitation process can develop. It is therefore very important that the gas content in the water in the cavitation tunnel is sufficiently high to provide an adequate level of cavitation nuclei.

6.3.3 Test Procedure

The standard procedure for testing in cavitation tunnels can be summarised as follows, see also Huse (1999):

1. Choose flow velocity in test section based on actual advance ratio, J .
2. Install aft-body model and adjust wake field by mesh screens
3. Install propeller model
4. With atmospheric pressure in the tunnel, adjust propeller rate of revolution (and/or flow velocity) until the propeller thrust is correct according to open water and propulsion tests in the towing tank. This is called the "thrust identity" principle.
5. Keeping flow velocity and rate of revolution from bullet 4 constant, reduce the tunnel pressure until the specified cavitation number is achieved.
6. Do necessary cavitation observation and measurements.

During the test the following parameters are measured:

- Propeller rate of revolution
- Thrust
- Torque
- Static tunnel pressure
- Water speed in the test section

In addition to the above measurements, visual observation of the propeller cavitation is an important part of the tests. The visual observations are done by stroboscopic illumination at different angular positions of the blades. Photography and high-speed film or video recording is often used for documentation. Based on experience one can already from the visual observations draw conclusions whether the actual cavitation is acceptable or not, and, if required, which modifications of the propeller geometry should be recommended to improve the performance with respect to cavitation. For instance, experience is that erosion is easily produced by bubble cavitation, particularly if the bubbles collapse on the blade surface, while limited amounts of sheet and vortex cavitation are considered harmless.

6.4 Maneuvering tests

6.4.1 General

The purpose of manoeuvring model tests is two-sided:

1. Direct test of the manoeuvring behaviour of the ship with active use of rudder during the test
2. Establish the hydrodynamic quantities required in the in the manoeuvring equations from the tests

For item 1, a large space will be required and these types of tests are commonly carried out in seakeeping basins. A free running, self-propelled model with steering gear and possibility of automatic rudder control is used. Maneuvering tests are usually carried out according to specified standard maneuvers. During the tests a prescribed use of rudder is applied as input. The horizontal motions of the model (i.e. surge, sway and yaw) and the actual rudder angle are measured during the tests. The tests results are used for determination of the maneuvering performance of the model. The most used standard maneuvers are the zig-zag test, the spiral tests and turning circle test.

The requirement to scaling for maneuvering tests is to use Froude scaling in addition to the geometrical similarity requirements. For dynamic tests also the inertia distribution must be correctly scaled, see chap 5.2. Possible scale effects will be introduced from viscous forces.

The most common and reliable method to determine the coefficients in the manoeuvring equations, see Berg (2000), is still model test results. The coefficients from model test can be obtained either from analysis of tests results with free running models or from test with fixed model where the forces and moments acting on the model is measured during the tests. For testing with fixed model three different approaches is used:

- Planar motion Mechanism (PMM) tests
- Towing tank tests
- Rotating arm tests

These methods are discussed in the following.

6.4.2 Towing Tank tests

In a towing tank the model can be towed at constant speed and yaw angle. The model must be free to pitch, roll and heave, but restrained in sway and yaw. The sway forces and yaw moment are measured as a function of towing speed and yaw angle. Both the linear and quadratic terms are obtained if tests are carried out for several towing speeds and yaw angles. The yaw angles are usually limited to be within 10 degrees as this is considered as a realistic maximum drift angle during manoeuvring operations.

Similar test can also be carried out for different rudder angles. The rudder forces are measured. From these tests also the influence of the rudder on yaw moment and sway forces can be established.

6.4.3 Planar Motion Mechanism (PMM)

This is the most used method for determination of the hydrodynamic coefficients in the maneuvering equations. PMM is mounted to the towing carriage in a towing tank or a seakeeping basin. A typical example of PMM set-up is shown in Figure 6.5. The tank has to be sufficiently wide to avoid interference between the model and the tank wall. For shallow water tests the water depth should be correctly scaled as the bottom effect may influence the measured forces.

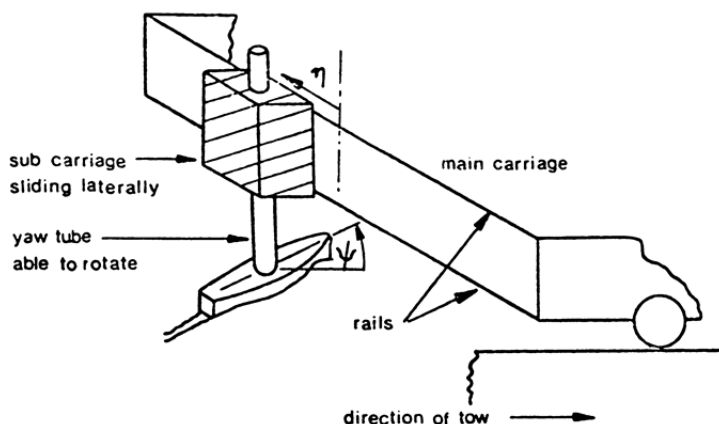


Figure 6.5 *Planar Motion Mechanism*

The model is usually connected to the PMM such that it is free to heave and pitch and fixed in roll. Great care is required when aligning the model and this should be checked before and after the test.

The following sequence of tests should be carried out:

1. Oblique towing tests,
2. Pure sway tests
3. Pure yaw tests
4. Yawing with drift.

During the tests the hull forces in surge and sway direction and the yaw moment are recorded. If rudder is applied the rudder lift forces should also be measured. The oscillation frequency should be selected sufficient low to be free from frequency dependence. Further interference with tank wall must be avoided. The drift angle, drift angle speed and sway speed should be varied to cover the realistic range during manoeuvring conditions.

A further description of recommended tests procedure for PMM is given by ITTC (1996), Manoeuvrability Committee.

PMM tests are regarded as the most reliable and controlled method for determination of the hull forces as input to the manoeuvring equations. The main draw back with PMM testing is the complexity and cost connected to running these tests. To establish a complete set of hull forces data a large number of test cases are required.

6.4.4 Rotating arm

In rotating arm tests the model is moved in a circular path by a mechanical driven rotating arm. The principle is shown in Figure 6.6. The model is restrained in roll. It is possible to vary the radius of rotation and also the drift angle can be varied. With this set up the model will have a correct combination of speed and radius for a turning circle test.

During the tests the sway force and yaw moment are measured. With this test method the sway and yaw coefficients together with the different non-linear coupling terms can be established. In addition surge and heel moment during turning can be measured.

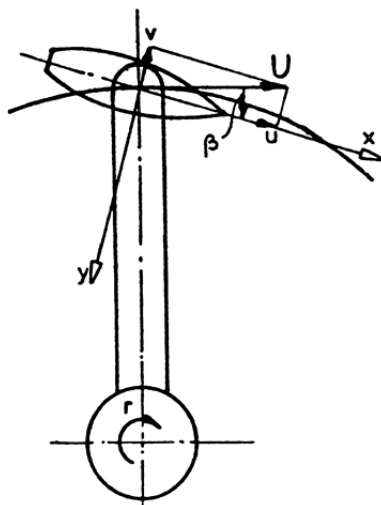


Figure 6.6 *Rotating arm Planar Motion Mechanism*

7 SEAKEEPING TESTING

7.1 General

Conventional ship testing as described in the previous section cover the calm water testing for ships. This is what we often call the classical model testing. In this chapter testing of ships in waves will be discussed.

For seakeeping, a term that can be interpreted as ship behaviour in rough weather, the following type of test results will be important:

1. Ship motions (heave, roll and pitch) and accelerations
2. Slamming loads (bottom slamming)
3. Green water on deck
4. Added resistance and speed reduction in waves
5. Global loads in hull beam

The first item is important for comfort evaluation (crew and passengers) and evaluation of criteria for voluntary speed reduction. Slamming loads are important for structural strength both locally and global (whipping) and will influence voluntary speed reduction. Green water is important for safety and possible loading on deckhouses and equipment. Added resistance determined the involuntary speed reduction and is an important parameter for fuel consumption. Optimisation of resistance performance based on only calm water resistance can end up with a design solution which is not the optimum, as the ship will see wave conditions where added resistance gives a significant contribution to the total resistance, in a large part of the total operation time. For a general discussion of seakeeping performance, see Lloyds (1989).

Seakeeping tests can be carried out in towing tanks (equipped with wave maker or in seakeeping basins/ocean laboratories. Towing tank testing is limited to head and following sea, while in larger basins arbitrary wave heading can be covered.

7.2 Test Requirement

For testing in waves, gravity forces will be the governing force contribution and the Froude scaling has to be applied. For scaling of waves this implies that the wave height follows the geometrical scale ratio and the wave period follows the square root of the scale ratio, see also chapter 2.4.

For seakeeping testing the dynamic motions of the model are the key results and hence inertia forces will be important. This implies that the mass distribution of the model needs to be correctly scaled, as discussed in chapter 5.2.

For seakeeping testing the main topic of interest is usually the wave frequency response. If slamming forces is a part of the purpose of testing one has to ensure adequate equipment and

sufficient sampling frequency to cover the very fast response of this type of loading, see also the discussion in chapter 4.10.

The models used for seakeeping testing are usually considered to be “infinitely stiff”. If whipping and/or springing responses are a part of the test purpose, also the global elastic properties of the hull model needs to be correctly scaled. This is discussed in detail in chapter 5.3. For these resonance frequency phenomena the response can be considered to be high frequency (HF) and well above the range of the wave frequency.

7.3 Test set up

Possible principle arrangements for connections between the model and carriage are illustrated in Figure 7.1. Connection type a) is only used for measurement of wave excitation forces. For alternative b), c) and d) the model is free to heave and pitch, but with different level of constraining the surge motions. In towing tank testing (only head and following seas) alternative c) and d) are most commonly used. Alternative d) will require a self-propelled model. For this case the surge connection has to be with very low friction. This can be achieved by using hinged mechanism, restrained sideways, but free to move vertically and longitudinally, connected at bow and stern of the model.

For Seakeeping basin testing alternative e) is the most commonly used. In this set up only the powering and instrumentation cables are connected between the model and carriage. The connection has to be sufficiently soft to avoid influence on the ship motions. This alternative will require a self-propelled model with heading control. A carriage system that is able to follow the model track will also be required. For testing in arbitrary wave heading a carriage with a sub-carriage for transverse motions will be required.

Alternative f) is a completely free running model. All instrumentation and powering supply have to be carried by the model. The measurements must be recorded onboard or transmitted by telemetry. This set-up does not require any carriage system. However the equipment onboard is heavy, especially batteries for propulsion power, and will therefore require a quite large model. Alternative f) is mainly used for testing models outside laboratories, on lakes and in the sea.

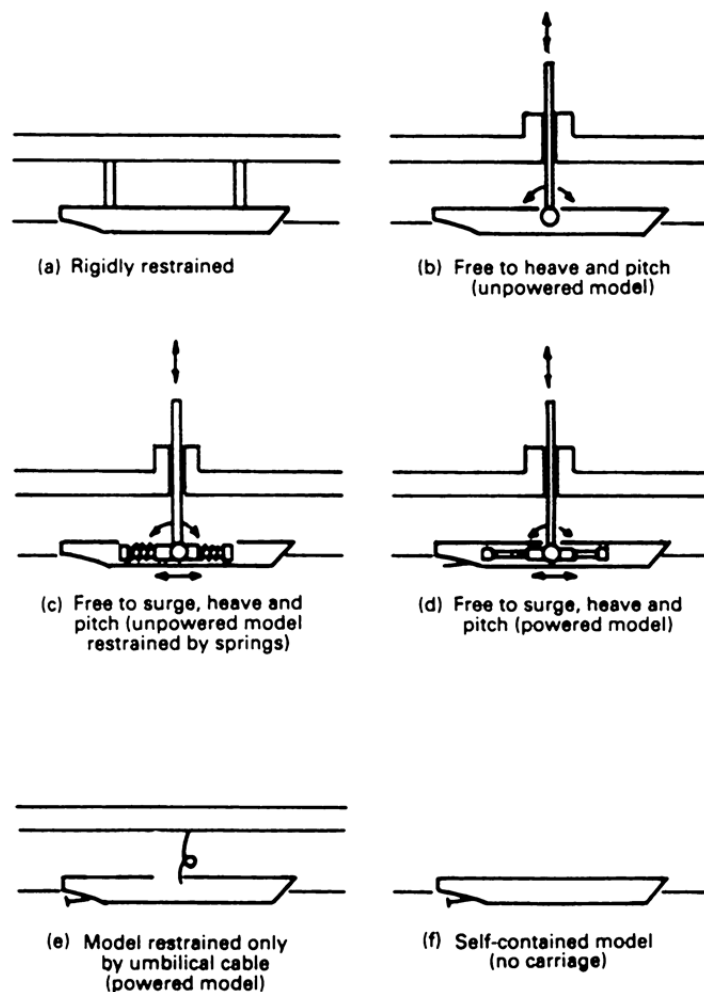


Figure 7.1 Possible arrangement for mounting the model under the carriage
(From Lloyd (1989))

7.4 Test Procedure

For seakeeping testing, both regular and irregular waves are commonly used. Regular wave testing is normally used for obtaining the motion RAO's and added resistance at the wave frequency and is often used for verification of numerical calculations. Irregular waves are used to study the performance and establish design values at actual conditions including statistical distribution and extreme values.

The wave calibration should be carried out prior to the testing and without the ship model in the tank to avoid wave reflection from the model on the wave measurements. In a long and narrow towing tank the wave characteristics can vary along the tank length. This is in particular a problem for short and steep waves. This variation is connected to the stability of the waves as they propagate downstream the tank and also to the effect of the tank walls. During the wave calibration the wave measurements should therefore be carried out in different positions along the tank to determine possible position dependency for the wave height (for regular waves) and spectral shape (for irregular waves).

If the phase information between the wave elevation and motion response of the model is required, it is necessary to measure the incident wave by a wave gauge mounted at the carriage in a known position relative to the position of the model. The difference in position between the wave gauge and model (measured in the wave direction) has to be accounted for when calculating the relative phase. It is also important to locate the wave gauge in a position where the distortion of the wave caused by the model is avoided.

Both self-propelled and towed model are used in seakeeping tests. In towing tests a prescribed towing speed is kept constant during the run. For self-propelled models two different procedures can be applied:

- Constant propulsion power applied during the run. The carriage speed adjusted to follow the model
- Constant carriage speed. Propulsion power adjusted during the run to follow the carriage.

The measurements during the test will depend on the actual purpose of the tests. A typical set of measurements during a seakeeping test will be:

- Towing resistance (when towing the model)
- Thrust, torque and rate of revolution (for self propelled models)
- Speed
- Ship motions; always heave and pitch, but also surge, sway, roll and yaw may be measured, depending on set-up.
- Vertical acceleration; typically at FP
- Relative motions; typically in bow and stern areas
- Green water on deck; measured by wave gauges on deck or by force transducers to measure amount of green water
- Impact loads; bottom slamming, bow flare or other exposed locations. Measured by pressure cells or force panels.
- Video recording

For a model running at a wave heading, β , ($\beta = 180^\circ$ is head sea) the encounter frequency, ω_e , is given from:

$$\omega_e = \omega - \frac{\omega^2 U}{g} \cos \beta$$

where ω is the wave frequency and U the ship speed. When testing in following waves the encounter frequency may be very low. This can introduce a practical problem as the number of waves encountered during one run along the tank will be low, and a number a repetition runs with different realizations of the incoming waves will be required to get a proper confidence of the statistical distribution of the responses.

7.5 Tank wall effects

The ship model will generate its own wave system, both due to diffracted waves and radiated waves due to the ship motions. These waves will reach the tank wall and be reflected back to the model as shown in Figure 7.2. If the model speed is low the reflected waves will hit the model as shown on the upper drawing in Figure 7.2, and the response of the model will be influenced.

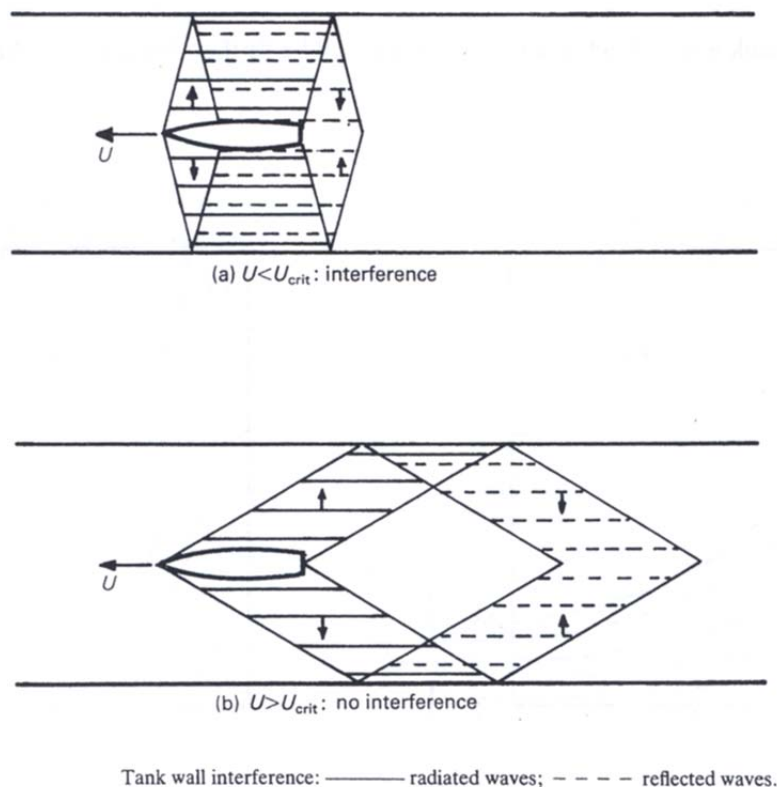


Figure 7.2 Illustration of tank wall effects. (From Lloyd (1989))

The phase velocity of the radiated waves is:

$$c_e = \frac{g}{2\omega_e}$$

The travelling distance is from tank centre (assuming the model in this position) to the tank wall and back to the model, i.e. equal the breadth of the towing tank, B . The travelling time is then

$$t_w = \frac{B}{c_e}$$

Interference will occur if the model moves a distance less than its own length, L_M during the time t_w , i.e. if :

$$U < U_{crit} = \frac{L_M}{t_w}$$

Combined with the equation for encounter frequency, ω_e , the following relation is obtained for the critical model speed in head sea waves:

$$U_{crit} = \frac{g}{2\omega} \left[\sqrt{1 + \frac{2L_M}{B}} - 1 \right]$$

Here, ω is the wave circular frequency. It follows that the critical speed increases with the wave length. The resulting critical Froude number is shown in Figure 7.3 for head sea and following waves. For following waves tank wall interference will always occur for model lengths greater than $B/4$, which is usually the case.

The tank wall effect as an error source will be further discussed in chapter 10.

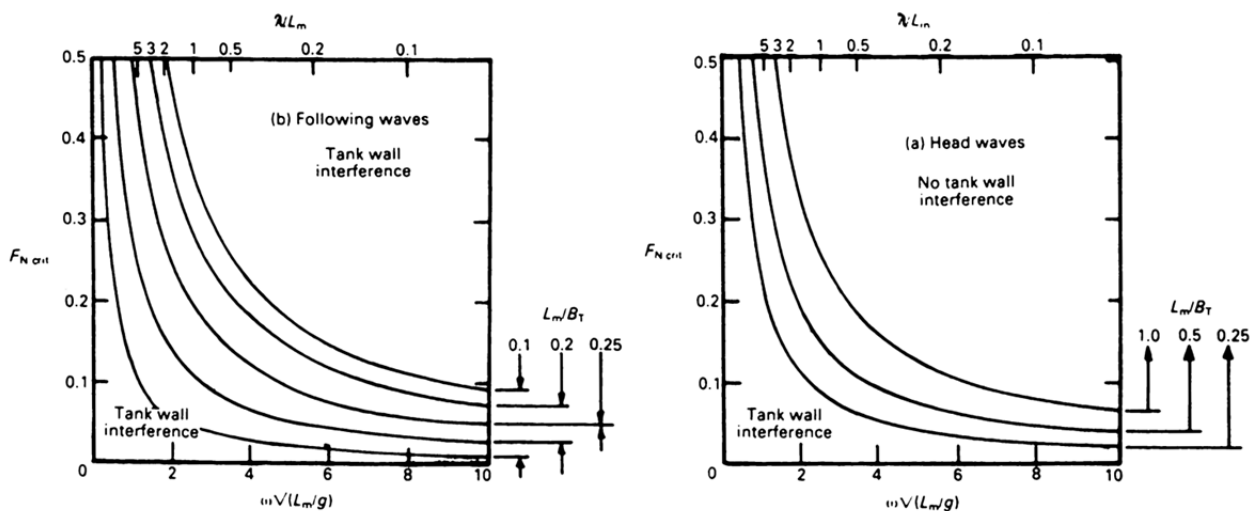


Figure 7.3 Critical Froude number for tank wall effects. (From Lloyds (1989))

8 OFFSHORE STRUCTURE TESTING

8.1 General

In this chapter testing of offshore structures will be discussed. Typical ship testing as described in the two previous sections cover ships designed and used for conventional transportation purposes. The term “offshore structures” is in this presentation interpreted as all other applications. Examples will be moored, floating platforms and ships applied for production and/or storage of oil/gas, fixed structures, risers, mooring systems, floating and submerged bridges, fish farming structures, etc.

Testing of offshore structures cover a wide range of model testing from simple decay test in calm water intended to determine hydrodynamic coefficients to set-ups where complex platform structures including mooring and riser system exposed to waves, wind and current are modelled.

Typical objectives for testing of offshore structures includes:

1. Determine hydrodynamic damping, added mass, motion RAO's and other hydrodynamic quantities used as input to numerical simulations.
2. Verify concepts to ensure that all important physical phenomena are properly understood and accounted for during the design phase.
3. Establish operational limits.
4. Generate data for calibration and verification of numerical tools for actual type of structure and loading conditions.

For new type of concepts item 2 will often be the most important. Many examples exist where model testing has revealed unexpected problems with new concepts. In some cases the problems are of such nature that they make the concept unfeasible. In other cases the problems may be of such a nature that they can easily be solved, once you are aware of them.

In Appendix B an example of a specification for testing of an offshore structure is presented. The actual case is a turret moored floating production and storage tanker (FPSO).

8.2 Test Requirements

Testing of offshore structures is for most cases carried out for fixed or moored structures, which means zero speed. Problems with wall reflection effects (see chap. 7.5) will therefore make the use of relatively narrow towing tanks very questionable for this type of testing. Also the requirements to wind and current generation are in general not available in towing tanks. Ocean laboratories will therefore be required in most cases for offshore testing.

The requirements to scaling of models and waves are to a large extent similar to for seakeeping testing (see chapter 7.2). Requirements to modelling of mooring systems are given in section 5.3.3.

The motion responses that can be observed for offshore structures are split into different frequency regimes dependent on excitation source and dynamic properties of the structures:

- Wave frequency (WF) motions, i.e. motions taking place in the frequency range of the used wave spectrum. The excitation is mainly linear wave forces.

- Low frequency (LF) motions, i.e. motion taking place at resonant frequency well below the wave frequency range. The excitation is mainly non-linear wave forces (wave drift forces), but also the dynamic wind and for some special cases current induced oscillation can be important excitation sources. This low frequency response is also often called slow drift motion.
- High frequency (HF) motions, i.e. motions taking place at resonance frequencies well above the range of the wave frequency. The excitation is mainly non-linear wave forces including impact loads.

The low frequency motions will be important for all type of moored structures. Depending on the water depth, typical resonance periods can be in the range 40-500 s. The low frequency motions are often found to be the main source both for platform motions and mooring forces.

The high frequency motions have been a problem for Tension Leg Platforms (TLP). The axial stiffness of the vertical tethers (usually steel tubes) connecting the TLP to the seabed introduces a resonance frequency in heave, roll and pitch. Typical resonance periods will be 2.5-4 s, which will be well below the wave period range for wave excitation. Another example of HF motions is whipping and springing of ships.

8.3 Deep water structures requirements

The discussion of scaling has so far been limited to cases where it is practically possible to achieve geometrical similarity. An example where it is difficult or impossible to correctly model the actual geometry of the system is offshore structures in deep water. Deep water is usually defined as water depths greater than 1000 m.

Traditionally, offshore structure testing has been carried out at a scale of about 1:50. It has been shown that when using standard equipment (wave makers, instrumentation, etc.) the scale ratio can be extended to about 1:100 without severe reduction of quality of measurement. The maximum water depth in existing test facilities is 10 m, see chapter 3.4. This limits the practical water depth to 500-1000 m for standard testing in existing test basins. Basins with much larger depths are not considered feasible of economical reasons. It should be noted that also the length/breadth have to be increased as well to be able to model the horizontal extent of the mooring system, see Figure 8.1

Different solutions of the problem have been suggested; see Stansberg et.al. (2000) and Bouchner et.al. (1999):

1. Use of ultra small scale model testing ($\lambda=1:\gg 100$).
2. Passive equivalent mooring system or truncated hybrid system.
3. Solutions with active control systems, based on real-time simulation of the mooring system response
4. Outdoor testing

For case 1 the complete system is modelled and no numerical calculations will be required. However increasing scale ratio will increase the scale effects, especially for cases where viscous forces are important. Physical modelling will be difficult. Note that mass and load scales with third

power of scale factor ($1/\lambda^3$). As an example scale 1:200 gives that 1 g in model scale corresponds to 8 tonnes in full scale. Wind and wave current generation will become increasingly problematic and waves will be significantly influenced by surface tension.

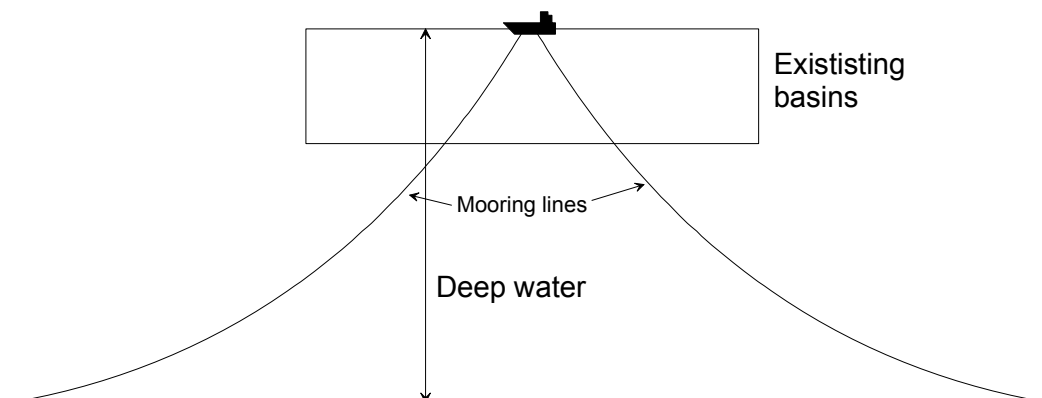


Figure 8.1 Required basin size for testing in deep water

For case 2 an equivalent and more shallow water mooring system, with properties as similar as possible as the deep water system, is established numerically. The equivalent or truncated system is used in the test. An example of mooring system truncation is shown in Figure 8.2. The mooring stiffness can usually be correctly modelled by this method, but mooring line and riser dynamics will not be correct. This method will therefore require extensive numerical simulations after the tests, where the dynamic coupling of the platform and mooring/riser system is treated. This process is illustrated in Figure 8.3. Using this method conventional model scale ratios can be used to cover applications in very deep water. The disadvantage is that one has to rely on numerical calculations (calibrated towards the shallow water tests) to establish design values for the actual deep water system.

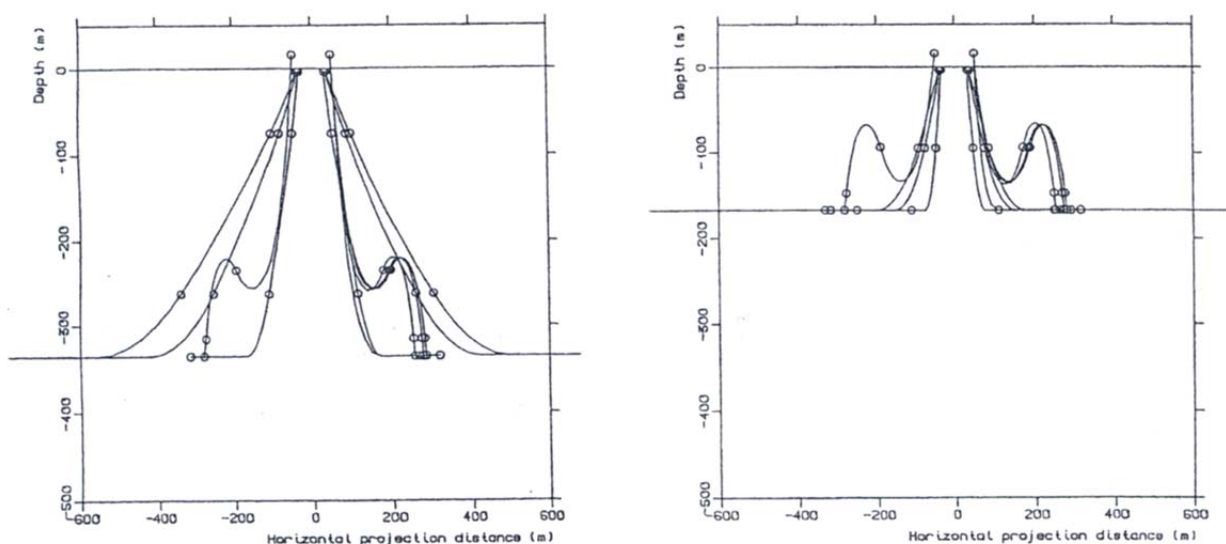


Figure 8.2 Illustration of truncation of mooring system. Left; Full system, Right; truncated system. (from Stansberg et.al. (2000))

Case 3 is in principle similar to case 2 using a truncated system, but now with active numerical control at the mooring line intersections with the basin bottom. The intention with the control is to

simulate a similar behaviour as the part of system not modelled would have generated. Complex online simulation systems will be required for this approach and the performance of the system will be dependent on correctly simulated control actions. Also this solution will therefore have to rely on the accuracy of numerical calculations.

Case 4 with outdoor testing may be a feasible solution for some cases and has been used, e.g. for testing of long risers in a current. However the fundamental problem with this approach is control of environmental conditions.

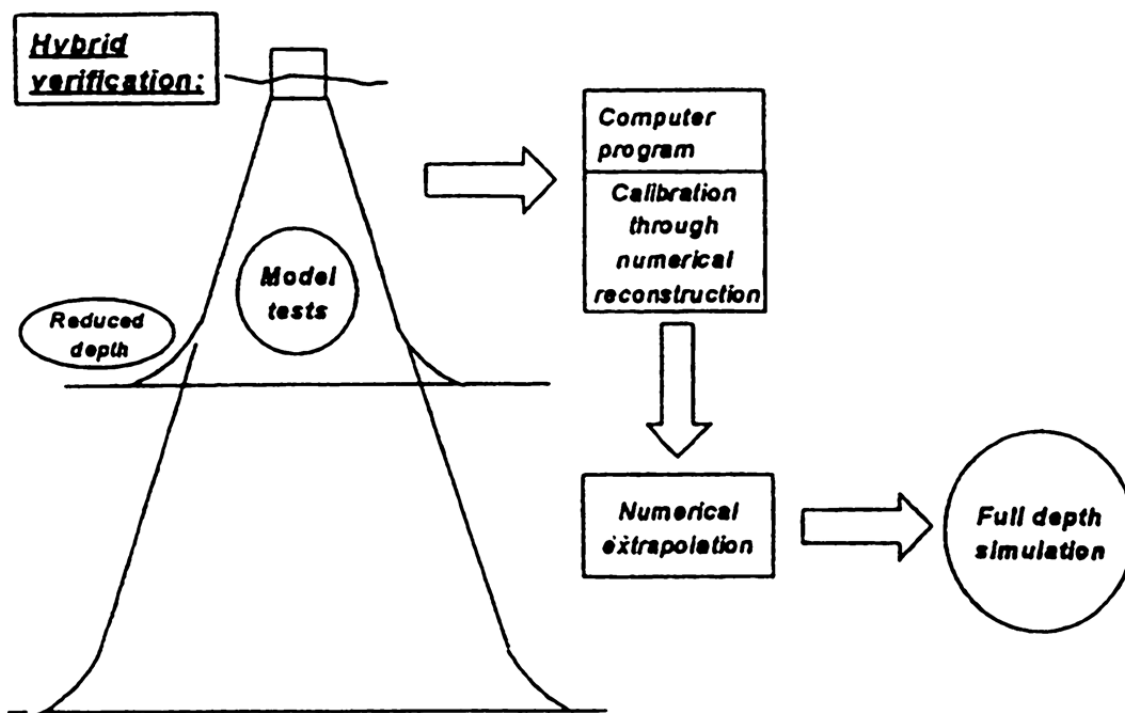


Figure 8.3 Illustration of hybrid verification procedure (from Stansberg et.al. (2000))

8.4 Test Procedure

For offshore structure testing, irregular waves are most frequently used. In a typical test set up both tests in short crested and long crested waves are often included. For generation of data for verification and calibration of numerical methods long crested waves are usually used.

As mentioned, testing of offshore structures can cover a wide range of complexity in test set ups, from simple decay tests in calm water to multi-body arrangements including mooring and riser system exposed to waves, wind and current. The test procedure will vary accordingly. For testing of moored structures the main steps in the test procedure can be summarised as follow:

- Environment calibration tests, including waves, wind and current. Carried out without the model installed. The calibration has to be carried out at the correct water depth and for the actual combination of wave and current conditions. During the calibration the measurements are carried at the mean position of the structure.
- Installation of mooring- and riser system and model in the basin. In basins with movable bottom, most of this work will be done with bottom in surface position.

- Static calibration tests for verification and calibration of system properties, including heel test of platform model for metacentric height verification, pull out tests for verification of mooring- and riser tension and geometry, etc.
- Decay tests to verify natural periods, damping and general dynamic performance, typically including platform heave, roll and pitch motions as well as surge and sway motions for mooring system.
- Tests in the defined wave-, wind- and current- conditions.

Tests are often carried out for different loading conditions of the ship/platform to cover the actual working range, typically fully loaded and ballast condition will be covered. As response of moored structure will be sensitive to the heading of the environment, several combinations of wind- waves and current headings are usually covered by the test programme.

The purpose of tests is often to verify the system performance in typical operating conditions and to establish the design values of the responses in extreme environmental conditions. In combination with different environmental directions and loading conditions a comprehensive test program with a significant number of tests will be required.

The measurements during the test will depend on the actual purpose of the tests. A typical set of measurements for testing of a moored platform/ship will be:

- Mooring line tension in all mooring lines
- Riser tension and shear forces/bending moments at platform connection.
- 6 degree of freedom platform motions.
- Accelerations at specified points
- Relative motions and wave run up at columns/bow area
- For ship structures; Green water on deck, Impact loads; bottom slamming, bow flare or other exposed locations.
- For Platforms; Impact loads towards deck structures and other exposed areas.
- Video recording

Typical duration of tests in irregular waves will be 3-6 hours (full scale time).

Analysis of the measurements is discussed in chapter 10.

9 REAL TIME HYBRID MODEL TESTING

Real time hybrid model testing means model testing in real time combination with numerical simulation. The idea is not really new, but the possibility to realize the idea is just recently occurred, due to the development of simulations and actuator technology.

The concept of real time hybrid model testing is best explained by an example; Passive anti-roll tanks are extensively used on many types of offshore ships, since they provide effective roll damping regardless of the forward speed of the ship. The sloshing flow inside the tank is hard to calculate by numerical methods, and the viscous effects require a model of the tank which is fairly large (more than a meter in length). There is of course a close two-way coupling between the sloshing water motions in the anti-roll tank and the rolling motions of the ship. The roll motions of the ship can be simulated fairly easily and accurately by industry standard programs like ShipX Vesim, Shipmo, or Wases. Thus, one have set up a hybrid model testing scheme where the ship motions are simulated using the ship simulator Vesim (which is using motion calculations from ShipX Veres), the motions calculated by Vesim are fed to a rig holding the model of the anti-roll tank, which then “shakes” the tank according to the simulated ship motions, and then the resulting forces from the tank on the rig are measured and fed back as input to the simulator in the next time step. This is illustrated in **Figure 9.1** below.

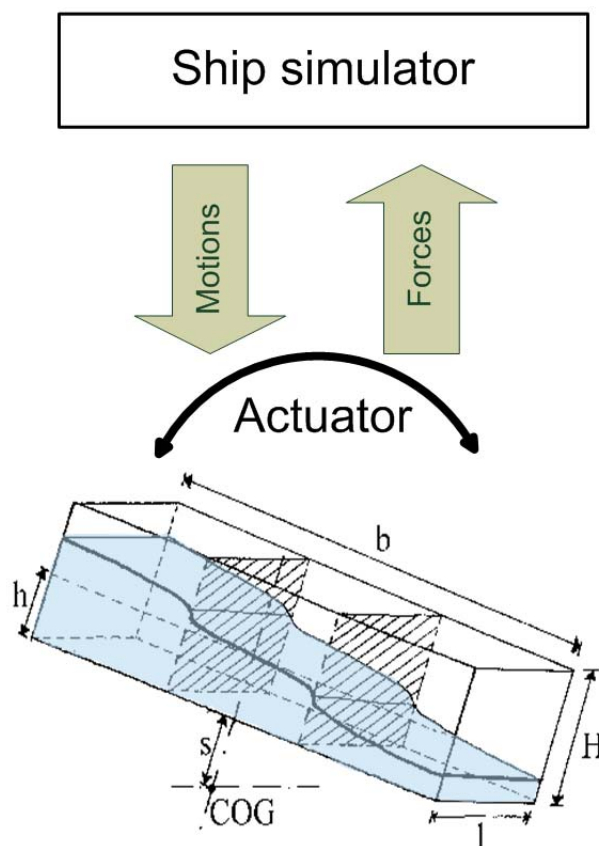


Figure 9.1 Principle sketch of hybrid testing of passive anti-roll tank

There are many types of tests which may benefit hugely from use of real time hybrid model testing techniques. Here are some examples:

9.1 Testing of floating offshore ships and platforms with mooring and flexible riser systems.

Currently, the water depth needs to be modelled in the same scale as the platform for the riser and mooring system dynamics to be modelled correctly. This places severe limits on possible model scales for verification of deep water installations – or requires the construction of extremely costly deep water model basins. The current solution is to test truncated systems, but this is not really a satisfactory solution. In a hybrid model testing scheme one would for instance model the platform, simulate the mooring and riser systems, apply the calculated forces on the platform in real time and feed the platform motions back to the simulations.

9.2 Testing of hydrofoil ships.

The hydrofoils require high Reynolds number and correctly modelled cavitation for correct performance, while the ship hull requires Froude scaling and a free water surface. Together, this requires a large towing tank with controlled air pressure (vacuum tank) with a very high speed carriage, something that doesn't exist. The hybrid model testing solution would be to test the ship hull in a towing tank while simulating the forces from the foil system, and/or to test the foil system in a high-speed cavitation tunnel and simulate the ship performance.

9.3 Testing of floating offshore wind turbines.

Due to wind gusts and the motions of the floating turbine tower, the forces from the turbine on the tower are highly dynamic. In addition, the electric generator and the pitch control system of the turbine are important for the response. All this might be modelled in a large ocean basin with a powerful wind generating system, but it requires a large model and a correspondingly huge basin. The hybrid model testing solution is for instance to test the tower in a normally sized wave basin, simulate the rotor and generator dynamics and apply the simulated forces from the turbine on the turbine tower model in real time.

9.4 Challenges in hybrid model testing

Hybrid model testing as outlined above might seem like a very simple and attractive technique, but there are good reasons why this technique is still not in routine use in most model basins. The initial example with the anti-roll tank is simpler than the other three examples because it is motions and not forces that are applied on the physical model. Applying specified forces are more challenging. The electrical (or hydraulic) actuators that are typically used will provide a specified position. It is then possible to place force transducers between the model and the actuator, and then have a local control loop to control the actuator to give the wanted force, but it adds complexity to the system, and the inevitable small time delays in such a control loop might introduce unwanted dynamics and even instability to the system. **Figure 9.2** shows another set-up for a hybrid test of a floating offshore structure, where the actuators are applying calculated displacements to the ends of truncated mooring lines. In this manner, one avoids the problem of applying known forces, but on the other hand, one gets the additional problem of simulating the dynamic response of the truncated mooring lines.

In the real time hybrid testing control loop the state of the model is first sampled, then the required actuation is computed based on simulation of the part of the system not included in the model test.

The sampling requires use of a low-pass filter to avoid Nyquist downfolding, and additional filtering might be required to remove noise from the signal. As discussed

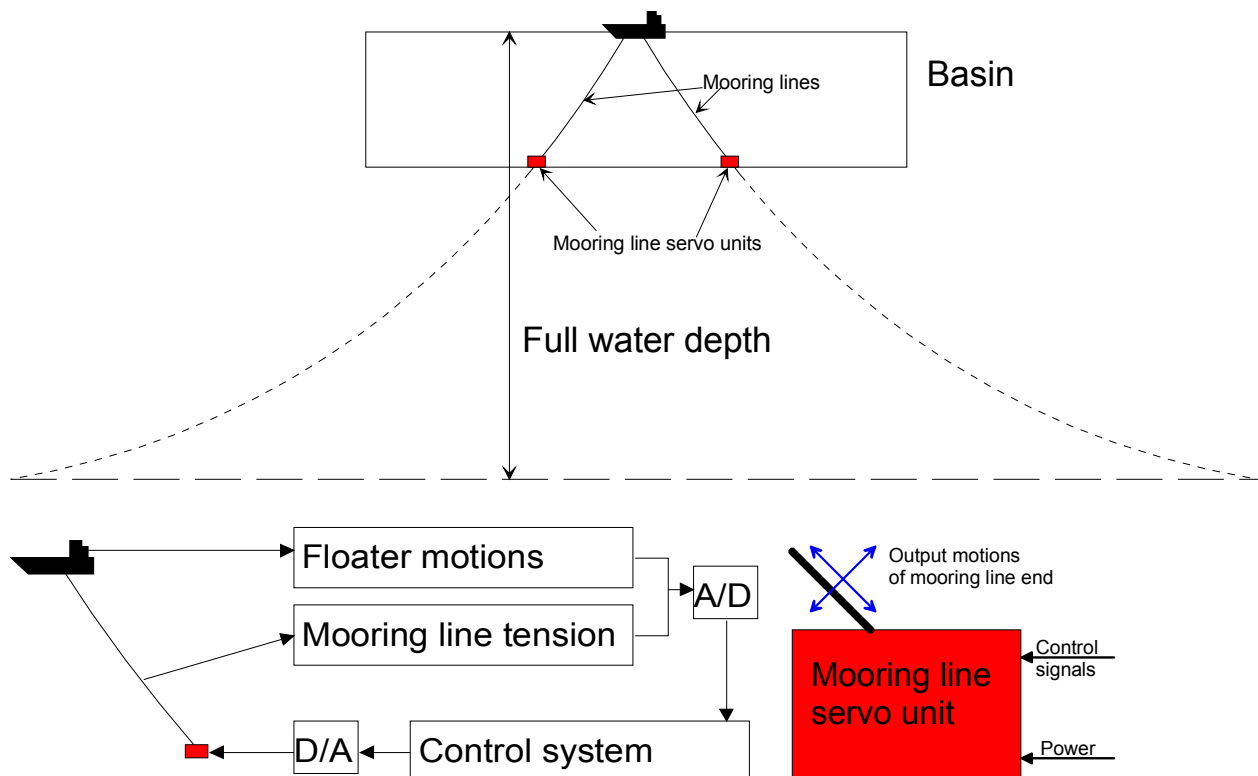


Figure 9.2 Possible solution for hybrid model test of floating offshore structure.

e

Time delay is also a problem for the simulation part. Time scales as $1/\sqrt{\lambda}$, so time goes quicker in model scale. Thus, the simulations must be fairly simple to be able to run in real time in model scale. This means that one might have to make special, simplified simulation models for the purpose of hybrid model testing. This is for instance the case for the floating moored offshore structure, where a full simulation of the dynamic response of the mooring and riser systems certainly won't run in real time model scale. This problem is becoming smaller as computer calculation speed is increasing, but it will continue to be a limitation for the foreseeable future.

10 ANALYSIS OF MEASURED DATA

10.1 General

The measurements from model tests will be recordings of time histories from all applied transducers in the test set up. The analysis of model test data will therefore be concentrated on time series analysis. The type of analysis to be performed will depend on which type of tests that have been carried out. Typical type of tests will be:

1. Static tests
2. Decay tests
3. Regular wave tests
4. Irregular wave tests

Analysis of each of the different type of tests is described in the following.

10.2 Static tests

With static tests we mean tests that are expected to give a constant measured value. Typical examples of such tests will be:

- Towing tests and propulsion tests in calm water
- Pull out tests

For such tests the mean value is the only test result of interest. However some care is required to avoid including the transient effects during start up. It will therefore be required to remove this part before the mean value is calculated. Plot of the measured time history will give a good control that steady state condition have been reached.

10.3 Decay test

Decay tests will give important information about natural frequencies, added mass and damping of a dynamic system. An example of measured response from a decay test is shown in Figure 10.1.

Let us consider a one-degree of freedom system with non-linear damping. The differential equation describing the motions is:

$$M\ddot{x} + B_1\dot{x} + B_2\dot{x}|\dot{x}| + Cx = 0$$

where M is the mass (including added mass), C is the restoring stiffness, B_1 is the linear damping and B_2 is the quadratic damping term. The natural frequency of the undamped system is given as:

$$\omega_0 = \sqrt{\frac{C}{M}}$$

From a measured natural period of the system and a known restoring stiffness the total mass can be calculated from the above equation. The added mass is now determined by subtracting the known structural mass of the system.

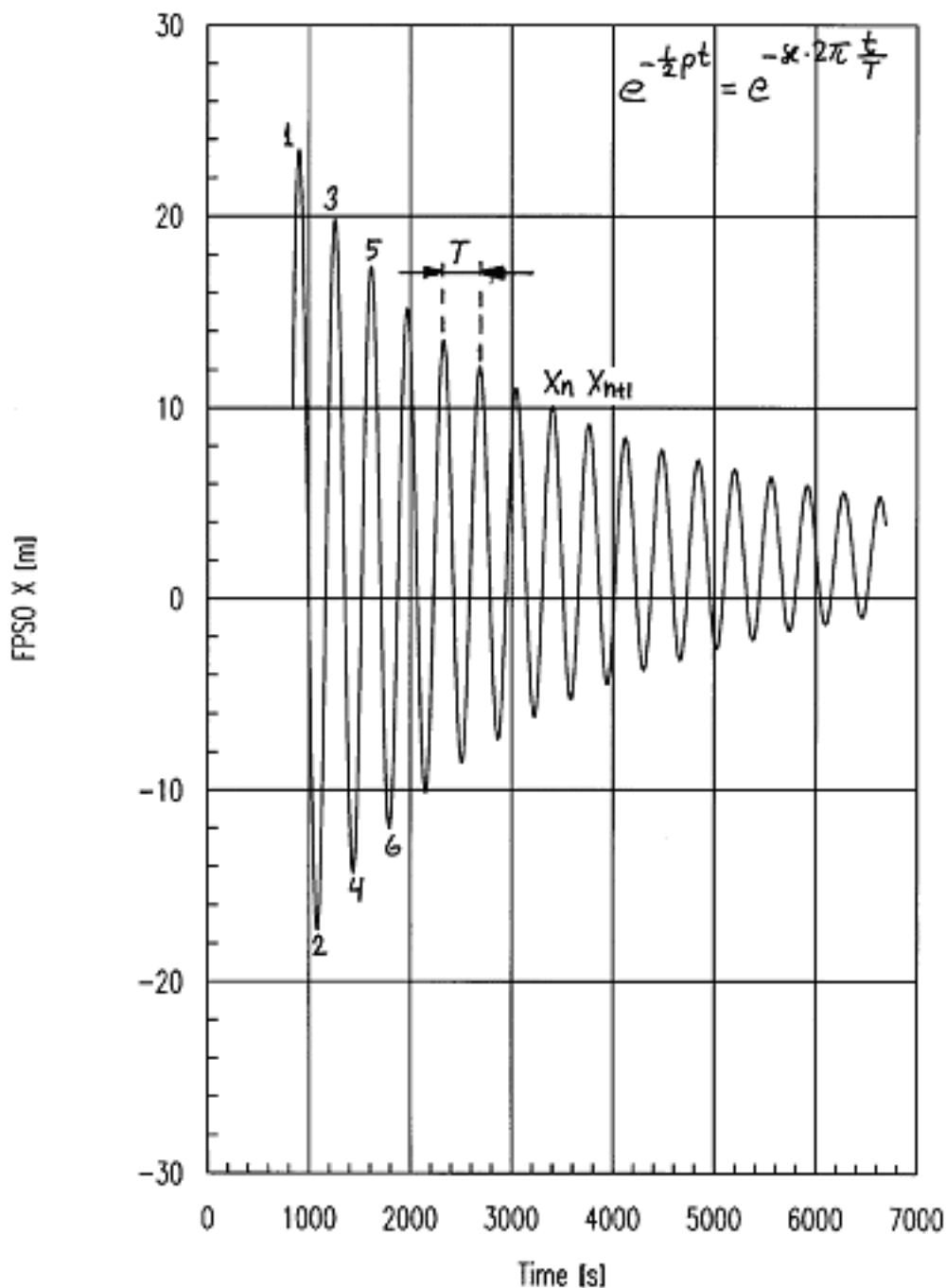


Figure 10.1 Example of measured response from a decay test

In the following the method for determination of linear and non-linear damping is outlined. The equation of motions can be divided by M and we get the standard form:

$$\ddot{x} + p_1\dot{x} + p_2\dot{x}|\dot{x}| + p_3x = 0$$

The analysis of this equation is based on well-known solution of a linear oscillating system in combination with the technique of equivalent linearization. Equivalent linearization implies that the non-linear damping term is replaced with a linear term. The equivalent linear term is determined from the requirement of equal damping energy per cycle. This requirement is satisfied using:

$$p_{EQ} = p_1 + \frac{8}{3\pi}\omega x_0 p_2$$

where x_0 is the motion amplitude of the relevant cycle and ω is the oscillation frequency. The linearized equation of motion can now be written as:

$$\ddot{x} + p_{EQ}\dot{x} + p_3x = 0$$

Assuming x_{i-1} and x_i are two succeeding amplitudes, the logarithmic decrement is defined as:

$$\Lambda = \ln\left(\frac{x_i}{x_{i+1}}\right)$$

The amplitudes x_i and x_{i+1} shall be spaced one damped natural frequency, T_d , apart. The damping ratio ξ is defined as the ratio between actual and critical damping:

$$\xi = \frac{p}{p_{cr}} = \frac{p}{2M\omega_0}$$

The general relation between the logarithmic decrement and the damping ratio is given as:

$$\Lambda = \xi\omega_0 T_d = 2\pi \frac{\xi}{\sqrt{1-\xi^2}}$$

For low damping ratios, typically $\xi < 0.2$, this relation might be approximated by:

$$\Lambda \approx 2\pi\xi$$

The equivalent damping coefficient, p_{EQ} , is given from:

$$p_{EQ} = 2M\omega_0\xi = \frac{2C\xi}{\omega_0}$$

p_{EQ} and Λ can now be obtained for each cycle from the measured logarithmic decrement. The results for Λ for each period are plotted versus the mean amplitude (mean of two successive amplitudes) or alternatively against the the equivalent velocity $\frac{8\omega x_i}{3\pi}$. An example is shown in

Figure 10.2 . p_1 is found from the figure from the intersection with the abscissa and p_2 is found from the slope of the curve. One should avoid using the first oscillation, due to transient effects, and the smallest amplitudes at the tail of the decay, due to inaccuracy.

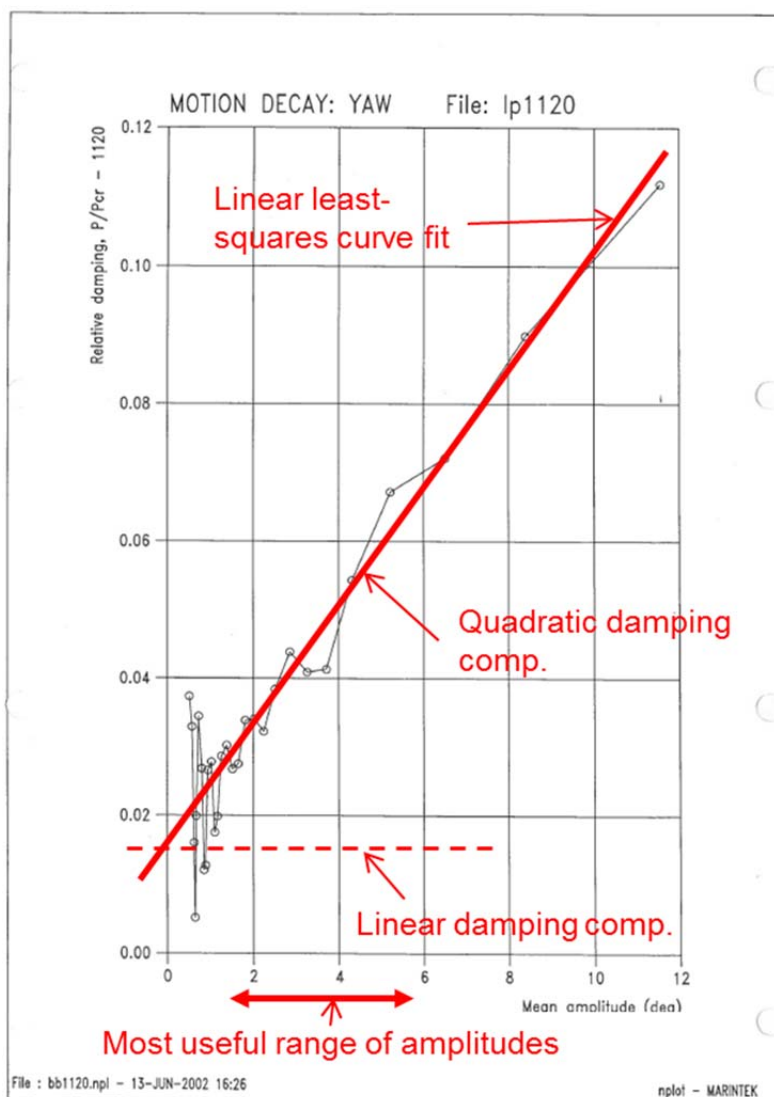


Figure 10.2 Example of measured damping from a decay test

The natural frequency of the damped, freely oscillating system, ω_d , is given from:

$$\omega_d = \omega_0 \sqrt{1 - \xi^2}$$

where ω_0 is the natural frequency of the undamped system defined above and ξ is the relative damping of the system.

10.4 Regular Wave Test

Regular wave tests are normally used for obtaining the RAO's of motions and loads. The analysis of regular waves requires that the input wave is sufficiently close to sinusoidal and that the wave is stable and stationary long enough to obtain steady state vessel motions. Steep regular waves may tend to be unstable as they propagate from the wave maker and down the tank. Wave breaking or transfer of energy to other wave frequencies may occur and the input wave reaching the vessel is no longer sinusoidal. Tank wall reflection will be another problem for testing in relatively narrow

tanks and introduce a non-stationary effect. Wave reflection effects as an error source will be further discussed in chapter 12.

It is important to ensure that a steady state response has been achieved for the time window used for the analysis. For wave periods close to any resonance period of a lightly damped system several oscillations will be required to achieve a steady state response. Careful inspection of the measured response time history will therefore be required before performing the analysis.

Assuming a harmonic input wave signal:

$$x(t) = X_A \sin(\omega_1 t)$$

where X_A is the wave amplitude and ω_1 is the wave frequency. For a linear system the measured response signal, $y(t)$, will also be a harmonic signal. The amplitude Y_A , can be easily obtained from the measured maxima and minima of the $y(t)$ signal. The phase angle ε , is obtained from the phase lag between the input wave signal and the measured response. The RAO (Response Amplitude Operator) or transfer function is defined as the ratio between the response amplitude and input wave amplitude:

$$RAO = \frac{Y_A}{X_A}$$

As discussed above the input wave may not be completely harmonic. Also, the tested system may introduce non-linearity's either due to non-linear wave loading effects or mechanical non-linearities (e.g. mooring forces or structural non-linearity's in the model). In practical model testing Fourier analysis of the measured results is almost always used. From the Fourier analysis the amplitude and phase of the different harmonic components, Y_i and ε_i , are obtained. The fundamental component is at the frequency of wave excitation ω_1 and the higher order components are at frequencies $\omega_n = n\omega_1$, where $n=2,3,\dots$. The RAO's are now defined as the ratio between the fundamental component of the measured response and the wave:

$$RAO = \frac{Y_1}{X_1}$$

In Figure 10.3 a typical example of plots of measured responses in regular waves are shown. The case considered is vertical wave forces acting on a fixed horizontal circular cylinder with diameter $D=0.5$ m. The first case shows the response for a small wave height, $H=0.04$ m. The system is close to linear. The second case is for the same wave period, but with wave height increased to $H=0.4$ m. Strong non-linearities are observed.

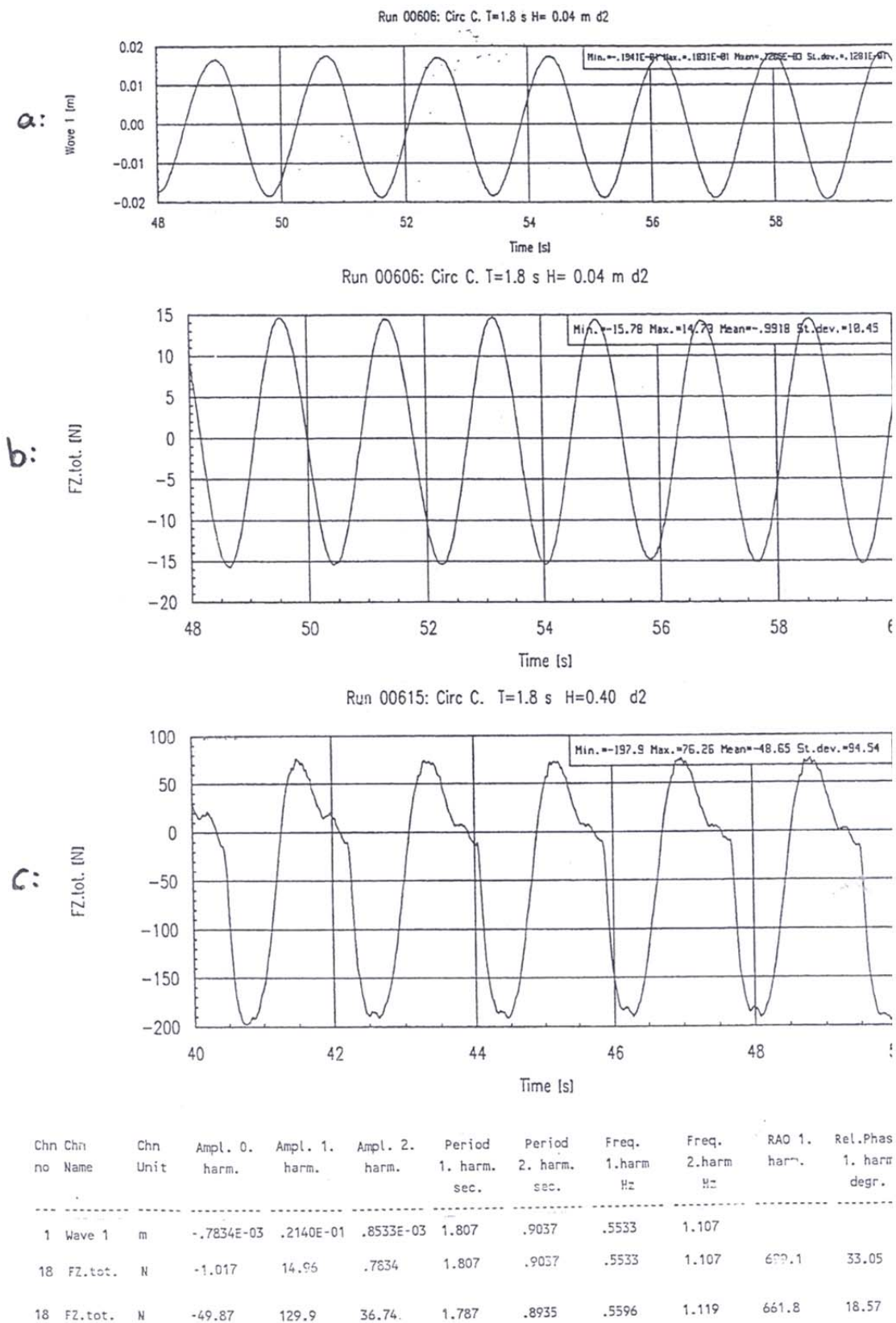


Figure 10.3 Examples of measured responses in regular waves. Vertical wave forces on horizontal circular cylinder. a: Input wave for $H=0.04$ m, b: Vertical forces for $H=0.04$ m, c: Vertical force for $H=0.4$ m

The results from the Fourier analysis are also included in the Figure 10.3. For the first case almost all energy is concentrated on the fundamental frequency (e.g the input wave frequency). For the last case significant contributions at the higher harmonic components are observed. The input wave signal is seen to be almost completely sinusoidal.

Testing in regular wave require one test for each frequency. It will therefore be relatively time consuming to obtain a complete transfer function covering an actual frequency range. Typically 10-15 tests at different frequencies will be required.

10.5 Irregular Wave Test

Irregular waves are intended to represent a realistic sea state and are therefore used for studying the actual responses including non-linear phenomena as high frequency (HF) and low frequency (LF) responses, impact loads and survivability in extreme sea states. To achieve realistic wave frequency response the energy spectrum (i.e the energy frequency distribution) of the input waves must be correct. For the low frequency motions it is also required that the wave group spectrum is correctly modelled. The wave group spectrum is the spectrum of the envelope curve of the wave train, see Figure 10.4.

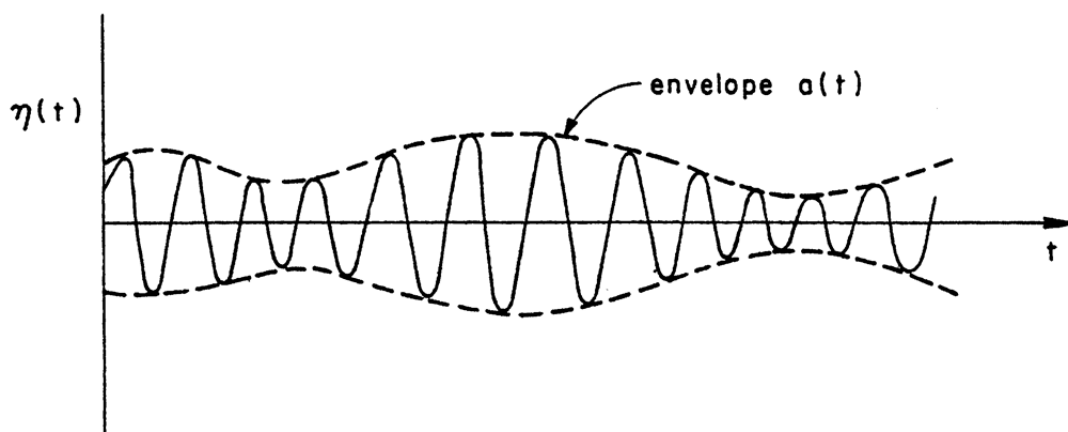


Figure 10.4 Envelope curve of the wave train.

10.5.1 General about stochastic processes

The measured time history from irregular wave tests will be a stochastic process that is a continuous function of time. It is therefore necessary to discuss some characteristics that classify a random process.

Stationarity:

Testing in irregular waves is almost exclusively based on that the input wave signal is a stationary process, which means that all the statistical properties, including probability distribution and density function of the process are unchanged by time. This means for example that for the process $x(t)$:

$$E[x(t)] = E[x(t + \tau)] \quad -\infty < \tau < \infty$$

where $E[x]$ is the expected value of x .

Homogeneous process

It is commonly assumed in analysis of waves that the process is not only stationary in time, but also homogeneous or stationary in space. This assumption implies that no change would be made of the statistical properties if the position of the measurements were shifted to a new location.

Ergodic

A stationary process is called ergodic when it is allowed to replace the averaging over space by an averaging over time. This implies for example that for stationary and ergodic process $x(t)$ we can write:

$$E[x_1(t)] = E[x_2(t)] = E[x(t + \tau)]$$

where $E[x_1]$ is the expected value of x at position 1. This assumption makes it possible to interchange the expected value of function $g(x)$ with the temporal average of $g(x)$:

$$E[g(x)] = \lim_{T \rightarrow \infty} \left\{ \frac{1}{T} \int_{-T/2}^{T/2} g(x) dt \right\}$$

A consequence of the ergodic property is that the wave registration at one single point can be used for characterisation of the sea state.

In the following analysis we will assume that the measured response is a *stationary* and *ergodic* stochastic process. Applying these assumptions, largely simplify the statistical treatment of the measured stochastic processes. Detailed description can be found in text books treating stochastically analysis, e.g. Price and Bishop (1974), Bendat and Piersol (1966) .

The autocorrelation and cross-correlation functions

The autocorrelation function $R_{xx}(\tau)$ correlates the value of the stochastic process x at time t to its value at a later stage $(t + \tau)$. In this way $R_{xx}(\tau)$ gives a measure of the correlation of the signals dependent on the time lag τ . The autocorrelation function gives a measure of the periodicity of the time series. A time series with which is periodic with period T will have a peak in the autocorrelation function at $R_{xx}(\tau = T)$. The autocorrelation function is defined as:

$$R_{xx}(\tau) = \lim_{T \rightarrow \infty} \left\{ \frac{1}{T} \int_0^T x(t)x(t + \tau) dt \right\}$$

Applied on two different signals $x(t)$ and $y(t)$ where $x(t)$ is the reference signal (wave input) and $y(t)$ is the measured response, the cross-correlation function is given from:

$$R_{xy}(\tau) = \lim_{T \rightarrow \infty} \left\{ \frac{1}{T} \int_0^T x(t)y(t + \tau) dt \right\}$$

This is a useful expression for achieving a relation between the wave input and measured response in a model test set up.

10.5.2 Spectral Analysis

In analysing model test results it will often be very convenient to transform the measured time history signal $x(t)$, to the frequency domain. This can be obtained by a spectral analysis in which the spectral density of the signal is developed. The spectral analysis is usually done by the Fast Fourier Transform (FFT) technique.

Assuming the process takes place over the time interval $(0 < t < T, T \rightarrow \infty)$. The power spectrum of $x(t)$, $S_{xx}(\omega)$ is defined as the Fourier transform of the autocorrelation function $R_{xx}(\tau)$:

$$S_{xx}(\omega) = \int_{-\infty}^{\infty} R_{xx}(\tau) e^{-i\omega\tau} d\tau$$

The cross spectrum between two signals $x(t)$ and $y(t)$ where $x(t)$ is the reference signal (wave input) and $y(t)$ is the measured response is given from:

$$S_{xy}(\omega) = \int_{-\infty}^{\infty} R_{xy}(\tau) e^{-i\omega\tau} d\tau$$

The linear transfer function between response and wave can be established from the cross-spectrum between the response and the input wave signal and the wave spectrum as follows:

$$H(\omega) = \frac{S_{xy}(\omega)}{S_{xx}(\omega)}$$

$H(\omega)$ is the complex transfer function. The Response Amplitude Operator (RAO) can be defined as the modulus of $H(\omega)$ and the phase, $\phi(\omega)$, is the phase angle of $H(\omega)$.

Alternatively the RAO can be obtained from the input wave spectrum and measured response spectrum directly as:

$$|H(\omega)|^2 = \frac{S_{yy}(\omega)}{S_{xx}(\omega)}$$

Using this formulation no phase information is obtained. The principles of this relation are illustrated in Figure 10.5.

In Figure 10.6 an example of results from a spectral analysis of measured pitch motions are shown. The measured wave spectrum, Pitch response spectrum, RAO and relative phase between the wave elevation and Pitch motions are shown. The RAO and relative phase are obtained from the complex transfer function $H(\omega)$.

The reference wave used in the calculation of the transfer function should be taken as the wave measured at the reference position without the model present. This is in order to avoid the effect of the wave system generated by the model. For test with a stationary model (e.g. fixed structures or moored vessels) this is straightforward to obtain, but for towed or free running models the reference position is not well defined.

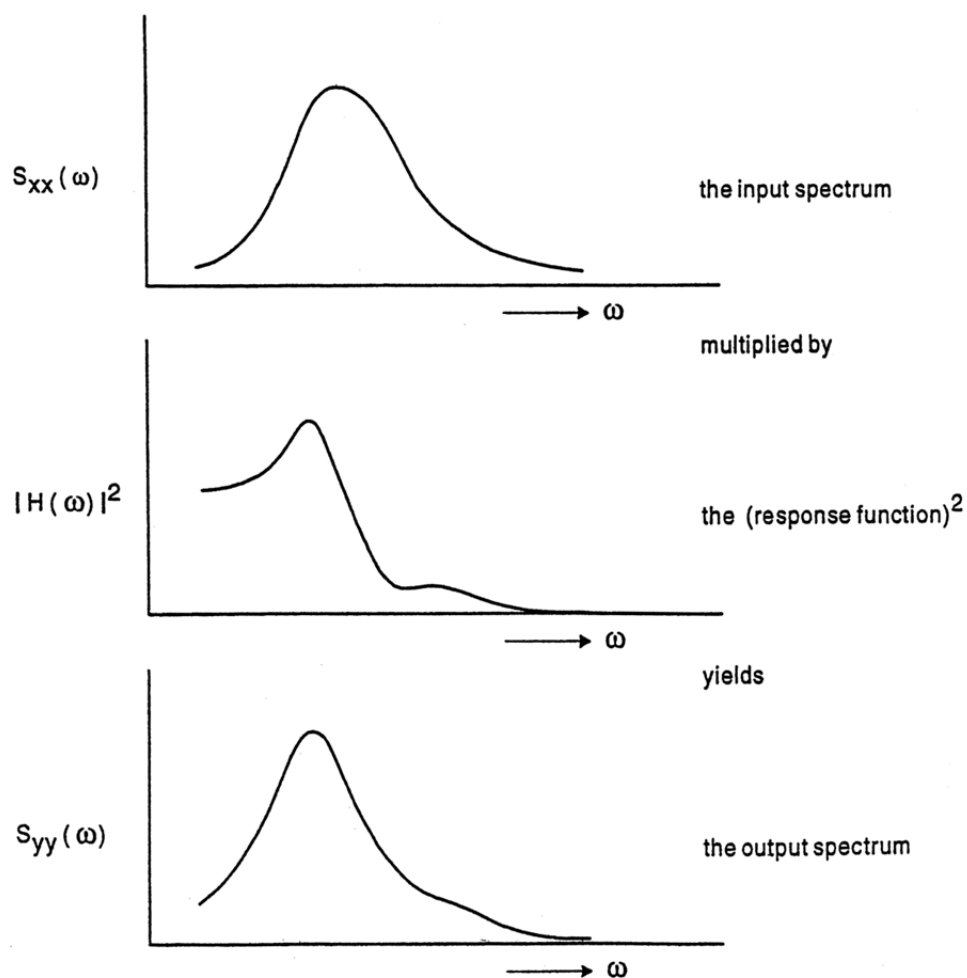


Figure 10.5 Example of relation between input wave spectrum, measured response spectrum and RAO.

The n 'th moments of the spectrum is defined as:

$$m_n = \int_0^{\infty} \omega^n S(\omega) d\omega$$

The different moments can be interpreted as follows:

$n=0$: m_0 = variance (σ^2) of the process or mean square response or area of spectrum

$n=2$: m_2 = second moment of the spectrum or mean square velocity of response

$n=4$: m_4 = mean square acceleration of response

The following parameters can be calculated from the spectral moments:

Standard deviation of response: $\sigma = \sqrt{m_0}$

Significant value of response: $x_{1/3} = 4\sqrt{m_0}$

Average period of response: $T_1 = \frac{m_0}{m_1}$

Average zero crossing period: $T_2 = \sqrt{\frac{m_0}{m_2}}$

Model Tests in Ocean Basin	
MARINTEK Project no. 5121 Plotted 93-11-24 for	Test no. 1305 Scale 1:80 File C01305 Conditions: TYPH.1: H=13.2 TP=14.7 C=1.60 Channel: PITCH Unit: deg. Filter: LP .3354 [Hz] s=.1118 [Hz]

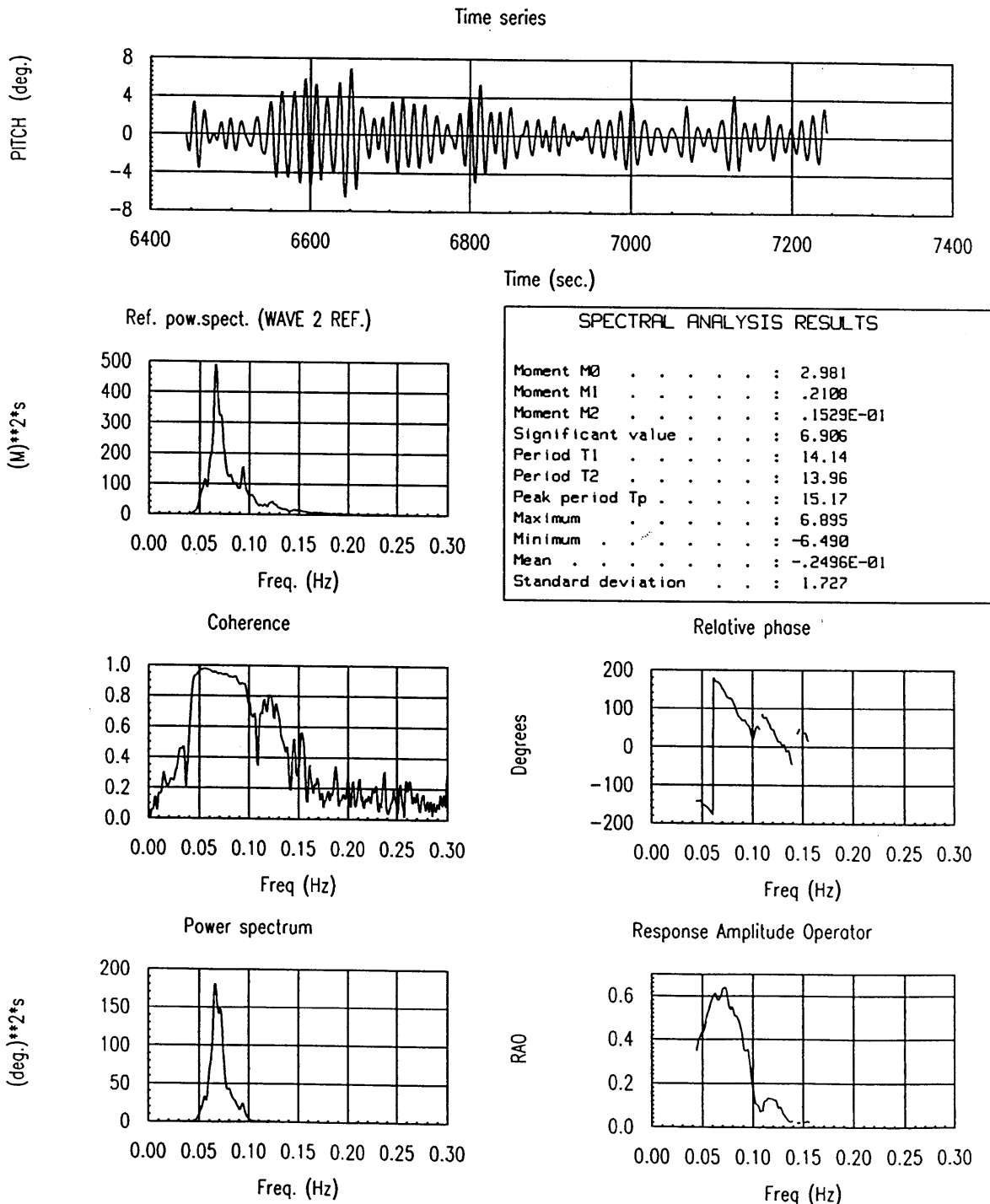


Figure 10.6 Example of result from spectral analysis (from MARINTEK Report).

A typical example of results from spectral analysis for a model test set up is shown in Table 10.1. For each of the measuring channels all the above-discussed parameters are listed.

Spectral Analysis Results

Test: 304 Test Id.: IRR H12.1 T14.1 C0.79 W35.0/-30 FL

Reference from test 304.1: Wave 2 cal

Chn no	Chn Name	Chn Unit	Moment M0	Moment M1	Moment M2	Moment M4	Per. T1 sec.	Per. T2 sec.	Peak period sec.	Sign. Val
1	Wave 1	m	9.397	.8027	.7897E-01	.3774E-02	11.71	10.91	13.49	12.26
2	Wave 3	m	9.123	.7894	.7987E-01	.4134E-02	11.56	10.69	13.66	12.08
5	REL.W.FORE	m	2.982	.3674	.5505E-01	.5039E-02	8.116	7.360	15.86	6.907
6	REL.W.MID.	m	6.616	.7092	.8880E-01	.5641E-02	9.329	8.632	13.56	10.29
7	TENSION L1	kN	.6141E+06	.1327E+05	961.3	512.0	46.27	25.28	112.2	3135.
8	TENSION L2	kN	.3067E+06	7360.	643.0	550.5	41.67	21.84	114.4	2215.
9	TENSION L3	kN	.2358E+05	1611.	241.2	257.6	14.64	9.889	14.30	614.3
10	TENSION L4	kN	4416.	379.6	99.33	203.3	11.63	6.667	13.52	265.8
11	TENSION L5	kN	7530.	527.2	129.5	258.2	14.28	7.624	113.0	347.1
12	TENSION L6	kN	.2156E+05	1003.	154.8	206.7	21.51	11.80	124.0	587.4
13	TENSION L7	kN	.3483E+05	1078.	201.4	278.5	32.31	13.15	133.5	746.5
14	TENSION L8	kN	.1770E+06	3468.	300.7	227.3	51.05	24.26	113.3	1683.
15	TENSION RG 1	kN	365.8	39.95	12.55	22.71	9.156	5.399	115.2	76.50
16	TENSION RG 2	kN	341.6	29.50	3.726	3.224	11.58	9.575	13.50	73.93
17	TENSION RG 3	kN	38.05	3.598	.9485	2.265	10.57	6.333	13.49	24.67
18	TENS. RBT1.1	kN	516.5	57.21	25.61	66.50	9.028	4.490	14.33	90.90
19	TENS. RBT1.2	kN	340.6	56.70	41.91	107.2	6.007	2.851	14.30	73.82
20	TENS. RBT2.1	kN	46.25	2.991	1.446	4.911	15.46	5.656	15.51	27.20
21	TENS. RBT2.2	kN	56.69	7.278	5.299	16.54	7.789	3.271	14.27	30.12
22	FX TURRET	kN	.1779E+07	.4292E+05	2775.	1240.	41.44	25.32	111.7	5335.
23	FY TURRET	kN	.7700E+06	.1543E+05	1238.	1150.	49.89	24.94	125.9	3510.
24	FZ TURRET	kN	.2698E+06	.1369E+05	1579.	1353.	19.71	13.07	112.2	2078.
25	FX Y TURRET	kN	.1729E+07	.4205E+05	2819.	1458.	41.12	24.77	111.2	5260.
26	MX TURRET	kNm	.1758E+06	7751.	1877.	5001.	22.69	9.678	133.2	1677.
27	MY TURRET	kNm	.2487E+06	.1339E+05	5287.	.1845E+05	18.58	6.859	113.3	1995.
28	MX Y TURRET	kNm	.2508E+06	.1372E+05	4857.	.1637E+05	18.29	7.186	113.3	2003.
29	X-ACC.TURR.	m/s^2	.9225E-02	.8690E-03	.1346E-03	.1785E-03	10.62	8.278	13.39	.3842
30	Y-ACC.TURR.	m/s^2	.8651E-01	.5843E-02	.4586E-03	.1217E-03	14.81	13.73	15.99	1.176
>> Reference channel:										
32	Wave 2 cal	m	8.890	.7623	.7552E-01	.3418E-02	11.66	10.85	13.52	11.93

Table 10.1 Example of tabulated results from spectral analysis (from MARINTEK Report).

10.5.3 Statistical analysis

The statistical analysis of the measured signals consists in calculating the statistical parameters and the statistical distribution of the process. The probability distribution function or the cumulative probability, $P(x)$, is the probability that a general value of the process $x(t)$ is less than or equal the value of x being considered. This is written as:

$$P(x) = P(x(t) \leq x)$$

The probability density function is defined from the relation:

$$p(x) = \frac{dP(x)}{dx}$$

or in other words: The probability that $a < x(t) < b$ is given by the probability density function such that:

$$P(a \leq x(t) \leq b) = \int_a^b p(x) dx$$

Two different probability distributions are of interest in the study of random wave generated responses:

- The distribution of the process itself, e.g. the distribution of the wave elevation $x(t)$ and the measured response $y(t)$.
- The distribution of amplitudes; e.g. distribution of the wave amplitudes x_A and measured response amplitudes, y_A in the tests.

The wave elevation for random waves is commonly adapted as a Gaussian (or normal distributed) process. The wave amplitudes can then be assumed to follow the Rayleigh distribution. The amplitude distribution is the most interesting quantities in the measurement of wave-induced motions. This distribution will therefore be discussed in some more details.

The cumulative distribution for the Rayleigh distribution is given as:

$$P(x) = 1 - \exp\left[-\frac{1}{2}\left(\frac{x - \mu_x}{\sigma_x}\right)^2\right] \quad \text{for } x \geq 0$$

Here μ_x is the mean or expected value of $x(t)$, defined as:

$$\mu_x = E[x] = \int_{-\infty}^{\infty} xp(x) dx$$

σ_x^2 is the variance of $x(t)$, defined as:

$$\sigma_x^2 = E\left[(x - \mu_x)^2\right] = E[x^2] - \mu_x^2$$

For a measured time series with N samples the mean value and the variance are calculated as follows:

$$\mu_X = \frac{1}{N} \sum_{i=1}^N x_i$$

$$\sigma_X^2 = \frac{1}{N-1} \sum_{i=1}^N (x_i - \mu_X)^2$$

Curves showing the cumulative distribution and the probability density distribution for the Rayleigh distribution are shown in Figure 10.7.

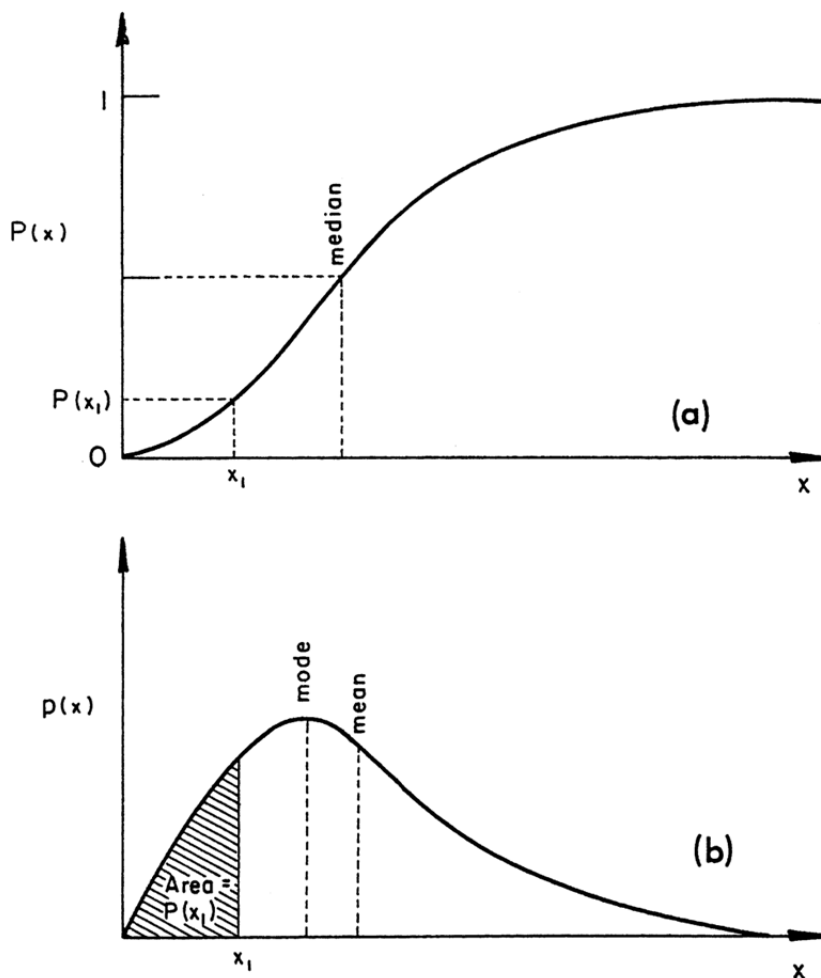


Figure 10.7 The Rayleigh distribution (a) cumulative distribution, (b) probability density.

As mentioned above the wave amplitudes can be assumed to follow the Rayleigh distribution. For wave induced linear responses the same assumption can be made. However for a broad range of practical important problems covered by model testing of ships and offshore structures the response is not linear. Non-linearities can be introduced by several reasons. Examples are:

- Surface zone non-linearity caused by non-vertical structure sides or structure in and out of water
- Excitation from higher order wave forces (drift forces)
- Non-linear drag forces
- Non-linear damping (important if resonance oscillation occur)

- Impact Loads
- Non-linear restoring stiffness (important for moored structure)

For all these situations the distribution of the response amplitudes will/may not follow the Rayleigh distribution. The more general Weibull distribution is therefore commonly used for fitting the measured data to a known distribution. To achieve this fit the statistical distribution derived from the measurements, $P(x_A)$, is plotted in Weibull scale. This is achieved by using logarithmic axis for x_A and the $P(x_A)$ -axis plotted as $\ln[-\ln(1-P(x_A))]$. Using the Weibull scale plotting will also emphasise the tail of the distribution, which will govern the prediction of the extreme amplitude values. From plotting the cumulative distributions in Weibull scale it is possible to analyse whether large extreme values measured in the tests are simply results of statistical uncertainties, or results from a more systematic trend.

The Weibull distribution is given as:

$$P(x_A) = 1 - \exp \left[-\frac{1}{G} \left(\frac{x_A - \mu_X}{\sigma} \right)^G \right]$$

where as before μ_X is the mean value of the process $x(t)$, σ is the standard deviation of the process and G is the shape parameter describing the slope of the Weibull curve. For $G=2$ gives the Rayleigh distribution and $G=1$ gives the Exponential distribution.

An example of plots of measured cumulative probability distribution of response amplitudes is shown in Figure 10.8. The straight line shown in the diagrams represent $G=2$, i.e the Rayleigh distribution. It is seen that for the first case the distribution follows closely to the Exponential distribution, while for the second case the distribution is close to Rayleigh distributed.

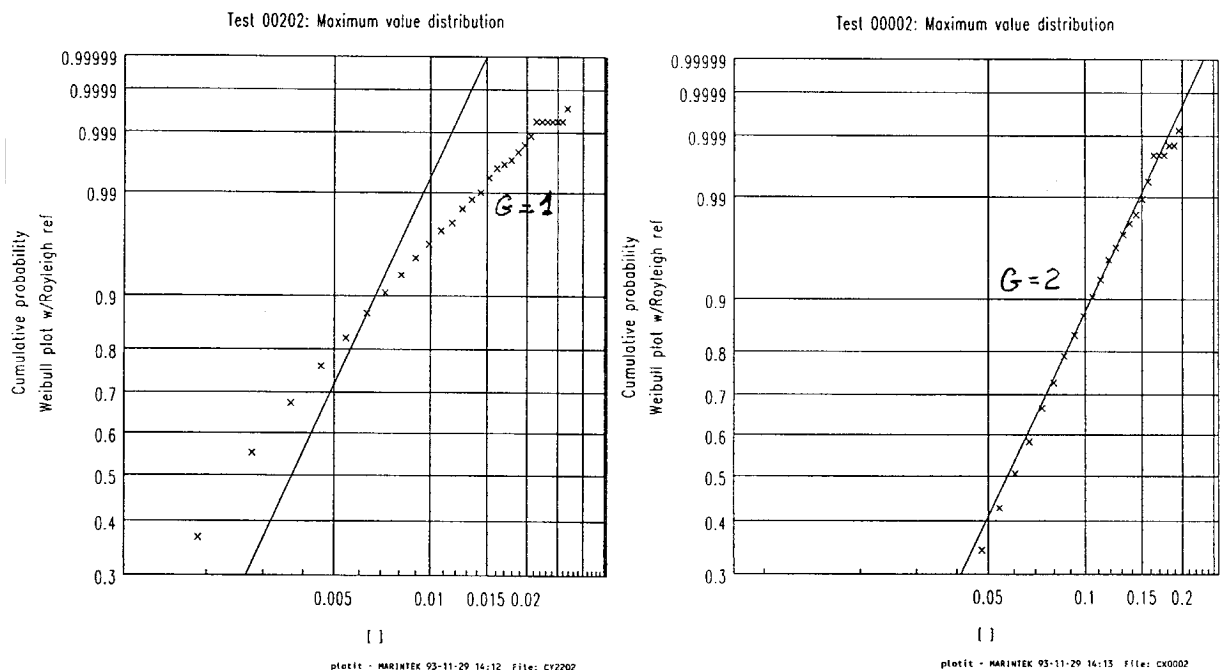


Figure 10.8 Examples of cumulative probability distributions plotted in Weibull scale.

In addition to the cumulative probability distribution discussed above a number of statistical parameters are obtained from the statistical analysis. They are summarised in the following.

Significant Values:

- Significant maxima; $x_{A/3}^+$: the mean of the highest one-third of the crest to zero values of x_A ,
- Significant minima; $x_{A/3}^-$: the mean of the highest one-third of the trough to zero values of x_A ,
- Significant double amplitude; $2x_{A/3}$: mean of the highest one-third of the maximum to minimum values of x_A ,

Maximum/Minimum Values:

- Maximum Value; $x_{A,MAX}$: Measured maximum value in the record.
- Minimum Value; $x_{A,MIN}$: Measured minimum value in the record.
- Largest double amplitude; $2x_{MAX}$: Largest measured crest to trough value in the record.

Skewness and the Kurtosis.

The Skewness is defined as the third central moment of the process:

$$\gamma_1 = E[(x - \mu_X)^3] = \frac{m_3}{\sigma_X^3}$$

The skewness provide an indication of the degree of asymmetry in the probability distribution about the mean value. For a Gaussian distribution the skewness will therefore be zero, but nonzero for a Rayleigh distribution.

The Kurtosis is defined as:

$$\gamma_2 = E[(x - \mu_X)^4] - 3 = \frac{m_4}{\sigma_X^4} - 3$$

The Kurtosis is zero for a Gaussian process.

A typical example of results from statistical analysis for a model test set-up is shown in Table 10.2. For each of the measuring channels all the above-discussed parameters are listed.

Statistical Analysis Results

Test: 2080 Test Id.: IRR H5.5 T9.5 C.55 W19/0 FL

Chn no	Chn Name	Chn. Unit	Mean value	Maximum value	Minimum value	Stand. dev.	No. of maxima	No. of minima	No. of meanupcro	Max. val. p-t-p	sign.val. p-t-p	sign.val. maxima	sign.val. minima	Skewness kurtosis	Excess of kurtosis	Estimated 3.0h-min	Estimated 3.0h-max
1	Wave 1	m	-.3793E-01	5.985	-5.203	1.390	1594	1594	1330	10.24	5.204	2.816	-2.595	.9939E-01	.1206	-5.293	6.058
2	Wave 3	m	-.1058E-01	6.166	-5.456	1.367	1623	1622	1328	11.03	5.096	2.807	-2.467	.1655	.3647	-5.313	6.610
5	REL.WAVE BOW	m	.9292E-01	14.42	-10.38	2.606	1456	1456	1241	22.98	10.16	5.320	-5.080	-.6970E-01	.2942	-9.948	12.76
6	HANGOFF TENS KN	KN	105.7	169.1	41.33	16.78	1557	1558	1105	104.6	56.29	136.7	76.67	.2072	-.3075E-01	40.91	173.6
7	FY RISER BOW KN	KN	70.89	156.9	-3.291	16.20	1585	1586	1076	102.4	49.58	100.3	42.58	.5328E-01	.7515	-5.728	151.3
8	FY RISER BOW KN	KN	3.071	56.18	-59.55	17.71	1580	1581	78	37.49	9.130	24.23	-18.41	-.2576	-.6932E-01	-64.35	58.69
9	FZ RISER BOW KN	KN	133.3	211.8	74.71	13.55	1384	1385	1156	116.5	48.59	160.2	108.7	.2665	1.541	70.27	210.3
10	RIS TENS BOW KN	KN	152.9	267.4	75.75	18.67	1376	1377	1111	156.1	64.99	189.6	119.1	.2413	1.236	69.82	261.5
14	RIS TENS BOT KN	KN	-9.597	71.30	-27.02	12.29	1217	1218	225	55.55	11.50	8.380	-21.92	1.414	2.610	-29.13	73.98
15	FY MOOR. BOW KN	KN	516.3	4264.	-14.05	503.8	1081	1082	163	2160.	348.5	1129.	108.5	2.234	6.688	-27.98	4161.
16	FY MOOR. BOW KN	KN	73.12	1191.	-765.0	140.7	1082	1082	50	621.5	65.81	202.9	-48.39	1.162	11.50	-747.3	1322.
17	FZ MOOR. BOW KN	KN	206.4	1416.	12.96	149.5	1138	1138	142	742.7	99.64	379.3	81.61	2.411	7.836	18.28	1392.
18	MOR TENS BOW KN	KN	575.0	4643.	34.22	529.1	1096	1097	151	2262.	362.0	1204.	154.2	2.343	7.289	33.14	4653.
19	FY MOOR. BOT KN	KN	-640.0	-78.62	-4672.	520.2	1019	1018	111	2822.	343.8	-228.1	-1294.	-2.303	7.196	-4541.	-50.72
20	FY MOOR. BOT KN	KN	-18.20	274.0	-640.0	61.44	1433	1434	139	354.5	26.79	27.36	-66.90	-3.230	23.07	-740.5	317.7
21	FZ MOOR. BOT KN	KN	-593.9	-357.4	-1881.	166.5	1212	1211	388	701.9	189.1	-428.0	-808.8	-2.194	6.647	-2015.	-356.0
22	MOR TENS BOT KN	KN	896.8	5074.	366.6	510.4	1151	1152	150	2277.	360.9	1487.	487.0	2.552	8.663	361.1	4913.
23	Wave 1 cal	m	-.8862E-01	6.240	-5.019	1.386	1574	1575	1325	10.97	5.191	2.942	-2.446	.1314	.1198	-5.036	6.553
24	Wave 2 cal	m	.6709E-01	7.453	-4.920	1.361	1581	1581	1326	10.18	5.129	2.915	-2.398	.1963	.3698	-4.864	7.225
25	Wave 3 cal	m	.8104E-01	7.658	-4.856	1.405	1552	1552	1314	10.37	5.290	3.050	-2.447	.2087	.2549	-4.820	7.111
26	X-POS.COG	m	-.354.7	-332.6	-366.0	5.665	421	420	44	27.89	3.678	-348.3	-360.5	1.181	1.538	-365.9	-332.9
27	Y-POS.COG	m	.3100	27.44	-18.83	9.373	1309	1309	22	5.517	1.266	12.02	-9.593	.2554	-.8111E-01	-1.030	26.98
28	Z-POS.COG	m	.9074E-02	1.194	-1.073	.3067	1576	1576	1111	1.971	1.072	.5908	-.5281	-.1104	-.1104	-1.030	1.194
29	ROLL	Deg.	-.2622E-01	1.251	-1.672	.2708	2676	2676	1525	2.340	.7372	.4096	-.5014	-.2287	.8735	-1.676	1.221
30	PITCH	Deg.	-.4387E-01	.9550	-1.100	.2543	1458	1458	1156	1.956	.9352	.4515	-.5158	.8343E-01	.3355E-01	-1.055	.9531
31	YAW	Deg.	-.4987	16.59	-14.56	6.410	574	574	24	19.13	1.845	6.205	-8.904	.2906	-.6084	-14.48	16.56

Table 10.2 Example of results from statistical analysis (from MARINTEK Report).

11 FULL SCALE MEASUREMENTS

Full scale measurements are in these lecture notes handled as the exception, rather than the rule. This might at first seem a bit awkward, since full scale is closer to the “true” situation. However, testing in full scale is usually time-consuming, very costly, and even if the uncertainty of scaling is avoided the uncertainty introduced by an uncontrollable environment might make the results less reliable.

Full scale tests are usually carried out in three different types of circumstances:

- Delivery of newbuildings (“Sea trials”)
- If a special problem has arisen, like propeller noise or excessive fuel consumption
- For Research purposes

We will now discuss each of these three cases, before some general considerations about the special challenges of full scale trials are made.

In addition to this comes ship monitoring systems. By this, we mean systems that are monitoring aspects of the performance of the ship during normal operation. Ship monitoring is covered in a separate section at the end of this chapter.

11.1 Delivery trials

In almost all shipbuilding contracts there are specific requirements for the speed the ship shall obtain at certain engine power levels. There are also very specific and grave consequences for deviations from the contracted speed. If the ship speed is smaller than the contract speed by, typically, 0.2 knots, the ship yard will have to pay a fee to the ship owner. If the deviation is large, for instance 1 knot, or even as small as 0.5 knots, the ship owner has the right to refuse to take ownership of the vessel. On the other hand, if the ship is faster than contracted, the yard usually gets a bonus. One might then think that this tempts the yard to quote a low speed, or specify a large engine to reach the specified speed, but doing this will most likely result in the yard losing in the competition for getting the contract in the first place. With this background it is easy to understand why delivery trials are important. It is also easy to understand why careful model testing to determine the trial speed before the ship is built is so common. If the model test shows that the ship is not going to meet the speed requirement it is still time to do fine-tuning of lines or propeller arrangement to improve performance. After the ship is built it is too late.

Delivery trials will always include speed trials. Usually double runs (running the same straight track in both directions) at not less than three different engine power levels. Other types of tests commonly performed are maneuvering trials, to ensure that the ship fulfills the IMO requirements for maneuverability. For high-speed crafts, the new IMO High speed craft code also includes requirements for seakeeping tests (see IMO: 2000 HSC Code (IMO 185E), Annex 9). In addition, there will usually be a lot of tests related to the correct performance of onboard systems, but these tests are of little interest to hydrodynamicists, and will not be discussed here.

11.1.1 Organization of delivery trials

When participating in a sea trial it is important to be aware of the organization and who is responsible, so we will give a brief overview: The Shipbuilder is responsible for organizing and execution of the sea trials. There will normally be appointed a Trial Leader, who is employed or hired by the Shipbuilder. The Trial Leader is responsible for all phases of the trial, but like all good executives he might delegate execution of different trials to different persons. When you participate in the sea trials it is very useful to locate and contact the Trial Leader.

Then there are usually several ship masters present. The shipyard will have a trial master to be responsible for the handling of the ship. The ship owner will usually have one or more ship masters present, usually the masters that are going to sail on the ship after delivery.

Measurements are performed by personnel engaged by the shipbuilder, or by third parties (like MARINTEK).

11.1.2 Speed trials

The purpose of the speed trials is to determine the speed-power characteristics of the ship at the contractual conditions, which is usually deep, calm water, no wind, sea temperature of 15 deg C, at a specified draught, usually design draught. Since the tests can rarely be carried out under these conditions, results will usually have to be corrected for the difference between specified and actual conditions.

Procedures for how to do sea trials are given in the international standard ISO 19019 and in the ITTC standard procedure "Procedure for the Preparation and Conduct of Speed/Power Trials". A short summary is given here:

Measurements:

- The speed is measured by (D)GPS or by clocking the time used to travel a measured mile. The shaft power should be found from RPM and shaft torque measured by strain gauge measurement on the propeller shaft(s), or by special torque meters. In practice, the extra cost of shaft measurements is often avoided and power is found from fuel consumption readings, but this method relies on engine manufacturer data on specific fuel consumption, which is often not very reliable.
- Water temperature should be measured. Water density shall preferably be measured, but is often found from the temperature and standard tables, based on assumed salinity.
- Wind speed and direction should be measured. Onboard wind indicators might be utilized, but it is preferable to bring a portable wind meter for an extra check as the ship instruments might not be properly calibrated.
- Water depth shall be noted and included in the report. Found from echo sounder or charts.
- Wave conditions shall be documented. Wave measurements by wave buoy are preferable, but seldom done. Instead, visual observation and estimation of wave height and direction is made. The best way to do this is to have several experienced persons do their own estimates, and then take the average.

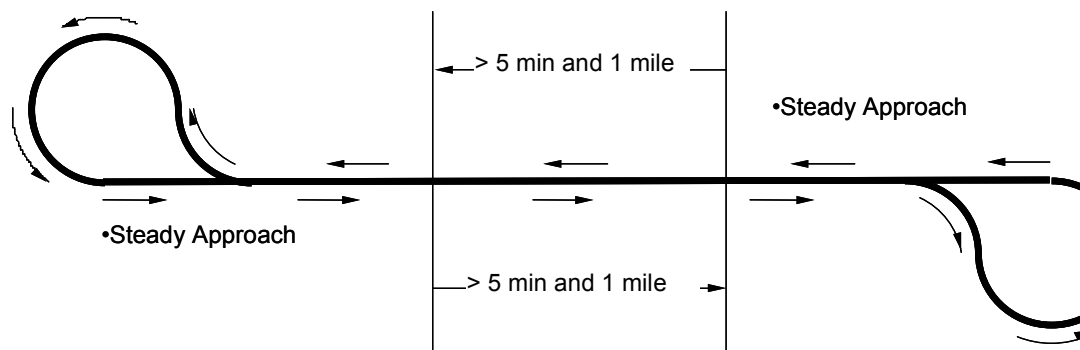


Figure 11.1 Recommended track for conducting speed trials

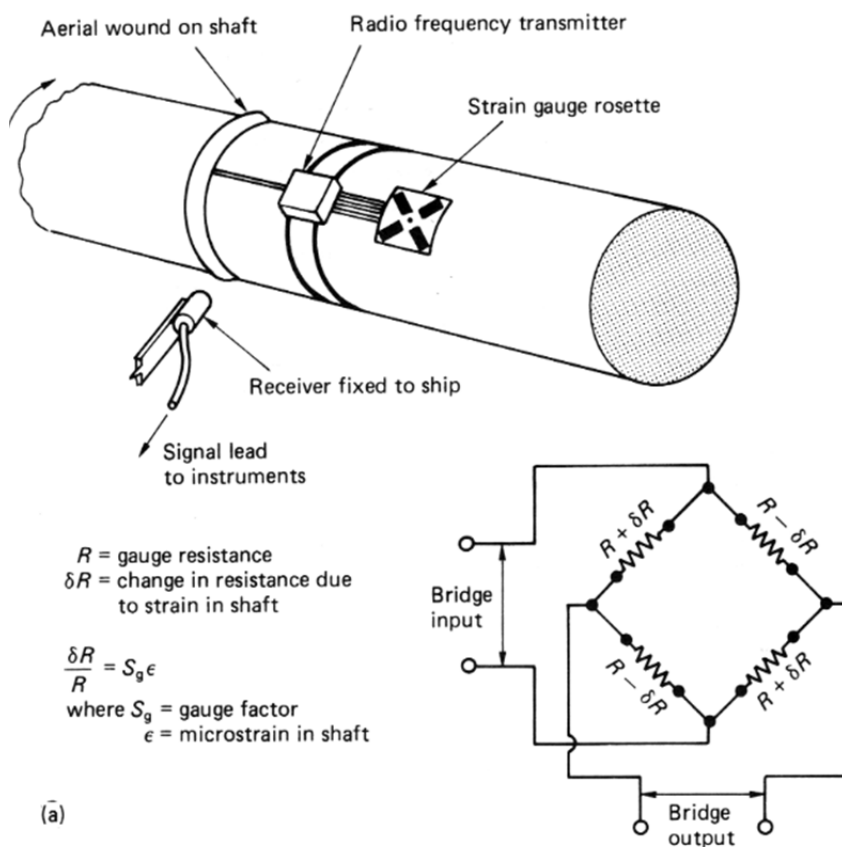


Figure 11.2 Measurement of shaft torque

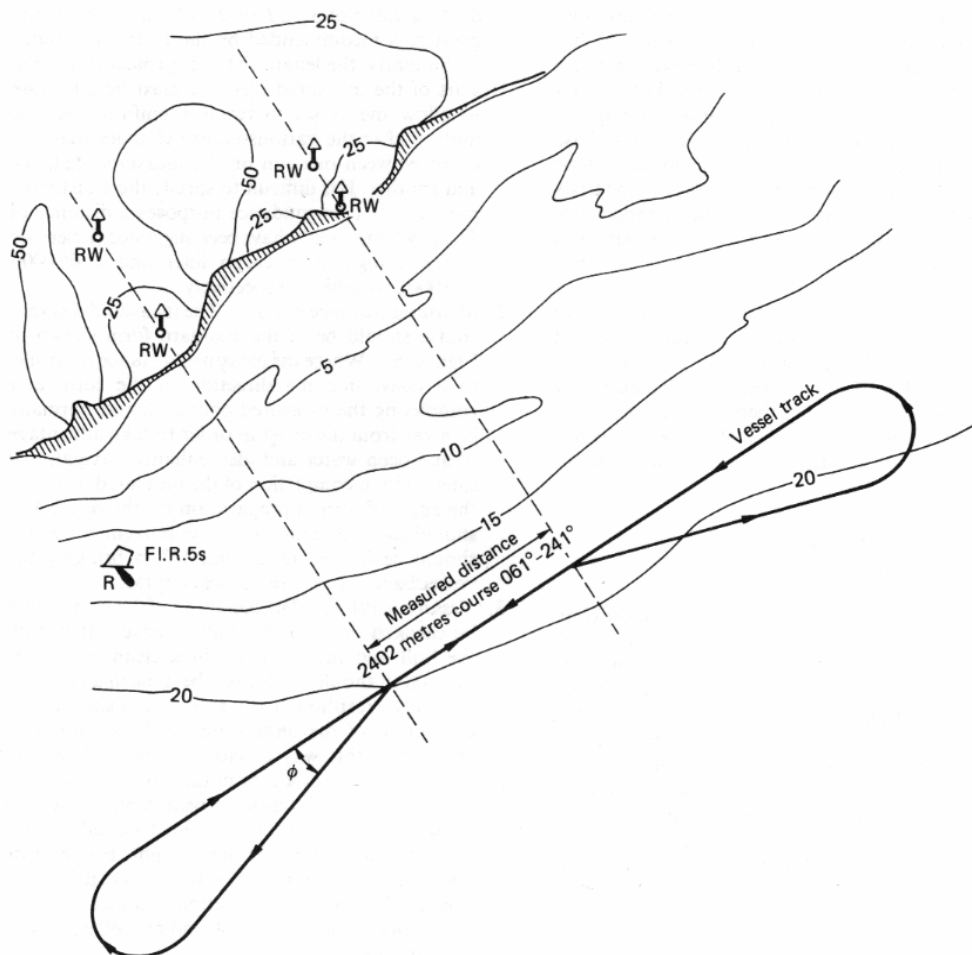


Figure 11.3 *Measured mile*

Performance:

The speed trials should always be done running the same track in both directions. After correcting the result of each run for wind and waves, the results are averaged in order to correct for the effect of current.

It is important that the course and speed have reached steady conditions before the run starts. This is achieved by a suitable approach run, as indicated in figures 11.1 and 11.3.

Use of rudder during the run should be minimized. If the ship is reasonably directionally stable, it is best to turn off the auto-pilot and run with the rudder fixed, or controlled by an experienced helmsman. If use of rudder is required it should be noted in the report.

Environmental conditions:

Typical contractual conditions:

- Sea state:
 - No waves
 - In practice: Beaufort 1 (Wave height 0.1 m)
- Wind
 - No wind

- In practice: Beaufort 2 (Wind speed ≤ 6 knots)
- Water depth h
 - Deep,
 - In practice: $h > 6.0\sqrt{A_M}$ and $h > \frac{1}{2}V^2$ (A_M is midship section area)
- Current
 - No current
 - No practical limit for when corrections are made. Use of double runs means that corrections are always included

Max acceptable trial conditions:

- Sea state
 - Preferably \leq sea state 3
 - Ultimately \leq sea state 5 (or up to sea state 6 for ships with $L > 100$ m)
- Wind
 - \leq Beaufort 6 (20 knots) (for ships with $L > 100$ m)
 - \leq Beaufort 5 (for ships with $L \leq 100$ m)
- Water depth h
 - $h > 6.0\sqrt{A_M}$ and $h > \frac{1}{2}V^2$ (A_M is midship section area)
 - Smaller depths require corrections for shallow water
- Current
 - Current of more than a few knots is unacceptable

When environmental conditions are above the contractual conditions, corrections will have to be done. Procedures for doing such corrections are given in International Standard ISO 15016, and in ITTC standard procedure "Procedure for the Analysis of Speed/Power Trial Data". Corrections for small differences in draught, difference in water temperature and density, wind, and shallow water are straight forward to apply and fairly accurate, while corrections for waves and use of rudder is difficult and not very reliable. For details, you are referred to the above mentioned documents. The ITTC standard is fairly close to the ISO standard, but using both might be helpful.

11.1.3 Bollard pull tests

Testing of bollard pull is common as part of delivery trials for tugs and anchor handlers. A very rugged pull meter is applied. The important part of the procedure is to minimise effects of boundaries (quay, bottom) (see Figure 11.4), and look for effects of water re-circulation (see Figure 11.5).

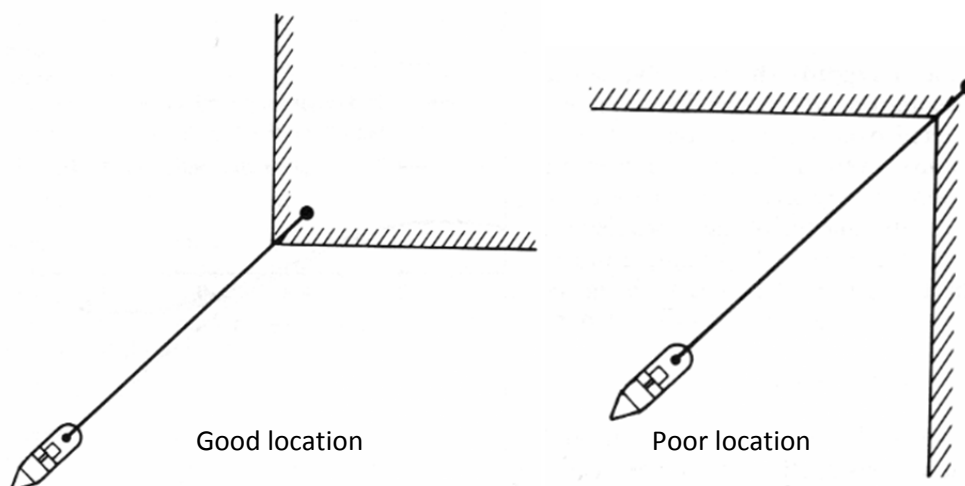


Figure 11.4 Good and bad locations for bollard pull test

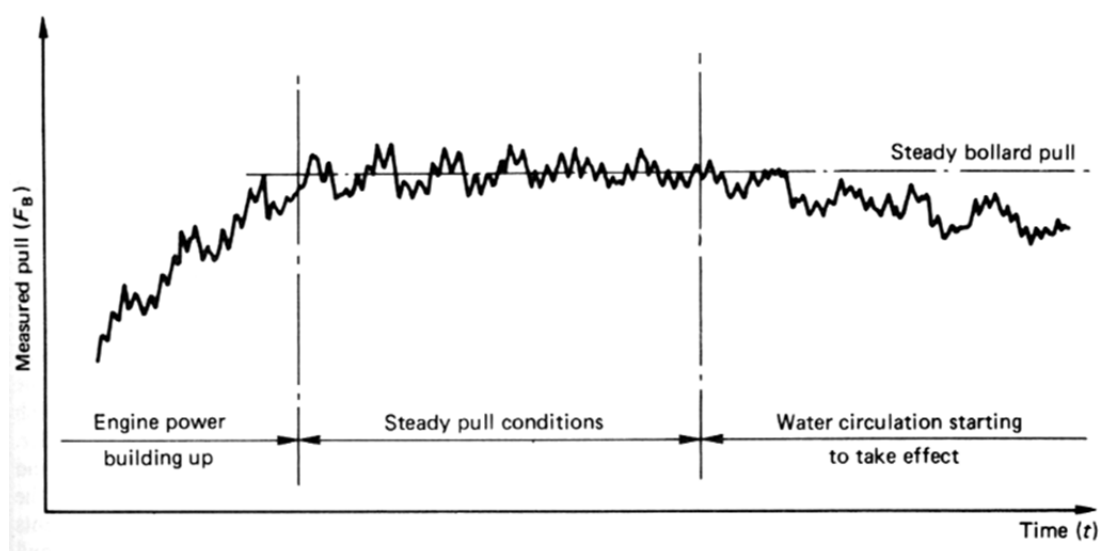


Figure 11.5 Selecting the proper part of the time series from a bollard pull test.

11.1.4 Manoeuvring trials

Trial types and execution are the same as in model scale. Standard tests are zig-zag, turning circle and stopping test.

Measurements:

- (D)GPS position measurement
- Gyro compass course
- Rudder angle
- Propeller revs

11.1.5 High speed craft

High speed craft will typically do speed trials the same way as conventional ships. The new IMO High speed craft code includes requirements for seakeeping and maneuvering tests (see IMO: 2000 HSC Code (IMO 185E), Annex 9). These tests can be summarized as follows:

- Stopping
 - Normal stop from max speed to zero
 - Emergency stop
 - Crash stop
- Cruise performance in two sea states
 - Normal conditions
 - Worst intended conditions
 - Measurements of accelerations, speed, wave heading
- Failure tests
 - Check that the ship, crew and passengers are not at risk if for instance the steering fails

11.1.6 Wave measurements

One of the main drawbacks of full scale testing is the problem of control and monitoring of the environment, and especially the wave condition. Control of the waves is of course out of the question. Wave monitoring is also surprisingly difficult. There are several alternatives:

- Visual observation – cheap and easy, but not reliable. Especially wave length is missing.
- Wave buoy – The best alternative, but when there is no stationary buoy in the area deploying and especially recovering the buoy will often represent a serious practical challenge.
- Wave radar – There are several different concepts on the market. Dedicated microwave radars are big and usually much too costly for ordinary sea trials. Systems using the X-band radar already on the ship are used on ships to some extent, but they have had problems measuring the correct wave height. Distribution of direction and wave period is fairly good on these systems. One example of such a product is Wavex, manufactured by Miros A/S in Asker, Norway. The complexity of installation of such systems means that temporary installation for the purpose of sea trials is not an attractive option.
- Bow-mounted altimeter. Measures the relative distance between the bow and the waves. Requires then accurate measurement of the vertical motions at the bow. Effect on the incoming waves from the presence of the ship might be a problem. Fairly reliable height and period, but wave direction must be visually estimated.

For visual observations, the Beaufort wind and wave scale is useful. However, it should be noted that the relation between wind and wave height is only valid for open sea. With limited fetch, the waves will be lower, shorter and steeper. Wave height and period can also be directly estimated from wind speed and fetch length.

Beaufort	Sea state	Description term Wind	Wave	Wind sp. [knots]		Wave height [m]	
				min	max	Probable	Max
0	0	Calm	Calm	0	1	0	0
1	0	Light air	Ripples	1	3	0.1	0.1
2	1	Light breeze	Small wavelets	3	6	0.2	0.3
3	2	Gentle breeze	Large wavelets	6	10	0.6	1
4	3	Moderate breeze	Small waves	10	16	1	1.5
5	4	Fresh breeze	Moderate waves	16	21	2	2.5
6	5	Strong breeze	Large waves	21	27	3	4
7	6	Near gale	Large waves	27	33	4	5.5
8	7	Gale	Moderately high waves	33	40	6	7.5
9	8	Strong gale	High waves	40	47	7	10
10	9	Storm	Very high waves	47	55	9	12.5
11	9	Violent storm	Exceptionally high waves	55	63	11.5	16
12	9	Hurricane	Exceptionally high waves	63	71	14	16
13	9	Hurricane	Exceptionally high waves	71	80	>14	>16
14	9	Hurricane	Exceptionally high waves	80	89	>14	>16
15	9	Hurricane	Exceptionally high waves	89	99	>14	>16

- **Table 11.1** The Beaufort wind and wave scale. See also <http://ioc.unesco.org/oceanteacher/resourcekit/M3/Formats/Codes/SeaState.htm>

11.2 Ship monitoring systems

Ship monitoring systems are systems that monitor certain aspects of the performance of the ship during normal operation. Thus, this is generally systems that are permanently installed onboard. This is a field in rapid development, driven by technological progress and the increasing need for ship owners to get detailed and reliable information about the performance of their fleet. Examples of such monitoring systems are discussed below.

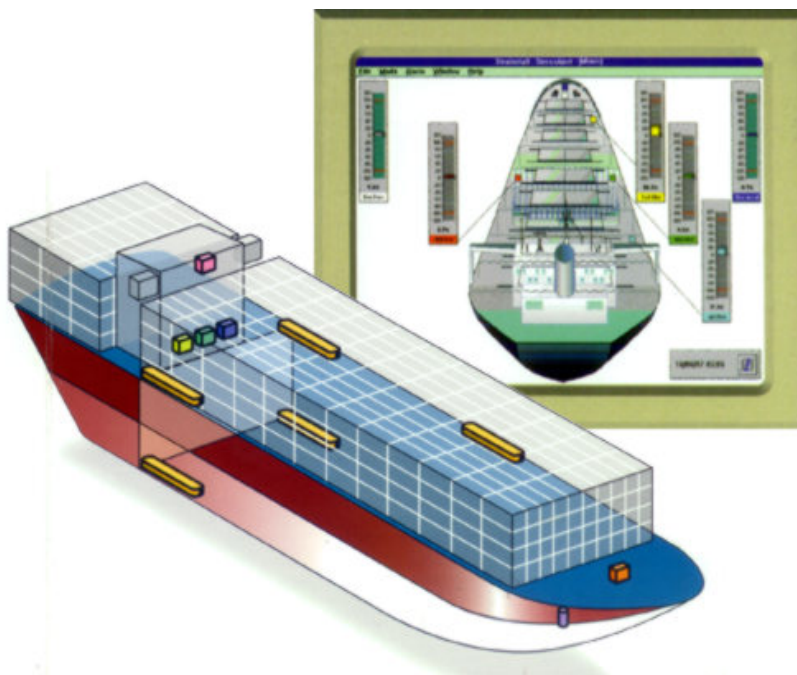


Figure 11.6 Hull monitoring system

11.2.1 Hull monitoring

This is monitoring of strain at strategic locations in the hull girder. The primary purpose is to monitor the development of fatigue damage. It is mandatory to have such a system on bulk carriers above 20 000 tonnes. The system will monitor the local strain and compute the expected remaining fatigue life. It is also used to avoid overloading when loading and offloading. There are many suppliers of such systems and the technology is well developed. Strain gauges are by far the most common sensor technology for this purpose, but fiber optics has also been used. Figure 11.6 shows an example of hull monitoring system.

11.2.2 Performance monitoring

Monitoring of speed and power performance is performed in order to optimize the operation and maintenance of merchant ships. The ship owner wants to monitor how the power requirement increases with time, so that optimum intervals for cleaning of hull and propeller can be achieved. The power supplied to the propeller is measured, preferably by a torsion (or power) meter installed on the propeller shaft. Speed is measured by speed log and GPS. It is the speed through water, which is what the speed log is supposed to measure, that is needed for the performance evaluation. However, the speed log measurements are notoriously unreliable, since they are located in the vicinity of the hull, so that they are influenced by the boundary layer and local pressure field. Since the local pressure field matters, waves and ship motions will cause noise in the measurement. Marine growth on the sensors is also a cause of measurement error.

A major problem with performance monitoring is to correct the measurement results for effects of wind, waves, current and loading condition. To help in the correction, extra measurements, like ship motions, incoming waves, wind etc. might be added to the system.

Traditionally, the monitoring of speed and power performance was made in terms of noon reports made by the crew and sent to the head office by fax or telex. Increasingly, systems that automatically log data at much higher sampling intervals than once per day are installed. The systems might collect the data on board or send them to shore by satellite link. There is a rapid technological development in this field.

11.2.3 HEMOS – Health Monitoring System

A novel kind of monitoring system is monitoring the performance of onboard systems, with the aim of detecting possible faults and to see how the systems are operated. A primary example of such a system is the HEMOS, developed by Rolls-Royce Marine, in close co-operation with the ship owner Farstad. As is illustrated on Figure 11.7, the system is collecting data from propulsion units, engines, tunnel thrusters, as well as operational data like speed, heading and position and sending these data in real time to Rolls-Royce offices on shore. Thus, this is primarily a system that allows the equipment supplier, in this case Rolls-Royce, to monitor the performance of their equipment. By doing this, the equipment supplier can learn more about how their equipment is actually used, and they might potentially detect failing equipment before it completely stops working. The idea for the system is taken from the air engine business of Rolls-Royce, where a similar system has been in operation for many years, on most of the engines sold by Rolls-Royce. Competitors of Rolls-Royce are working on similar systems.

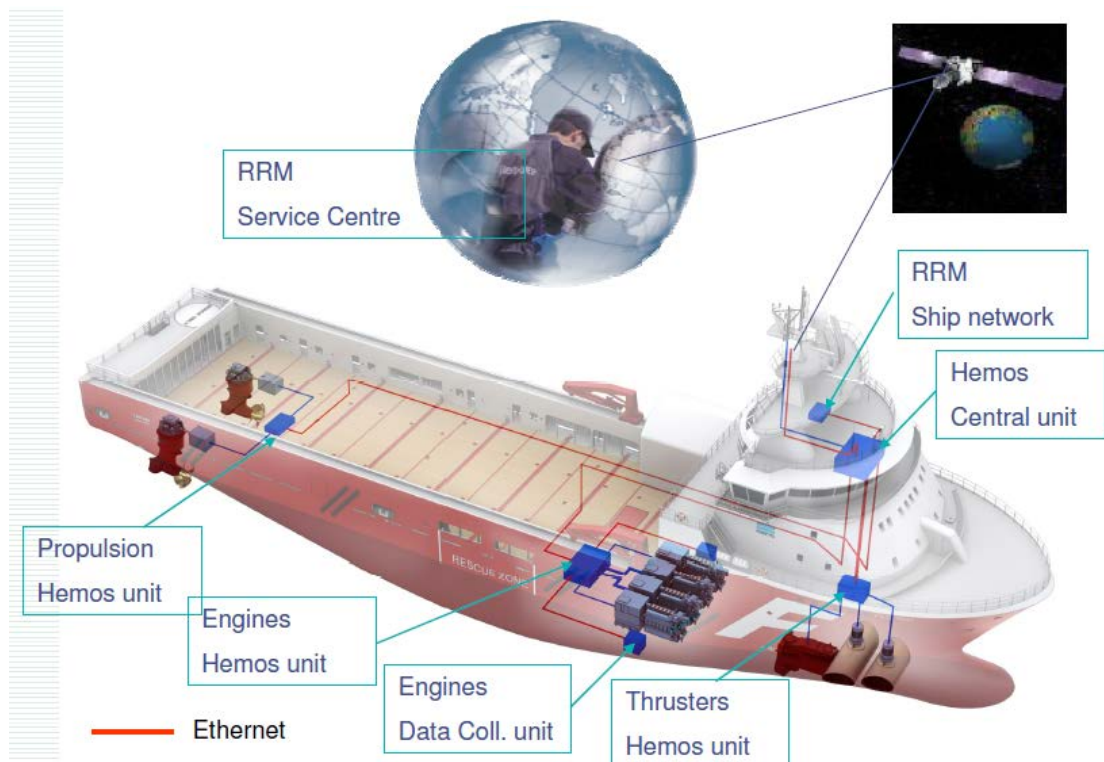


Figure 11.7 *HEMOS Health Monitoring System by Rolls-Royce Marine*

12 ERROR ANALYSIS

12.1 Introduction

It is important to keep in mind when performing all kinds of physical experiments that there is inherent uncertainty in all measured data. A test result is really just one example of the range of possible outcomes of the experiment. If the experiment is repeated it is very unlikely that exactly the same measurement result is obtained. It is of course very important to know how far the measured value could be from the unknown, true value. To know this, one has to perform so-called uncertainty analysis. Systematic use of uncertainty analysis in ship and offshore model testing is a relatively new phenomenon, which has arisen during the last 10 years. A good uncertainty analysis is especially important when using experiments to verify computer codes or a theoretical method.

Verification of CFD codes by model experiments has been a driving force in increasing the awareness of uncertainty in conventional hydrodynamic testing.

When designing an experiment to answer a certain question, for instance if the proposed bulb design change of a ship will actually decrease the fuel consumption, one should always keep in mind what is the uncertainty of the experiment compared to the required accuracy of the answer to the question. For the mentioned example, if the measured resistance reduction is 2% and the uncertainty of measurement is 3%, we have in fact not documented a resistance reduction. To document a resistance reduction of 2%, we will need to perform an experiment with an uncertainty that is significantly less than 2%.

In this chapter we will start with a short introduction to uncertainty analysis of experiments in general. This section (11.2) relies heavily on the lecture note by Svein Ersdal, which is included in Annex D. For an in-depth treatment of this subject we recommend the book by Coleman and Steele (1999). Details of uncertainty analysis of towing tank tests are found in Longo and Stern (2005) and in the ITTC Recommended Procedures, which can be found at the ITTC Permanent website:

<http://ittc.sname.org/documents.htm>

After the section on general uncertainty analysis, we go on to discuss specific error sources of special importance in experimental hydrodynamics.

12.2 Uncertainty analysis

12.2.1 Basic Concepts

The aim of an uncertainty analysis is to give a quantitative measure of how reliable a measured or calculated value is. The word error is used for the difference between a measurement result and the “true” value, while uncertainty is the statistical representation of error.

The uncertainty is usually quantified in terms of the *confidence interval*. A 95% confidence interval of for instance 2 N means that 95% of all readings of a particular measurement will be within 2 N from the “true” value. In other words it means that the probability that the true value will be within the confidence interval is 0.95.

Two types of errors are considered in the analysis: *bias* and *precision errors*. Bias errors are systematic errors, errors that are not revealed by repetition of the experiment– while precision

errors are “scatter” in the results, found by comparing the results of repeated measurement. There is really no clear distinction between the two, since the amount of bias error depends on how large part of the experiment is repeated. For instance, in case of a towing test of a ship model, the bias and precision errors will be very different if the repetition only includes running the model several times in the tank, or if it involves building a new, but supposedly equal model and testing it in another facility. It is still important to distinguish between the two types of uncertainty, and when performing the uncertainty analysis, we must choose *the replication level*, that is how large part of the experimental set-up that is re-made as part of the repetition. Including more factors in the repetition reduces the bias error, and that is a good thing, since the bias error cannot be measured, but must be “estimated” by some kind of qualified guess. Calibration is the key to reduction and quantification of bias error. By measuring a known quantity with the same test set-up as used on the real experiment, one can at least in theory, eliminate the bias error.

12.2.2 Calculation of precision error

The precision error can be calculated from repeated measurements, and we will show the procedure here. For a start, it is common to assume that if a measurement is repeated infinitely many times the measured values will follow a Gaussian distribution around a mean. The Gaussian distribution is called the *parent distribution*. The Gaussian distribution is given as:

$$f(X) = \frac{1}{\sigma\sqrt{2\pi}} e^{-\frac{(X-\mu)^2}{2\sigma^2}}$$

Where μ is the mean and σ is the standard deviation. For N samples, the mean \bar{X} is given as:

$$\bar{X} = \frac{1}{N} \sum_{j=1}^N X_j$$

And the standard deviation S_x is given as:

$$S_x = \sqrt{\frac{1}{N-1} \sum_{j=1}^N (X_j - \bar{X})^2}$$

It should be noted that the mean is itself normally distributed with mean μ . The standard deviation of the means depends on the number of samples according to the following relation:

$$S_{\bar{X}} = \frac{S_x}{\sqrt{N}}$$

For the parent distribution the confidence interval of a sample is given by:

$$\text{Prob}(X_j - t\sigma \leq \mu \leq X_j + t\sigma) = \gamma$$

Where γ is the confidence interval, typically $\gamma=0.95$. $t \approx 1.96$ for a normal distribution when $\gamma=0.95$. For a finite number of samples the standard deviation of the parent distribution, σ , is unknown. Also t is then unknown. This equation can be rewritten as:

$$\text{Prob}\left(-t \leq \frac{X_j - \mu}{S_x} \leq t\right) = \gamma$$

Where the variable $\frac{X_j - \mu}{S_x}$ is random and follows a Student's t distribution with N-1 degrees of freedom. The value of t may then be found from:

$$t = F^{-1}\left(\frac{1}{2}(1 + \gamma)\right)$$

Where $F^{-1}()$ is the inverse of the cumulative density function for the t-distribution. Note that

F^{-1} is a function of degrees of freedom N-1. N is still number of samples. The relationship between t and number of samples is given in Figure 12.1. It is seen that when the number of samples increase the value of t goes towards the value of t for a normal distribution. t can be computed in Excel by the function TINV(1-0.95;N-1) (in this case for 95% confidence).

The precision limit for a sample is now easily found from:

$$P_x = t S_x$$

Note that this is the precision limit of one sample of an experiment, but that to calculate this precision limit you need to have more than one sample. We will discuss this more thoroughly later. The precision limit of the mean of N repetitions is given by:

$$P_{\bar{x}} = t \frac{S_x}{\sqrt{N}}$$

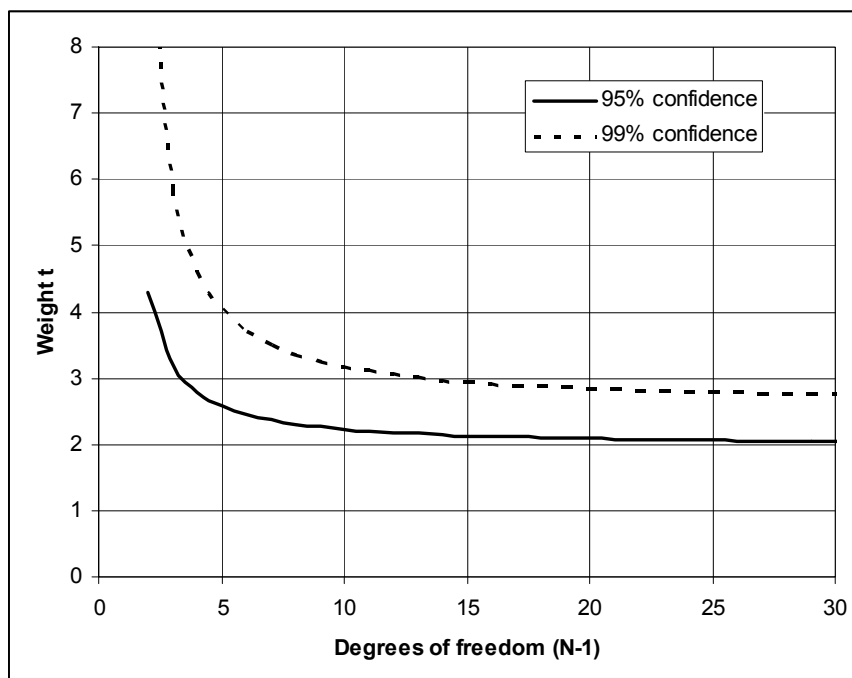


Figure 12.1 The weight t for estimating confidence intervals using Student's t distribution

It is seen from Figure 12.1 that the value of t decreases rapidly with increasing number of samples for less than about 10 samples. From the previous equation it is seen that this will result in rapid decrease in the precision limit of the mean of the samples. Thus, repeating experiments up to about 10 times is an efficient way of decreasing the precision limit. The precision limit of one sample shall ideally not change with changing the number of samples – when N is increasing t will decrease, but S_x will increase due to more samples. That is the point of the Student's t distribution, to compensate for the fact that S_x will be much smaller than σ when the number of samples is low. However, the *uncertainty* of S_x will decrease with increasing number of samples. Thus, to calculate a sensible value for S_x you need several samples.

So in a world without small budgets and not enough time all experiments would be repeated at least 10 times, so we could calculate the precision error and also reduce the uncertainty. In practice this is seldom possible. It is also usually not required to repeat the experiment in order to reduce the uncertainty. In order to calculate the precision error it is still required to have repeated tests. This is often solved by repeating only one of many conditions, and assume that the precision limit found for this condition is representative also for the other conditions. For instance for a towing test with a ship model you would only repeat one of the speeds, not all, and only at one loading condition. It could also be argued that you could use the precision limit found for one large tanker model for all similarly sized tanker models, and so on.

Example: Calculation of precision limit for a towing test

The towing test with a ship model is repeated 15 times for one speed.

The standard deviation of the measured resistance for the 15 tests is $S_x=0.185$ N.

This gives a precision limit $P_x = S_x \cdot t_{15} = 0.185 \cdot 2.145 = 0.396$ N

The average resistance of the 15 tests is 41.65 N. The uncertainty of the resistance measurement

(of a single test) is then: $\frac{0.396}{41.65} = 0.0095 = 0.95\%$

The standard deviation of the mean of the 15 tests is $\frac{0.185}{\sqrt{15}} = 0.0478$.

This gives a precision limit for the mean $P_{\bar{x}} = S_{\bar{x}} \cdot t_{15} = 0.0478 \cdot 2.145 = 0.102$, which gives an uncertainty of $\frac{0.102}{41.65} = 0.002 = 0.2\%$.

Thus, it is seen that a number of repeated tests is required to calculate the precision error of a single test, and that the uncertainty of the mean of several tests is significantly smaller than the uncertainty of a single test.

12.2.3 Chauvenet's criterion for rejecting outliers

Data samples that deviate significantly from the majority of the data samples are called *wild points*, or outliers. If no physical explanation is found, the data point might still be disregarded, even if no particular error source is identified. An accepted criterion for rejection of a sample, when no particular reason for deviation is found, is Chauvenet's criterion. It states that samples within a band around the mean with probability of exceedence less than $1 - \frac{1}{2N}$ should be retained. This limit can be expressed as a weight on the standard deviation:

$$t_{\text{chauvenet}} = F^{-1}\left(\frac{1}{2}(1 + p)\right)$$

Where $p = 1 - \frac{1}{2N}$ is the limit probability based on N samples. Note that in this case $F(\)$ is the cumulative density function of the normal distribution, also for small values of N . Values of $t_{\text{chauvenet}}$ is plotted in Figure 12.2.

Samples with higher deviation from the mean than:

$$|X_j - \bar{X}| > t_{\text{chauvenet}} \cdot S_x$$

may then be disregarded.

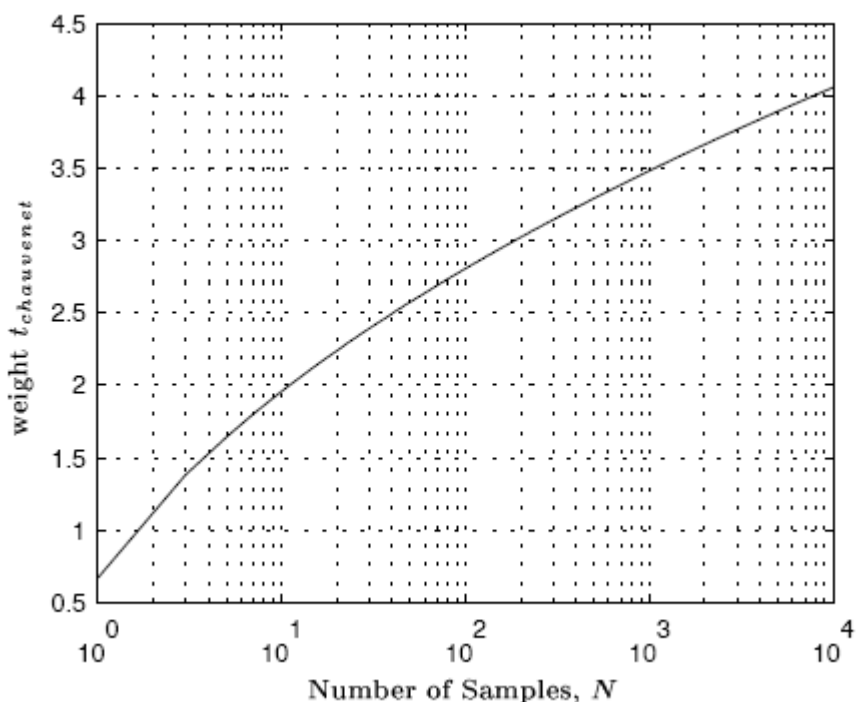


Figure 12.2 The weight $t_{\text{chauvenet}}$ in Chauvenet's criterion for rejection of outliers

12.2.4 Estimating bias errors

In contrast to precision errors, there is in general no straight-forward way of quantifying bias errors. ITTC has provided an example calculation of uncertainty of a towing test, which can be used as an example of how to estimate bias errors. A good example there is the estimation of the bias error

related to the accuracy of the geometrical shape of the model. It is assumed that the modeling accuracy is ± 1 mm, and that the model is ballasted to correct weight, not draught. The maximum error in displacement can be calculated from the modeling accuracy, and the effect on resistance of increased or decreased draught due to error in volume is calculated. This then represent the bias error of modeling accuracy on model resistance.

An important source of bias error is calibration. If the calibration of a sensor is incorrect, this will turn out as a bias error. Uncertainty of calibration factors can in turns be divided in precision and bias, where the precision error can be found from repeated calibrations. Bias errors of the calibration can be hard to determine, and it could be tempting to ignore it. Good calibration procedures will ensure that calibration bias errors are small.

Another source of bias error is blockage effect, and the procedure used to correct for blockage effect, if that is applied. In this case it seems reasonable to search the literature for alternative ways of correcting for blockage, compare them, and make a qualified guess of the uncertainty based on the comparison.

12.2.5 Error Propagation

When calculating the uncertainty, one should consider the final end result, and by “final end result” we mean the answer to the question initially being asked. If the question is “what is the total resistance of a particular ship model?”, asked for instance as part of validation of a CFD code, one need not include the scaling to full scale in the uncertainty analysis. If the question is “what is the ship resistance?”, also the conversion to full scale must be included. The equations relating the measured quantities (in the above example that might be the number of pulses from the carriage speed pulse counter and the voltage read from the dynamometer strain gauges) with the final end result, are called *data reduction equations*. The data reduction equations affect how the uncertainty of individual factors influences the total uncertainty. The data reduction equations might also contribute to the bias errors, in case they are not an entirely true representation of the “real world”. An example of this is the scaling of ship resistance to full scale; something that we know is only an imperfect assumption of a reality too complex to model entirely correct.

We will now briefly show how the influence on the final end result of the different error sources is calculated. The reduction equation can in general be written as:

$$X = f_r(Y_1, Y_2, \dots, Y_N)$$

Where X is the result for which the uncertainty is sought, f_r is the functional relation and Y_i is the parameters on which X depends. Assuming that a small change in a parameter Y_i results in a small change in X , Taylor expansion gives:

$$\begin{aligned} X &= \widehat{X} + \sum_{i=1}^N \frac{\partial \widehat{X}}{\partial Y_i} \Delta Y_i + \frac{1}{2} \frac{\partial^2 \widehat{X}}{\partial Y_i^2} \Delta Y_i^2 + O(\Delta Y_i^3) \\ &\simeq \widehat{X} + \sum_{i=1}^N \frac{\partial \widehat{X}}{\partial Y_i} \Delta Y_i \end{aligned}$$

From this the *influence coefficient* is defined as

$$\kappa_i = \frac{\partial \widehat{X}}{\partial Y_i}$$

and the *elemental error* is then:

$$e_i = \frac{\partial \widehat{X}}{\partial Y_i} \Delta Y_i = \kappa_i \cdot \Delta Y_i$$

The elemental errors are calculated independently for bias and precision errors. For precision errors ΔY_i can be found from repeated measurements, while for bias errors ΔY_i must be estimated, as discussed previously. The recommended practice is to calculate ΔY_i to 95% confidence limit. Calculation of the influence coefficients requires knowledge of the mathematical relation between the parameters and the result. If elemental error sources are independent the combined effect of the errors are found by summation as:

$$e = \sqrt{\sum_{i=1}^N e_i^2}$$

To find the total error, bias and precision errors must be combined. Approximately 95% coverage of the true value is reached by using:

$$e = \sqrt{e_S^2 + e_B^2}$$

Where e_S is precision error and e_B is bias error. Simple summation of e_S and e_B gives about 99% coverage.

If \widehat{X} is the measurement and e is the total error found using the above procedure with a confidence interval of 95%, then we know that the true value X is found in the interval

$$X = \widehat{X} \pm e$$

with a probability of 95%. Thus, the error e is given in the same physical unit as the measurement X . It is common to quote a *relative error*, defined as:

$$e_r = \frac{e}{\widehat{X}}$$

12.3 Discussion of Error Sources

Performing uncertainty analysis as briefly outlined above, and as described by for instance Coleman and Steele (1999), might be very time-consuming, easily more time consuming than the experiment itself. In routine testing, one usually relies on past experience of agreement between model test results and full scale trials, which gives a good indication of the inherent uncertainty of the end result. Due to the difficulties in estimating the bias errors, this “gut feeling” for the uncertainty might be just as reliable as the results of a formal uncertainty analysis. However, the formal uncertainty analysis will provide documentation, and it will give information about what are the most important contributions for the total uncertainty, thus giving information about what parts of

the experimental set-up that should be improved. For novel test types, where there is no large database of experience to provide proof that the test gives valid results, it is indeed recommended to perform an uncertainty analysis as an integral part of the planning and setting up of the experiment.

In addition to Coleman and Steele, the proceedings and Recommended Procedures of ITTC provides specific guidance on how to perform uncertainty analysis of standard ship model tests. As a starting point we will in the following discuss some of the most important error sources of model testing of ship and offshore structures:

1. Scale effects
2. Incorrect modelling of structures (geometry, weight distribution etc)
3. Incorrect modelling of environment
4. Instrumentation and measurements error
5. Error in analysis and interpretation of tests results.

The last error source are not limited to model tests, but are equally important for evaluation of numerically obtained results and for results from full scale measurements.

It should be noted that except item 4 *Instrumentation and measurements error* in the list above, this is mostly sources of bias error. The precision errors are easier to identify, but harder to generalise, since they usually depend on types of transducers and details of the experimental facilities and test set-up.

12.3.1 Reynolds number scale effects

As discussed in chapter 2 the different requirements to achieve dynamic similarity in model and full scale can in general not be satisfied simultaneously. Testing of ships and offshore structures are for most practical situation influenced by surface wave effects, either from incoming waves or wave generated by the motions of the structure. Gravitational forces will govern surface wave formation. This implies that for these conditions equality in Froude number in model and full scale must be achieved. Froude scaling is therefore assumed as basis for the discussion of scale effects.

Applying Froude scaling the difference in full scale and model scale Reynolds number will be (assuming the same fluid viscosity):

$$\frac{Re_F}{Re_M} = \frac{L_F U_F}{L_M U_M} = \lambda^{3/2}$$

Using a scale ratio of 1:50 gives a factor for Reynolds number equal to about 350. The difference in Reynolds number is the main source for scale effects in model testing of ship and offshore structures. The importance of the scale effects and how to account for them will depend on the actual type of tests. Scaling of towing resistance of ships is the classical scaling problem and it is probably the only case for which a reasonably rational and proven scaling procedure exists. The scaling procedures used today for ship resistance is a result of large efforts over a very long period of time. This topic is discussed in detail in the basic courses in Hydrodynamics and will not be treated here. Reference is made to Steen (2011).

In the following scale effects will illustrated by considering two different cases, the wake distribution at propeller position of a ship and the drag forces on cylindrical elements.

12.3.2 Scaling of Wake distribution

Due to the differences in Reynolds number in model and full scale there may be scale effects on the wake distribution. Difference in wake fraction will influence propeller thrust and rudder normal forces. It is therefore important to account for the scale effects. A practical method to scale the wake distribution has been suggested by Sasajima and Tanaka (1966). The basic ideas of the method are:

- The viscous wake field is obtained by subtracting the potential wake (obtained from calculations or experiments) from the measured total wake
- The viscous model wake should be corrected in such a way that when going from model to full scale the momentum in the wake should be reduced by the same fraction as the viscous resistance. This is obtained by moving all points on the wake contours in the map towards the centre-plane by the ratio of full scale to model scale viscous resistance
- Add the full-scale viscous wake field to the potential wake (not influenced by scale effects) to obtain the complete full scale wake distribution.

An example of measured and scaled wake distribution is shown in Figure 12.3. (from Huse, 1974).

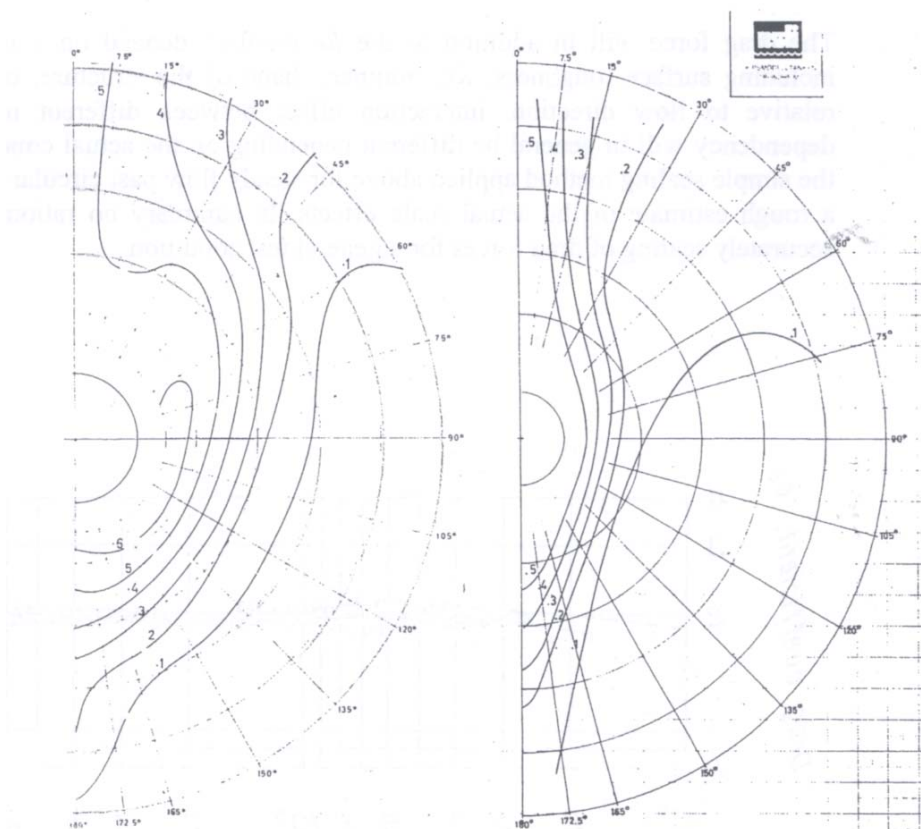


Figure 12.3 Original model wake distribution (left) and scaled wake distribution (right).

12.3.3 Scaling of drag forces

In Figure 12.4 and Figure 12.5 the drag coefficient for a squared shaped cylinder with sharp corners and a circular cylinder are shown as function of Reynolds number. The drag coefficients C_D is given from the drag force according to:

$$dF_D = 1/2 \rho C_D DU^2$$

The results are for steady flow. For the cylinder with sharp corners, Figure 12.4, it is seen that the drag force is almost independent of Re . This implies that for structures with sharp corners the scale effects will be negligible and Froude scaling can be directly applied without corrections.

For the circular cylinder case a pronounced effect of Re is observed. Four different flow regimes are defined. The definition of these regimes is included in Figure 12.5. (from Sarpkaya and Isaacson (1981)). The scale effects can in principle be evaluated using the results given in Figure 12.5 by comparing the C_D value for model scale and full-scale Re values. For full scale conditions we will for most cases be within the Post-Supercritical flow regime ($Re > 3 \cdot 10^6$), which gives $C_D \approx 0.7$, see Figure 12.5. In model scale we will usually be within the Subcritical flow regime, which gives $C_D \approx 1.2$. This implies that for this case the viscous drag forces are significantly over-predicted in the model tests. The scaling error is obtained as the ratio between the model scale and full-scale C_D values.

The drag force will in addition to the Reynolds number, depend on a number of parameters, including surface roughness, KC number, shape of the structure, orientation of structure relative to flow direction, interaction effect between different members etc. The Re dependency will in general be different depending on the actual condition. This implies that the simple scaling method applied above for steady flow past a circular cylinder can only give a rough estimate of the actual scale effects. In summary no rational procedure exists for accurate scaling of drag forces for a general test condition.

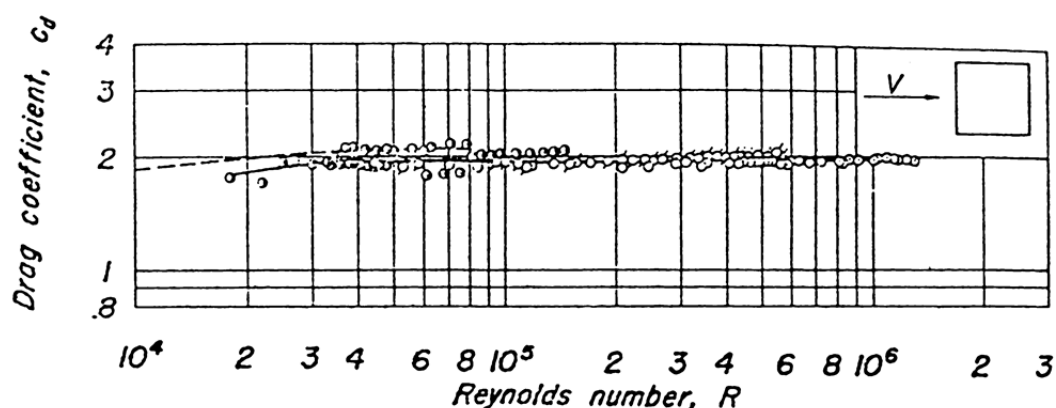


Figure 12.4 Drag coefficient for squared cylinder with sharp corners in steady flow.

	A Subcritical	B Critical	C Supercritical	D Post-supercritical
Boundary layer	laminar	transition	turbulent	turbulent
Separation	about 82 deg.	transition	120 - 130 deg.	about 120 deg.
Shear layer near separation	laminar		laminar separation, bubble turbulent reattachment	turbulent
Strouhal number	$S = 0.212 - \frac{2.7}{Re}$	transition	0.35 - 0.45	about 0.29
Wake	Re < 60 laminar; 60 < Re < 5000 vortex street Re > 5000 turbulent	not periodic		
Approximate Re range	< 2×10^5	2×10^5 to 5×10^5	5×10^5 - 3×10^6	> 3×10^6

Incompressible flow regimes and their consequences.

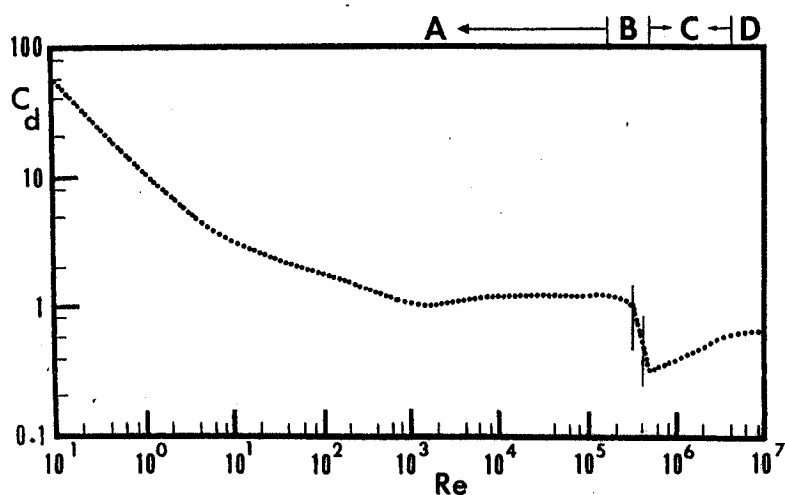


Figure 12.5 Drag coefficient for circular cylinder in steady incident flow.

12.3.4 Scale effects on responses

In general scale effects may be important for all cases where viscous forces gives a significant force contribution, either as pressure drag or as skin friction forces. To make an evaluation of possible error sources from scale effects it is therefore necessary to have a good understanding of the physics of the actual hydrodynamic problem.

For wave frequency motions on floating structures the excitation forces are normally dominated by mass forces and not by drag forces. If the frequency range is far from resonance frequencies, the motion response will not be influenced by damping forces and the scale effects will be negligible. Close to resonance frequency, damping is important and the scale effects for the wave frequency motions can be important.

For High frequency and Low frequency motions of structures we are dealing with a low damped system at resonance. For such systems the motion responses will depend on the damping and scale effects will occur if viscous forces represent an important damping contribution. This is often the case. In ANNEX C a practical procedure to quantify the scale effects on Low Frequency motions of a moored vessel is given (Huse and Matsumoto, (1989)).

12.3.5 Errors due to structural modelling

It is of practical reasons not possible to include all details and mechanical properties of a full scale structure into a model. Simplifications have to be made. Errors due to structural modelling can be split into two different categories:

1. Modelling inaccuracies that include errors in shape, weight distribution etc.
2. Modelling simplifications.

Modelling inaccuracies can be controlled by careful checking of the model prior to testing. It is common praxis to check all main dimensions of the model as well as weigh, draft, trim and metacentric height (by inclination tests) before the test program is started and any deviation can be identified.

It is more difficult to assess the effect of model simplifications. As an example, the mooring system of floating structures was in the early stage of testing of offshore structure, often modelled with horizontal, above water springs. The idea was to get the correct restoring effect. Later on it was found that the dynamics of the mooring lines could give a large contribution to the line tension and also give an important contribution to the low frequency damping. The used simplification in mooring system modelling could therefore introduce a large underestimation the maximum mooring line forces and also over predict the slow drift motions.

In general one should always try to model the properties of the full-scale structure as close as possible. If simplifications are introduced, possible consequences for the test results have to be carefully evaluated.

12.3.6 Errors due to Environmental modelling

Modelling of the environment in model testing can represent an error source due to the following factors:

1. Waves (wave height and period), wind and current modelling
2. Physical limitations of the test facility.

For waves, wind and current the variation in space and time can represent an important error source. The most important physical limitations of the test facility are the tank walls and the limited water depth.

12.3.6.1 Wave parameters and spectral shape

When propagating from the wave maker the properties of the waves may change downstream. This is in particular a problem for short and steep waves and most pronounced in a long and narrow towing tank. During the wave calibration the wave measurements should therefore be carried out in different positions along the tank to verify the wave data along the entire test track.

For testing in irregular waves the shape of the wave spectrum is an important error source, see Guedes Soares (1990). Characterisation of the used spectrum only by the standard parameters, H_s , T_p and γ is therefore not sufficient and it is required to ensure that the measured spectrum shape is in agreement with the theoretical shape. For comparison with numerical calculations the measured spectral shape should be used in the calculations.

12.3.6.2 Tank Wall Effects - Wave reflection

The model will generate its own wave system. For testing of stationary structures diffracted waves and radiated waves due to the ship/platform motions will be generated. These waves will reach the tank wall and the wave generator and will be reflected back to the model. In this way a transverse wave system will gradually be developed. For ships with forward speed, the stationary wave system due to the forward speed will also be reflected from the tank walls.

The tank wall interference effects can have a very important effect on the experimental results. In Figure 12.6 results from measurements of vertical wave forces acting on a fixed hemisphere in regular waves are shown, see Zhao et. al (1988) for further details. The test was carried out in a conventional towing tank. The intention with the test was validation of a numerical code. Calculations were carried out both with and without tank wall effects. It is seen from the figure that the tank wall effects are very important. At some wave frequencies, corresponding to the resonance frequencies of the transverse wave system in the tank, the vertical force drops to a value that is an order of magnitude lower than the predicted value without wall reflections. Including the tank wall effect in the numerical model is seen to give a very good agreement between test results and calculations. This example clearly illustrates the importance of using equivalent conditions when comparing model test results and numerical calculations.

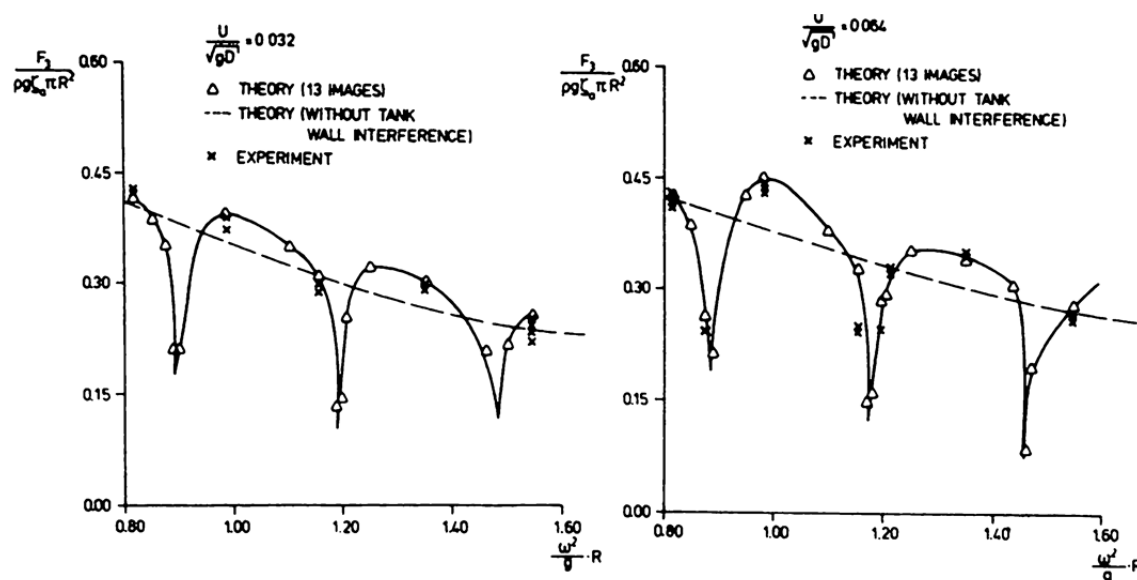


Figure 12.6 Comparison between numerical and experimental results for first order vertical wave forces on a hemisphere – Effect of tank wall interference

The results in Figure 12.6 clearly show the limitation of using conventional towing tanks for testing of stationary or low speed models. If used for this type of testing great care is required in the interpretation of the test results. Using a large basin with wave beaches at two sides will largely reduce this problem, but the reflected waves from the wave maker and the side without a beach may still to some extent influence the results.

12.3.7 Instrumentation and measuring errors

The accuracy of transducers will be influenced by the actual measuring range, linearity, possible hysteresis, tendency of drift, calibration accuracy etc. It is therefore very important to ensure that the used instrumentation in test set up have the required properties. Choice of instrumentation has

to be made based on a good understanding of the governing physical and hydrodynamic phenomena to be tested.

Transducers are often influenced by the temperature. For slow variations in temperature this can introduce drift in the measured signal. This effect can be controlled by regularly updating measurements towards a known value (often based on zero readings). If the temperature changes abruptly it will be much more difficult to identify the temperature effect on the measurement. An example is measure of impact pressure. When the pressure cell hit the water the temperature change abruptly due to difference in air and water temperature. The temperature change occurs at the same time as the impact pressure and it is very difficult to split between the two contributions. Direct use of the measured signal can therefore give totally misleading results for this case.

Many sensors based on strain gauges experience a notable drift in the signal shortly after the amplifier has been turned on. This is due to the heat produced by the current going through the strain gauge, which is causing small thermal deformations of the metal to which the strain gauges are glued. To minimise such errors, a zero reading should be made some time after turning on the amplifiers.

Careful calibration procedures are important to minimise measurement errors. At commercial model test institutions standard procedures for instrument calibration is included as a part of the Quality Assurance (QA) system.

As a rough estimate the following measuring accuracy can be applied (based on model scale):

- Wave probes: 1 mm
- Accelerometers: 0.5 % of measured value
- Force transducers: 1-5 % of measured value
- Optical position measurements 0.5 mm
- Optical angle measurements 0.1 deg.

13 MODEL TESTS VS NUMERICAL CALCULATIONS

13.1 General

In Table 12.1 an overview of the most important qualities of physical models (which means model testing) and numerical models are shown. The table is taken from Aage (1992).

<i>Qualities</i>	<i>Physical Models</i>	<i>Numerical Models</i>
Representation	Very Good	Limited by available theories and computer power
Accuracy	Good	Good within validity limits
Scale Effects	Yes	No
Reliability	Very Good	Risk of human errors
Credibility	Very Good	Prima facie not good
Flexibility	Not Good	Good
Execution	Long	Low with standard programs
Cost	High	Development cost high

Table 12.1 *Physical versus Numerical Models (from Aage (1992))*

The comments listed in the table represent general evaluation of the capabilities of the two different tools to obtain reliable results. The “ranking” will of course depend on the actual case, the complexity of the problem and how appropriate the available test facility and the numerical code are for the actual case.

The main advantage of model tests is the possibility to model very complicated situations. Assuming a realistic modelling, one can be quite sure that all important physical phenomena are properly covered. This is in particularly important for new concepts or for new applications of established design solutions. The main problems with model tests are the lack of flexibility in changing design condition, scale effects, and costs.

From the table it is concluded that model testing has an important role to play in the analysis of complex designs applied in general environmental conditions.

As numerical calculations evolve and become more accurate and easier to use, the importance of model testing for routine verification of the performance of ships and offshore structure becomes smaller. Calculations are slowly taking over the routine work, but the need for verification of numerical methods and the development of new and technologically demanding structures means that experiments and model basins are almost as important today as they were 30 years back.

13.2 Model tests for Validation of Numerical Calculations

Validation of a numerical code means to check that the computer program is consistent with the physical reality. For this purpose model tests plays an important role.

To carry out a computer code validation using model test results we need to identify error sources both for the model tests and for the numerical model. In principle an uncertainty analysis should be applied to both numerical analysis and experimental results. A procedure for uncertainty analysis for seakeeping calculations is given by Faltinsen and Svendsen (1990). The error sources in the numerical calculations are classified as numerical errors (meaning errors relative to the theoretical basis of the program), physical errors (which is errors caused by the theoretical assumptions and simplifications used as basis for the theory) and human errors. The effect of each error source must be systematically investigated by numerical calculations.

It is not possible to define a detailed general validation procedure. The validation procedure will be dependent on the actual problem to be considered, the numerical code to be validated and what type of experimental data that is available. A possible procedure for validation of a computer program for seakeeping analysis is outlined in the following.

Steps in a validation procedure for wave induced ship motions:

1. Equal model loading condition; Ensure that the following parameters is the same in the model tests and numerical calculations:
 - Geometry
 - Vessel draft and trim
 - Metacentric height (GM_T and GM_L)
 - Radius of gyration r_{xx} r_{yy} and r_{zz}
2. Equal environmental data; Examine the environmental data used in model tests.
 - Wave height H and period T at position of testing for regular waves. For irregular waves H_s , T_p and spectral shape.
 - Possible deviation in wave data along test track.
 - Effect of water depth? If yes, shallow water to be included in calculations
 - Test results influenced by diffracted and reflected waves, including tank wall effects?
3. Equal test condition; Ensure that the model tests and calculations are carried out for the same test cases including parameters as:
 - Forward speed
 - Wave heading
 - Transient effects in model tests (and also in calculations if time simulations)

4. Natural periods; Compare calculated and measured resonance periods in heave, roll and pitch. Causes to possible deviations to be explained (mass terms or restoring terms, if decay; damping contributions).
5. Influence of difference in conditions between model tests and prototype; Establish by numerical calculations the effect of possible differences between model test conditions and calculation condition case on the results.
6. Influence of error ranges on results; Establish by numerical calculations the effect of error ranges for the different parameters on the final results.
7. Comparison of wave results;

Regular Waves:

- RAO
- Phase
- Added resistance / speed reduction

Irregular waves:

- Standard deviation
- Statistical distribution
- Extreme values
- RAO's
- Added resistance / speed reduction
- (Green water, Impact Loads etc., depending on actual case)

14 REFERENCES

- Aage, C. (1992), "Relevance of Model Testing in Irregular Seas and Current", Proc. of OMAE 1992.
- Bendat, J.S. and Piersol, A.G. (1966). "Measurements and Analysis of Random Data", John Wiley & Sons, Inc.
- Berg, T.E. (2000), "Ship Manoeuvring", Department of Marine Hydrodynamic, NTNU.
- Buchner, B, Wichers, J.E.W. and de Wilde, J.J (1999), "Features of the State-of-the-Art Deepwater Offshore Basin", Offshore Technology Conference, paper OTC 10814, Houston, Texas
- Chakrabarti, S.K (1999). "Modeling Laws in Ocean Engineering", in Developments in Offshore Engineering, Wave Phenomena and Offshore Topics, Edited by J.B. Herbich, Gulf Publishing Company, ISBN 0-88415-380-0
- Coleman, H. and Steele, W.G. (1999). "Experimentation and Uncertainty Analysis for Engineers, Second Edition", Wiley-Interscience, ISBN 0 471 12146 0
- Dean, R.G. and Dalrymple, R.A. (1991). "Water Wave Mechanics for Engineers and Scientists", in Advanced Series on Ocean Engineering – Volume 2. World Scientific, USA
- Dunn, P.F. (2005), "Measurement and Data Analysis for Engineering and Science", McGraw-Hill. ISBN 0-07-282538-3
- Goldstein, R.J (1983). (ed.) "Fluid Mechanics Measurements", Hemisphere Publishing Company, Washington, USA
- Guedes Soares, C. (1990), "Effect of Spectral Shape Uncertainty in the Short Term Wave Induced Ship Responses", Applied Ocean Research, Vol 12, pp.150-159.
- Hermundstad, O.A, Aarsnes, J.V. and Moan, T. (1995), "Hydroelastic Analysis of a Flexible Catamaran and Comparison with Experiments", FAST '95, Lybeck, Germany, Vol I, pp 487-500
- Huse, E. (1999). "Experimental Methods in Marine Hydrodynamics", Department of Marine Hydrodynamic, NTNU.
- Huse, E. (1974). "Effects on afterbody forms and afterbody fins on the wake distribution of single-screw ships.", NSFI report R-31.74..
- Huse, E. and Matsumoto, K. (1989). "Viscous Surge Damping of Floating Production Vessels Moored at Sea", 8th OMAE Conference, The Hague.
- Huse, E. and Tørum, A. (1981). "NHL – Ocean Laboratory Design Philosophy", Int. Symp. on . Hydrodynamic in Ocean Engineering, Trondheim, Norway
- ITTC (1996). Report from Propulsor Committee, 21st int. towing tank conference, Trondheim, Norway
- ITTC (1996). Report from Manoeuvrability Committee, 21st int. towing tank conference, Trondheim, Norway

ITTC Symbols & Terminology, Recommended Procedures and Quality Systems manual:
<http://ittc.sname.org/documents.htm>

Lloyds, A.R.J.M. (1989), "Seakeeping, ship behaviour in rough weather", Ellis Horeood Limited. West Sussex, England

Longo, J, Stern, F. (2005), "Uncertainty Assessment for Towing Tank Tests With Example for Surface Combatant DTMB Model 5415", Journal of Ship Research, Vol. 49, No. 1, March 2005, pp. 55–68

Maeda, H. (1991). "Modelling techniques for dynamic of ships", Phil. Trans R. Soc. London, Vol 334, pp 339-355.

Naeser, H. (1981). "NHL – Ocean Basin Capabilities and Limitations", Int. Symp. on . Hydrodynamic in Ocean Engineering, Trondheim, Norway

Newland, D.E. (1975). "Random Vibrations and Spectral Analysis", Longman, London

Olsen O.A. (1992). "Instrumenteringsteknikk", Tapir Trondheim.

Sasajima, H. and Tanaka, I. (1966), "On the Estimation of Wake of Ships" 11th International Towing Tank Conference Proceedings, Tokyo.

SNAME (1967). "Principles if Naval Architecture", The society of Naval Architects and Marine Engineers, New York.

Sarpkaya, T and Isaacson, M. (1981), "Mechanics of Wave Forces on Offshore Structures", Van Nostrand Reinhold Company.

Stansberg, C.T., Øritsland, O. and Kleivan, G., (2000), "VERIDEEP Reliable Methods for Laboratory Verification of mooring and Stationkeeping in Deep Water", Offshore Technology Conference, paper OTC 12087, Houston, Texas

Steen, S., (2011), "Motstand og Propulsjon. Propell og foilteori", Kompedium UK-2011-99 i TMR4247 Marin Teknikk 3. Institutt for Marin Teknikk.

Stoot, W.F. (1959)"Some Aspects of Naval Architecture in the Eighteenth Century", Transaction of Institution of Naval architects, 101,31

Taylor, E.S. (1974). "Dimensional analysis for engineers", Clarendon Press, Oxford

Walderhaug, H. (1983), "Eksperimentell Marin Hydrodynamikk", Department of Marine Hydrodynamic, NTNU.

White, F.M. (2005) "Fluid Mechanics", fifth edition, McGrawHill, ISBN007-124343-7

Zhao, R. Faltinsen, O.M., Krokstad, J. and Aanesland, V. (1988), "Wave-Current Interaction Effects on Large-Volume Structures", BOSS '88, Trondheim, Norway.

15 INDEX

- 6 DoF, 35
- accelerometer, 36
- AD converter, 30, 46
- AD-converter, 48
 - range, 48
 - resolution, 48
- added mass, 79
- Added resistance, 73
- afterbody model, 20
- amplifier, 30, 46
 - frequency range, 52
 - rise time, 52
- analog, 30
- atmospheric pressure, 15
- autocorrelation function, 94
- Bendat and Piersol, 54, 94
- Berg, 70
- bias error*, 115, 119
- blockage effect, 57
- bollard pull, 109
- Bouchner, 80
- boundary layer
 - turbulent, 68
- bridge balancing, 46, 56
- bridge excitation, 46
- British method, 65
- Buckingham's Pi-theorem, 8
- bulk carrier, 113
- calibration, 29, 55
- calibration curve, 55
- calibration factor, 55
- capacitance transducer, 34
- carriage, 74
- catamaran, 59
- cavitation, 15, 68
 - pressure pulses, 68
- cavitation number, 15, 18, 20
- cavitation tests, 63
- cavitation tunnel, 15, 16, 20
- centre of gravity, 57
- CFD, 115, 120
- Chakrabarti, 8
- charge amplifier, 46
- Chauvenet's criterion, 119
- Coleman and Steele, 115
- commutative probability, 100
- confidence interval*, 115
- continental method, 65
- Crash stop, 111
- cross spectrum, 95
- cross talk, 44
- cross-correlation function, 94
- current, 29
- current generator, 29
- DA-converter, 48
- data acquisition, 30, 46
- decay test, 87
- digital, 30
- dimensionless quantities, 12
- Doppler shift, 42
- Dunn, 5
- dynamic similarity, 8, 9, 68
- dynamometer, 43
- elastic fluid forces, 9
- elastic model, 13, 34, 61
 - Backbone model, 61
 - Hinged model, 61
- elastic models, 9
- environment calibration, 82
- equivalent damping coefficient, 89
- ergodic process, 94
- error, 115
- Excel, 117
- Farstad, 113
- Fast Fourier Transform, 95
- fatigue life, 113
- FFT, 95
- field measurement technique, 43
- filter, 30
- filters, 46
 - band pass, 46
 - high pass, 46
 - low pass, 46
- flap wave maker, 23
- Floating bridge, 59
- floating platforms, 79
- folding, 51
- Froude number, 10, 68, 122

Froude scaling, 12, 13, 28, 70, 122
 Froude, William, 6
 full bridge, 33
 Gaussian distribution, 116
 Gaussian process, 103
 General Acoustics, 45
 geometrical similarity, 8, 14
 geometry, 60
 global loads, 59
 Global loads, 73
 Goldstein, 30
 GPS, 110
 gravitational forces, 9
 Green water, 73
 gyration radius, 57
 gyro, 35
 Gyro compass, 110
 half-bridge, 33
 HEMOS, 113
 Hermunstad, 62
 High speed craft, 111
 homogeneous process, 94
 Hottinger, 48
 hull monitoring system, 113
 hull vibrations, 68
 Huse, 5
 hydrodynamic damping, 79
 hydroelastic, 60
 hydroelastic problems, 13
 hydroelasticity, 13
 ice tank, 18
 IMO, 105

- High Speed Craft code, 105

 impact loads, 39, 52, 80
 inductive transducer, 33
 inertia forces, 9, 57
 ISO, 109
 ITTC, 42, 71, 109, 115, 119, 122
 JONSWAP, 26
 Keulegan-Carpenter number, 12
 kinematic similarity, 8
 kinematic viscosity, 10
 Kurtosis, 103
 Laser Doppler Velocimetry, 42
 LDV, 40, 42

- seeding*, 42

 Length of record, 54
 Leonardo da Vinci, 6
 logarithmic decrement, 89
 low frequency motions, 80
 Mach's number, 10
 Maeda, 60
 manoeuvring, 69
 manoeuvring tests, 63
 Marin, 29
 Marine Cybernetic Laboratory, 23
 mass, 57

- distribution, 57

 MCLab, 29
 measurement bridge, 32
 metacentric height, 59
 moment of inertia, 57
 monohull, 59
 mooring line, 34
 mooring lines, 13
 Mooring lines, 59
 mooring system, 60
 multidirectional waves, 26
 Newland, 26
 noise, 68
 normal distribution, 116
 NPD spectrum, 29
 Number of samples, 54
 Nyquist frequency, 51
 ocean basin, 16
 ocean laboratory, 22
 offshore structures, 79
 Olsen, 30
 operational limits, 79
 optical system, 34
 Particle Image Velocimetry, 43
 Peerlesspool, 5
 pendulum test, 58
 phase angle, 91
 piezo-electric, 37
 pitot tube, 40
 PIV, 43

- seeding*, 43

 Planar motion Mechanism, 70
 Planar Motion Mechanism, 70
 PMM, 70
 position measurement, 34

potentiometer, 35
 power spectrum, 95
 Prandtl pitot tube, 40
precision error, 115
 precision limit, 117
 Pressure cell, 38
 pressure forces, 9
 Pressure measurements, 37
 Pressure Profile Systems, 39
 pressure sensing film, 39
 pressure sensitive paint, 40
 pressure transducers, 37
 Price and Bishop, 94
 probability distribution, 100
 propeller
 diameter, 68
 speed of advance, 68
 thrust, 43
 torque, 43
 propeller dynamometer, 64
 propulsion test, 63
 PSP, 40
 RAO, 79, 90, 95
 Rayleigh distribution, 100
 regular wave, 90
replication level, 116
 resistance dynamometer, 63
 resistance measurement, 63
 Response Amplitude Operator, 95
 Reynolds number, 10, 68, 122
 riser, 34
 risers, 13, 59
 Rolls-Royce, 113
 Rotating arm tests, 70
 rudder, 69
 sampling frequency, 46, 48, 50
 Samuel Fortey, 6
 sand strip, 64
 Sarpkaya and Isaacson, 124
 Sasajima, 123
 scale effects, 122, 125
 scaling ratios, 12
 sea trials, 106
 Sea trials, 105
 seakeeping, 73
 seakeeping test, 18
 seismic cables, 59
 servo needle wave probe, 46
 Ship monitoring system, 112
 Ship motions, 73
signal-to-noise ratio, 49
 Significant value, 96
 similarity
 dynamic, 8, 9
 geometrical, 8
 kinematic, 8
 Six degrees of freedom, 34
 Skewness, 103
 slamming, 39, 73
 Slow drift motion, 80
 slow drift motions, 29, 53
 spectral analysis, 95
 speed log, 113
 speed trials, 106
 springing, 13, 59
 standard deviation, 116
 Standard deviation, 96
 Stansberg, 80
 stationary process, 93
 Steen, S., 63, 67, 122
 stochastic process, 93
 stopping test, 110
 strain gauge, 31, 33
 Strouhal number, 12
 Student's t distribution, 117
 studs, 64
 surface forces, 9
 Swedenborg, Emanuel, 6
 Tanaka, 123
 tare, 56
 Tekscan, 39
 temperature drift, 56
 Tension Leg Platforms, 59, 80
 test duration, 53
 towing carriage, 18
 towing tank, 16
 towing test, 63
 transducer, 30, 31
 resonance frequency, 52
 transducer drift, 56
 transfer function, 25
 Trial Leader, 106

- trim post, 64
- turbulence stimulator, 64
- turning circle, 110
- UltraLab, 45
- ultrasound wave probe, 45
- uncertainty, 115
- uncertainty analysis, 115
- vacuum tank, 18
- validation, 130
- vapour pressure, 15
- variance, 96
- velocity measurement, 40
 - non-intrusive, 43
 - ultrasonic, 40
- video based systems, 34
- viscous forces, 9
- voluntary speed reduction, 73
- wake fraction, 123
- Walderhaug, 5
- wave
 - amplitude, 91
 - frequency, 91
- wave absorption, 27
- wave beach, 18, 27
- wave drift forces, 29
- wave elevation, 44
- Wave frequency, 79
- wave frequency phenomena, 53
- wave maker, 18, 23
- wave probe, 44
- wave reflection, 27
- wave spectrum, 25
- Weber number, 68
- Webers number, 11
- Weibull distribution, 102
- Wheatstone bridge, 31, 33
- whipping, 13, 59, 73
- White, 8
- Wind generation, 28
- Young's modulus, 14
- zero crossing period, 97
- zero level, 56
- Zeroing, 56
- Zhao, 127
- zig-zag, 110

ANNEX A

EXAMPLE OF REPORTING FROM MODEL TEST

The content of a model test report will depend on the type of testing, the extent of the tests and requirements to reporting form the client. A typical lay out of the model test report may be as follows:

1 Summary

- Summary of the test results and the main conclusion from the model test.

2 Introduction

- General info about the project
- Objectives of the test

3 Description of Test Set - Up

- Model scale
- Test Facilities
- Test arrangement
- Model description; main dimensions, loading conditions etc.
- Model calibration and verification

4 Measurements and Data Acquisition

- Description of used instrumentation (type of transducers). Position of transducers on model or in basin etc.
- Notion and sign conventions
- Co-ordinate system applied for the measurements
- Data acquisition, filtering
- Measuring accuracy
- Control and check routines

5 Environmental Conditions (only relevant for testing in waves)

- Wave, wind and current data used in the tests (when relevant)
- Calibration of environmental conditions

6 Test Programme

- Detailed description of the test program for each type of test (static tests, decay tests, regular wave tests or irregular wave tests) with numbering of tests. All relevant input parameters to be specified (i.e. wave, wind and current condition, speed, loading condition etc.)

7 Data Analysis

- Scaling of results from model to full scale
- Filtering applied during the measurements and analysis
- Analysis carried out and method description for different type of tests (static test, decay tests, wave tests etc.)

8 Presentation and discussion of Results

- Presentation of main results (Detailed results usually in Appendixes)
- Interpretation on evaluation of results for main parameters.
- Evaluation of scale effects

APPENDIXES

Will typically include more detailed information from the tests than what is given in the main report. Examples will be:

- Detailed description of calibration procedures and results
- Wave calibration tests
- Description of analysis methods
- Measured Time series
- Detailed results from analysis (filtering, spectral and statistical analysis)

ANNEX B

EXAMPLE OF MODEL TEST SPECIFICATION

Introduction

Model tests with a turret moored tanker shall be carried out. The tanker model is a standard North Sea shuttle tanker.

The tests shall cover environmental conditions corresponding to typical operational conditions as well as design condition based on the 100 years return period storm.

The model test will be performed at Marintek, Trondheim.

Objectives

The main purpose of the model tests will be verification of the present design. The motions and sea-keeping performance of the tanker as well as the mooring loads are determined for both operating and extreme environmental conditions. The results will also serve as input to calibration and verification of the theoretical and numerical design analyses.

The objectives of the model tests with the moored tanker can be summarized as follows:

- To verify numerical predictions of system global responses, maximum offsets and mooring line tensions;
- To verify numerical predictions of the vertical, horizontal and moment loads transferred from the Turret system to the tanker.
- To measure and estimate the green water effects and possible bottom slamming loads
- To establish the maximum roll and pitch motions
- To quantify the damping of the low frequency motion;
- Forces in the mooring system
- To identify the most critical combination of metocean loads and validate the design of the mooring system;
- To investigate any potential interference problems between tanker mooring system and flexible riser;

Model description

The models shall be constructed to a linear scale of 1:50 .

The water depth is xxx m.

The total test set up include the following components:

- Tanker
- Turret
- Mooring System
- Riser System

Tanker Description

Main data for the tanker:

Parameter	Loaded	Ballast
Length between Perpendiculars, L_{PP}		
Length over all, L_{OA}		
Draft at F, d_{FP}		
Draft at AP, d_{AP}		
Breadth Moulded, B		
Transverse Wind Area		
Longitudinal Wind Area		
Freeboard, main deck f_{MD}		
Freeboard at Bow, f_{BOW}		
Freeboard at Trunk deck, f_{TD}		
Displacement		
Roll Radius of Gyration r_{xx}		
Pitch Radius of gyration r_{yy}		
Yaw Radius of gyration r_{zz}		
Transverse metacentric height, GMt		

Table 1 *Main Particulars of Tanker.*

Both the loaded and ballast condition shall be used (see also Table 1):

The tanker model shall be constructed in accordance with the Yard drawings. The main dimensions, mass and inertia properties of the tanker shall be accurately modeled. The tanker model shall match the prototype's characteristics including the superstructure.

The model will be fitted with equipment for measuring bending moments and shear forces, at two stations of the tanker, at midship position and aft of the Turret. Bending moments shall be measured relative to the pitch, roll and yaw axes of each station and shear force measurements shall include both horizontal and vertical components. The instrumentation shall be designed so as not to distort the model's global responses.

Turret Model

The turret model will be constructed to scale in accordance with the turret design and the line attachment positions will be according to design drawings. The position of the turret will be at position $xxx \cdot L_{pp}$ from FP.

The loads shall be measured in 5 degrees of freedom; forces in x-, y- and z-direction and moment about x- and y-axis. Hence the turret will be free to rotate about the vertical z-axis.

Mooring System

The mooring system consist of 8 evenly distributed mooring lines (i.e. 45° between each line). Mooring line 1 shall be directed towards large wave maker.

Each of the eight mooring lines has the following composition:

Segment type (from anchor)	Length m	Nominal diameter Mm	Axial stiffness EA kN	Weight in air kN/m	Submerged weight kN/m
Chain					
Wire Rope					
Chain					
Wire Rope					

Line pretension = xxx kN (fairlead at depth 15m)

Horizontal distance between anchor and fairlead = xxxx m

Water depth = xxx m

All mooring lines shall be physically modeled in terms of mass, submerged weight and total leg elasticity.

Riser System

The riser system consists of one off xx'' flexible riser in Steep-Wave configuration

The following parameters describe the configuration:

Horizontal distance between top and bottom end connection	:	xx m
Length of bare riser section below buoyancy section	:	xx m
Length of buoyancy section	:	xx m
Length of bare riser section above buoyancy section	:	xx m
Net submerged weight of bare section	:	xxx kN/m
Net buoyancy of buoyancy section	:	xxx kN/m
Outer diameter of bare riser	:	xxx m

The riser configuration will be modeled geometrical correct from the turret table to the sea bottom with the above weight distribution.

Test Program

Still Water Tests

The following still water tests shall be performed:

- (a) Static offset tests to verify stiffness characteristics of the mooring system.
- (b) Extinction tests to measure the low-frequency surge damping and natural period.
- (c) Pitch, heave and roll natural periods for all loading conditions.
- (d) Current load test to verify loads applied by specified current velocity.
- (e) Wind load tests test to verify loads applied by specified wind velocity.

Irregular Wave Test

In Table 2 tentative test program for the irregular wave are specified. The following notations are used:

- H_s : Significant wave height
- T_p : Spectral Peak period
- γ : Wave Spectrum Peaked-ness parameter
- α_{wave} : Wave heading relative current
- U_w : Wind speed, 1 hour mean, at 10 m above sea level
- α_{wind} : Wind heading relative current
- U_c : Current speed

The wind and wave heading given in the table represent the heading relative to current direction. (fixed in the laboratory). The wind spectrum is to be taken as the NPD spectrum.

Intact mooring system is assumed except for one test condition where the most loaded line shall be broken.

For offloading conditions, sufficient combinations of directions of wind, current and wave direction shall be investigated to ensure the critical cases are found.

- Vertical acceleration at
- Global bending moments and shear forces in two transverse cuts
- Tension in mooring lines and riser.

Data acquisition

Data shall be sampled at minimum model scale rate of xxx Hz for the irregular wave tests. For the measurement of pressure and impact forces a sampling rate of xxx Hz shall be applied for tests using the design sea states.

The data recording duration in irregular waves shall be long enough to achieve sufficiently small band width in the spectral analysis. The test duration shall not be less than 3 hours prototype time. A sufficient lapse of time shall be allowed between tests to avoid any distortion of the new generated environment by the previous test.

Analysis

All calculations of spectral analysis and mooring line tension transfer functions shall be documented with band width, record length, sampling estimates. All data analysis shall be provided in both tabular and plot format. Statistical and spectral analysis shall be carried out on all channels. Statistical analysis shall include mean, standard deviation, zero crossing periods, and minimum and maximum values. All results shall be presented in prototype scale.

Required test accuracy

1) Mooring system

Extinction tests to calibrate stiffness and natural periods of the moored system. The measured stiffness and natural periods shall be within $\pm x \%$.

2) Current and Wind Generation

The current velocity profile over the top x % of the water depth shall be modeled in still water.

Wind simulation will be performed by fans. The speed of fans shall be adjusted so that the mean value of analytical or measured data obtained from wind tunnel test is matched for the various tested wind headings.

3) Wave Generation

Acceptable tolerances on the values of significant wave height (H_s), and spectral period (T_p), shall be $\pm x \%$. Wave envelope spectral shall be provided to verify the absence of unrealistic wave reflection in the basin.

Test Documentation

The final report shall contain, as a minimum:

- Detailed description of test set-ups and program;
- Description of models;
- Description of wind, waves, and current modeling;
- Results of static deflection, extinction and current tests;
- Zero crossing statistics of all channels;
- Response amplitude operator plots of all relevant channels (including phase angles);
- Weibull extreme value plots of all channels;
- Mean, standard deviation, minimum and maximum values of all channels;
- Selected time histories of representative portions of each test;
- First and second order waves spectra comparing measured and theoretical;
- High and low frequency numerical filtering of main loads and motions.

Still Photography and Video

Still photographs shall be provided tanker model, the mooring legs and force transducers, the tank set-ups including wave probes, and the wind and current measurement positions.

Video recording of all wave tests by the following cameras:

- Above water camera (roof and side)
- Two underwater camera to observe the mooring lines and riser response

ANNEX C

VISCOUS SURGE DAMPING OF FLOATING PRODUCTION

VESSEL MOORED AT SEA

Huse, E. and Matsumoto, K. 8th OMAE Conference, 1989, The Hague.

VISCOUS SURGE DAMPING OF FLOATING PRODUCTION VESSELS MOORED AT SEA

E. Huse
Marintek
Trondheim, Norway

K. Matsumoto
NKK Corporation
Yokohama, Japan

--

ABSTRACT

The present paper deals with the surge damping, and thus resonant surge motions of ships moored at sea. A procedure for estimation of viscous surge damping is described. The procedure consists in applying the theory and available data for skin friction on an infinite plane wall in oscillatory flow by referring to an area identical to the wetted surface of the ship. Then a "form factor in oscillatory flow" is defined in analogy with the form factor used in traditional ship resistance theory.

Experimental measurements on a tanker model show that the two form factors are of the same magnitude. Assuming the form factor to be independent of Reynolds number the procedure can also be used as a logical basis for evaluating scale effects in model tests with ships in waves moored at sea.

Possible physical contributions to the form factor are discussed. Experiments with flat plates show that "end effects" can only explain a small fraction of the total form factor. Theoretical calculations indicate that the velocity increase along the hull surface due to the potential flow field can also only explain a small fraction of the total form factor.

1. INTRODUCTION

A characteristic feature of moored offshore structures is their slow oscillatory motions at resonant frequencies. They take place well outside the frequency range of the wave spectrum, and are excited mainly by second order wave forces. In surge direction, for instance, the first order motions occurring

at wave frequencies are normally smaller than the resonant surge. Since the resonant motions are often dominating, they are correspondingly important to the peak offsets of the vessel, to the peak loads in the mooring lines, riser design requirements, etc.

First order motions of platforms and ships can today be calculated quite accurately by theoretical methods. Second order motions are more uncertain. Present-day theories for calculating the excitation forces have limitations, and particularly the system damping cannot be calculated on a purely theoretical basis. For low-damped systems at resonance, the motion RAO at resonance is to a first approximation inversely proportional to the damping. The accurate prediction of damping therefore becomes very important in the prediction of motions, maximum offsets and mooring line peak loads.

Main contributions to the surge damping of moored platforms and ships arise from

- a. radiation of waves due to motions
- b. wave drift damping
- c. drag and friction damping of main structure including effects of appendages, roughness, marine growth etc.
- d. drag forces on mooring lines
- e. friction between mooring lines and seabed

The present paper deals exclusively with item c above. Furthermore it is concentrated on moored ships.

2. BASIC IDEA AND SCOPE OF INVESTIGATION

Complete theoretical calculation of the viscous surge damping requires solution of the boundary layer equations for oscillatory flow around arbitrary bodies. Recent developments in computer capacities and numerical methods for boundary layer calculations have been considerable. Nevertheless, their complexity and cost are still such that simple and approximate calculations combined with model testing are necessary in engineering practice. In model testing there is today the problem in testing moored vessels that no standard procedures exist for evaluating possible scale effects. At least they are not so well established and verified as they are for instance in traditional resistance testing of ship hulls.

The present paper presents an engineering approach and shows how it can be used for calculation of viscous surge damping as well as serving as a logical basis for scaling the results of model tests with moored ships in waves. The procedure consists in applying the theory and available data for skin friction on an infinite plane wall in oscillatory flow by referring to an area identical to the wetted surface of the ship. Then a "form factor in oscillatory flow" is defined in analogy with the form factor used in traditional ship resistance theory.

Thus, if we have sufficient empirical information on typical values for the form factor in oscillatory flow, we have also a very simple procedure for calculating viscous surge damping. Furthermore, if we, in analogy with ship resistance theory, assume that the form factor in oscillatory flow has the same value in model and full scale we also have a logical basis for evaluating scale effects in model testing of moored ships.

Fig. 1 illustrates the basic idea. In this diagram R_n is the Reynolds number defined by

$$R_n = \frac{\omega x_0^2}{\nu}$$

where

ω = circular frequency of vessel surge motion

x_0 = amplitude of surge motion

ν = kinematic viscosity

The friction coefficient C_{osc} is defined by

$$C_{osc} = \frac{F_d}{\frac{1}{2} \rho (\omega x_0)^2 S} \quad (1)$$

where

F_d = amplitude of viscous force component in phase with the surge velocity

ρ = density

S = wetted surface

The points marked "model" and "ship" in Fig. 1 are meant to represent the ship-shaped hull, while the curve represents data for an infinite flat plate oscillating in its own plane.

It should be carefully noticed that the "friction line" shown in Fig. 1 is of course basically different from the friction lines used in ship resistance work.

Our "form factor in oscillatory flow" as used in this paper is defined by (see Fig. 1).

$$k_{osc} = \frac{a}{b} \quad (2)$$

This definition is consistent with the one in Ref. 6.

Basic hypotheses of this paper now are:

- The value of k_{osc} will not vary very much between hulls of similar shape. Thus if we have some typical values for k_{osc} , they are more generally applicable.
- The value of k_{osc} is independent of Reynolds number.

In the subsequent sections the above procedure is worked out in more detail for practical application, and some experimental data are provided, indicating that the form factor in oscillatory flow is of approximately the same magnitude as the traditional form factor obtained from resistance tests.

3. OSCILLATORY FLOW ON FLAT PLATE

The problem of laminar oscillatory flow on an infinite flat plate was first treated by G. Stokes and is well known as Stokes' second problem, Ref. 1. According to the solution of Stokes' second problem, the friction coefficient C_{osc} is

$$C_{osc} = f_w \cdot \cos \phi \quad (3)$$

where

$$f_w = 2/\sqrt{R_n}$$

$$\phi = \pi/4$$

The angle ϕ in the above formula represents a phase lag between total skin friction force and free stream velocity. Since we are dealing with damping considerations, we are only interested in the friction force component in phase with the velocity. Therefore the factor $\cos \phi$ has been included in the expression for C_{osc} in Eq. 3.

As shown in Appendix 1 a series of decay tests with flat plates oscillating in their own plane have been performed. The results are shown in Fig. 2 together with the theoretical line of Eq. 3. The agreement is excellent.

Turbulent oscillatory flow and friction on an infinite flat plate have been treated by many researchers, especially in connection with the kinematics and dynamics of the fluid motion in the wave boundary layer near the seabed in shallow water. Various semiempirical theories and experimental data have been published. Reviews of these works are given in Refs. 2 and 3.

Among them Jonsson, Ref. 4, gave a simple approximate expression of turbulent friction coefficient on a smooth infinite flat plate as

$$f_w = 0.09 \cdot R_n^{-0.2} \quad (4)$$

Jonsson gives no information on phase lag.

Myrhaug, Ref. 5, presented the friction coefficient and phase lag in smooth, infinite plate, turbulent flow by the following implicit equation. Constants in the equation were determined from turbulent flow data.

$$\frac{2\kappa^2}{f_w} = [\ln(4.5 \cdot C \cdot R_n \cdot f_w)]^2 + B^2 \quad (5)$$

$$\phi = \sin^{-1} \left[\frac{B}{\kappa} \cdot \sqrt{f_w/2} \right] \quad (6)$$

where

$$\begin{aligned} \kappa &= 0.4 = \text{Karman's constant} \\ B &= 1.28 \\ C &= 0.30 \end{aligned}$$

Examples of f_w and ϕ values obtained from Eqs. 5 and 6 are given in Table 1.

In Fig. 2 the friction line according to Myrhaug's formula is shown, corrected for phase lag according to the phase angles shown in Table 1. The line according to Jonsson's formula has been corrected for phase lag according to the same phase angles.

4. EXPERIMENTAL DETERMINATION OF FORM FACTOR IN OSCILLATORY FLOW

The form factor k_{osc} has been determined experimentally for a 1:45 scale model of a large tanker in fully loaded condition. Model dimensions are:

length b.p.	5.785 m
breadth	0.7939 m
draught	0.3077 m
wetted surface	7.111 m ²
block coefficient	0.84

Body plan of the vessel is shown in Fig. 3.

A simple calm water surge decay test was done in MARINTEK's Ocean Laboratory, which is 80 m long and 50 m wide. The model was suspended in horizontal lines and springs above water. The axes of the springs were kept horizontal by means of vertical lines extending up to the roof structure of the building. By this system one obtains a purely linear spring coefficient and, more important, there is no mechanical friction that can disturb the test results. The surge motion of the model was measured by the OPTOPOS system, which is an electro-optical system for motion measurements (requiring no mechanical contact with the model).

The stiffness of the springs was chosen to give a resonant surge period of 18.5 seconds, model scale. Start amplitude for the decay test was 0.7 m, and the recording was done over the subsequent 80 surge periods.

The time trace of the surge motion was analysed as described in Appendix 2. The resulting C_{osc} values are plotted in Fig. 2, giving a form factor

$$k_{osc} = 0.60$$

when referring to the Jonsson flat plate formula.

The model has also been subject to resistance tests, towing in both forward and reverse directions. The resulting form factors in stationary flow were

$$\begin{aligned} k &= 0.50 \text{ in forward direction} \\ \text{and} \\ k &= 0.68 \text{ in reverse direction} \end{aligned}$$

5. PHYSICAL FLOW CONSIDERATIONS ON FORM FACTORS

In this section an attempt is made to split the form factor into its different physical contributions and to discuss their magnitudes. They are also compared with those in stationary flow.

First of all, when doing a calm water surge decay test there will always be a certain damping due to wave generation. By definition this is not part of the viscous damping, and must be considered as a source of error in the testing technique. An evaluation based on theoretical calculations shows that in the present tests the wave generation has produced a negligible damping compared to the viscous one.

The first contribution to K_{osc} to be discussed is the effect of the finite length of the vessel, or "end effect". The Jonsson formula is based on an infinite plate, while the finite length of the ship hull means that its bow and stern will move in and out of a wake which is different from the boundary layer along the parallel body or an infinite flat plate. As explained in Appendix 1 this end effect has been determined experimentally for flat plates. Applying the results of a flat plate of the same length as the hull model, the contribution of the "end effect" to K_{osc} is in the range of 0.05 to 0.10 depending on the ratio of motion amplitude to plate length.

A second physical contribution to K_{osc} is the effect of the flow curvature around the hull, which means that the local velocities will be different from the flat plate case. As shown in Appendix 3 the potential flow field around the hull has been calculated theoretically. The skin friction has been calculated by the Jonsson formula, using local input velocities along the hull corrected for the potential flow. The resulting contribution to K_{osc} was evaluated to be about 0.03.

None of the above two contributions can explain the measured K_{osc} of about 0.60. Thus there must be other physical contributions which are much more important. A possible hypothesis is that the pressure distribution over the hull is influenced by the boundary layer flow, or that one has in fact a sort of pressure drag in addition to the skin friction force.

This pressure drag is consistent with suggested physical explanations of the form factor in stationary flow (resistance theory).

A very important observation is that the measured form factor in oscillatory flow, K_{osc} , is very close to the form factors measured in stationary flow during forwards and reverse resistance towing tests with the same model. Since only one hull model has been tested it may be premature to consider this a general conclusion. More tests cases would definitely be desirable. In the meantime, the best recommendation for engineering purposes would be to assume that the form factor in oscillatory flow has the same value as the one in stationary flow. This

means that in evaluation of viscous surge damping the vast amount of empirical information on form factor from resistance testing can be applied.

In fact there is at least one previous publication in which measured surge damping has been compared to calculations based on flat plate skin friction, Ref. 6. It is known, however, that those measurements were done with the model suspended in springs and lines running over pulleys. The pulley friction has probably lead to erroneously large surge damping.

For the purpose of scaling results of wave tests with moored ships, one may assume that the oscillatory flow form factor, K_{osc} has the same value in model and full scale, i.e. it is independent of Reynolds number. This hypothesis can not be proved on the basis of available experimental data. However,

- the above discussion indicates a close relationship with the resistance form factor, and
- the assumption that the resistance form factor is independent of R_n does according to many year's practical experience give accurate prediction of ship resistance.

Thus it should not be unrealistic to apply the same hypothesis also in the oscillatory flow case.

6. SCALING OF RESONANT SURGE MOTIONS

In the previous sections a practical procedure for evaluating the viscous surge damping of a moored vessel has been presented. In addition the same principles can be used as a basis for scaling surge damping from model tests, and thus for scaling of resonant surge motions of a moored ship.

Let us consider a general case including both constant, linear and quadratic damping forces. In case of sinusoidal excitation the equation of motion of such a system is

$$m\ddot{x} + b_0 \frac{\dot{x}}{x} + b_1 \dot{x} + b_2 |x| \dot{x} + cx = F_0 \sin(\omega t) \quad (7)$$

Let us assume that mass m , stiffness c and excitation force amplitude F_0 are not subject to scale effects, i.e. they scale according to Froude's model law. Let us further assume that the relative system damping is small so that with sinusoidal excitation we shall also have approximately sinusoidal motion, i.e. at resonance

$$x = x_0 \sin(\omega_r t - \pi/2) \quad (8)$$

where ω_r is the resonant circular frequency.

Physically the second term on the left hand side of Eq. 7, $b_0 \dot{x}/|x|$ represents a damping force which is independent of motion amplitude. This is a realistic description of for instance mechanical friction between mooring lines and seabed, friction in case of mechanical connection between model and carriage, etc.

The linear damping force (third term in Eq. 7) physically describes wave generation damping. It also approximates the wave drift damping. The fourth term in Eq. 7 represents quadratic damping, for instance due to skin friction, pressure drag, drag force on mooring lines, etc.

The energy dissipation per cycle due to a damping force F_d is in general given by

$$\Delta E = \int F_d \cdot dx \quad (9)$$

where the integration is done over one complete cycle. The energy dissipation per cycle due to constant, linear and quadratic damping forces in Eq. 7 are obtained as follows, respectively,

$$\Delta E_0 = 4 b_0 x_0 \quad (10)$$

$$\Delta E_1 = \pi b_1 \omega_r x_0^2 \quad (11)$$

$$\Delta E_2 = \frac{8}{3} b_2 \omega_r^2 x_0^3 \quad (12)$$

For a system oscillating at constant amplitude the total energy dissipation per cycle due to damping forces has to be equal to the energy delivered by the excitation force, which can be calculated by substituting the excitation force $F_0 \sin(\omega t)$ for F_d in Eq. 9.

The result is

$$\Delta E_{ex} = \pi F_0 x_0 \quad (13)$$

From Eqs. 10 through 13, we thus have

$$\pi F_0 x_0 = 4b_0 x_0 + \pi b_1 \omega_r x_0^2 + \frac{8}{3} b_2 \omega_r^2 x_0^3$$

or

$$F_0 = \frac{1}{\pi} (4b_0 + \pi b_1 \omega_r x_0 + \frac{8}{3} b_2 \omega_r^2 x_0^2) \quad (14)$$

Eq. 14 is valid for model as well as full scale. Using indices m and s to indicate the model and full scale ship respectively, the excitation force amplitude scales

$$F_{0s} = F_{0m} \cdot \lambda^3 \frac{\rho_s}{\rho_m} \quad (15)$$

where

λ = geometrical scaling factor
 ρ = density of water

From Eqs. 14 and 15 we now obtain

$$U_s = U_m \cdot \lambda^3 \frac{\rho_s}{\rho_m} \quad (16)$$

where

$$U = 4b_0 + \pi b_1 \omega_r x_0 + \frac{8}{3} b_2 \omega_r^2 x_0^2 \quad (17)$$

Considering the coefficients b_0 , b_1 and b_2 to be known in model as well as full scale, and also considering the model motion amplitude x_{0m} to be known (measured), Eq. 16 represents a second order equation in the unknown full scale motion amplitude x_{0s} . Solving this equation gives us the general scaling formula.

$$x_{0s} = \frac{3}{16b_{2s}\omega_{rs}} \left[-\pi b_{1s} + \sqrt{(\pi b_{1s})^2 - \frac{32}{3} b_{2s} (4b_{0s} - \lambda^3 \frac{\rho_s}{\rho_m} U_m)} \right] \quad (18)$$

A part of the quadratic damping coefficient b_{2s} might be due to viscous damping on the hull, and it is also a function of motion amplitude x_{0s} as given in the previous section of the present paper. In that case, when x_{0s} is obtained by Eq. 18 some iteration calculations may be necessary.

Eq. 18 gives the full scale motion amplitude at resonance in regular waves when the corresponding model motion amplitude and damping coefficients in full and model scale are known.

Let us then consider scaling of test results in irregular waves. Of particular interest is the significant value of the low frequency part of the motion, i.e. after low-pass filtering of the motion signal, leaving only the spectral peak around resonance.

For a linear system it is known (see for instance Ref. 8) that

$$\frac{x_{0s}}{x_{0m}} = \frac{b_m}{b_s}$$

and

$$\frac{x_{1s}}{x_{1m}} = \sqrt{\frac{b_m}{b_s}}$$

where

b = linearized damping coefficient in the equation of motion

$x_{1/3}$ = significant value of low-frequency motion

From the above expressions we get

$$\frac{x_{1/3}^s}{x_{1/3}^m} = \sqrt{\frac{x_{0s}}{x_{0m}}} \quad (19)$$

where the motion amplitudes x_0 refer to regular waves, and are subject to scaling according to Eq. 18. As mentioned above the basic assumption behind Eq. 19 is linearity. For a system with nonlinear damping no such simple formula exists for quantification of significant motion. From general experience with linearization of such systems one would expect that Eq. 19 is sufficiently accurate for most practical applications in scaling model results.

In practical application of Eq. 19 the question arises:

Having measured the significant value $x_{1/3m}$, which level of motion amplitude x_{0m} referring to regular waves should be used? This is a subject of further investigations. Until the results of such investigations are available, a reasonable recommendation would be to use an x_{0m} value equal to $x_{1/3m}$.

A brief outline of a complete procedure for scaling resonant surge motions in regular waves will be as follows:

- a. Measure the model motion amplitude at resonance x_{0m}
- b. Measure or estimate the coefficients b_0 , b_1 and b_2 for model scale
- c. Estimate the same coefficients in full scale
- d. Calculate the full scale motion amplitude at resonance x_{0s} from Eq. 18

In case of irregular waves the significant value of the low-frequency part of the motion can be scaled by Eq. 19 after scaling of the resonant motion in regular waves.

The previous sections of the present paper have discussed in detail how one of the damping contributions, the viscous one, can be scaled. Detailed discussion of other contributions as listed in section 1, practical procedures for their determination, etc. is beyond the scope of the present paper.

The magnitude of the scale effect correction on surge motion due to scale effect on viscous surge damping will be very different from case to case, so that no general figure on its magnitude can be given. In many cases the surge damping due the mooring system (Ref. 7) and/or the wave drift damping can

be as much as one order of magnitude higher than the viscous hull damping. In carefully conducted model tests these contributions will not be subject to scale effects, and the total scale effect on resonant surge will be very small.

As one extreme case of relatively low viscous surge damping let us assume that the energy dissipation due to viscous damping on the hull model is 10 percent of the total energy dissipation due to damping forces. Let us further assume that the remaining 90 percent of the energy dissipation is divided into halves due to linear damping force, e.g. wave drift damping, and due to quadratic damping force, e.g. mooring line damping, and assume that both of them are free from scale effects.

When the ship reported in the present paper is applied with model motion amplitude at resonance of 0.5 m, the model and full scale skin friction coefficients (Fig. 2) differ by a factor of 3. In this case the above correction procedure gives scale effect correction factor

$$\frac{x_{0s}}{\lambda \cdot x_{0m}} = 1.05$$

for resonant motion in regular waves. The correction factor for significant value of low frequency surge in irregular waves becomes

$$\frac{x_{1/3}^s}{\lambda \cdot x_{1/3}^m} = 1.02$$

As the other absolute extreme let us consider the case where viscous hull damping is dominating to the extent that other sources of surge damping can be neglected. In practice this could nearly be the case for a tanker moored to an articulated tower in an area of small waves but high wind velocities, so that wind gusting is the main source of resonant surge excitation. For the same model with the same motion amplitude as above the correction procedure gives scale effect correction factors of 2.03 and 1.42 on resonant amplitude in regular wave and significant value of low frequency surge, respectively.

7. CONCLUSIONS

- The concept of form factor in oscillatory flow is used, defined on the basis of measured viscous surge damping of a ship hull and the theoretical skin friction of oscillating infinite plates.

- Experiments on a typical tanker model show that this form factor in oscillatory flow has about the same magnitude as the traditional form factor obtained in ordinary resistance tests.
- The application of a form factor in oscillatory flow together with the flat plate friction formula represents a simple engineering approach to evaluation of viscous surge damping.
- Assuming the form factor to be independent of Reynolds number the same basic principles can be used for evaluating scale effects on model test results from testing moored ships in waves. Depending on conditions the scale effect on the resonant surge amplitudes can be anything from a factor close to 1.0 (no scale effect) to a factor of 2.0.
- Experiments with flat plates show that "end effects" can only explain a small fraction of the total form factor. Theoretical calculations indicate that the velocity increase along the hull surface due to the potential flow field can also only explain a small fraction of the total form factor.

R_n	f_w	ϕ (deg)
10^5	0.00668	10.6
10^6	0.00419	8.4
10^7	0.00283	6.9
10^8	0.00202	5.8

Table 1 Semi-empirical calculations of f_w and ϕ for smooth turbulent flow using Eqs. 5 and 6.

APPENDIX 1. FLAT PLATE EXPERIMENT

In order to verify the theory on the laminar flow around the oscillating infinite flat plate described in Sec. 3 of this paper, and to get some information about the end effect of the plate (or the effect of finite dimensions of the plate), the damping coefficient due to skin friction on plates was directly measured by decay tests using the pendulum mechanism in MARINTEK's Ocean Laboratory.

Fig. 4 shows the test set-up. A flat plate with smooth surface A was fixed to the pendulum C. The basic principle of the test is to have the pendulum act as an exciter of horizontal motion of the plate. The energy dissipation can then be obtained very accurately from the decay of pendulum motion amplitude. The tests were performed with a pendulum length of 7.2 m and pendulum mass of 200 kg. Long and short plates were tested. Their lengths were 5.0 m and 2.5 m respectively, and the draft D was 1.173 m for both plates.

In order to compare the measured damping coefficient with the theory for infinite flat plate, end effect of the plate was corrected by the following procedure:

Measurements were performed for a long and a short plate. Here we assume that the measured damping coefficient consists of 2 contributions:

- the skin friction on an oscillating infinite plate multiplied by the area of the plate, and
- the end effect.

If we also assume that the end effect has the same magnitude for both long and short plate, we can obtain the skin friction F for a short plate excluding the end effect as

$$F = F_l - F_s$$

where

$$F_l = 2F + F_e$$

= measured skin friction on a long plate.

$$F_s = F + F_e$$

= measured skin friction on a short plate.

$$F_e = \text{end effect.}$$

The experimentally obtained friction coefficients are shown in Fig. 2 together with the theoretical line of Eq. 3 given in Sec. 3 of this paper. The theory shows good agreement with the experiments.

The experimental results show that the ratio of end effect to skin friction on the long plate

$$r_e = \frac{F_e}{2F}$$

depends on the amplitude ratio r_a defined by

$$r_a = \frac{x_0}{L_1}$$

where

$$x_0 = \text{horizontal motion amplitude}$$

$$L_1 = \text{length of long plate.}$$

The end effect ratio increases from 0.05 at an amplitude ratio of 0.020 to 0.10 at an amplitude ratio of 0.055.

APPENDIX 2 ANALYSIS METHOD

The surge decay tests on the ship model were analyzed by assuming that the surge motion satisfies an equation of the form

$$m \ddot{X} + \frac{1}{2} \rho S C_{osc} |\dot{X}| \dot{X} + C X = 0$$

where m , ρ , S , C_{osc} , and C have already been defined in the main body of this paper. The basic principle of the analysis is to determine the value of C_{osc} so that the energy dissipation per cycle represented by the damping term in the above equation becomes equal to the energy dissipation measured in the decay test.

If we assume that the surge motion is a pure sinusoidal motion as

$$X = X_0 \sin(\omega t) \quad (20)$$

The energy dissipation per cycle in this system can be given by

$$\begin{aligned} \Delta E &= 4 \int_0^{X_0} \frac{1}{2} \rho S C_{osc} | \dot{X} | \dot{X} dX \\ &= \frac{4}{3} \rho S C_{osc} \omega^2 X_0^3 \end{aligned} \quad (21)$$

By using the measured amplitudes in the decay test, the energy dissipation per cycle can also be expressed by

$$\Delta E = \frac{1}{2} m \omega^2 (X_i^2 - X_{i+1}^2) \quad (22)$$

where X_i is the amplitude of the i 'th oscillation. There is one period difference between X_i and X_{i+1} . From Eqs. 21 and 22 the friction coefficient C_{osc} is obtained as

$$C_{osc} = \frac{3m}{8\rho S} \cdot \frac{X_i^2 - X_{i+1}^2}{X_0^3} \quad (23)$$

Measured surge motion X is not purely sinusoidal as in Eq 20, due to the decaying amplitudes. For the analysis, therefore, the mean value of X_i and X_{i+1} was used for X_0 in Eq. 23 as follows.

$$C_{osc} = \frac{3m}{8\rho S} \cdot \frac{X_i^2 - X_{i+1}^2}{\left(\frac{X_i + X_{i+1}}{2}\right)^3} \quad (24)$$

APPENDIX 3. FLOW CURVATURE CONSIDERATIONS

An attempt was made to evaluate if flow curvature due to potential flow around the hull could influence the skin friction, and thus represent a considerable contribution to the skin friction. The procedure was as follows:

- the wetted surface of the hull was divided into altogether 630 surface elements
- the potential flow field around the hull was calculated by a "Hess and Smith type" computer program
- the local velocity at each surface element, corrected for the potential flow field, was used in calculating the skin friction by the Jonsson formula
- the longitudinal components of the friction force on all elements were summed up to obtain the total skin friction including the effect of flow curvature.

The result was that the above procedure increased the skin friction by 2.5 percent compared to the flat plate of equal wetted surface.

REFERENCES

- [1] Schlichting, H., "Boundary-Layer Theory" 7th Edition. McGraw-Hill, New York, 1979.
- [2] Jonsson, I.G., "A new approach to oscillatory rough turbulent boundary layers", Ocean Engineering, Vol. 7, pp. 109-152, 567-570, 1980
- [3] Myrhaug, D., "Modeling rough turbulent wave boundary layers", Encyclopedia of Fluid Mechanics (N.P. Chermisnoff, editor), Gulf Publishing Company, Houston, Vol. 6, pp. 1229-1335, 1986.
- [4] Jonsson, I.G., "Wave boundary layers and friction factors", Proc 10th Conf. Coastal Engng., Tokyo 1966, Vol. I, pp. 127-148, Am.Soc. Civ. Engrs., New York.
- [5] Myrhaug, D., "A rational approach to wave friction coefficients for rough, smooth and transitional turbulent flow", Division of Marine Hydrodynamics, Norwegian Institute of Technology, Trondheim, 1988, to appear in Coastal Engineering.
- [6] Faltinsen, O.M. et. al. "Slowdrift Damping and Response of a moored ship in Irregular Waves", Proceedings OMAE, Tokyo, 1986.

[7] Huse, E., and Matsumoto, K., "Practical Estimation of Mooring Line Damping", Paper No. 5676, Offshore Technology Conference, Houston 1988.

[8] Hoof, J.P. "Advanced Dynamics of Marine Structures", pp:167-169, John Wiley & Sons, 1982

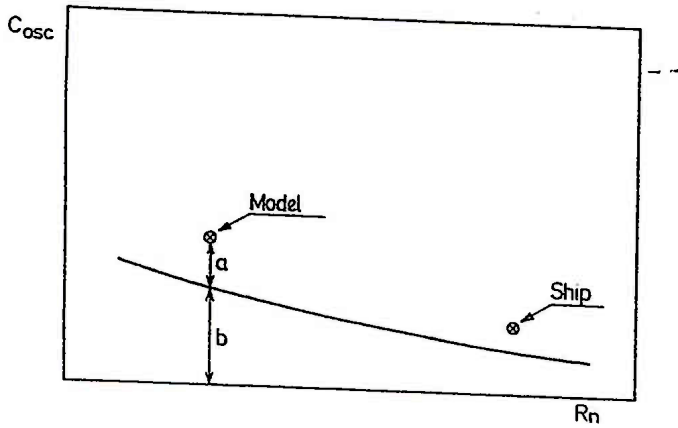


Fig. 1 Definition of basic principles

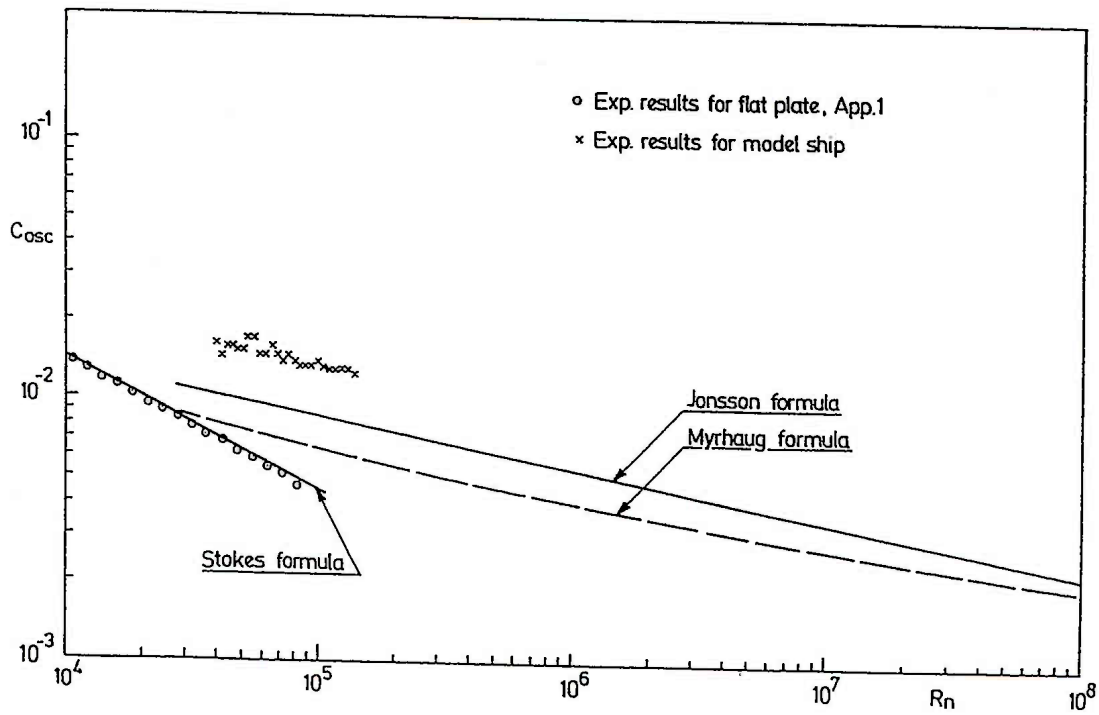


Fig. 2 Friction coefficient C_{osc} versus R_n

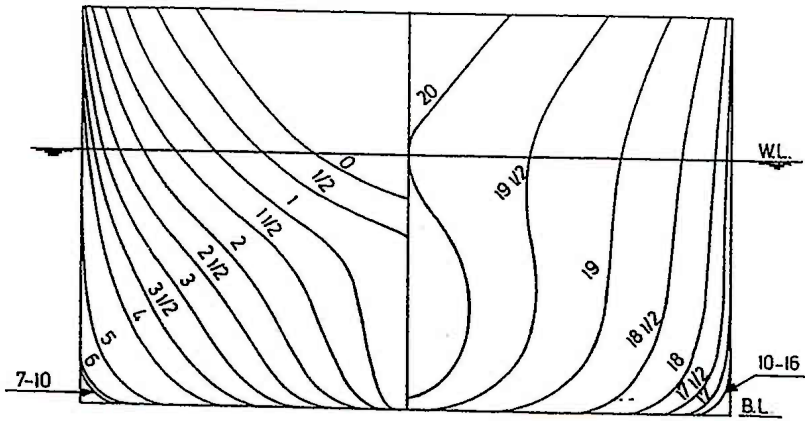


Fig. 3. Body plan of vessel

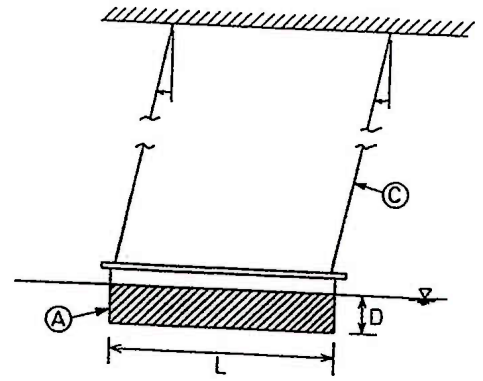


Fig. 4 Pendulum test set-up for flat plate

LECTURE NOTE: ERROR ANALYSIS OF EXPERIMENTS

S. Ersdal

August 10, 2004

1 Basic statistics

The aim of an error analysis is to give a quantitative measure of how reliable a measured or calculated value is. Normally this is presented as a confidence interval, e.g 95%. This means that the probability that the true value is within the given interval is 0.95. In the following the word error will be used to describe the distance between a measured or calculated value and the true, but unknown, value. The word uncertainty may be used for the statistical estimate of the same thing.

All analysis here refers to so called time wise experiments, i.e. the measured quantity is measured at a single location at different times. The alternative, sample-to-sample experiments, in which the quantity varies in space but not in time may in marine applications be the interesting for applications as thermodynamic properties of water and material properties of material. For the towing tank experiments considered here such variations are not considered.

1.1 Bias, precision and total error

Two types of errors are considered in the analysis: *bias* and *precision* errors. The difference is illustrated in figure 1 taken from Coleman and Steele (1989). The figure also illustrate the *total* error as the sum of bias and precision errors. A main assumption in this analysis is that if an infinite number of measurements were taken the precision error would follow a Gaussian distribution. The bias error would then be the difference between the mean of this distribution and the true value. The trouble with these definitions is of course that the true value is unknown, so in practice a alternative definition is needed.

To do this the concept of replication level is introduced. When repeating an experiment the replication level describes what exactly is repeated, here in tree levels. At the zeroth order replication the measured quantity is assumed absolutely constant in time, so that only variations inherent in the measurement system it selves contributes to the error. For example, calibration of load cells before mounting it in the experimental setup should give zeroth order replication. In this case the true value is known, so bias and precision can be estimated in the normal sense. At first-order replication level the instrumentation and setup is fixed, but the time is running. This corresponds to repeating the experiment keeping the instrumentation constant. Repeated runs in a tow tank is a good example. Nth level replication includes all other possible changes when repeating the experiment, form changing a pressure cell, to performing a similar experiment in another laboratory, with different personnel.

Since the bias error in the zeroth level replication usually can be accounted for in the calibration model, a more practical distinction between precision and bias error is as follows. The precision error is given by the variation of first order replication while bias error is included at Nth order replication. This immediately reveal the main problem of evaluating the bias error, it can in practice not be measured. Estimates must be based on experience and more or less educated gusses. On the other hand the precision error can be estimated to a reasonable degree by repeating the experiment.

1.2 Sample population and confidence interval

If the measurement is repeated an infinite number of times, the main assumption here is that the measured value will be normal, or Gaussian, distributed around a mean. This *parent distribution* is characterized by the mean μ and the standard deviation σ , and expressed by

$$f(X) = \frac{1}{\sigma\sqrt{2\pi}} e^{-\frac{(X-\mu)^2}{2\sigma^2}} \quad (1)$$

here $f(X)dx$ is the probability that a single measurement X will lie between X and $X+dX$. The measurement is of course never repeated an infinite number of times. The statistic properties of interest is therefore

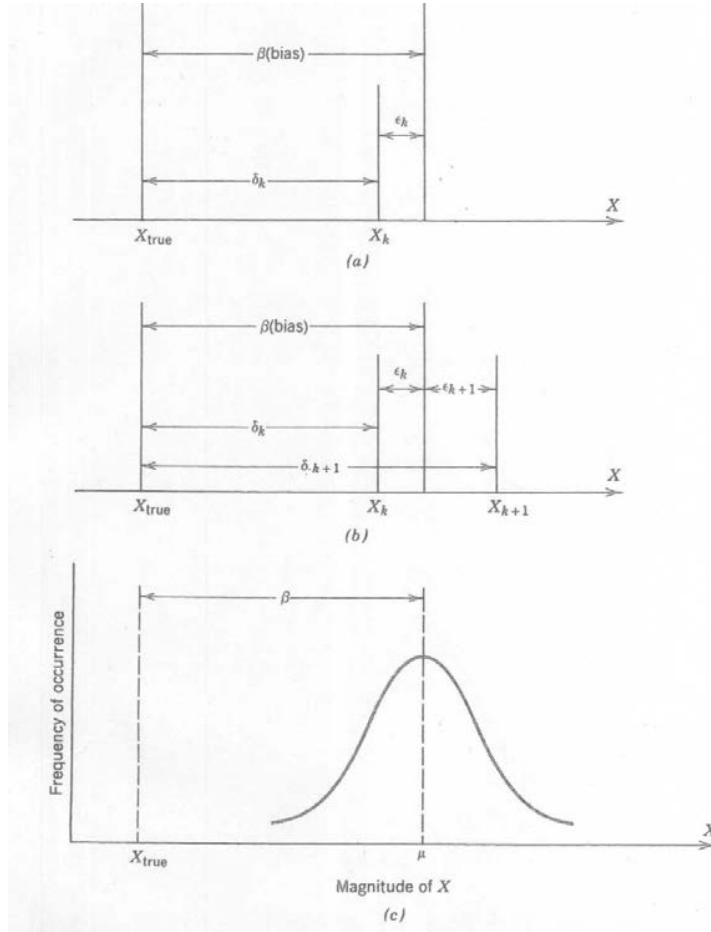


Figure 1: *Errors in the measurements of a variable X: a) single reading, b) two readings, c) infinite number of readings. From Coleman and Steele (1989)*

based on a *sample population* that consist of a finite number of samples drawn from the parent distribution. For the sample population the mean is given by

$$\bar{X} = \frac{1}{N} \sum_{j=1}^N X_j \quad (2)$$

where N is number of samples (measurements) X_j . The precision index, or standard deviation, of the sample population is defined by

$$S_x = \sqrt{\frac{1}{N-1} \sum_{j=1}^N (X_j - \bar{X})^2} \quad (3)$$

Working with a sample population, the mean in equation (2) will depend on the set of samples taken from the parent population. Thus the mean it selves is normally distributed with mean μ (mean of the parent distribution) and standard deviation (Kreyszig 1988)

$$S_{\bar{x}} = \frac{S_x}{\sqrt{N}} \quad (4)$$

For the parent distribution the confidence interval of a sample is given by

$$Prob(X_j - t\sigma \leq \mu \leq X_j + t\sigma) = \gamma \quad (5)$$

where $t \simeq 1.96$ for a normal distribution and confidence level $\gamma = 0.95$, i.e the 95% confidence interval. For the sample population, the standard deviation is unknown thus the value of t is not given. Equation (5) can

be rewritten

$$Prob \left(t \leq \frac{X_j - \mu}{S_x} \leq t \right) = \gamma \quad (6)$$

where the variable $\frac{X_j - \mu}{S_x}$ is random and follows a Student's t distribution, with $N - 1$ degrees of freedom. The value of t may be found from (Kreyszig 1988)

$$t = F^{-1} \left(\frac{1}{2}(1 + \gamma) \right) \quad (7)$$

where $F^{-1}(\cdot)$ is the inverse of the cumulative density function for the t -distribution, again with $N - 1$ degrees of freedom. Figure 2 gives values of t for 95% and 99% confidence intervals. For $N > 30$ the value $t = 2$ is acceptable (International Towing Tank Conference 1990). The precision limit for a sample is then

$$P_x = tS_x \quad (8)$$

and for the mean of N repetitions

$$P_x = t \frac{S_x}{\sqrt{N}} \quad (9)$$

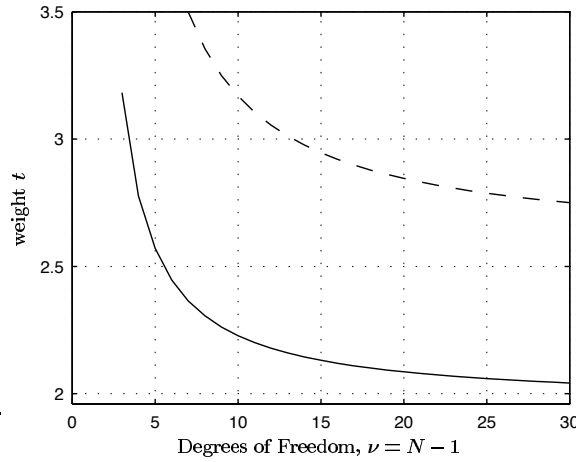


Figure 2: The weight t for estimating confidence intervals: — 95% confidence; -- 99% confidence. Ordinate axis corresponds to 95% confidence for a normal distribution: $t=1.96$

1.3 Chauvenet's criterion for rejecting outliers

Data samples that appears significantly out of line with the majority of samples are called *wild* points, or *outliers*. If the reason for such discrepancy is obvious and verifiable, such points can be disregarded. In cases where the reason is harder to explain, an acceptable criterion for rejection of a sample is the Chauvenet's criterion. This states that samples within a band around the mean with probability of exceedence less than $1 - \frac{1}{2N}$ should be retained. This limit can be expressed as a weight on the standard deviation:

$$t_{chauenet} = F^{-1} \left(\frac{1}{2}(1 + p) \right) \quad (10)$$

where $p = 1 - \frac{1}{2N}$ is the limit probability based on N samples. Note that in this case $F(\cdot)$ is the cumulative density function of the normal distribution, also for small values of N . Values of $t_{chauenet}$ are plotted in figure 3.

Samples with higher deviation from the mean than:

$$|X_j - \bar{X}| > t_{chauenet} S_x \quad (11)$$

may then be disregarded, and new mean and standard deviation can be found based on the remaining data. The procedure can only be performed once.

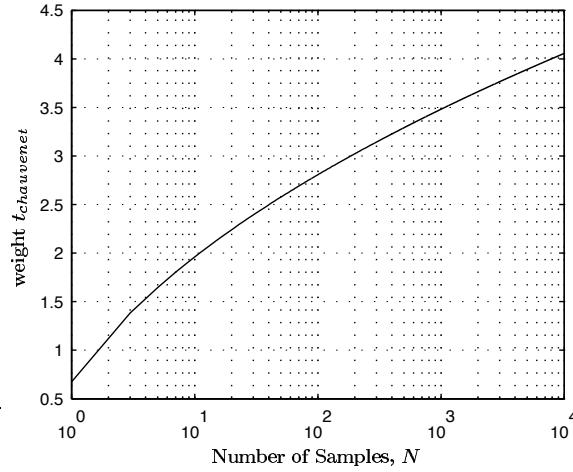


Figure 3: The weight $t_{\text{chauvenet}}$ in Chauvenet's criterion for rejection of outliers

1.4 Bias error estimation

The precision limits in equation (8) and equation (9) is only valid for the precision part of the error, while the bias cannot be treated this way. This follows from definition, the bias error does not change when the measurement is repeated. Note that the higher the replication level of repeated measurements, the fewer unknown bias errors there are in the results. This means that errors that must be estimated if the experiment is performed only once, might be included in a statistical analysis if the experiment is repeated.

Known and well defined bias errors, like constant terms in a calibration model, are usually corrected for and not included in the error analysis. The rest, for example the uncertainty of the constant term in the calibration model, must be estimated in some way. The approach is to establish a bias error limit B that with a given confidence represents the unknown bias. In order to establish this limit simplified estimates, experience or more or less educated guesses must be applied.

2 General Uncertainty Analysis

The parameter actually measured is seldom the final result of the test. For example, when measuring force with a strain gauges the parameter actually measured is an electrical resistance. Based on the change in resistance, a force is calculated, and then usually non dimensionalized. The final result is therefore a function of several parameters, both inherit in the measurement method and in the preferred way to present the result.

2.1 Reduction equation

The functional relationship is called the *reduction equation* and is expressed:

$$X = f_r(Y_1, Y_2, \dots, Y_N) \quad (12)$$

where X is the measurement (sample) and the reduction equation f_r is a function of N parameters $Y_1 \dots Y_N$. Examples for the experiments in later chapter of such parameters are calibration factors, tow speed and model dimensions but also less obvious factors like temperature and thermodynamic properties of water. The first step of the error analysis is to establish a list of parameters that must be considered. In the following these parameters are denoted *elemental error sources*.

Assuming that a small change in a parameter Y_i results in a small change in the measured value, Taylor expansion gives:

$$X = \hat{X} + \frac{\partial \hat{X}}{\partial Y_i} \Delta Y_i + \frac{1}{2} \frac{\partial^2 \hat{X}}{\partial Y_i^2} \Delta Y_i^2 + \mathcal{O}(\Delta Y_i^3) \quad (13)$$

$$\simeq \hat{X} + \frac{\partial \hat{X}}{\partial Y_i} \Delta Y_i \quad (14)$$

From this, the *influence coefficient* is defined as

$$\kappa_i = \frac{\partial \hat{X}}{\partial Y_i} \quad (15)$$

and the elemental error is:

$$e_i = \frac{\partial \hat{X}}{\partial Y_i} \Delta Y_i = \kappa_i \Delta Y_i \quad (16)$$

In most cases the absolute value of ΔY_i is not known. Rather it is given as a precision limit based on a confidence interval as described in the previous section. The recommended practice is the 95% confidence interval, where the probability of the actual ΔY_i being less or equal to the estimated value is 95%:

$$\Delta Y_i = P_{Y_i} = P_i \quad (17)$$

or for bias error

$$\Delta Y_i = B_{Y_i} = B_i \quad (18)$$

Where P_i and B_i are the precision and bias limit of parameter Y_i respectively.

2.2 Error propagation

If all elemental error sources are independent, the combined effect on the measured value (error propagation) is:

$$e = \sqrt{\sum_{i=1}^N (\kappa_i e_i)^2} \quad (19)$$

The precision and bias errors are calculated separately:

$$e_P = \sqrt{\sum_{i=1}^N (\kappa_i P_i)^2} \quad (20)$$

$$e_B = \sqrt{\sum_{i=1}^N (\kappa_i B_i)^2} \quad (21)$$

where subscript P is denotes precision and B denotes bias error.

The total error may be found by

$$e = \sqrt{e_P^2 + e_B^2} \quad (22)$$

According to Coleman and Steele (1989) this gives approximately a 95% coverage of the true value. The alternative is to sum the errors

$$e = e_P + e_B \quad (23)$$

This gives 99% coverage if the bias and precision errors are of the same order and 95% coverage if one is negligible compared to the other. International Towing Tank Conference (1990) recommends both to be reported, but only the former will be discussed in later chapters.

If \hat{X} is the erroneous measurement and e is the total error from equation (22), the true value X is found in the interval

$$X = \hat{X} \pm e \quad (24)$$

with a probability of 95%. This of course requires that the 95% confidence interval is used throughout the analysis. It is also assumed that the bias error is symmetric, which is not always the case. If not, a high and low limit must be established from equation (22).

Here the error has the same unit as the measured value it selves. An alternative is to define a *relative error*:

$$e_r = \frac{e}{\hat{X}} \quad (25)$$

so that

$$X = \hat{X} (1 \pm e_r) \quad (26)$$

The relative error can be calculated by using a *relative influence coefficient*:

$$\kappa_{ri} = \frac{1}{\hat{X}} \frac{\partial \hat{X}}{\partial Y_i} \quad (27)$$

in equations (20) - (21) .

3 Measurement Errors

The following steps are listed in International Towing Tank Conference (1990) in order to create an uncertainty interval for a measurement:

1. identify all error sources
2. determine the individual precision and bias errors for each error source
3. determine the sensitivity of the end result to error sources
4. create the total precision interval
5. create the total bias uncertainty
6. combine total bias and precision either by addition or *root sum square* method (equation (22))
7. declare results from 4)-6) separately.

The first two steps are the tough ones. A possible approach is to start with the reduction equation and then consider its parameters and what might influence them. Then the replication level must be considered in order to distinguish between precision and bias errors. The question is typically if the experiment is repeated, and which uncertainties are covered by repetition.

The influence coefficients is found by partial derivation of the reduction equation, either analytically if possible or numerically by changing input parameters to a numerical procedure.

The ITTC report use a slightly different way to calculate the precision error than the one outlined above. Rather than establishing a precision limit P for each parameter Y , a total precision limit is calculated

$$S_{result} = \sqrt{\sum_{i=1}^N (\kappa_i \delta_i)^2} \quad (28)$$

The precision error is then given by

$$e_P = t_{95} \frac{S_{result}}{\sqrt{M}} \quad (29)$$

where t_{95} is the weight based on a 95% confidence interval and M is the number of times the test is repeated. To find t_{95} from a student's t distribution an average degree of freedom is required, weighted by the magnitude and degree of freedoms of the individual precision indexes S_i . This is done by the Welch-Satterthwaite approximation:

$$\nu_{result} = \frac{(\sum S_i^2)^2}{\sum \frac{S_i^4}{\nu_i}} \quad (30)$$

This do not seem to give a simplification compared to calculating a precision limit for each elemental error source, so this method is not applied here.

4 Modeling errors

The word model is used in at least three different contexts in this thesis. First there is the physical models used in the experiments, i.e the hardware actually put in the water in order to measure force or response. Next there is the mathematical model used to describe some physics, possibly on several levels. Thus the hydrodynamic force model is a mathematical model used in the simulation of the motion of a cable, a higher level mathematical model. Finally there is a numerical model, here used to describe the implementation of a mathematical model, thus including the numerical methods and other approximations made to actually solve the equations given by the mathematical models. Hopefully it will be clear from the context what is actually meant in each case.

The flow diagram in figure 4 is adapted from International Towing Tank Conference (1990) and describes the modeling and validation process. Note the distinction between verification and validation, the former being the process of checking that the implemented code actually gives a true representation of the mathematical model(s), while the latter is to verify that the numerical model is an adequate representation of the physical reality. Roughly speaking the verification will in the following be done by comparison to analytical results for special test cases, while validity of the numerical model is based on comparison to experiments.

A confidence interval of the numerical model is established in the same way as for the experimental results, considering the numerical model a reduction equation and estimating limits for each parameter. Error sources to be considered are indicated in figure 4.

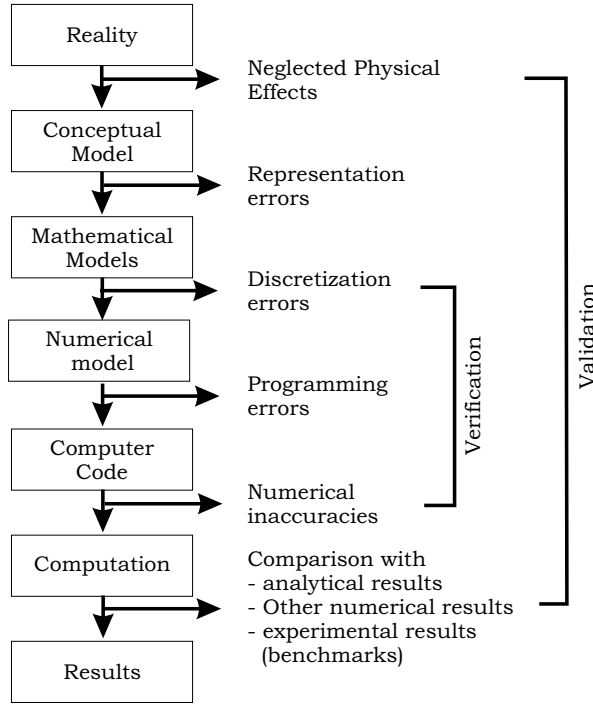


Figure 4: Modeling and validation process. From recommendations in International Towing Tank Conference (1990)

4.1 Comparing model and experiment

In comparing measured and calculated results the distinction between measurement errors and modeling errors are not always obvious. This is the case for parameters not explicitly stated in the reduction equation, so that a numerical model is necessary to estimate sensitivity. In the following parameters of this type will be treated as modeling errors while the term measurement errors will be reserved for uncertainties in the actual measurement.

Plotting experimental results and errors in the same plots as numerical results and errors gives a good impression of the overlap of the two, but might require a lot of plots. An alternative, quantitative way of presenting the comparison between model and experiment is suggested to be:

$$R_{me} = \frac{\sqrt{(tS_{mc})^2 + e_{mod}^2}}{e_{exp}} \quad (31)$$

Here S_{mc} is the standard deviation of the difference between the numerical and experimental answer, t is the weight and should correspond to the weight used in the error estimates, e_{exp} is the estimated experimental error and e_{mod} the estimated modeling error. The formula is based on a comment by Coleman and Steele (1989) on regression uncertainty. The idea is that the discrepancy between model and experiment must be considered together with the measurement and modeling errors. If the ratio R_{me} is unity or less, the value estimated from the model is within the combined uncertainty of the measurement. This is the best comparison that can be obtained with the experimental data set, and the model should then be acceptable. For R_{me} larger than unity the model with the lowest ratio gives the best representation of the measured value. This representation works best if the error in the measured data does not vary to much from case to case.

5 Example: Lift Coefficient of a cylinder

In this example the lift, or transverse forces, on a rigid cylinder at low angle of attacks are measured. The experimental setup is shown in figure 5. There is a force sensor in each end of the test section, thus the total force is a sum of two measurements. The force sensors are a standard strain gauges based design used extensively by MARINTEK, while all velocities are encoder outputs from the carriages. The model was

Table 1: *Parameters of the test section*

Length	L	2.03 m
Diameter	d	0.051 m
Dry Weight	m	1.875 Kg
Water density	ρ	998.5 Kg/m ³
Dyn. viscosity	ν	1.05×10^{-6} m ² /s
Length to diameter ratio	$\frac{L}{d}$	39.2
Structural mass to Added mass ratio	$\frac{m_s}{\rho \pi \frac{d^2}{4}}$	0.46
Roughness	$\frac{k}{d}$	29.5×10^{-6}

ran both in the large towing tank and in MCLab. In both laboratories a Heidehein MGC+ were used for amplification, filtering and analog to digital conversion of all measurements. Although same make and model, two different units were used. In the towing tank a sample frequency of 200 Hz and a filter cutoff frequency of 100 Hz were used. For the followup experiments in the MCL the sampling frequency was reduced to 120 Hz, filtering at 40 Hz. All force signals were recorded in Volts, while calibration and all data analysis were performed on a PC using MATLAB[®].

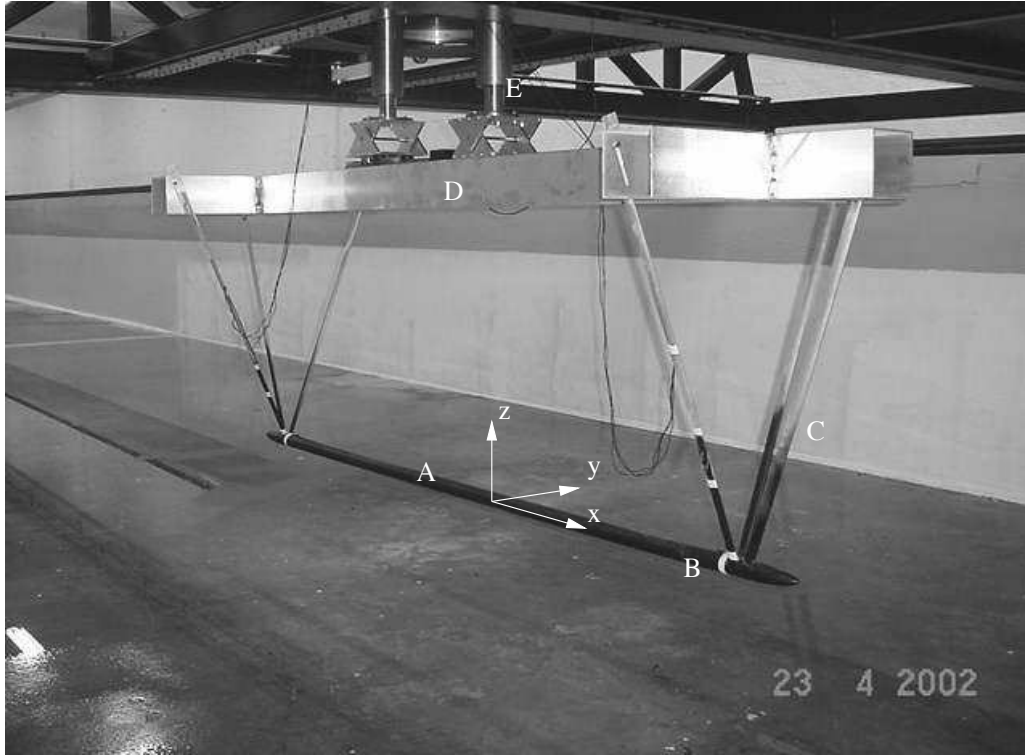


Figure 5: *The Model mounted under the carriage: A -test section, B -Force sensor housing, C -end supports and struts, D -yoke*

Important parameters are given in table 1.

In the towing tank, each run were performed in both directions for each combination of velocity and angle. Six repetitions are therefore available for these data points. This will be used to illustrate the difference between a 1st and a 2nd order replication analysis.

5.1 Reduction Equations

The presented results of the experiments is the lift coefficient as a function of angle off attack α coefficients. Denoting the measured forces from the two force sensors with superscripts f and a for forward and aft sensor

respectively, the reduction equation is

$$C_l(\alpha) = \frac{F_y^a + F_y^f}{\frac{1}{2}\rho U^2 dL} \quad (32)$$

$$(33)$$

To generalize, the reduction equations contain measured forces, a dynamic pressure $q = \frac{1}{2}\rho U^2$ and representative dimensions. The error sources are grouped according to this.

5.2 Precision and bias limits for force measurements

For the force measurements, there are three replications levels available:

- The sensors were calibrated after assembly. By rotating the sensor and the spacer it was mounted on, known weights of 10-500 grams were applied in directions 0,90,120,180,240, and 270 degrees with respect to the positive n axis. This gave more than 120 points on which to build a 2-D calibration model incorporating cross-talk and alignment errors:

$$F_n = k_1 V_1 + k_2 V_2 \quad (34)$$

Here F_n is the known force in direction n , V_{1-2} are the measured voltages in the two directions of the sensor and k_1 and k_2 are coefficients found by the least square fit method. The result is 4 sets of coefficients. This is the zeroth replication level.

- The measurements are time series where the time series are at least 15 seconds long. The forces used in the analysis is the mean of this time measurements and represents a 1'st replication level.
- At least some of the time series are repeated six times, representing a 2'nd order replication level with 3 degrees of freedom. Here variations in alignment and velocity are included in the data set, so the precision level should be higher for this case.

Precision limits are given in table 2. For zeroth order replication the value is the 95% confidence interval of the calibration model. The 1'st order level uses the forward runs on the third day, while the 2'nd order includes all measured data. Six data points is assumed for all angles in this case. For the higher order levels the precision is given by:

$$P_x = t \frac{S_x}{\sqrt{N}} \quad (35)$$

In table 2 the median is given rather than the mean. The median is the value for which the probability of exceedence is 50%. In other words, half the calculated limits are below this limit, and half the limits are above it. Since relatively few values (mostly $\alpha > 20$) are quite high compared to the limit for most cases, the median is more representative than the mean. From inspection of the raw data it was found that for 1'st order replication the value does not vary with angle of attack, thus the variation is mainly due to velocity.

For $\alpha > 20^\circ$ the model was observed to oscillate and the standard deviation of the time series increases by a factor five or more. This is reflected in the max value of the precision level. For second order replication the z direction results are much higher than expected, particularly since these value should be less sensitive to small variations in angle of attack than the y-direction. This may imply unsteady flow pattern for the high angles.

The highest limits are found for the highest measured values, so the relative error is more constant than the precision levels indicates. Typically, the precision limit is about 5% of the measured values, at least in the y-direction.

The 2'nd order level is here included for comparison only. Since there is a small difference in speed in forward and back wards runs, the resulting precision limits is too high. When estimating the final error from repeated runs, the coefficients are calculated for all data series, then the mean and the precision level is established.

Identified sources of bias errors in the force measurements are

Vibrations (B_{01}) Since the total force on cylinder is measured, all inertia forces due to vibration induced by the carriage and its drive system are included in the measurements. But these are assumed to have zero mean, and the effect is included in the precision errors in table 2. The effect of vibration on the averaged hydrodynamic damping forces depends on the work done by the cylinder on the fluid, which again depends on the actual motion of the cylinder. From decay test of the model mounted on the

Table 2: Precision and bias limit ranges and medians (in N) on force measurements. All velocities and angles included. (na -not applicable)

Replication Level	Samples N	Weight t	y-direction			z-direction		
			min	max	median	min	max	median
0 th	120	2		0.015			0.028	
1 st	4000	2	0.021	0.616	0.048	0.029	0.248	0.066
2 nd	6	2.57	0	3.615	0.096	0.04	9.35	0.35
Bias errors								
	Vibration	B_{01}	0.0	0.15	0.0025	1.5×10^{-6}	0.008	0.0015
	Cylinder End	B_{02}	0	0.0022	4.4×10^{-5}		na	
	Strut Wake	B_{03}		na			0.0015	
Measured Force		$ F_n $	0	37.387	0.615	4.00×10^{-4}	1.991	0.368

carriage the lowest eigenfrequency is found to be 9 Hz. The highest shedding frequency is found for 2.5 m/s tow speed and 30 degrees yaw angle. The estimated value is $f_v = 4.9 - 6.86$ where the low value corresponds to subcritical flow (Strouhal number $S_t = 0.2$) and the high limit corresponds to transcritical flow, $S_t = 0.28$ (Faltinsen 1990). Since the in line oscillating force has twice the frequency of the vortex shedding, there is a possibility of matching load and eigenfrequency for the extreme cases. Oscillation of the model was observed, both visually and in the force measurements, for velocities above 1.5 m/s and angles above 20 degrees. For the remaining tests no oscillation of the model was observed and the motion of the cylinder is assumed limited to the 0.1 mm clearance of the pin of the sensor to the fitting in the test cylinder. For the case of VIV, Faltinsen (1990) give a simple relation between drag coefficient and amplitude of oscillation:

$$\frac{C_d}{C_{d0}} = 1 + 2 \left(\frac{A}{d} \right)_{max} \quad (36)$$

Here C_{d0} is the drag coefficient without vibration, A is the amplitude and d is the cylinder diameter. Although the current case is not VIV, this represent an upper limit. The bias due to vibration can then be expressed

$$B_{01} = 2 \left(\frac{A}{d} \right)_{max} F_0 = 0.004 F_0 \quad (37)$$

Where F_0 is the measured force.

Cylinder end effects (B_{02}) To ensure that all forces actually goes trough the force sensor a gap between the test cylinder and the support is necessary. The boundary layer thickness at the forward gap is found to $\delta^* \simeq 1.2$ mm, about the same as the 1 mm gap opening. It is then assumed that the tangential flow velocity at the gap is small and that potential forces from sudden change in diameter can be neglected. The analysis is then limited to include frictional forces due to low speed flow between the outer plate of the support and the protrusion at the cylinder end. This is assumed to be similar to a 2D channel flow, see right part of figure 6. The height of the channel is $h = 1$ mm, the breath $b = 4$ mm (the length of the protrusion on the cylinder end), and the length $l = \frac{1}{2}\pi\frac{d}{2}$, i.e half the circumference of the cylinder. From Blevins (1992, Table 13-4) the shear force on the walls are:

$$\tau = \frac{h}{2l}(p_1 - p_2) \quad (38)$$

Here $(p_1 - p_2)$ is the pressure drop through the channel. The pressure difference on the upstream and leeward side of the cylinder can be estimated by the dynamic pressure of the cross flow so that $(p_1 - p_2) \simeq \frac{1}{2}\rho(U \sin(\alpha))^2$. With equal flow on both side of the protrusion, the total force on the cylinder end is

$$B_{02} = \tau 2bl = hb \frac{1}{2} \rho (U \sin(\alpha))^2 \quad (39)$$

Analysis Errors The use of a well documented and tested tool like MATLAB[®] should reduce the number of bugs in the computer analysis scripts, and there is no way to quantify the possibility of bugs. Another question is which part of the measured time series to use in analysis. All recordings were started before

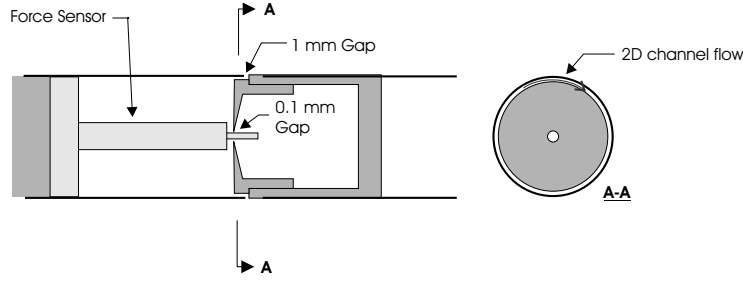


Figure 6: Model detail: Test section end

Table 3: Precision and bias limit for (in m/s) on reference velocity. All velocities and angles included. (na -not applicable)

Replication Level	Samples N	Weight t	Tow speed [m/s]			
			1.0	1.5	2.0	2.5
1'st	4000	2	8.28×10^{-5}	1.2×10^{-4}	1.52×10^{-4}	1.85×10^{-4}
Bias errors						
Residual flow		B_{04}	0.004			
Generated waves		B_{05}	6.8×10^{-4}	0.0027	0.011	0.024

the actual run, so that all transient effects are present in the time series. The part of the time series used in averaging are identified based on the tow velocity, with a time delay from constant velocity was achieved to assumed steady state forces of at least 5 seconds. From visual inspection of selected force traces no transients were observed beyond this time, but no further analysis were done.

Wake of the struts (B_{03}) In planning the experiments it was estimated that the pressure recovery in the wake of a single strut should be quick enough so that it did not create a force on the test section. From runs with zero angle it is seen that there is a small vertical force on the forward sensor. This is most likely due to the combined effect of all three struts. Since the effect of angle of attack is uncertain, it cannot simply be subtracted from the results, but is included as an bias uncertainty limits. It only influences force in the z-direction.

For the y-direction it is found that the presence of the struts have a major influence on the initial vortex formation on the cylinder nose. This effect is studied by comparing rotation in yaw to results from rotating in pitch in the discussion of the results.

The range and median of the bias limits are given in table 2. For the most part, the bias error is an order of magnitude lower than the precision limits.

5.3 Precision and bias limits for dynamic pressure

The dynamic pressure is given by

$$q = \frac{1}{2} \rho U^2 \quad (40)$$

Of these parameters only the speed is measured, and also represent the largest uncertainty with respect to bias, so the analysis will concentrate on this.

The tow speed is measured by a counter mounted on the carriage rails. The precision error is given by equation (35) and listed for 1'st order replication in table 3. The speed is slightly different on forward and backward run due to the speed control on the carriage, so there is to few data points to include 2'nd order replication here.

The bias errors are:

Residual flow (B_{04}) The waiting time between runs was minimum 4 minutes, based on experience and visual observation of the waves in the tank. An estimate of the level of residual flow can based on far

wake theory. The mean velocity deficit at the center of a plane (or 2-D) wake is given by (Blevins 1992, p.267)

$$\frac{u_1}{U} = 1.2 \left(\frac{x}{C_d D} \right)^{-\frac{1}{2}} \quad (41)$$

For an axi-symmetric body the relation is

$$\frac{u_1}{U} = 0.35 \left(\frac{x}{(C_D A)^{\frac{1}{2}}} \right)^{-\frac{2}{3}} \quad (42)$$

Here u_1 is the maximum velocity in the wake A the characteristic area on which C_d is based, and U the free stream velocity. Equations 41 and 42 refers to a coordinate system fixed to the moving body. Switching now to a plane fixed with respect to the fluid and normal to the direction of motion, as in 2D+t theory, the diffusion of the wake becomes a function of time by the substitution $x = \frac{U}{t}$:

$$u_1 = U 1.2 \left(\frac{U t}{C_D D} \right)^{-\frac{1}{2}} \quad (43)$$

$$u_1 = U 0.35 \left(\frac{U t}{(C_D A)^{\frac{1}{2}}} \right)^{-\frac{2}{3}} \quad (44)$$

for plane and axi-symmetric wakes respectively. In this fixed plane the velocity u_1 is the actual velocity at the center line, not the velocity deficit, since the body fixed coordinate moves with a velocity U with respect to the fixed system. Table 4 lists the resulting velocity for the cylinder (axi-symmetric) and a strut (plane) at $t=240$ s. The tow speed is set to $U = 2.5$ m/s and it is assumed that the diffusion in the fixed plane is not affected by the fact the the motion of the cylinder actually has stopped at some time $t < 240$.

Table 4: *Estimated residual velocity u_1 after 4 minutes*

	C_D	d/A	u_1
Test Cylinder	0.01	$\pi dL = 0.32 \text{ m}^2$	0.002
Strut	0.1	0.01 m	0.004

The result for the strut is then used in table 3. There is also the possibility of residual flow due to remaining waves, but since these could not be observed this is neglected.

Generated Waves (B_{05}) The depth at which the cylinder is towed is a trade of between rigidity of the model and the influence of the free surface. In this case the cylinder was towed at a depth of 0.4 m, or 8 d . The amplitude of velocity at a given depth is

$$u_A = \sqrt{kg} \zeta_A e^{-kh} \quad (45)$$

where $h = 0.4$ m is the tow depth, $\omega = \sqrt{gk}$ is the circular frequency of the wave, and ζ_A is the amplitude of the wave elevation at the surface. The expression uses assumes infinite water depth. The wave number is given by $k = \frac{2\pi}{\text{wavelength}}$ where the max wave length is $\lambda = 2\pi \frac{U^2}{g}$ for transverse waves and $\lambda = \frac{4\pi}{3} \frac{U^2}{g}$ for divergent waves (Faltinsen 2004). High wave numbers means slower decay with depth, so the transverse waves should be critical. On the other hand, the only waves that could be observed during the experiment were divergent waves from the strut. The Froude number for the struts is 1.84 for $U = 1.0$ m/s which is in a range where the divergent waves are dominant (Faltinsen 2004). By observing the wash on the tank walls, it was concluded that the wave amplitude never exceeded 5 cm. The bias limit is then estimated by:

$$\zeta_A = 0.05 \text{ m} \quad (46)$$

$$k = \frac{3}{2} \frac{g}{U^2} \quad (47)$$

$$B_{05} = \sqrt{\frac{3}{2}} U \zeta_A e^{-kh} \quad (48)$$

The second parameter in the dynamic pressure is the water density. The density and viscosity of the water in the tank used for calculating dynamic pressure and Reynolds number are given in table 1. These values are based on a measured water temperature of 18.2 °C and taken from tables used at MARINTEK. The variation of the temperature in the tank is very low, so the same temperature is used for all days. The biases are:

$$\begin{aligned} \text{Density} & & B_{06} &= 0.1 \frac{Kg}{m^3} \\ \text{Dynamic Viscosity} & & & 5.0 \times 10^{-9} \frac{m^2}{s} \end{aligned}$$

The dynamic viscosity is only used when calculated Reynolds number, and is not included in the error estimate. .

5.4 Precision and bias limits for Alignment and dimensions

Alignment The yaw angle was set manually using a fixed protractor. The angle was set by the same person all day, ensuring that the same reference was used each time. The bias limit was then estimated to

$$B_{06} = \pm 0.25^\circ \quad (49)$$

Running both directions with zero angle of attack revealed no difference in z-direction force thus no error in pitch alignment could be observed. Since such forces may be very small, a precision error equal to the yaw precision are applied anyway.

Model dimensions (B_{07}) All dimensions are kept constant during analysis, thus there should be no precision errors. The length and diameter of the test section were measured to an accuracy of ± 0.5 mm. Then

$$B_{07} = 0.5\text{mm} \quad (50)$$

5.5 Influence Coefficients

The influence coefficient becomes

$$\kappa_i = \frac{\partial \hat{C}_l}{\partial Y_i} \quad (51)$$

where Y_i is the parameters in equation (33). Below, the parameters are index by the alphabet rather than numbers, to separate from error source indexes. The sensitivity to variation in a single sensor is

$$\kappa_a = \frac{\partial}{\partial F_y^f} \left(\frac{F_y^a + F_y^f}{\frac{1}{2}\rho U^2 dL} \right) = \frac{1}{\frac{1}{2}\rho U^2 dL} \quad (52)$$

and similar for F_y^a . For error in the velocity the sensitivity is

$$\kappa_b = \frac{\partial}{\partial U} \left(\frac{F_y^a + F_y^f}{\frac{1}{2}\rho U^2 dL} \right) = -2 \frac{F_y^a + F_y^f}{\frac{1}{2}\rho U^3 dL} \quad (53)$$

for both normal forces and moments. The sensitivity to variation in density is

$$\kappa_c = \frac{\partial}{\partial \rho} \left(\frac{F_y^a + F_y^f}{\frac{1}{2}\rho U^2 dL} \right) = -\frac{F_y^a + F_y^f}{\frac{1}{2}\rho^2 U^2 dL} \quad (54)$$

and finally for variation in diameter

$$\kappa_d = \frac{\partial}{\partial d} \left(\frac{F_y^a + F_y^f}{\frac{1}{2}\rho U^2 dL} \right) = -\frac{F_y^a + F_y^f}{\frac{1}{2}\rho U^2 d^2 L} \quad (55)$$

and similar for variation in length.

The angle of attack α is not included in the reduction equations, so the sensitivity cannot be expressed this way. But since the angle of attack is varied, the relationship between the force and the angle of attack is known from the experiment. This of course is the reason for doing the experiments in the first place. The sensitivity κ_e can therefore be estimated by a numerical derivation of the measured results, with respect to the given angle of attack.

5.6 Total error estimates

To avoid division by zero when calculating a relative error, only $\alpha \geq 1^\circ$ are included in the following results. Figure 7 shows the relative errors for C_l calculated based on the forward runs the 3rd day. This represents a 1st order replication approach. The bars give the contributions from the source described above. The part of the bars representing force and dynamic pressure (*Dyn. Pres.*) includes both precision and bias errors for these sources. The solid line gives the total error from equation (22), the quadratic sum of the error contributions.

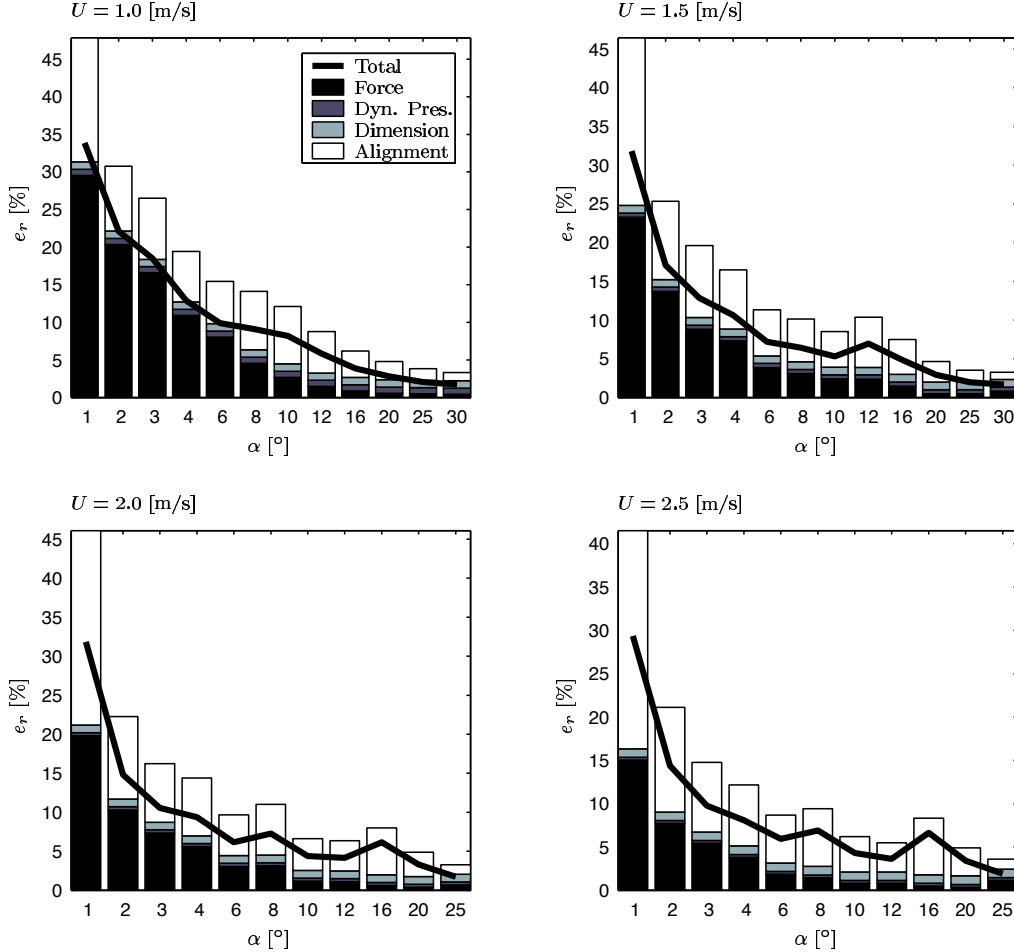


Figure 7: Relative errors based on 1st order replication analysis. Calculation is for C_{n2}

Figure 8 gives the relative errors from the 2nd order replication. In this case a coefficient is calculated for each run, and the precision error is based on the variation of these values. Six repetitions are assumed for all angles. By repeating the test series errors due to variation of the set angle and the residual velocity will be included in the precision part, so B_{04} and B_{07} are not included in the bias error estimates. This is the main reason for repeating the experiments. Note difference in legend between the two plots. For 2nd order replication there is only one precision error and it is given separately. The remaining sources are all bias errors.

Comparing the two methods, the 1st order replication gives high errors for low angles and a little low errors for medium and high angles compared to 2nd order replication. Particularly at the lowest angles it seems that the error due to variation in angle of attack is lower than the estimate in B_{07} . For higher angles the comparison is reasonable, which hopefully indicates that no large error sources are omitted in the analysis.

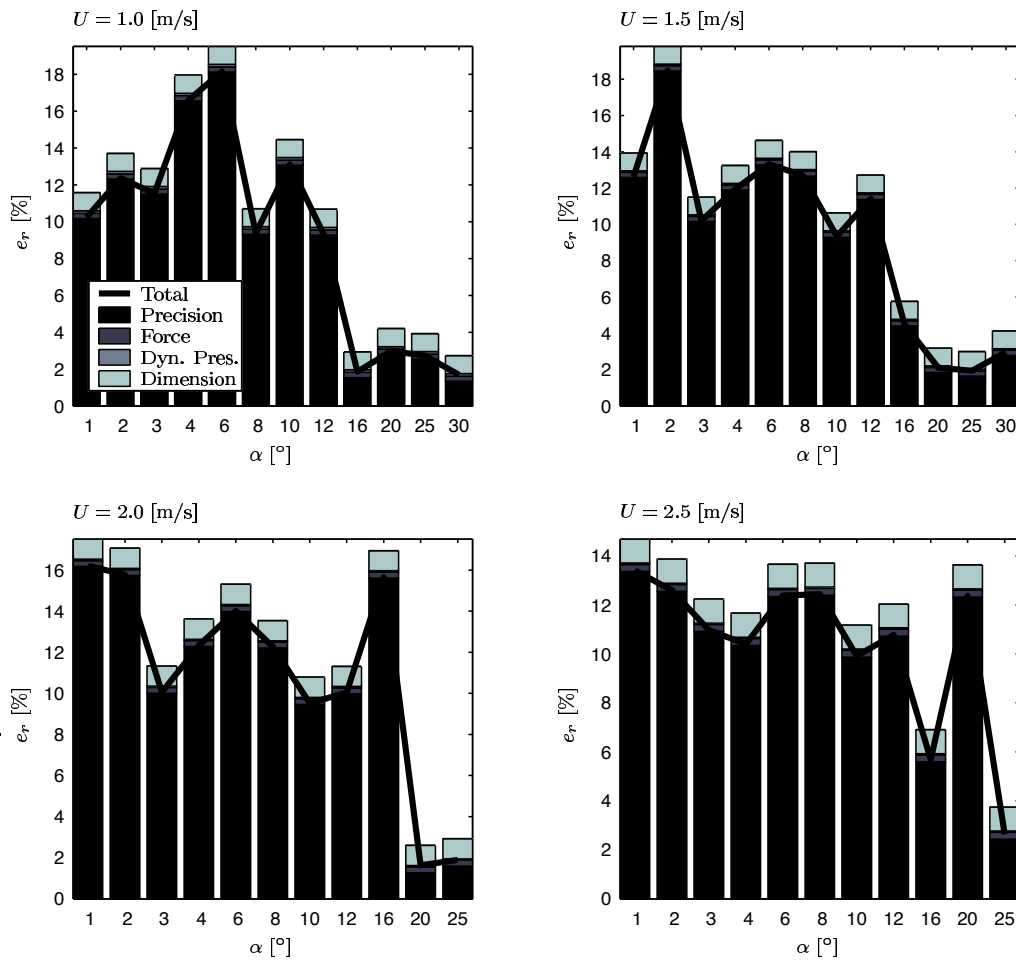


Figure 8: Relative errors based on 2'nd order replication analysis. Calculation is for C_{r2}

References

- BLEVINS, R. D. (1992). *Applied Fluid Dynamics Handbook*. Krieger Publishing Company.
- COLEMAN, H. AND W. STEELE (1989). *Experimentation and Uncertainty Analysis for Engineers*. Jon Wiley and Sons.
- FALTINSEN, O. M. (1990). *Sea Loads on Ships and Offshore Structures*. Cambridge University Press.
- FALTINSEN, O. M. (2004). Hydrodynamics of high-speed marine vehicles. Lecture notes.
- International Towing Tank Conference (1990). *Report of the Panel on Validation Procedures*. International Towing Tank Conference. 19'th.
- KREYSZIG, E. (1988). *Advanced Engineering Mathematics* (6 ed.). Jon Wiley and Sons.

	ITTC – Recommended Procedures and Guidelines	7.5 – 02 03 – 01.4 Page 1 of 10	
	Performance, Propulsion 1978 ITTC Performance Prediction Method	Effective Date 2008	Revision 02

Table of Contents

<p>1. PURPOSE OF PROCEDURE 2</p> <p>2. DESCRIPTION OF PROCEDURE 2</p> <p> 2.1 Modifications of the 1978 ITTC Performance Prediction Method.....2</p> <p> 2.2 Definition of the Variables.....2</p> <p> 2.3 Analysis of the Model Test Results3</p> <p> 2.4 Full Scale Predictions4</p> <p> 2.4.1 Total Resistance of Ship.....4</p>	<p> 2.4.2 Scale Effect Corrections for Propeller Characteristics.7</p> <p> 2.4.3 Full Scale Wake and Operating Condition of Propeller7</p> <p> 2.4.4 Model-Ship Correlation Factor.....8</p> <p>3. VALIDATION 9</p> <p> 3.1 Uncertainty Analysis9</p> <p> 3.2 Comparison with Full Scale Results ...9</p> <p>4. REFERENCES 9</p>
--	--

Edited by 22 nd ITTC QS Group 1999	Approved
15 th ITTC 1978 pp388 – 402 17 th ITTC 1984 pp326 - 333 18 th ITTC 1987 pp266 - 273	15 th ITTC 1978, 17 th ITTC 1984 and 18 th ITTC 1987
Date	Date

	ITTC – Recommended Procedures and Guidelines	7.5 – 02 03 – 01.4 Page 2 of 10	
	Performance, Propulsion 1978 ITTC Performance Prediction Method	Effective Date 2008	Revision 02

1978 ITTC Performance Prediction Method

1. PURPOSE OF PROCEDURE

The procedure gives a general description of an analytical method to predict delivered power and rate of revolutions for single and twin screw ships from model results.

2. DESCRIPTION OF PROCEDURE

2.1 Introduction

The method requires respective results of a resistance test, a self propulsion test and the characteristics of the model propeller used during the self propulsion test,

The method generally is based on thrust identity which is recommended to be used to predict the performance of a ship. It is supposed that the thrust deduction factor and the relative rotative efficiency calculated for the model remain the same for the full scale ship whereas on all other coefficients corrections for scale effects are applied.

In some special cases torque identity (power identity) may be used, see section 2.4.4.

2.2 Definition of the Variables

C_A Correlation allowance
 C_{AA} Air resistance coefficient
 C_{App} Appendage resistance coefficient
 C_D Drag coefficient

C_F Frictional resistance coefficient
 C_{FC} Frictional resistance coefficient at the temperature of the self propulsion test
 C_{NP} Trial correction for propeller rate of revolution at power identity
 C_P Trial correction for delivered power
 C_N Trial correction for propeller rate of revolution at speed identity
 C_R Residual resistance coefficient
 C_T Total resistance coefficient
 D Propeller diameter
 F_D Skin friction correction in self propulsion test
 J Propeller advance coefficient
 J_T Propeller advance coefficient achieved by thrust identity
 J_Q Propeller advance coefficient achieved by torque identity
 K_T Thrust coefficient
 K_Q Torque coefficient
 K_{QT} Torque coefficient achieved by thrust identity
 k Form factor
 k_P Propeller blade roughness
 N_P Number of propellers
 n Propeller rate of revolution
 n_T Propeller rate of revolution, corrected using correlation factor
 P Propeller pitch
 P_D, P_P Delivered Power, propeller power
 P_{DT} Delivered Power, corrected using correlation factor

	ITTC – Recommended Procedures and Guidelines	7.5 – 02 03 – 01.4 Page 3 of 10	
	Performance, Propulsion 1978 ITTC Performance Prediction Method	Effective Date 2008	Revision 02

P_E, P_R	Effective power, resistance power
Q	Torque
R_C	Resistance corrected for temperature differences between resistance- and self propulsion test
Re	Reynolds number
R_T	Total resistance
S	Wetted surface
S_{BK}	Wetted surface of bilge keels
T	Propeller thrust
t	Thrust deduction factor
V	Ship speed
V_A	Propeller advance speed
w	Taylor wake fraction in general
w_Q	Taylor wake fraction, torque identity
w_R	Effect of the rudder(s) on the wake fraction
w_T	Taylor wake fraction, thrust identity
Z	Number of propeller blades
β	Appendage scale effect factor
ΔC_F	roughness allowance
ΔC_{FC}	Individual correction term for roughness allowance
Δw_C	Individual correction term for wake
η_D	Propulsive efficiency or quasi-propulsive coefficient
η_H	Hull efficiency
η_0	Propeller open water efficiency
η_R	Relative rotative efficiency
ρ	Water density in general

Subscript “M” signifies the model
Subscript “S” signifies the full scale ship

2.3 Analysis of the Model Test Results

The calculation of the residual resistance coefficient C_R from the model resistance test

results is found in the procedure for resistance test (7.5-02-02-01).

Thrust T_M , and torque Q_M , measured in the self-propulsion tests are expressed in the non-dimensional forms as in the procedure for propulsion test (7.5-02-03-01.1).

$$K_{TM} = \frac{T_M}{\rho_M D_M^4 n_M^2} \quad \text{and} \quad K_{QM} = \frac{Q_M}{\rho_M D_M^5 n_M^2}$$

Using thrust identity with K_{TM} as input data, J_{TM} and K_{QTM} are read off from the model propeller open water diagram, and the wake fraction

$$w_{TM} = 1 - \frac{J_{TM} D_M}{V_M}$$

and the relative rotative efficiency

$$\eta_R = \frac{K_{QTM}}{K_{QM}}$$

are calculated. V_M is model speed.

Using torque identity with K_{QM} as input data, J_{QM} is read off from the model propeller open water diagram, and the wake fraction

$$w_{QM} = 1 - \frac{J_{QM} D_M}{V_M}$$

V_M is model speed.

In case of using torque identity the relative rotative efficiency

$$\eta_R = 1.0$$

The thrust deduction is obtained from

	ITTC – Recommended Procedures and Guidelines	7.5 – 02 03 – 01.4 Page 4 of 10	
	Performance, Propulsion 1978 ITTC Performance Prediction Method	Effective Date 2008	Revision 02

$$t = \frac{T_M + F_D - R_C}{T_M}$$

where F_D is the towing force actually applied in the propulsion test. R_C is the resistance corrected for differences in temperature between resistance and self-propulsion tests:

$$R_C = \frac{(1+k)C_{FMC} + C_R}{(1+k)C_{FM} + C_R} R_{TM}$$

where C_{FMC} is the frictional resistance coefficient at the temperature of the self-propulsion test.

2.4 Full Scale Predictions

2.4.1 Total Resistance of Ship

The total resistance coefficient of a ship without bilge keels is

$$C_{TS} = (1+k)C_{FS} + \Delta C_F + C_A + C_R + C_{AAS}$$

where

- k is the form factor determined from the resistance test, see ITTC standard procedure 7.5-02-02-01.
- C_{FS} is the frictional resistance coefficient of the ship according to the ITTC-1957 model-ship correlation line
- C_R is the residual resistance coefficient calculated from the total and frictional resistance coefficients of the model in the resistance tests:

$$C_R = C_{TM} - (1+k)C_{FM}$$

The form factor k and the total resistance coefficient for the model C_{TM}

are determined as described in the ITTC standard procedure 7.5-02-02-01.

The correlation factor for the calculation of the resistance has been separated from the roughness allowance. The roughness allowance ΔC_F per definition describes the effect of the roughness of the hull on the resistance. The correlation factor C_A is supposed to allow for all effects not covered by the prediction method, mainly uncertainties of the tests and the prediction method itself and the assumptions made for the prediction method. The separation of ΔC_F from C_A was proposed by the Performance Prediction Committee of the 19th ITTC. This is essential to allow for the effects of newly developed hull coating systems.

The 19th ITTC also proposed a modified formula for C_A that excludes roughness allowance, which is now given in this procedure.

- ΔC_F is the roughness allowance

$$\Delta C_F = 0.044 \left[\left(\frac{k_s}{L_{WL}} \right)^{\frac{1}{3}} - 10 \cdot Re^{-\frac{1}{3}} \right] + 0.000125$$

where k_s indicates the roughness of hull surface. When there is no measured data, the standard value of $k_s = 150 \times 10^{-6}$ m can be used.

- C_A is the correlation allowance.

C_A is determined from comparison of model and full scale trial results. When using the roughness allowance as above, the 19th ITTC recommended using

$$C_A = (5.68 - 0.6 \log Re) \times 10^{-3}$$

to give values of $\Delta C_F + C_A$ that approximates the values of ΔC_F of the original 1978 ITTC method. It is recommended that each institution main-

	ITTC – Recommended Procedures and Guidelines	7.5 – 02 03 – 01.4 Page 5 of 10	
	Performance, Propulsion 1978 ITTC Performance Prediction Method	Effective Date 2008	Revision 02

tains their own model-full scale correlation. See section 2.4.4 for a further discussion on correlation.

- C_{AAS} is the air resistance coefficient in full scale

$$C_{AAS} = \frac{1}{2} \rho_A V_S^2 C_{DA} \frac{A_{VS}}{S_S}$$

where, A_{VS} is the projected area of the ship above the water line to the transverse plane, S_S is the wetted surface area of the ship, ρ_A is the air density, and C_{DA} is the air drag coefficient of the ship above the water line. C_{DA} can be determined by wind tunnel model tests or calculations. Values of C_{DA} are typically in the range 0.5-1.0, where 0.8 can be used as a default value.

If the ship is fitted with bilge keels of modest size, the total resistance is estimated as follows:

$$C_{TS} = \frac{S_S + S_{BK}}{S_S} [(1+k)C_{FS} + \Delta C_F + C_A] + C_R + C_{AAS}$$

where S_{BK} is the wetted surface area of the bilge keels.

When the model appendage resistance is separated from the total model resistance, as described as an option in the ITTC Standard Procedure 7.5-02-02-01, the full scale appendage resistance needs to be added, and the formula for total resistance (with bilge keels) becomes:

$$C_{TS} = \frac{S_S + S_{BK}}{S_S} [(1+k)C_{FS} + \Delta C_F + C_A] + C_R + C_{AAS} + C_{AppS}$$

There is not only one recommended method of scaling appendage resistance to full

scale. The following alternative methods are well established:

- 1) Scaling using a fixed fraction:

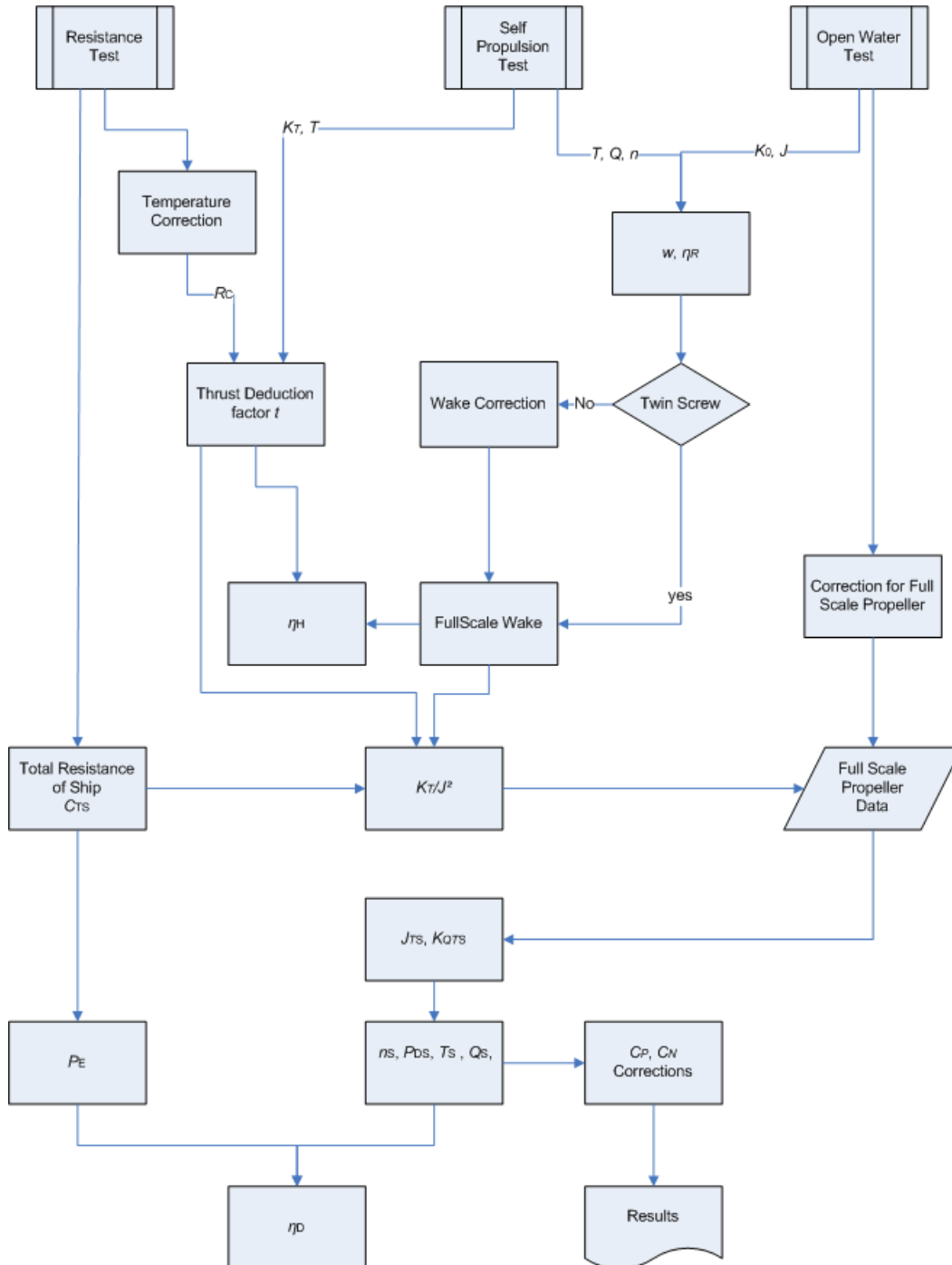
$$C_{AppS} = (1 - \beta) \cdot C_{AppM}$$

where $(1-\beta)$ is a constant in the range 0.6-1.0.

- 2) Calculating the drag of each appendage separately, using local Reynolds number and form factor.

$$C_{AppS} = \sum_{i=1}^n (1 - w_i)^2 \cdot (1 + k_i) \cdot C_{FSi} \cdot \frac{S_i}{S_S}$$

where index i refers to the number of the individual appendices. w_i is the wake fraction at the position of appendage i . k_i is the form factor of appendage i . C_{FSi} is the frictional resistance coefficient of appendage i , and S_i is the wetted surface area of appendage i . Note that the method is not scaling the model appendage drag, but calculating the full scale appendage drag. The model appendage drag, if known from model tests, can be used for the determination of e.g. the wake fractions w_i . Values of the form factor k_i can be found from published data for generic shapes, see for instance Horner (1965) or Kirkman and Klöetsli (1980).



	ITTC – Recommended Procedures and Guidelines	7.5 – 02 03 – 01.4 Page 7 of 10	
	Performance, Propulsion 1978 ITTC Performance Prediction Method	Effective Date 2008	Revision 02

2.4.2 Scale Effect Corrections for Propeller Characteristics.

The characteristics of the full-scale propeller are calculated from the model characteristics as follows:

$$K_{TS} = K_{TM} - \Delta K_T$$

$$K_{QS} = K_{QM} - \Delta K_Q$$

where

$$\Delta K_T = -\Delta C_D \cdot 0.3 \cdot \frac{P}{D} \cdot \frac{c \cdot Z}{D}$$

$$\Delta K_Q = \Delta C_D \cdot 0.25 \cdot \frac{c \cdot Z}{D}$$

The difference in drag coefficient ΔC_D is

$$\Delta C_D = C_{DM} - C_{DS}$$

where

$$C_{DM} = 2 \left(1 + 2 \frac{t}{c} \right) \left[\frac{0.044}{(Re_{c0})^{\frac{1}{6}}} - \frac{5}{(Re_{c0})^{\frac{2}{3}}} \right]$$

and

$$C_{DS} = 2 \left(1 + 2 \frac{t}{c} \right) \left(1.89 + 1.62 \cdot \log \frac{c}{k_p} \right)^{-2.5}$$

In the formulae listed above c is the chord length, t is the maximum thickness, P/D is the pitch ratio and Re_{c0} is the local Reynolds number with Kempf's definition at the open-water test. They are defined for the representative blade section, such as at $r/R=0.75$. k_p denotes the blade roughness, the standard

value of which is set $k_p=30 \times 10^{-6}$ m. Re_{c0} must not be lower than 2×10^5 .

2.4.3 Full Scale Wake and Operating Condition of Propeller

The full-scale wake is calculated by the following formula using the model wake fraction w_{TM} , and the thrust deduction fraction t obtained as the analysed results of self-propulsion test:

$$w_{TS} = (t + w_R) + (w_{TM} - t - w_R) \frac{(1+k)C_{FS} + \Delta C_F}{(1+k)C_{FM}}$$

where w_R stands for the effect of rudder on the wake fraction. If there is no estimate for w_R , the standard value of 0.04 can be used.

If the estimated w_{TS} is greater than w_{TM} , w_{TS} should be set as w_{TM} .

The wake scale effect of twin screw ships with open sterns is usually small, and for such ships it is common to assume $w_{TS} = w_{TM}$.

For twin skeg like stern shapes a wake correction is recommended. A correction like the one used for single screw ships may be used.

The load of the full-scale propeller is obtained from

$$\frac{K_T}{J^2} = \frac{S_s}{2D_s^2} \cdot \frac{C_{TS}}{(1-t) \cdot (1-w_{TS})^2 \cdot N_p}$$

where N_p is the number of propellers.

With this K_T / J^2 as input value the full scale advance coefficient J_{TS} and the torque coefficient K_{QTS} are read off from the full scale

 INTERNATIONAL TOWING TANK CONFERENCE	ITTC – Recommended Procedures and Guidelines	7.5 – 02 03 – 01.4 Page 8 of 10	
	Performance, Propulsion 1978 ITTC Performance Prediction Method	Effective Date 2008	Revision 02

propeller characteristics and the following quantities are calculated.

- the rate of revolutions:

$$n_s = \frac{(1 - w_{TS}) \cdot V_S}{J_{TS} \cdot D_S} \quad (\text{r/s})$$

- the delivered power of each propeller:

$$P_{DS} = 2\pi\rho_s D_S^5 n_s^3 \frac{K_{QTS}}{\eta_R} \cdot 10^{-3} \quad (\text{kW})$$

- the thrust of each propeller:

$$T_S = \left(\frac{K_T}{J^2} \right) \cdot J_{TS}^2 \rho_s D_S^4 n_s^2 \quad (\text{N})$$

- the torque of each propeller:

$$Q_S = \frac{K_{QTS}}{\eta_R} \cdot \rho_s D_S^5 n_s^2 \quad (\text{Nm})$$

- the effective power:

$$P_E = C_{TS} \cdot \frac{1}{2} \rho_s V_S^3 S_S \cdot 10^{-3} \quad (\text{kW})$$

- the total efficiency:

$$\eta_D = \frac{N_P \cdot P_{DS}}{P_E}$$

- the hull efficiency:

$$\eta_H = \frac{1 - t}{1 - w_{TS}}$$

2.4.4 Model-Ship Correlation Factor

The model-ship correlation factor should be based on systematic comparison between full scale trial results and predictions from model scale tests. Thus, it is a correction for any systematic errors in model test and powering prediction procedures, including any facility bias.

In the following, several different alternative concepts of correlation factors are presented as suggestions. It is left to each member organisations to derive their own values of the correlation factor(s), taking into account also the actual value used for C_A .

(1) Prediction of full scale rates of revolutions and delivered power by use of the $C_P - C_N$ correction factors

Using C_P and C_N the finally predicted trial data will be calculated from

$$n_T = C_N \cdot n_s \quad (\text{r/s})$$

for the rates of revolutions and

$$P_{DT} = C_P \cdot P_{DS} \quad (\text{kW})$$

for the delivered power.

(2) Prediction of full scale rates of revolutions and delivered power by use of $\Delta C_{FC} - \Delta w_C$ corrections

In such a case the finally trial predicted trial data are calculated as follows:

$$\frac{K_T}{J^2} = \frac{S_S}{2D_S^2} \cdot \frac{C_{TS} + \Delta C_{FC}}{(1 - t) \cdot (1 - w_{TS} + \Delta w_C)^2 \cdot N_P}$$

With this K_T/J as input value, J_{TS} and K_{QTS} are read off from the full scale propeller characteristics and the following is calculated:

$$n_T = \frac{(1 - w_{TS} + \Delta w_C) \cdot V_S}{J_{TS} \cdot D_S} \quad (\text{r/s})$$

$$P_{DT} = 2\pi\rho_s D_S^5 n_T^3 \frac{K_{QTS}}{\eta_R} \cdot 10^{-3} \quad (\text{kW})$$

	ITTC – Recommended Procedures and Guidelines	7.5 – 02 03 – 01.4 Page 9 of 10	
	Performance, Propulsion 1978 ITTC Performance Prediction Method	Effective Date 2008	Revision 02

(3) Prediction of full scale rates of revolutions and delivered power by use of a C_{NP} correction

For prediction with emphasis on stator fins and rudder effects, it is sometimes recommended to use power identity for the prediction of full scale rates of revolution.

At the point of K_T -(J)-Identity the condition is reached where the ratio between the propeller induced velocity and the entrance velocity is the same for the model and the full scale ship. Ignoring the small scale effect ΔK_T on the thrust coefficient K_T it follows that J-identity correspond to K_T - and C_T -identity. As a consequence it follows that for this condition the axial flow field in the vicinity of the propeller is on average correctly simulated in the model experiment. Also the axial flow of the propeller slip stream is on average correctly simulated. Due to the scale effects on the propeller blade friction, which affect primarily the torque, the point of K_Q -identity (power identity) represents a slightly less heavily loaded propeller than at J-, K_T - and C_T -identity. At the power identity the average rotation in the slipstream corresponds to that of the actual ship and this condition is regarded as important if tests on stator fins and/or rudders are to be done correctly.

In this case, the shaft rate of revolutions is predicted on the basis of power identity as follows:

$$\left(\frac{K_Q}{J^3}\right)_T = \frac{1000 \cdot C_P \cdot P_{DS}}{2\pi\rho_S D_S^2 V_S^3 (1-w_{TS})^3}$$

$$\frac{K_{Q0}}{J^3} = \left(\frac{K_Q}{J^3}\right)_T \cdot \eta_{RM}$$

$$n_S = \frac{(1-w_{TS}) \cdot V_S}{J_{TS} \cdot D_S}$$

$$n_T = C_{NP} \cdot n_S$$

3. VALIDATION

3.1 Uncertainty Analysis

Not yet available

3.2 Comparison with Full Scale Results

The data that led to 1978 ITTC performance prediction method can be found in the following ITTC proceedings:

- (1) Proposed Performance Prediction Factors for Single Screw Ocean Going Ships (13th 1972 pp.155-180) Empirical Power Prediction Factor (1+X)
- (2) Propeller Dynamics Comparative Tests (13th 1972 pp.445-446)
- (3) Comparative Calculations with the ITTC Trial Prediction Test Programme (14th 1975 Vol.3 pp.548-553)
- (4) Factors Affecting Model Ship Correlation (17th 1984 Vol.1 pp274-291)

4. REFERENCES

- (1) Hoerner, S.F. (1965) "Fluid-Dynamic Drag". Published by the author.
- (2) Kirkman, K.L., Klöetsli, J.W. (1980) "Scaling Problems of model appendages", 19th American Towing Tank Conference, Ann Arbor, Michigan



**ITTC – Recommended
Procedures and Guidelines**

**7.5 – 02
03 – 01.4**
Page 10 of 10

**Performance, Propulsion
1978 ITTC Performance Prediction
Method**

Effective Date
2008

Revision
02